(2)

LOW COST 2-D HEATSHIELD MATERIALS

AD A113928

Final Technical Report : MMT Project 3381

MARCH 5, 1982

Report Period May 28, 1979 Through November 21, 1981

Prepared Under Contract DAAK40-79-C-0150

Prepared For:

U.S. Army Missile Command
Redstone Arsenal, Alabama 35898

Prepared By:

FIBER MATERIALS INCORPORATED
BIDDEFORD, MAINE 04005

LOW COST 2-D HEATSHIELD MATERIALS

Final Technical Report : MMT Project 3381

MARCH 5, 1982

Report Period May 28, 1979 Through November 21, 1981

Prepared Under Contract DAAK40-79-C-0150

Prepared For:

U.S. Army Missile Command
Redstone Arsenal, Alabama 35898

Prepared By:

FIBER MATERIALS INCORPORATED
BIDDEFORD, MAINE 04005

UNCLASSIFIED

SECURITY CLASSIFICATION OF THIS PAGE (When Data Entered)

REPORT DOCUMENTATION PAGE	READ INSTRUCTIONS BEFORE COMPLETING FORM
1. REPORT NUMBER	2. GOVT ACCESSION NO. AD-A113 928	3. RECIPIENT'S CATALOG NUMBER 3381
4. TITLE (and Subtitle) LOW COST HEATSHIELD MATERIALS	5. TYPE OF REPORT & PERIOD COVERED Final Technical Report May 1979 - November 1981
	6. PERFORMING ORG. REPORT NUMBER W/A 1655
7. AUTHOR(s) R. L. Burns J. B. Smith P. Dara	8. CONTRACT OR GRANT NUMBER(s) DAAK40-79-C-0150
9. PERFORMING ORGANIZATION NAME AND ADDRESS Fiber Materials, Incorporated Biddeford Industrial Park Biddeford, Maine 04005	10. PROGRAM ELEMENT, PROJECT, TASK AREA & WORK UNIT NUMBERS
11. CONTROLLING OFFICE NAME AND ADDRESS U.S. Army Missile Command DRSMI-IYD Redstone Arsenal, AL 35898	12. REPORT DATE March 1982
	13. NUMBER OF PAGES 203
14. MONITORING AGENCY NAME & ADDRESS (if different from Controlling Office) DCASMA Boston 666 Summer Street Boston, MA 02210	15. SECURITY CLASS. (of this report) Unclassified
	15a. DECLASSIFICATION/DOWNGRADING SCHEDULE

16. DISTRIBUTION STATEMENT (of this Report)

Approved For Public Release,

Distribution Unlimited.

17. DISTRIBUTION STATEMENT (of the abstract entered in Block 20, if different from Report)

18. SUPPLEMENTARY NOTES

MICOM Project Engineer: Bob Park DRDMI-EAT

19. KEY WORDS (Continue on reverse side if necessary and identify by block number)

Heatshields	Ablatives
Braiding	Erosion
Silica Tapes	Ablation
Prepregging	Rubber-modified-silica-phenolic

20. ABSTRACT (Continue on reverse side if necessary and identify by block number)

Heatshield materials were manufactured using braided and prepregged rubber-modified-silica-phenolic (RMSP) tapes as opposed to bias-cut broad-goods. This program demonstrated the manufacturing technology using both flat and tubular braided materials.

Material test and evaluation was made by comparing the ablation erosion and thermal/mechanical properties of RMSP heatshield materials fabricated with braided versus bias-cut materials.

DD FORM 1 JAN 73 1473 EDITION OF 1 NOV 65 IS OBSOLETE

UNCLASSIFIED

SECURITY CLASSIFICATION OF THIS PAGE (When Data Entered)

TABLE OF CONTENTS

LIST OF FIGURES

LIST OF FIGURES (Cont.)

LIST OF FIGURES (Cont.)

LIST OF FIGURES (Cont.)

LIST OF FIGURES (Cont.)

LIST OF TABLES

LIST OF TABLES (Cont.)

Preface

The effort described within this report was sponsored by the U.S. Army Missile R&D Command, Redstone Arsenal, Alabama, under Contract DAAK40-79-C-0150. The contracting officer's technical representative was Mr. Bobby C. Park DRDMI/EAT. The Fiber Materials, Incorporated Project Engineer was Mr. Robert Burns. Task leaders for material fabrication and testing were Mr. Ray Sylvain and Mr. Peter Barry.

This report has been reviewed by the U.S. Army Missile Command and has been approved for distribution.

1.0 SUMMARY

Heatshield materials were successfully manufactured using braided tapes consisting of rubber-modified-silica-phenolic (RMSP) and glass reinforced phenolic resin. Tests and evaluations consisting of ablation, erosion, thermal and mechanical properties were used to evaluate the performance of heatshield materials fabricated from braided versus conventional bias-cut broadgood tapes. Analyses of test results indicated that heatshield materials tapewrapped with braided tapes provided similar properties except for mechanical strengths.

Braiding of tapes offer advantages over commercial bias-cut materials. The advantages include the ability to manufacture continuous tapes at the desired width plus a balanced tape construction. Also, cost benefits can be realized from the elimination of slitting and stitching operation which are currently required for bias-cut broadgoods. The stitching of bias tapes also results in randomly located splice joints in the final heatshield product.

A series of tasks were undertaken in this program to evaluate and demonstrate the technology of fabricating heatshield materials using braids. Numerous manufacturing approaches were taken and demonstrated, with the final result being a manufacturing demonstration. Drawbacks of braided materials were also identified and these specifically relate to the selection of braid design and prepregging problems. Additional efforts are required in these areas to optimize the braided tape technology for heatshield applications.

2.0 INTRODUCTION

The overall objective of this program was to develop the manufacturing technology necessary for fabricating low cost heatshield materials using a continuous/spliceless prepreg tape and to demonstrate this technology by fabricating and evaluating subscale hardware. It was also the objective to utilize state-of-the-art (SOTA) wrapping methods which have been established for a variety of strategic heatshield materials.

Fabrication of a prepreg tape which is continuous offers both potential cost and performance advantages over bias-cut tapes which are currently being used to manufacture heatshields. To understand this rationale, a review of current SOTA heatshield fabrication methods is discussed.

The majority of composite heatshield structures are fabricated using tape-wrapping techniques. This process essentially consists of wrapping strips of prepregged tape (i.e., resin impregnated and B-staged material) around a mandrel which is representative of the structural shape of the heatshield. (Refer to Figure 1.) The strips of tape are wrapped at an angle to either the surface or the centerline of the mandrel. The angle the tape forms to the mandrel's surface is called either the "wrap angle" or "shingle angle" of the heatshield. An angle greater than 0° is necessary for aerodynamic, ablation and insulation considerations. When wrapping at an angle to the mandrel surface, the tape is required to stretch and conform. The magnitude of the required conformability is dependent on the diameter of the structure, the wall thickness requirements of the heatshield and the desired shingle angle. In essence the inside and outside diameters of the tape require different magnitudes of stretch and conformability. This is commonly referred to the wrap ratio, which is the quotient obtained from the outside diameter and inside diameter which the tape forms on

Figure 1. Schematic of Tapewrapping Process

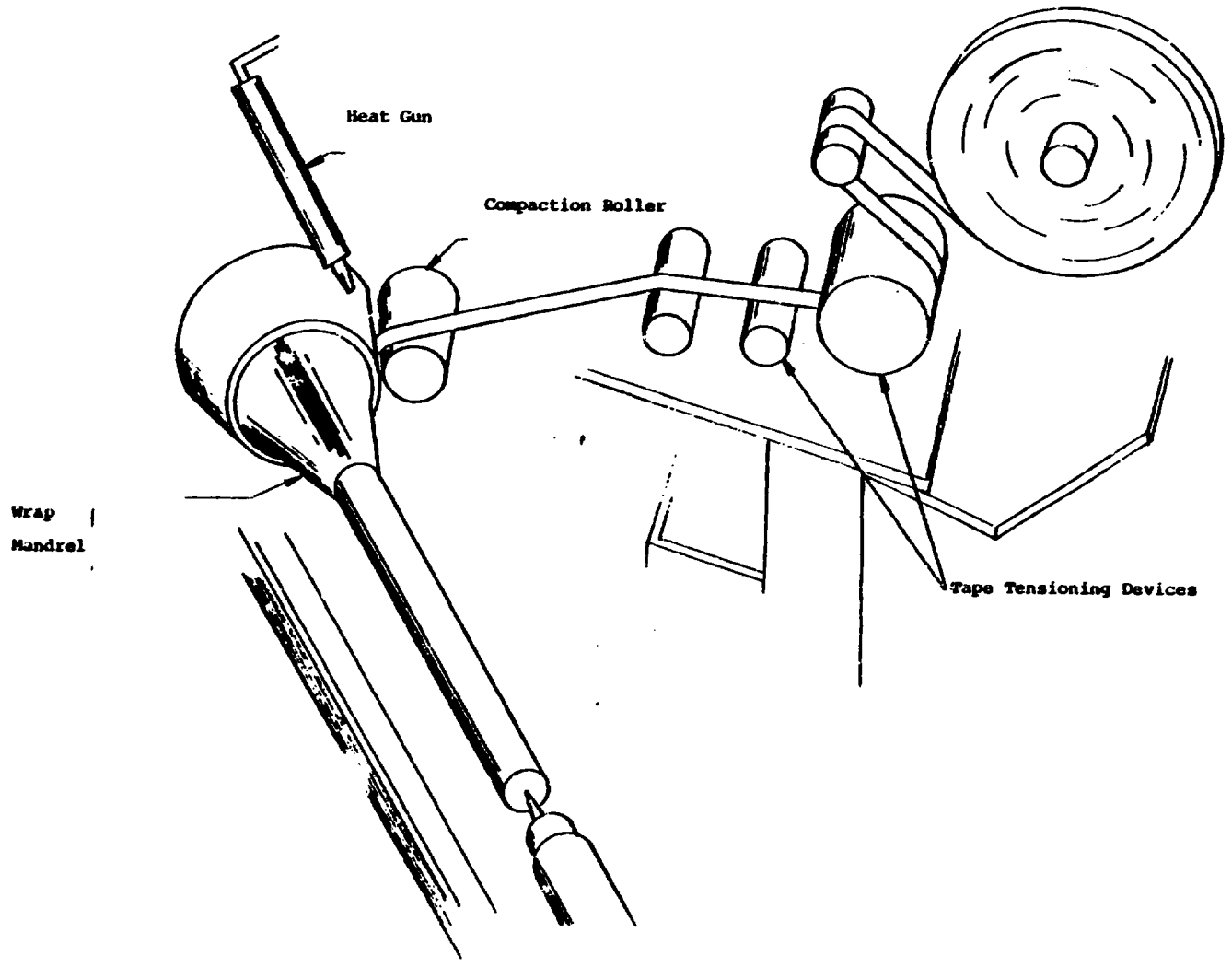

the mandrel.

Tape wrapped heatshields were originally developed in the late 1950's and early 1960's for use on IRBM's developed by the U.S. Army. The manufacturing methods have not advanced significantly since.

Conventionally woven fabric or tapes (i.e., the warp and fill yarns cross at right angles) do not provide the stretch and conformability characteristics necessary to manufacture a tapewrapped heatshield which contains a shingle angle greater than a few degrees. This is a result of the continuous yarns in the circumferential direction of the tape. The stretching ability of the tape (i.e., straight tape) is essentially nonexistant; therefore, the variation in the required inside to outside diameters of the tape wrapped heatshield do not permit their use. To overcome this problem, materials manufactured for tape wrapping are obtained by weaving conventional broadgoods, impregnating and B-staging with the selected resin system and then cutting strips at a 45° angle to the edge of the fabric. (See Figure 2.) This material is referred to as bias-cut tapes.

The strips of bias-cut tapes are subsequently joined by either overlapping or butting the ends. Joining is accomplished by stitching the overlapped or butted tape lengths. Bias-cut tapes provide the needed conformability since neither the warp or fill yarns are continuous. In addition, the material has the ability for limited stretch since movement of the yarns are permitted.

There are drawbacks to using bias-cut materials which are related to either cost and/or potential performance problems. In terms of cost, the length of the individual strips of tape is limited by the width of the woven broadgoods. For example, most broadgoods are manufactured between forty (40) inches to seventy-two (72) inches wide and the corresponding length of a single bias-cut

Figure 2

PREPARATION OF CONVENTIONAL BIAS TAPES

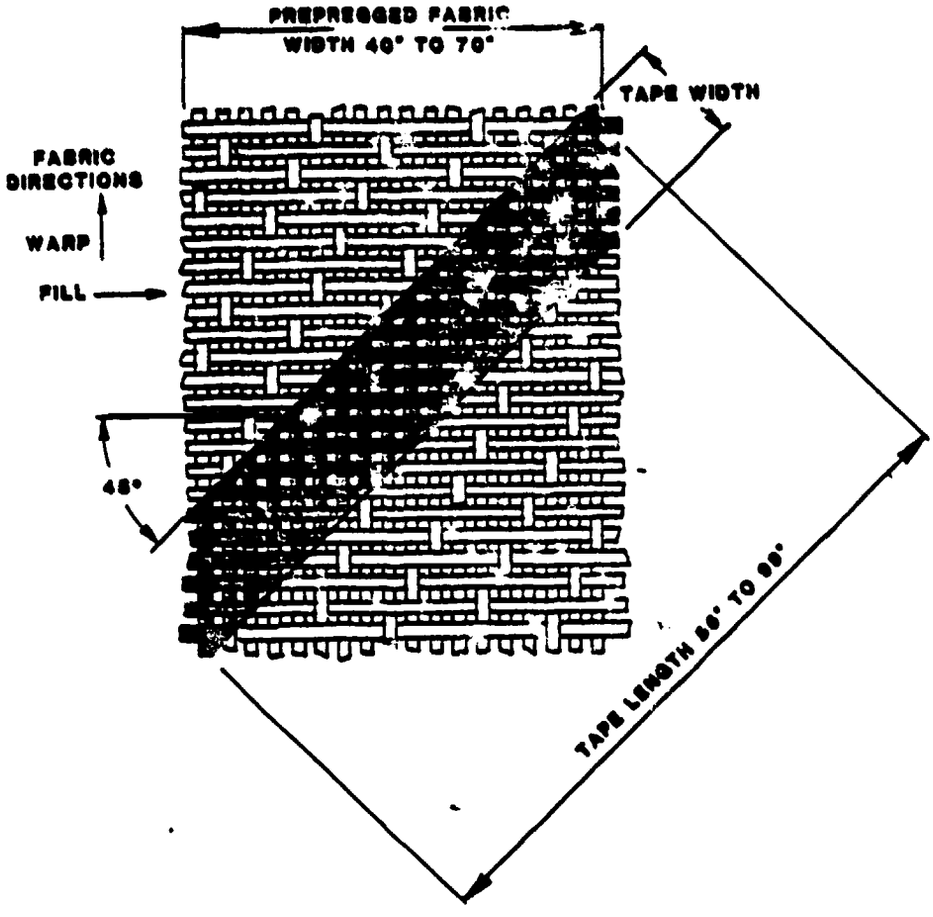

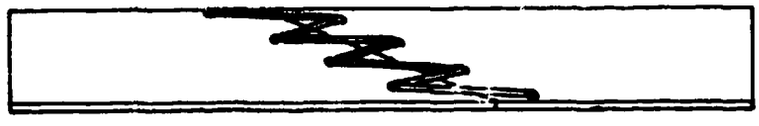

BUTT SPLICE

OVERLAY SPLICE

strip is fifty-six (56) inches to one hundred (100) inches long. The costs involved to stitch the lengths of tape varies for different materials, however, the stitching operation adds 15% to 20% to the material cost.

The potential drawbacks of bias-cut tapes are two-fold with respect to heatshield performance. First, woven broadgoods contain an inbalance in weave construction. The fiber volumes are unequal in the warp and fill direction due to the variation in yarn end count (i.e., yarn ends per linear inch). High quality fabrics used for manufacturing prepregged tapes contain a four (4) percent difference in yarn volume between the warp and fill direction. Second, the splice joints result in a random distribution throughout the fabricated heatshield. These discontinuities vary in location because the circumference of a conical shaped structure changes constantly along its central axis, hence, splice joints are randomly located.

The effects of having different warp and fill yarn counts which protrude to the heatshield surface and the presence of radome splice joints on the ablating surface have been extensively studied. The primary purpose of these have been to analytically model and identify their effect(s) on the flow field and roll torque characteristics. These analyses provided only limited success and were not positively verified by ground simulation and flight testing. However, elimination of yarn inbalance and minimizing splice joints would result in more reproducible and predictable heatshields.

An alternate method for producing tapes is by braiding. The manufacture of fiber reinforced tapes using a braiding approach offer three main advantages. First, the tape can be fabricated at the desired tape width. This eliminates the fabric slitting operation required for conventional bias-cut materials. Second, braided materials can be made continuously, thus eliminating stitching operations. Also, braiding provides the capability to tailor the reinforcement

in terms of stretch/conformability. For example, the angle the yarns form at their crossover point can be controlled, thus providing a tape which contains either high stretch (low braid angles) or very low stretch (high braid angles).

Standard commercial braiding equipment can be used to fabricate continuous tapes. Any yarn which can be handled or woven on conventional looms or winding equipment can also be braided.

The simplest way to describe braiding is to illustrate a maypole dance with figures that represent braiding machine carriers. (See Figure 3). In this illustration the characters pass inside and then outside of each other traveling in opposite directions on different tracks. The ribbon which the characters hold forms a spiral around the pole. The weave pattern formed by the ribbon is typically called a "basket weave". When an even number of characters are used, a tubular braid is formed. When an odd number of characters are used, a flat braid is formed. This is accomplished by reversing the direction of the characters at a designated point on the track called terminals and shifting to a different track.

A braided tape is defined by its shape (whether flat or tubular), the braid angle (which is the angle the yarns form with respect to the edge of the tape), yarn count (which is the number of yarn ends wound on each braiding machine carrier), packing (which describes the fineness of the weave), and the addition of warp yarns (can be accomplished by inserting yarns through warp tubes). These tubes are located equally spaced around the braiding track and for every two braid carriers a machine contains one warp tube. The warp yarns do not spiral around the braid (tubular braid) or travel from edge to edge (flat braid) but lay straight in the braid parallel to the centerline of the tape. (Refer to Figure 4).

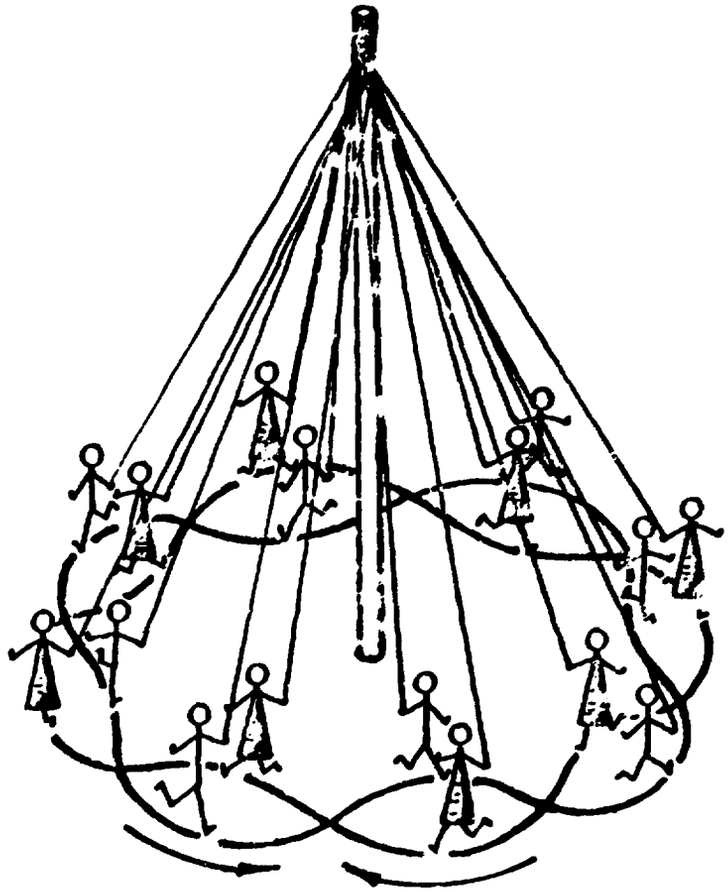

FIGURE 3 BRAIDING PROCESS ILLUSTRATION

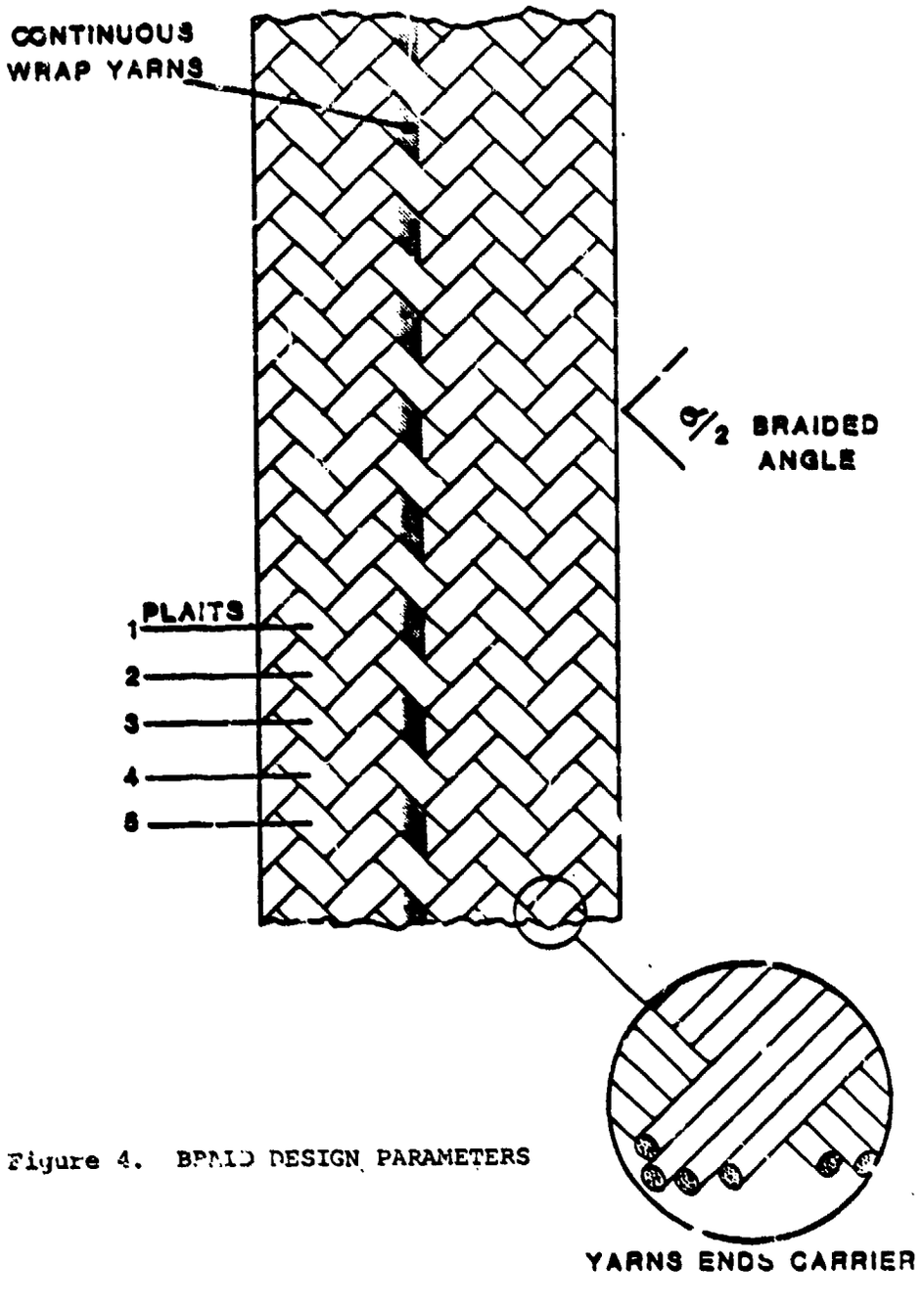

Figure 4. BRAID DESIGN PARAMETERS

A braid design is controlled by the type of yarn selected, the number of braiding machine carriers, the number of yarn ends wound on each braid carrier and the location of the braiding point. The braiding point is centrally located above the braiding machine and by adjusting it up or down the braid angle and yarn packing can be altered. These parameters are controlled in combination with the speed of the take-off equipment. The type of yarn selected, machine carriers and yarn ends per braid carriers control the physical characteristics of the braid. For example, using a single end, very fine yarn (i.e., low denier), the maximum obtainable braid diameter (tubular braid) or width (flat braid) is limited by the number of machine carriers. To obtain a wider tape, a machine which contains a higher number of carriers or multiple ends of yarn must be used.

To carry out the program objectives, a series of tasks were identified which would result in the development and demonstration of heatshields manufactured with a braided tape. The following section discusses the approach to the manufacturing technology development.

2.1 Approach

The intent of this program was to develop the manufacturing technology using continuous/spliceless braided tape and demonstrate its application to current U.S. Army heatshield requirements.

The first task was a heatshield material requirements review to enable selection of a heatshield material and construction for manufacturing technology development. The Pershing II ballistic missile was selected as the baseline with material requirements being defined based on the anticipated aerodynamic

heating, predicted trajectories and erosion resistance requirements. With the heatshield requirements defined, factors such as yarn type, shingle angle, and heatshield wall thickness were considered in establishing material selection.

Under the second task, baseline fabrication studies were conducted to identify a braid design. The braiding process was selected to be suitable for manufacturing tapes which contain the fiber types, fiber volume and physical processing characteristics consistant with heatshield requirements. Identified were material constructions adaptable to commercial braiding and SOTA tape-wrapping equipment. Unacceptable were material constructions which required major alterations to braiding equipment or the redesign of the wrapping lathe. The desired characteristics of the braid were a material which exhibited the conformability, high yarn packing (i.e., plaits/inch is synonymous with picks/inch for a woven material) and handling characteristics of commercially available bias-cut tapes. The braid construction and design parameters selected for investigation consisted of flat braids, tubular braids, variations in braid angle, the addition of continuous warp yarns and all of these parameters compared against variations in the number of yarn ends for braiding machine carriers.

Once a braid construction(s) was selected, prepregging procedures were determined. The approach to this task was to define prepreg characteristics or goals. These properties were established using laboratory prepregging equipment and subsequent characterization. Characterization consisted of resin content, volatiles and flow properties of the tape. Once laboratory procedures were optimized, the methods used were then transferred to production equipment.

Demonstration of tapewrapped hardware plus test and evaluation was the next task used in the approach. Hardware consisting of molded flat panels and tapewrapped cylinders were evaluated for manufacturability of braided tape with SOTA

manufacturing procedures. Tests were selected to enable a comparison of materials fabricated with braid and conventional bias-cut tapes.

As a final task, subscale heatshields were fabricated as demonstration hardware. The heatshield size, half-angle and wall thickness were selected as being representative of current U.S. Army requirements.

It should be noted that the tasks identified in the program approach were not undertaken in a defined chronological order. The program approach was designed to enable each succeeding task to provide feedback. A summary of the program approach/tasks is illustrated in Figure 5. From this flow chart it is seen that the evaluation phases affected one another and problems encountered in a particular task required solving in the previous operation.

It should also be noted that the technical requirements of this program were modified midway through the program. The majority of the braid tape development was demonstrated using glass/phenolic materials following the approach described in this section. However, prior to fabrication of the demonstration hardware, the selection of rubber-modified-silica-phenolic (RMSP) material was made. This material was selected to enable demonstration of the braiding technology with a material that was identified for use on a current U.S. Army missile system. Selection of this material required repeating the evaluation tasks prior to conducting a manufacturing demonstration. The selection of silica yarn also required additional braid design evaluation and prepregging trials. The details of this effort will be discussed in the subsequent section.

Figure 5.

SUMMARY

PROGRAM APPROACH/TASKS

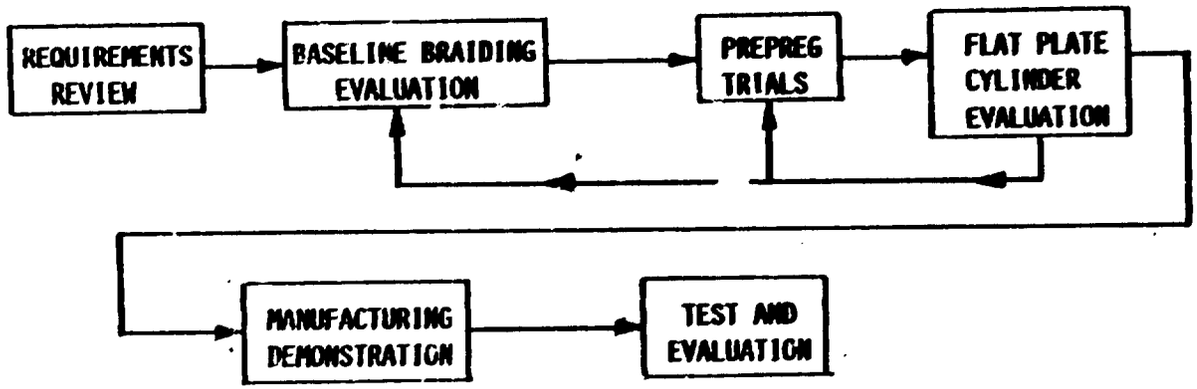

3.0 MANUFACTURING TECHNOLOGY DEVELOPMENT

3.1 Material Requirements Review

As discussed previously, the objective of this task was to determine the material requirements, and select a reinforcement (yarn) and matrix material (resin). The approach was to review the current and projected U.S. Army heatshield requirements with special emphasis on the Pershing II flight environment. The evaluation of the heatshield environment consisted of the heat flux history, total integrated heating, backface temperature limitations, vehicle velocities, body shape, and potential flight trajectories.

Two problems made it difficult to obtain the necessary information to make an accurate heatshield sizing and material determination. First, the Pershing II design requirements and projected mission had not been completely defined at the time the information was needed. Second, the information required had limited access because of security reasons. However, an analysis of the heatshield material requirements were made based on limited information and assumptions. The information obtained for this analysis consisted of cold wall heat rates as a function of position on the vehicle and time for flights of 400, 632 and 880 nautical miles (nm) and is summarized in Figure 6. The 880 nm flight presented the most severe aerodynamic heating condition of the three (3) flights. The geometry of the vehicle,which is shown in less detail in Figure 6, indicated that the forward portion of the heatshield began at station 7. To determine the heating rate history, the 880 nm flight cold wall heat flux for station 7 was integrated by segmenting the area under the curve into five (5) simple geometric shapes as shown in Figure 7. The total integrated heating was determined to be 4375 Btu/Ft^2. This value,in conjunction with the cold wall heating rates indicated in Figure 6, is low as compared to typical reentry

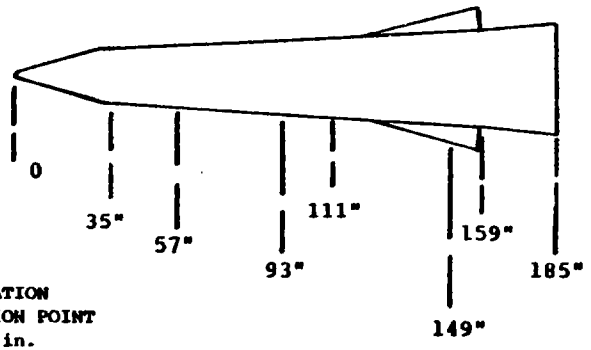

STATION	LOCATION
0	STAGNATION POINT
1	5 in.
2	15
3	25
4	34.7
5	35.7
6	36.7
7	37.8

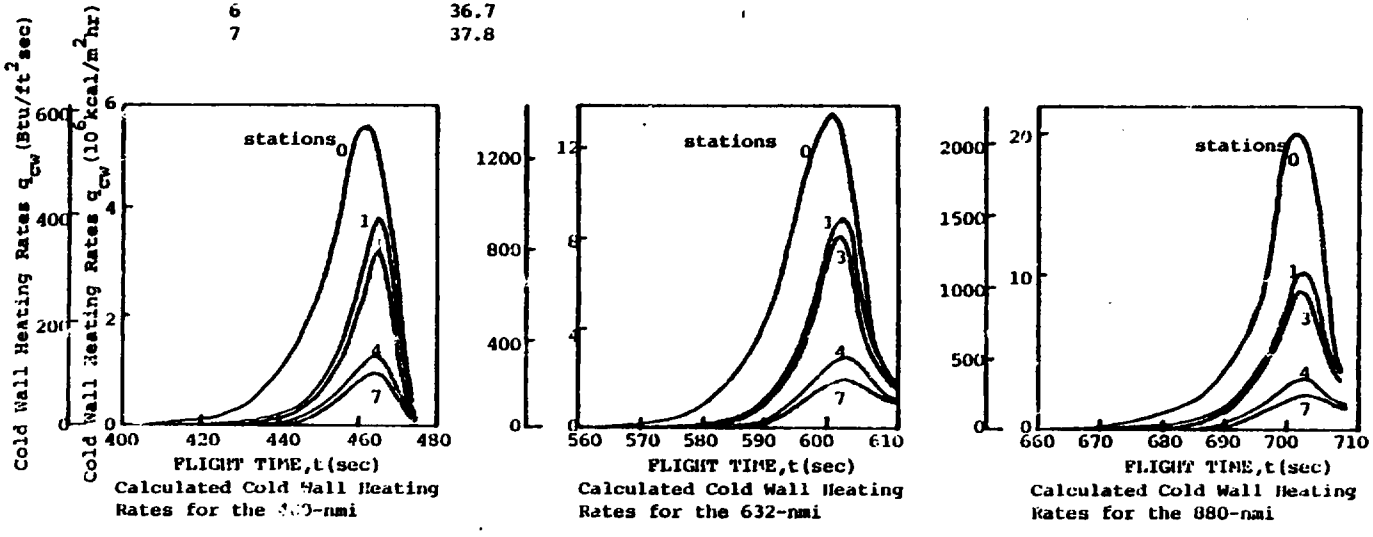

Figure 6.

VEHICLE GEOMETRY AND PROJECTED HEATING RATES

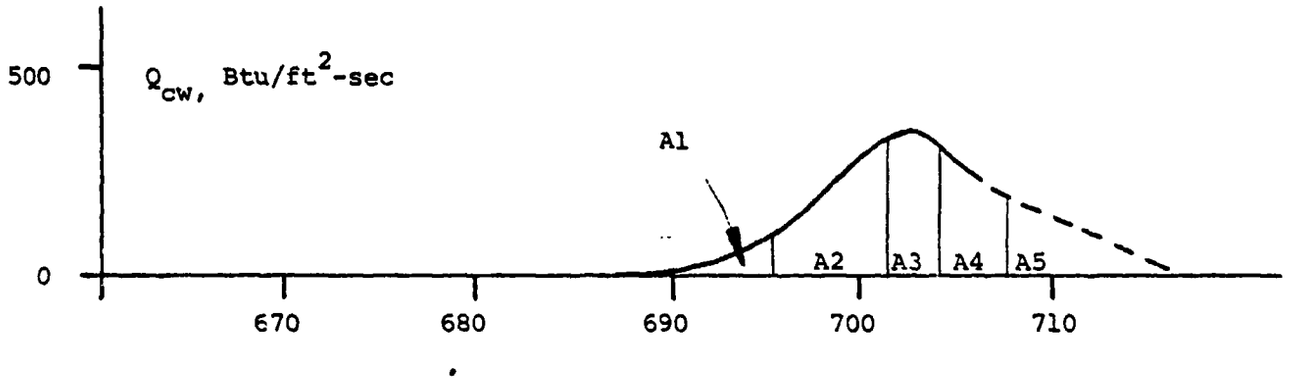

Region	A1	A2	A3	A4	A5
Heat Flux (Btu/ft^2)	321	1500	643	750	1161

$$Q_A = Q_{A1} + _{A2} + _{A3} + _{A4} + _{A5} = 4375 \text{ Btu/ft}^2$$

$$\bar{Q} = Q_A/20 \text{ seconds} = 219 \text{ Btu/ft}^2\text{-sec}$$

Figure 7. Heat Flux Calculations For 880-nmi Flight

vehicle environments.

To determine the generic class of heatshield material required (i.e., carbon, silica, quartz,etc.) a review of thermal and ablative properties were made. A summary of the thermal and ablative properties of selected heatshield materials is presented in Table 1. These materials represent the various generic material types which were considered for selection. Carbon/phenolic (CP) has typically been used where superior ablation performance is required. Its performance is significantly superior when compared to the other generic material types. However, this statement must be qualified in that the mission must be severe enough to take advantage of the superior ablation performance, otherwise the high thermal conductivity of CP is a drawback. Based on the limited mission data available, it is assumed that minimal to negligable ablation would occur using CP. Therefore, the attributes of CP would not be utilized and selection of either a silica, glass, or quartz system would be more appropriate because of their superior insulation properties.

The information reviewed for this task (i.e., references 9 through 13) plus inspection of the data listed in Table 1 and Figure 6 suggests that little or no ablation would occur even if generic silica materials were used. The analysis for making a material selection used this assumption since inadequate heatshield erosion requirements were available.

Based upon this assumption, carbon reinforced heatshields are eliminated as being unnecessary. That left the generic silica reinforced materials, plus others such as nylon reinforced materials and cold wall ablators. In fact, based on the data available,cold wall ablators such as fluropolymers and epoxy-urethane would probably meet the mission requirements; however, these materials are typically cast or molded and not within the scope of the program.

TABLE I

THERMAL, PHYSICAL AND ABLATION PROPERTIES OF VARIOUS HEATSHIELDS[1.2]

	Teflon	Nylon Phenolic	Glass Phenolic	Silica Phenolic	Carbon Phenolic
Ablation Temperature(^{o}F)	1340	4500	3500	3500	6500
K (Btu/Hr-ft-^{o}R)	0.14	0.17	0.28	0.25	0.8
Density (gm/cc)	2.18	1.21	1.73	1.55-1.65	1.47
Cρ(Btu/lb-^{o}R)	0.26	0.43	0.28	0.25	0.4
Emissivity	0.15	0.8-0.9	0.6	0.7	0.8-0.9
Heat of Ablation, Q*, (Btu/lb)	$950+\eta(H_s-H_w)$	$1500+\eta(H_s-H_w)$	$1100+\eta(H_s-H_w)$	$2960+\eta(H_s-H_w)$	$5970+\eta(H_s-H_w)$
Blowing Coefficent					
ηt (turbulent)	0.50	-	0.25	0.57	-
ηL (laminar)	0.17	0.50	-	0.41	0.74

H_s= stagnation enthalpy

H_w= enthalpy of the wall

Q*= Figure of merit=heat required to remove per unit mass due to ablation

A second review of the thermo-physical and ablation data presented in Table 1 suggests that nylon reinforced phenolic has excellent insulation and ablation properties when compared to the generic silica (i.e., glass, quartz, silica) heatshield materials. In theory, this is so; however, the insulation properties of nylon phenolic are preserved only if the char layer remains adhered. There is some evidence based on review of references that the char layer formed by nylon phenolic strips away due to aerodynamic forces. Also, there may be chemical instabilities and shelf life (i.e., storage) problems in that internal stresses can vary and increase with time as a result of fabrication processes. Due to these uncertainties, which may be unfair stigmatization of nylon phenolic and because of limited data, nylon phenolic was eliminated from any further consideration.

The ranking of generic silica materials according to ablation performance for moderate to high heat flux environments are in the following descending order: quartz, silica (Refrasil®) and glass phenolic. The thermal properties of these materials are similar. The major difference is ablation properties where high aerodynamic shear forces tend to "peel" away the low melt layer formed by glass reinforced phenolic. But, as discussed previously, the heating environment is low and it is assumed that the corresponding shear forces are also low. Therefore, the superior ablation properties of quartz would not being taken advantage of. When costs are considered, quartz is nearly an order of magnitude greater than silica and the same is true for silica as compared to glass. Low observables (i.e., trace element impurities) were not considered or identified as a critical property of the heatshield material. Therefore, based on the heatshield requirements which were determined from the anticipated heating rates, data review and cost consideration, glass/phenolic was selected as the material system for demonstrating the braiding manufacturing technology.

Prior to initiating baseline braiding studies, heatshield wall thickness values were calculated to determine the physical characteristics of the required glass braid (i.e., tape width is a function of the wall thickness of the heatshield). The required wall thickness was determined as a function of the thickness of insulation material required to limit the backface temperature to a predetermined value, plus the material removed due to ablation. To determine this, complex digital computer codes (i.e., ACE, Aerothermal Chemical-Equilibrium and CMA, Charring-Material-Ablation) are used. However, significant material property data are required as inputs for these codes, plus specific flight environment parameters such as recovery enthalpy, surface pressure and heat transfer coefficients. The data required to support these computations were unavailable and, as discussed previously, it was assumed little or no ablation occurs. To determine the heatshield wall thickness requirements, an appropriate "hand" calculation technique was selected which would yield an acceptable estimate of the required heatshield insulation thickness required for preliminary design purposes. This approach assumes that no ablation takes place and that heatshield thickness is a function of the insulation requirements only.

In this approach, the transient reentry heating problem is substituted with a hypothesized equivalent steady-state heat transfer approach where the backface of the heatshield is assumed to be perfectly insulated. For this simple radiation insulation shield, the problem is now one of finding the temperature response of one (1) finite element where the exposed side is at constant temperature and the other side perfectly insulated.

The solution to the problem is:

$$\frac{\Delta Tr}{\Delta Tw} = 1-4/\pi \sum_{m=0}^{\infty} \frac{(-1)^m}{(2m+1)} \left\{ \exp \left[\frac{-(2m+1)^2 \pi^2 \alpha t}{4 X_i^2} \right] \right\}$$

Where:

α = Diffusivity of the heatshield (averaged over the charred and virgin states)

t = Time of which the heat flux is exposed.

x_i = Heatshield insulation thickness required.

Such that:

Tw = The heated surface temperature

Tr = The maximum backface temperature permitted

To = The initial material temperature (70°)

This equation can be expressed in graphical form as a function of the parameter $K\rho t/C_p W_i^2$ This is shown in Figure 8.

K = Thermal conductivity

ρ = Density

c = Heat Capacity

W_i = The required heatshield mass per unit of area.

Figure 9 illustrates solution curves for various assumed values of T_R (backface temperature limit) Tw (maximum heatshield surface temperature), and t (time exposure to the heat flux). The most stringent condition is given by Tw = 5500°R, T_R = 200°F, and t = 25 seconds which yields a heatshield thickness requirement (x_i) of 0.352 inches.

Realistically, a backface surface temperature of 200°F is a stringent value. Typically values of 400-500°F are more commonly used. If this were the case, an adequate heatshield thickness of 0.26 inches would be used. However, the limitation of the backface surface temperature is unknown, hence a conservative value of 0.35-0.40 inches was determined. This thickness was subsequently used

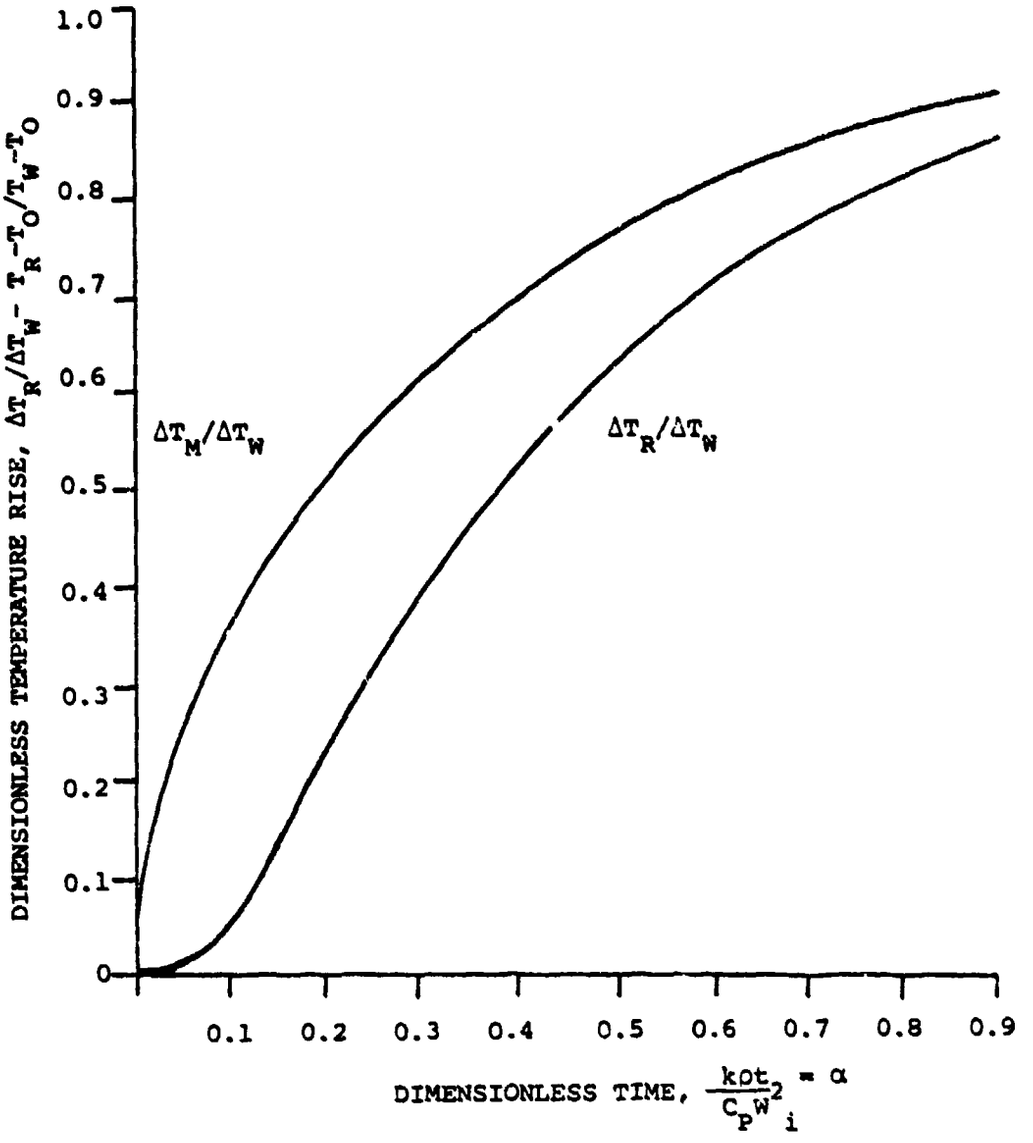

Figure 8 REAR AND MEAN TEMPERATURE RISE IN A FINITE MEDIUM WITH CONSTANT SURFACE TEMPERATURE (T_W) AND INSULATED REAR BOUNDARY

T_M = Mean Temperature over Heatshield Thickness

T_R = Maximum Backface Temperature Allowed

T_W = Front Surface Wall Temperature

T_o = Material Initial Temperature

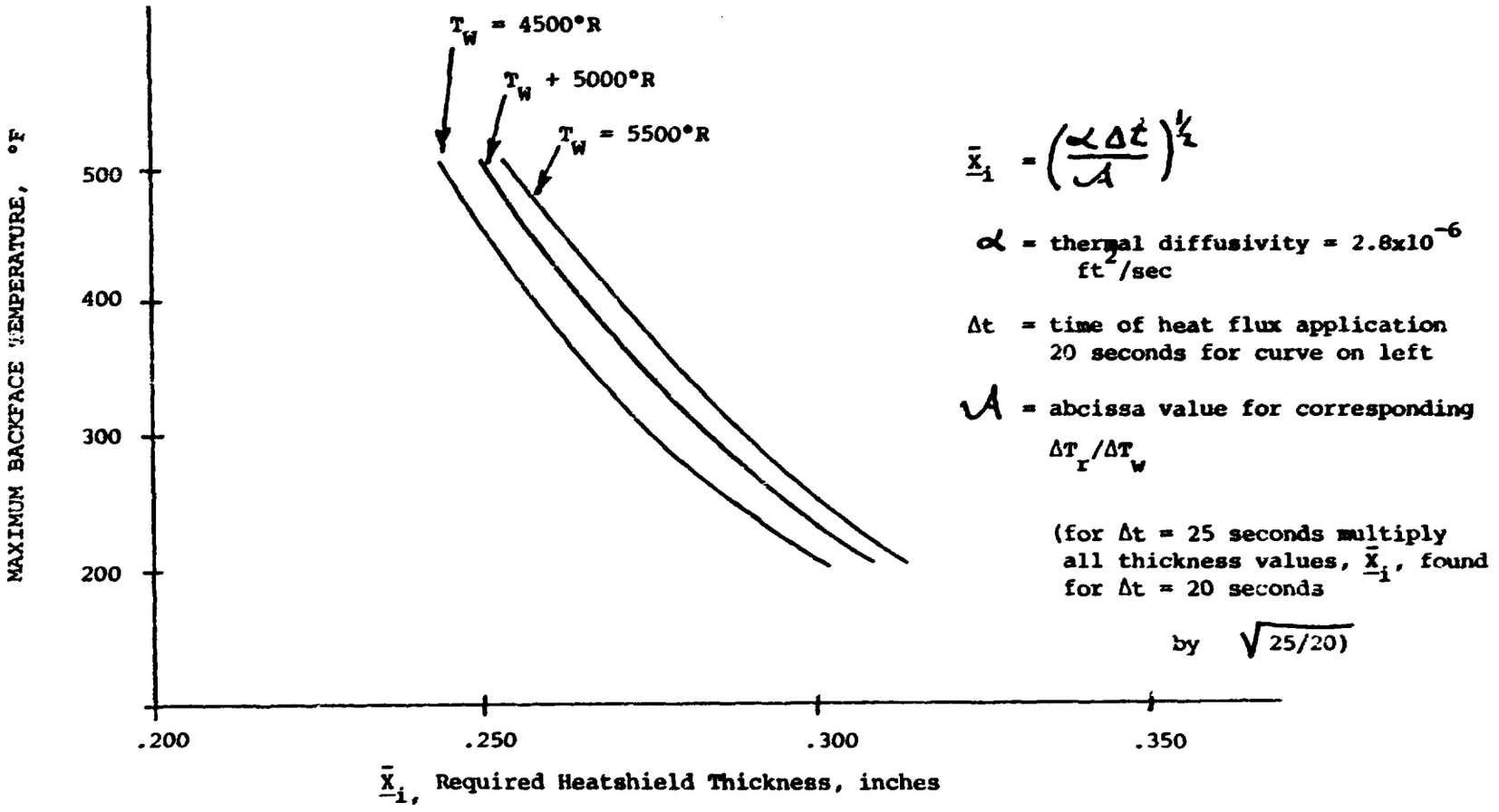

Figure 9 Required Heatshield Thickness versus Maximum Backface Temperature (Glass Phenolic)

to determine the physical size of the braid required to tapewrap demonstration and test hardware using a braided tape.

It should be noted that the determination of a heatshield material and thickness requirement used assumptions and liberties. It was planned not to limit the braiding technology to just glass phenolic materials corresponding to a specific heatshield thickness. The approach enabled a variety of reinforcements to be fabricated using braiding techniques.

3.2 Baseline Fabrication Studies

The objective of this task was to establish the braided tape construction. Design goals consisted of fabricating a material which was conformable, contained high yarn packing, capable of subsequent prepregging and one which was applicable to commercial braiding techniques.

The design parameters which were selected for review consisted of the number of yarn ends per braiding machine carrier, the braid angle, the addition of warp yarns and the evaluation of flat braided tapes. These design parameters were selected to determine the effect on the tape thickness, stretch/conformability and qualitative evaluation of their handling properties.

This task was initiated prior to the selection of heatshield material (i.e., material requirements were being defined concurrently with baseline design studies). A S-2 glass yarn was selected to evaluate the various braid constructions. Table 2 lists a summary of the braid design parameters which were selected.

TABLE 2

SUMMARY OF BRAID DESIGN PARAMETERS

Braid Angles: 30°, 45°, 60°, 80°
Yarn ends per carrier: 1, 2, 3, 4
Warp yarns: Single warp yarn, forty (40) warp yarns
Machine Carriers: 80, 77
Shape: Tubular, flat

Table 3 lists the matrix of candidate braid designs. It can be seen from this matrix that design parameters were isolated to determine their effects on the properties of the braid.

Plans were to fabricate thirty (30) feet of each braid design and both qualitatively and quantitatively evaluate their characteristics. Qualitative evaluation consisted of stretch and conformability testing. Commercially available silica/phenolic was purchased to enable a comparison. Conformability testing consisted of draping the "as braided" tape over a wrapping mandrel to simulate a 45° shingle. Selected tubular braids were also slit, see Figure 10, to determine any benefit from this approach. A qualitative judgement was then made of the tapes ability to conform. Subsequently, to examine the stretch characteristics, selected samples that were judged as conformable (i.e., formed to the mandrel surface without wrinkling or bulking) were then prepregged and mounted in a universal tensile testing machine. A load-extension curve was generated and the measured increase in gage section was determined at various load levels. Commercial bias-cut silica/phenolic tape was also included in this matrix. This enabled a more accurate comparison of the braid's stretch characteristics.

Quantitative evaluation of the various braid designs was conducted by prepregging selected designs and molding bars for subsequent testing. Prepregging was conducted with Monsanto's SC1008 phenolic resin using laboratory prepregging equipment. The molded bars were examined for density, porosity, residual volatile content and fiber/resin content. It should be noted, that for selection of the braid, major emphasis was placed on the resulting fiber volume and ply thickness. Prepregging parameters had not been established at this time, therefore, the resin content was not a determinant of the braid design

TABLE 3

BRAID DESIGN MATRIX-CANDIDATE DESIGNS

Identification Number	Yarn Ends Carrier	Braid Angle(θ°)	Comments
1	1	45	STD basket weave
2	1	45	40 warp yarns
3	1	80	STD basket weave
4	1	60	STD basket weave
5	1	30	40 warp yarns
6	1	60	40 warp yarns
7	1	45	Single warp yarns
8	1	80	Single warp yarn
9	1	60	Single warp yarn
10	1	45	Flat braid

Note 1: This same sequence was followed for 2, 3, and 4 yarns per braid carrier.

Note 2: All tubular braids used 80 machine carriers and all flat braids contained 77 machine carriers.

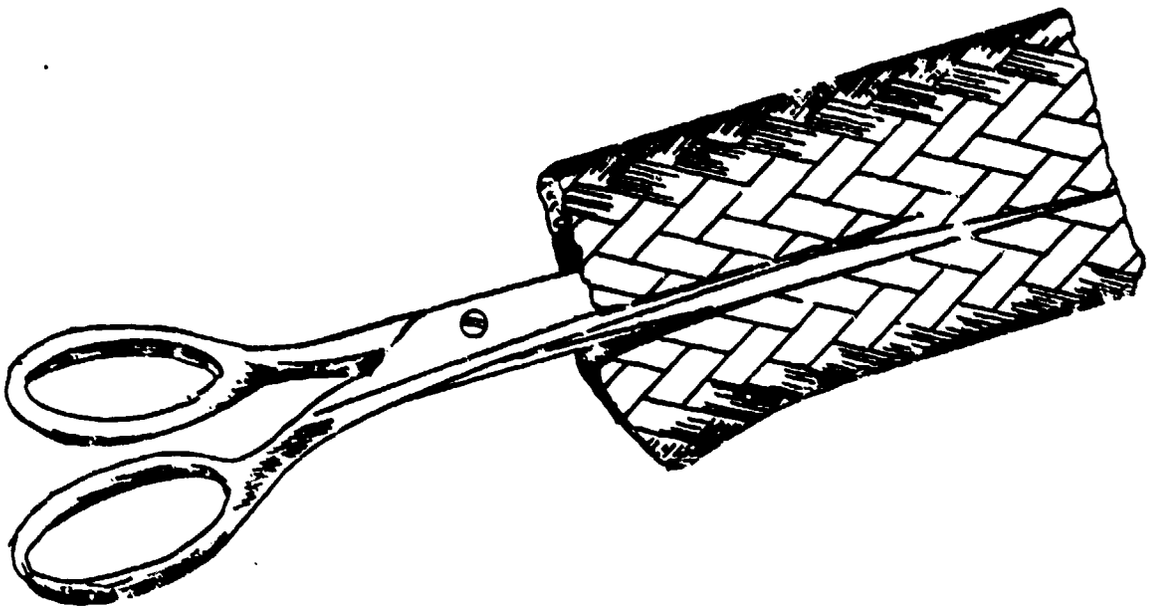

FIGURE 10 REPRESENTATIVE SKETCH OF SLITTING OF TUBULAR BRAID

The results of these evaluations were as follows:

Addition of Warp Yarns: The addition of single continuous warp yarns in the axial direction of the braid did not appear to affect the conformability of the braid. However, the insertion of multiple warp yarns prevented the tape from conforming to the mandrel surface. The intent of the warp yarn insertion was to maintain the shape and cross-section of the braid not knowing what degree of yarn packing and handling characteristic would be obtained. The warp yarns (since they are straight and continuous) reduce the ability of the braid to stretch. Multiple warp yarns restricted the movement the braid and these braid designs had stretch and conformability properties which were similar to a straight tape. Therefore, the addition of multiple warp yarns was dropped from further design consideration.

Braid Angle: The original plans called for evaluating braided materials with a 30°, 45° and 60° braid angle. However, it can be seen from Table 3 that 30° braids were not fabricated and an 80° braid angle was substituted. During the initial braiding trials it was determined that braid angles of less than 45° were difficult to manufacture with reproducible results. Angles of less than 45° required very high yarn packing beyond both the capabilities of the braiding machine and the capability of the yarn. For example, to obtain this braid angle required lowering the machine braiding point. As yarn formed into a tubular braid, the take-off was not capable of applying adequate tension to pull the braid. Slippage of the tape which caused variation in braid angle and/or breakage of yarn occurred. Therefore, an 80° braid angle was selected to replace the 30° braid. The 80° material was easily manufactured, but since the yarns form a very high angle to the edge of the braid little conformability was

realized. In essence, the 80° braid had characteristics of a straight tape and eliminated any need for further evaluation.

The 45° and 60° braids exhibited the ability to conform and stretch to a mandrel surface. It should be kept in mind that a 45° braid angle is similar in construction to a bias-cut tape. These designs were selected for further evaluation.

Yarn Ends/Carrier: This parameter was included in the baseline design studies for two (2) purposes. First, the number of yarn ends was varied in order to determine the physical size (i.e., width) of the resulting braid. Numerical techniques exist to determine the resulting tape width; however, variations result from different yarn packings using different materials. Second, the effects increased yarn ends have on stretch and conformability characteristics needed to be evaluated.

The braids which contained only one (1) or two (2) yarn ends produced a braid which was too narrow for tapewrapping. Slitting of the tubular braid would provide a tape with adequate width; however, this operaion was considered undesirable since it would add cost to the final tape product. The low yarn end count braids were therefore dropped from further evaluation.

Flat Braids: Flat braids were selected for evaluation in the event that a tubular braid could not be used for tapewrapping. A tubular braid can be slit to form a flat shape, but this operation must be performed subsequent to prepregging. If a tubular braid is slit prior to prepregging, the yarns tend to unravel and the handling properties of the braid are very poor. Flat braids resulted in narrow tape widths plus showed limited ability to conform. This was limited by the nature of the edges. In a flat braid an individual yarn traverses the width of the tape from side-to-side. The edges of a flat braid resist any deformation which restricts the tape conformability.

Flat braids were dropped from further evaluation. Table 4 lists a summary of the braided tape designs which were molded into flat laminates. Note that some braid designs were discontinued prior to molding. The nomenclature used in Table 4 for identifying the various braid designs is explained as follows:

Example: Braided Tape Design Nomenclature

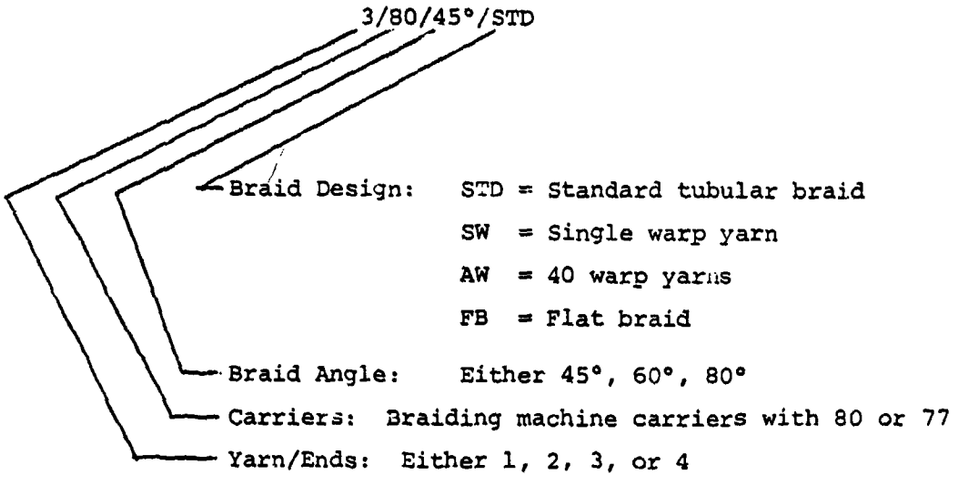

From Table 4 the variation in physical properties of the braids can be seen. Conformability data has not been provided for reasons discussed previously; this was a qualitative assessment. In general, there is not a direct correlation between braid design and physical characteristic (i.e., thickness) of the braid. The thickness measurements are indicative of the layer spacing which would be obtained in a molded laminate. The trends observed from this data indicate that:

a) Tapes which contained higher braid angles resulted in higher laminate densities. This is believed to be a result of "ply nesting" which was observed under microscopic (i.e., metallographic) examination.

TABLE 4

SUMMARY - PHYSICAL PROPERTIES OF
CANDIDATE BRAID DESIGNS AND FLAT LAMINATES

Sample #	Identification	Braid Characteristics Thickness (in) Tubular	Slit	Laminate Characteristics Density g/cc	Fiber Volume %	Fiber Weight %
1.	1/80/45°/Std.	0.030	0.014	2.07	68	82.1
2.	1/80/45°/AW	-	-	2.01	66	82.0
3.	1/80/80°/Std.	0.029	0.016	NOT MOLDED		
4.	1/80/60°/Std.	0.027	0.013	2.11	71	83.8
5.	1/80/30°/AW					
6.	1/80/60°/AW					
7.	1/80/45°/SW	0.043	0.022	2.07	68	81.9
8.	1/80/80°/SW	0.023	0.010	NOT MOLDED		
9.	1/80/60°/SW	0.046	0.015	2.04	67	82.2
10.	1/77/45°/FB	-	0.024			
11.	2/80/45°/Std.	0.058	0.020	1.96	69	87.7
12.	2/80/45°/SW	0.053	0.022	1.96	69	87.7
13.	2/80/45°/AW					
14.	2/80/60°/Std.	0.037	0.016	2.03	70	85.6
15.	2/80/60°/SW	0.040	0.021	2.08	72	85.9
16.	2/80/60°/AW					
17.	2/80/80°/Std.	0.033	0.016	NOT MOLDED		
18.	2/80/80°/SW	0.066	0.029	2.13	73	85.1
19.	2/80/80°/AW					
20.	3/80/45°/Std.	0.091	0.027	2.00	71	88.3
21.	3/80/45°/SW	0.091	0.029	1.97	70	88.5
22.	4/80/45°/Std.	0.131	0.037	1.98	70	88.0
23.	3/80/60°/Std.	0.058	0.023	2.00	70	87.4
24.	3/80/60°/SW	0.061	0.026	1.95	68	86.8
25.	4/80/60°/Std.	0.081	0.027	2.01	71	87.9
26.	3/80/80°/Std.	0.039	0.020	2.14	74	86.5
27.	3/80/80°/SW	0.041	0.019	2.07	71	85.1
28.	4/80/80/Std.	0.046	0.024	2.12	73	85.6
29.	Same as #2					
30.	2/77/45°/FB	-	0.046	2.00	67	83.4
31.	3/77/45°/FB	-	0.050	1.95	68	87.1
S/P*	545					

* Commercial Silica/Phenolic Prepreg.

b) Tapes manufactured by braiding resulted in significantly higher fiber volumes as compared to commercial silica phenolic materials. This trend is qualified in that selected tests for prepreg resin content indicated that the braided tape resin solids content was two-thirds of commercial silica/phenolic prepreg. This would account for some of the difference in fiber volume, but the trend still indicated that braided materials had higher fiber volume.

The results of the braided tapes selected for additional conformability tests are shown in Table 5. As discussed previously, six (6) inch long specimens of prepregged tape were mounted in a universal tensile testing machine. The percent strain (i.e., tape stretch) and percent reduction in tape width were measured on a four (4) inch gage length of the tape. These results should not be construed as quantitative data; however, the data does provide an indication of relative conformability characteristics.

To perform these tests a twenty (20) pound load cell in conjunction with a constant cross-head speed of 0.25 inch/minute was used in an attempt to arbitrarily simulate extreme and severe tapewrapping conditions. The results were taken from the stress/strain curves at a four (4) pound load. It was at this value that approximately 80% of the total strain occurred and it was prior to physical damage to the braid. The conformability for the standard braid designs were similar where equivalent yarn ends were used, but the 45° braid angle material had a lower reduction in tape width. The commercially available silica/phenolic material exhibited a very high reduction in tape width, but this was not unexpected. The sides of a bias-cut tape were

TABLE 5

BRAIDED TAPE CONFORMABILITY TEST RESULTS

Identification	Reduction in Tape Width (%)	Strain @ 4# (%)
1/80/45°/Std.	12.5	5.1
1/80/60°/Std.	57.8	8.1
1/80/45°/SW	25.0	1.2
1/80/80°/SW	37.5	17.9
2/80/45°/Std.	33.0	17.5
2/80/45°/SW	28.5	14.3
2/80/60°/Std.	4.5	2
2/80/60°/SW	44.0	14.5
2/80/80°/SW	9.1	9.7
3/80/45°/Std.	20.8	14.3
3/80/45°/SW	20.8	13.1
4/80/45°/Std.	25.8	15.5
3/80/60°/Std.	32.1	13.9
3/80/60°/SW	32.1	15.6
4/80/60°/Std.	28.1	16.3
3/80/80°/Std.	54.0	4.1
3/80/80°/SW	40.0	38.5
4/80/80°/Std.	27.9	3.2
1/77/45°/FB	-	15.6
2/77/45°/FB	-	8.3
3/77/45°/FB	-	5.6
Silica/Phenolic	68.7	19.0

unrestrained. A specimen of 4/80/45°/STD. was slit and tested for comparison to the bias-cut tape and a similar reduction width of 62% resulted. Width reduction in a tubular braid is not necessarily desirable since it may cause wrinkling or distortion in the tapewrapped structure.

As a result of the braid fabrication and evaluation, the braid design selected for manufacturing technology development was four (4) yarn ends per carrier, using eighty (80) carrier tubular braid design with a 45° braid angle (i.e., 4/80/45°/STD). The design selection was based upon the following:

a) A 4/80/45° braid provided adequate width for subsequent wrapping operations and part fabrication.

b) The selected design exhibited stretch and conformability characteristics similar to commercially available bias-cut silica/phenolic prepreg.

c) The braid design selected was reproducible in terms of manufacturability.

d) High fiber volumes were realized.

e) The braid contained high fiber packing, but it permitted resin impregnation during laboratory prepregging operations.

As a result of the requirements review, glass/phenolic was identified as an acceptable material candidate. The yarn designated for subsequent program tasks was braided E-glass which was fabricated into a 4/80/45°/STD braid design.

3.3 Process and Materials Optimization

The objectives of this task were to develop the prepregging procedures for braided tapes. Laboratory prepregging procedures were established and then transferred to production equipment. The prepregged tapes were then used to fabricate cylinders and flat plates. The information obtained from the manufacturing of the laminates and data generated on their physical properties was used as feedback. Subsequently, the prepregging and/or braid designs were modified as required.

Two goals were established for the braided prepregs. First, property goals defined were a resin solids content of 30% ± 5% and a residual volatile content of 6% ± 3%. These properties are typical of commercially available bias-cut tapes and are discussed in prior sections. Second, the intent of the program was not to develop new tapewrapping procedures and processing methods, but to utilize existing tapewrapping procedures with a braided tape.

To establish the prepreg procedures, an initial quantity (i.e., 42 pounds) of tubular E-glass yarn was obtained and braided. The yarn type used was designated ECG75 1/2, a product of PPG Industries. This yarn has a similar denier to the S-glass yarn which was used for the baseline braiding evaluations. It should be noted that the initial fourty-two pound quantity of E-glass yarn did not contain the desired phenolic compatible finish; instead, it contained a starch-oil finish which is commonly used for weaving glass fabrics. Nine hundred (900) pounds of E-glass yarn was ordered with an epoxy compatible finish; however, this material had not been received at the initiation of this task; therefore, the forty-two pound quantity was used to prevent delays. The E-glass yarn was woven into twenty-five (25) yards of 4/80/45° tubular braid and four hundred (400) yards of 5/80/45° tubular braid.

As previously discussed, a four yarn ends per carrier braid was designated for the baseline design; however, a review of the tape width resulting from the four yarn ends braid design (4/80/45° braid) with twenty degree shingle angle indicated marginal excess material (less than two tenths of an inch) would be available for machining after frusta tapewrapping and curing. At this stage of the manufacturing technology development, the molding characteristics of the braided tapes was not completely understood. Therefore, the 5/80/45° was selected to insure adequate material was available for tapewrapping.

The prepreg parameters, (1) resin solids content, (2) volatiles content and (3) stretch and conformability, were first established using laboratory equipment. This set-up consisted of weighted metering rolls, a resin tank and an air circulating oven for resin staging. Samples of both the 4/80/45° and 5/80/45° braid were processed to establish baseline prepreg properties. Typically, three foot long sections of braid were processed. The braids were all staged at 300°F for four (4) minutes. The average resin solids content and volatiles content were the same for both braid designs (19% and 3.4% respectively). The volatiles content was within the goals established for the prepreg (i.e., 6% $\pm$ 3%), but the resin solids content was significantly lower (i.e., 30% ± 5%); although representative of the prepreg properties obtained on the S-glass material fabricated for the baseline braid evaluation. The low resin solids content was attributed to the incorrect yarn finish previously discussed. Stretch and conformability tests were performed on the prepregged samples using a universal tensile testing machine. The results were nearly identical in terms of percent stretch and reduction in tape width as those previously obtained on the S-glass braids with the same design.

Prior to processing materials in the tapeline facility, (see Figure 11) staging conditions were determined which would result in similar flow properties and volatile contents for laboratory procedures. Translation of the laboratory staging times to tapeline velocities is shown in Table 6.

TABLE 6

Laboratory Staging Translated to FMI Tapeline Facility

Laboratory Oven B-Stage Time (minutes)	Tapeline Velocity (ft/min)
6.5	15
5.5	20
4.5	25
3.5	30

Note: The staging temperature was 300°F

A quantity of short-length (i.e., six foot sections) braids were processed in the tapeline to determine the optimum method of resin impregnation. Since a tubular braid was being used, there were concerns about the ability of the resin to penetrate and coat the interior surfaces of the braid. The initial trials indicated that pre-soaking the braid in phenolic resin in addition to passing the braid through the resin bath resulted in a more homogeneous resin distribution and it also resulted in a resin solids content which approached the established goal.

The tapeline staging conditions were modified as a result of the needed resin soaking cycle, thereby requiring additional trials. Short lengths of braid were used to conserve material. To process short lengths of braid in the tapeline facility, a sacrificial leader was bonded to the leading edge of the short braid section. The tapeline facility requires a minimum of fifty yards of tape to completely fill the staging towers and in production the first and last fifty yards that exits the staging towers is typically

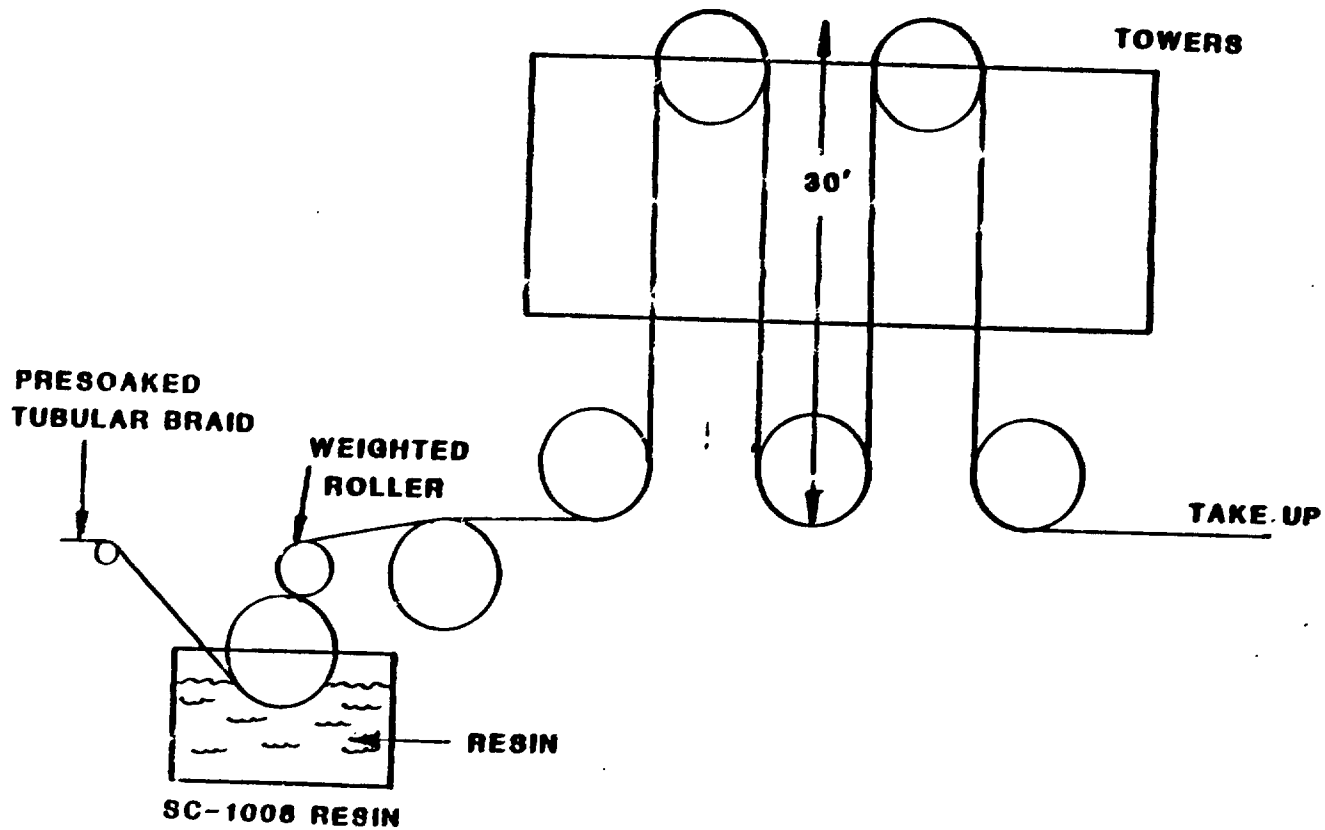

Figure 11. SCHEMATIC OF TAPE LINE FACILITY

discarded. Therefore, sacrificial leader yarns were used as the discarded material.

Results realized from the short length tape line evaluation were two-fold. First, reproducibility of the braided sections was poor. Both resin solids content and volatiles varied from section to section by up to 80%. Second, there was a severe modification to the design of the braided tapes. The braid angle was increased and there was a significant reduction in the width of the tape (i.e., stretching of the tape).

To determine whether the resin soaking cycle and feed mechanisms of the tapeline were contributing to the variations in resin solids and stretching, additional samples were impregnated only in the tapeline then staged under laboratory (i.e., circulating oven) conditions. The results of additional laboratory tests indicated that good resin solids reproducibility within 5% was obtained and stretching did not occur.

A one-hundred twenty (120) yard sample of 5/80/45°/tubular braid was pre-pregged on the tapeline facility in an effort to determine if the inconsistancies were a result of using short braid lengths. The prepreg was divided into three sections containing forty yards each. Ten samples which were equally spaced from each section of prepreg were removed and tested. The results of the tests conducted on these samples are listed in Table 7.

TABLE 7

Prepreg Test Results-120 yd section of 4/80/45°/tubular braid

Locations	% Volatiles Content*	% Resin Solids*
First 30 yds.	2.03	20.0
Middle 30 yds.	1.22	13.9
Last 30 yds.	1.97	15.1

* Average of ten equally spaced samples

It can be seen from the results in Table 7 that significant inconsistencies were still present. In addition, the prepreg properties were not within the property goals established. The major concern, however, was the stretching of the braid during the prepreg process. The 120 yard section had a reduction in width that averaged 18% and increased the braid angle to greater than 60° making it unusable for tapewrapping. The low volatile content indicated that the material was "over-staged" (i.e., the tape was heated to either too high a temperature or for an excessive period of time). The resin solids were also low, but this was not of concern at the time since, as previously discussed, the improper yarn finish provided poor wetting characteristics.

The results of the short and long length braid prepregging trials indicated that the laboratory conditions could not be directly translated to the production (i.e., tapeline facility) equipment. The problem of obtaining the proper volatile content was not of major concern since additional trials could be performed by varying both the temperature and tape velocity through the staging towers. However, of major concern was preventing the stretching of tape since any significant increase in the braid angle rendered the material unusable for subsequent wrapping.

Additional process trials indicated that the stretching of the braid occured as the tape entered and traveled up the staging towers. The two towers are thirty feet each in height and since the braid is being pulled through these towers, the physical weight of the impregnated braid caused the stretching to occur.

Production techniques were devised for eliminating the stretching of the braid. The objective of these plans was to maintain the braid angle as close to 45° as possible. Preliminary attempts consisted of stitching the edge of the tubular braid through its thickness in an attempt to freeze the braid angle. The stitch would be removed after prepregging. The stitch failed to prevent stretching. This approach failed because the stitch itself stretched concurrently with the braid. Warp yarns were also added to the tubular braid in both short and continuous lengths. These yarns prevented stretching only in the section of the tubular braid where they were located. This resulted in a non-uniform cross-section of the tape. Adding more warp yarns could have solved the problem, but these yarns would have to be removed since leaving them in the prepreg would restrict the ability of the tape to conform. This was previously determined in the baseline braid evaluation.

A number of other plans were designed to eliminate the stretching of the braided tapes. These consisted of: braiding tapes with a prepregged yarn, fabricating a new prepreg line; expanding the braid after prepregging; design off-speed rollers to reshape the braid after prepregging; using a flat braid that could be subsequently slit; and lastly, modifying the staging conditions

Braiding with a prepregged yarn required excessive cost. This approach also required significant modification to the braiding equipment consisting of modified tensioning devices and the addition of heated air to the braiding point. This approach was dropped because it mandated significant equipment development.

The fabrication of a horizontal prepreg line was also eliminated for cost and time considerations. However, the use of a horizontal prepreg line was demonstrated. Samples of braided tape were sent to Fiberite, Incorporated of Winona,

Minnesota. They operated a laboratory prepreg line which is horizontal and utilizes a belt to carry, rather than pull, the tape through the staging ovens.

The use of off-speed rollers was eliminated from further consideration because of technical problems and time considerations. The intent of this approach was to fabricate motorized rollers near the exit end of the staging towers. The rollers would operate at different speeds to apply pressure to the tape in an effort to reshape (i.e., change the braid angle to the original woven condition) the braid.

Expanding the braid after prepregging, modifying the staging conditions, and using a flat braided tape were selected and pursued. Expanding the braid over a tapered mandrel was demonstrated in the laboratory. The tubular tape was pulled over to a point which increased the braid width (i.e., thus reducing the braid angle) to a point where it was slit into two separate flat braids. This material demonstrated the ability to stretch and conform to a tapewrapped surface. A tool was therefore designed and built to accomplish the procedure in a production mode. Refer to Figure 12 for the design of the tool.

Fabrication of flat braids which obtained adequate widths for subsequent wrapping presented problems. It should be noted that under the baseline braid design evaluation, a flat braid did not provide the desired stretch and conformability characteristics. However, once the edge of the flat braid is slit after prepregging, it exhibits properties similar to a conventional bias-cut tape. The problem concerning the fabrication of the flat braid was related to the braiding operation. When attempting to fabricate a fine yarn ends per braid carrier into a flat configuration, inconsistent cross-sectional

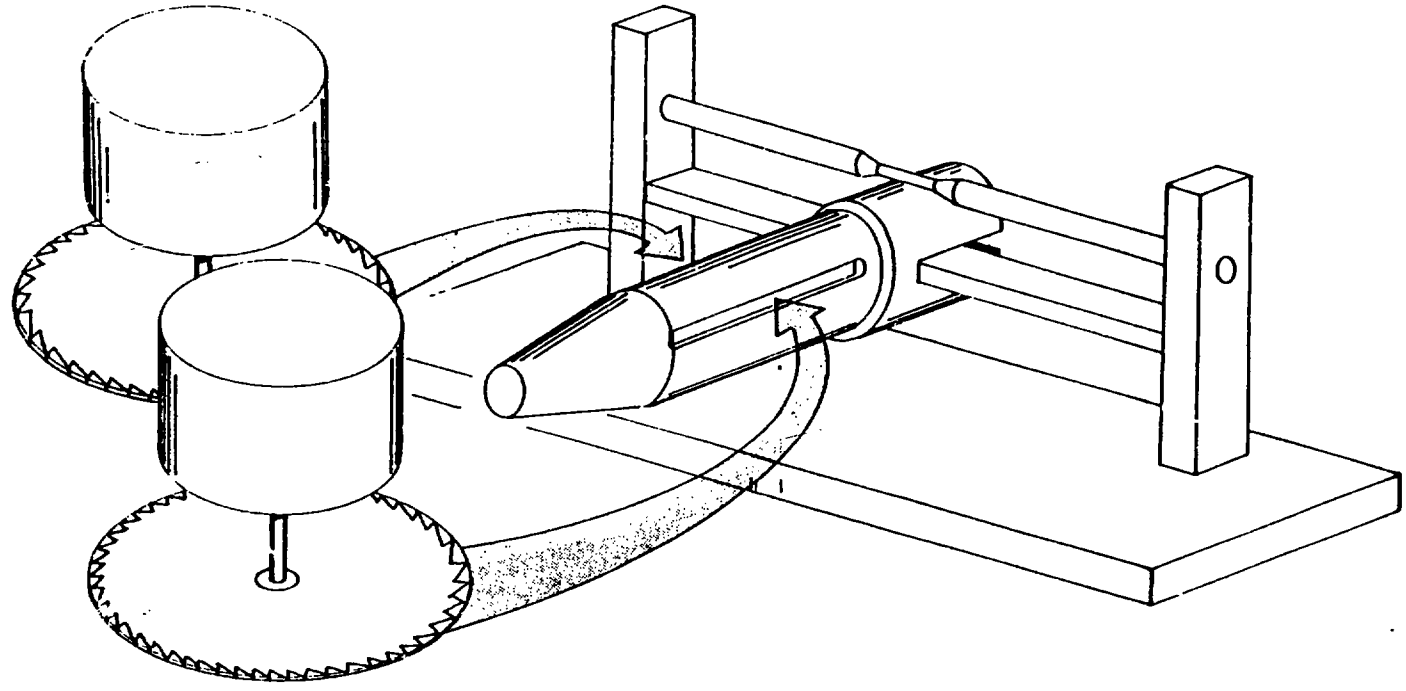

Figure 12. ILLUSTRATION OF BRAID RE-EXPANSION AND SLITTING TOOL

thickness and variation in braid angle was realized. To solve this problem, significant modifications (i.e., replacement of braid carriers) were required. This approach was set aside and the reshaping of the braid, plus modifications of the staging conditions, pursued.

Additional quantities of 5/80/45°/stand and tubular braid were fabricated for evaluation. This braid was manufactured for the same E-glass yarn (i.e., PPG ECG75 1/2); however, an epoxy compatible finish was supplied on the yarn. The braid was divided into lots and subsequently processed through the tape-line facility. The initial runs demonstrated the same problems (i.e., stretching and reduction in width) as previously experienced. It was decided to reduce the staging time, using the rationale that reduced staging would permit the braid to expand to its original shape. The braid "as woven" can be stretched by applying tension; when the tension is released it relaxes to its original shape because of yarn packing characteristics. It is felt that by reducing the staging time the resin would be "soft" enough to permit relaxation of the braid.

Reduced staging time provided positive results. Approximately twenty pounds were initially processed and used for subsequent tapewrapping of a frustum. The tubular tape processed well and tapewrapping of a subscale heatshield was successful. Additional quantities of 5/80/45°/tubular E-glass braid were manufactured. The characteristics of these lots of material are listed in Table 8.

TABLE 8

Properties of E-glass tubular braids prepregged with reduced staging conditions.

FMI Log Indent.	% Resin Solids	% Volatiles	Qty (lbs)	Results
15211	17.37	3.30	15	Rejected
15211A	23.36	4.46	25	Accepted
15222	26.64	6.48	14	Accepted
15222A	21.44	3.32	16	Rejected
15231	21.20	2.17	16	Rejected
15283	24.73	5.16	27	Accepted

Each lot of tape referenced in Table 8 was used to tapewrap a subscale frustum. Acceptance or rejection of the lot was based qualitatively on its conformability and handleability during tapewrapping. All of the tapes listed in Table 8 provided the stretch and conformability required, and rejection was made on the tape's ability to debulk during wrapping or adherence to previous layers. It can be seen that materials which had a low volatile content (i.e., "boardy") were rejected. It should be noted that the pre-soaking time was also increased for all lots subsequent to #15211 in an effort to increase the resin solids content.

Flat laminates were also processed from the acceptable lots of material by stacking layers of tape and molding them in a heated platen press. This operation was performed to identify the maximum density of the material, thus enabling a determination of the debulking properties of the material during tapewrapping. The average laminate density achieved was 2.07 gm/cc. The tapewrapping frusta were wrapped and cured in the "as wrapped" condition (i.e., without any external pressure) and subsequently machined. The average resulting density was 1.86 g/cc. This figure was well within the debulking ability of conventional bias-cut materials which typically average 80%-90%.

Additional prepreg trials were conducted and modifications to the process were made. The properties of Lot #15283 (refer to Table 8) were established as baseline properties. Modifications made to the prepregging process consisted of the addition of a cooling box located at the exit of the staging towers and permitting the staging towers to preheat for thirty (30) minutes minimum prior to the processing of the braid. Also, the motorized take-up reel located after the staging tower was eliminated. These modifications were instigated as a result of the first additional trial run (Lot #15221). This trial resulted in

a tape which was significantly understaged and had a 20% reduction in tape width. The understaged condition (i.e., wet condition of the prepreg) was caused by not allowing the prepreg towers to reach steady-state conditions. The stretching of the tape was attributed to the motorized take-up equipment coupled with the understaged prepreg. The take-up equipment applied an axial load to the prepreg causing it to stretch. The motorized equipment was replaced with a container where the prepreg was subsequently spooled after it had cooled to room temperature.

An additional quantity of approximately 700 yards of E-glass tubular braid was fabricated for verifying prepreg process parameters. The tubular braid was 5/80/45°/standard tubular braid using ECG-75 1/2 glass yarn. The 700 yards was divided into lots and prepregged. All the lots were soaked in SC1008 phenolic resin for a minimum of thirty minutes prior to entering the tapeline equipment. The braided tape was staged for 5.1 minutes at 300°F which relates to a tape velocity through the towers of 21 feet/minute. The properties of the resulting prepreg tapes are shown in Table 9.

TABLE 9

Properties of Braided, Prepreg Tapes - Tubular Braid
5/80/45° Standard-Monsanto SC1008 Phenolic Resin

Lot No.	Volatiles(%)	Resin Solids(%)	Tape Width*	Quantity(yds)
15321	6.03	22.7	1.0	20
15322	3.54	21.4	1.1	115
15323	5.67	21.9	1.1	169
15324	4.65	20.1	1.1	223
15325	5.46	22.1	1.1	188

*Width is measured as the diameter of the tubular braid.

All lots of prepreg were accepted except for lot number 15321, which as previously discussed was understaged and had been stretched. The remaining lots (i.e., 15322, 15323, 15324, 15325) were similar in properties to the

previously accepted lots which were used for wrapping subscale frusta (i.e., lot 15283).

A quantity of prepreg from lot 15324 was removed for determining shelf life properties of the prepreg. This material was sealed in a low permeable polymeric film and stored at 15°F in a freezer. At one month intervals, samples were removed and tested for volatile content, resin solids, and flow properties. The results of these tests are listed in Table 10. It appears from these results that the minimum shelf life of the braid when properly stored (i.e., below 20°F) was six months.

TABLE 10

Shelf Life Characteristics of Braided Prepreg Tape
Lot 15323, Stored at 15°F

Property	MONTHS 1	2	3	4	5
% Volatiles	5.67	3.75	4.11	4.31	4.76
% Resin Solids	21.9	22.2	21.2	21.6	21.8
% Total Flow	16.2	15.1	13.4	17.4	16.3
Laminate Thickness (in)	0.026	0.025	0.025	0.025	0.025

Physical properties of the subscale frustum wrapped from lot 15383 were determined to evaluate its (i.e., frustum) uniformity. The frustum was sectioned at 90° intervals and test coupons were removed for determining the physical parameters. The resulting properties are listed in Table 11.

TABLE 11

Physical Laminate Properties of Frustum Wrapped with Tubular E-Glass Prepreg, Lot 15283

	Specimen Location							
	0° FWD	0° AFT	90° AFT	90° AFT	180° FWD	180° FWD	270° AFT	270° AFT
Bulk Density (g/cc)	1.84	1.85	1.79	1.83	1.76	1.78	1.84	1.83
Apparent Density (g/cc)	2.04	2.02	2.05	2.04	2.04	2.04	2.05	2.03
Residual Volatiles*(%)	0.17	0.17	0.12	0.12	0.13	0.12	0.16	0.10
Resin Content *(Wt %)	22.4	23.7	21.2	22.5	19.6	23.4	21.9	22.8

* Residual Volatiles determined at 320°F for 9 minutes.
Resin Content determined at 1050°F for 3 hours.

Considering the molding technique used to cure the frustum (i.e., no external pressure, oven cured at free-standing position on the wrap mandrel) the physical properties were uniform.

Flat laminates were fabricated from the additional prepreg trials (i.e., lots 15322 through 15325) to enable machining of test specimens (i.e., thermal/mechanical, ablation, erosion specimens) and to enable an evaluation of the physical properties of the laminates to verify the reproducibility of the prepreg. A total of sevel laminates were fabricated; one from each spool of prepreg. Each laminate consisted of 82 plys (41 tubular braids) and was molded at 300 psi and 325°F for one hour minimum. The physical properties of the flat laminates are listed in Table 12.

TABLE 12

Physical Properties of Flat Laminates Fabricated From Braided Prepreg

Laminate Ident.	Tape Lot #	Thickness (in)	Ply Thickness (in)	Density (g/cc)	Flash Flow (%)
15326	15325(A)	2.17	0.027	2.07	9.9
15327	15325(B)	2.09	0.026	2.14	6.9
15328	15322	2.09	0.026	2.10	5.3
15329	15324(A)	2.14	0.026	2.10	8.7
153210	15323(A)	2.08	0.025	2.19	9.1
153211	15324(B)	2.17	0.026	2.15	6.8
153212	15323(B)	2.10	0.026	2.09	10.5

A frustum was also fabricated from each lot of prepreg tape. (i.e., lots 15322 through 15325) to evaluate the reproducibility of the material. The results obtained from the flat laminates listed in Table 12 indicated that improved consistency was required. The molding conditions were also evaluated during additional fabrication trials to determine the minimum pressure required to obtain maximum density and minimum ply layer spacing. Pressures between 15 psi to 300 psi were evaluated. It was determined that pressures greater than 55 psi provided adequate compaction to obtain consistent high density and minimum ply spacing.

The causes for inconsistency of laminate properties were attributed to lower than desired resin content coupled with excess flow during the laminate molding of flat laminates and autoclave curing of subscale frusta. The excess resin flow was more noticeable in the flat laminates; it was not totally unexpected because of the low staging condition of the prepreg. The high resin flow characteristics of the prepreg could easily be controlled by altering the curing cycle (i.e., variations in the time-temperature-pressure

cycle can be modified to accomplish additional staging during molding). However, it was felt that the variation and low degree of the prepreg's resin solids content caused inconsistancy.

Efforts to increase the resin content of the prepreg consisted of using grooved rollers during impregnation, addition of silica filler to the resin, and increasing the solids content in the resin system.

Grooved prepreg rollers were fabricated for evaluation. Typically, the rollers used during prepregging were flat and tended to squeeze resin from the tape. The grooved rollers contained slots which were approximately 0.050" deep and spaced on a 0.100" centers. These slots left excess resin on the tape as it entered the staging towers. To increase the viscosity of the resin, powdered silica was added to the resin system. The resin solids content was increased to 75% by vacuum evaporating the alcohol solvent (i.e., typically SC1008 phenolic resin is supplied with a 50% resin solids content in alcohol).

All these approaches provided only marginal increases in resin content of the prepreg. At this point, the finish on the glass yarn became suspect. To determine whether the prepreg process methods were causing the low solids content, a sample of silica braid was fabricated and prepregged. A resin solids content of 32%-36% was achieved which is comparable to commercially available material. This also indicated that the prepreg procedures and process methods were acceptable. Further analysis of the glass fibers used to fabricate the tubular braids showed that residual starch oil was present. As previously discussed, a large quantity of E-glass yarn ordered from PPG Industries contained an epoxy compatible finish which could also be used with phenolic resin. The identification of the finish is proprietary to PPG; however, further inquiry revealed that starch-oil was also present in the epoxy compatible finish to improve handling and weaving characteristics.

Subsequently, additional lots of tubular 5/80/45°/standard braid were fabricated. A procedure was outlined using a mild caustic solution to wash the residual starch-oil finish off the yarn. However, it was at this point in the program that technical redirection was given by MICOM to develop the braiding technology using rubber-modified-silica-phenolic material (RMSP). This will be discussed further in the next section of this report.

As a result of the program redirection, further efforts using glass/phenolic were terminated. However, the groundwork for the manufacturing technology was successfully demonstrated using glass reinforced tubular braids.which enabled a determination of the manufacturing and process procedures which were directly applied to the RMSP material.

4.0 MANUFACTURING TECHNOLOGY DEMONSTRATION USING RMSP

The braided heatshield program was redirected to develop the manufacturing technology of heatshield materials using braided rubber-modified-silica-phenolic (RMSP). The program was redirected as a result of coordination meetings with representatives of system contractors and the COTR plus the anticipated costs required to establish the baseline data for an unproven heatshield material. Coordination meetings were held at Martin Marietta Aerospace Division to brief cognizant personnel of the braided technology development. There were significant objections to the selection of glass phenolic material due to the lack of a material data base. Also, the specific gravity of glass phenolic is higher than the currently used material (i.e., RMSP) resulting in an increased weight penalty. A significant data base was previously demonstrated with RMSP and personnel at these meetings felt that glass phenolic could not survive the mission requirements, specifically the heating environment.

As discussed in the first section of this report, the intent of this program to demonstrate the braided tape technology with the objective of applying the results towards a current or future U.S. Army system. For these reasons, the selection of RMSP was warranted.

The selection of RMSP required reiteration of selected development tasks previously performed with glass phenolic. Specifically, techniques for obtaining a braided silica material required development. The following section discusses the demonstration phase of the program using braided RMSP.

4.1 Silica Braid Development

Two (2) approaches were selected for obtaining a braided silica. The first method consisted of directly braiding a silica yarn. It should be noted, however, that silica yarn was available in limited forms. Silica yarn was available as bo

cordage and yarn from HITCO of Gardena, California. The cordage was available in either 0.040" or 0.053" diameter with corresponding yields of 700 yds/lb and 330 yds/lb respectively. This material was significantly larger than desired and the resulting braid would contain a high ply thickness. The high tape thickness and weight resulting from braided cordage would be difficult to handle and use for tapewrapping. One (1) yarn form of silica was also available which had a nominal diameter of 0.020" and a yield of 3280 yds/lb. This yarn was similar in size to the ECG75 1/2 glass yarn previously used.

A forty (40) pound quantity of silica yarn was purchased for braiding trials. The yarn was HITCO's product code FYT 100-Z. Plans were to fabricate both a tubular and flat braid for comparison to braids fabricated from glass. The braid designs selected were a 4/80/45° standard tubular and a 4/77/45° flat braid.

Initial braiding trials showed that the silica yarn was extremely fragile and and not adaptable to high-speed commercial braiding equipment. Modifications were required to the eighty (80) carrier braiding machine to enable handling of silica yarn. These consisted of speed control and rebuilding of the carrier tensioning devices. Tubular braids were successfully fabricated on a sixteen (16) carrier braiding machine which contained carrier speed control and proper tension devices. The approach of directly braiding silica yarn was put on hold pending the results of the alternate approach to obtain a braided silica tape. It should be noted that the cost of silica yarn is high (>$40.00/lb) when compared to the cost of commercially available "MSE" tapes (i.e., $17.00-25.00 per pound). The cost of a prepregged silica tape by directly braiding the yarn was estimated to be $50.00 to $55.00 a pound which is more than twice the cost of the commercially available material. The direct braiding of silica yarn was put on hold for this reason

also.

The second approach to obtain a silica consisted of braiding E-glass yarn and subsequently leaching the glass into silica. The leaching process is basically a hot acid washing and heat treating process where impurities in the glass are dissolved and washed away thus increasing the level of silica content in the yarns. This process is used by HITCO to manufacture Refrasil™ yarn and cordage. During the leaching process significant yarn shrinkage occurs (i.e., approximately 20%). Braided E-glass designs were selected to evaluate the effects of the leaching process on the final braid designs. A total of six (6) samples, each containing 100 feet, were fabricated for leaching evaluation. The braids consisted of both flat and tubular braids using five (5) and four (4) yarn ends per carrier of ECG75 1/2 glass yarn using seventy-seven (77) and eighty (80) carriers respectively. A summary of the braid designs fabricated for leaching trials is shown in Table 13.

TABLE 13

CANDIDATE E-GLASS BRAID DESIGNS
FABRICATED FOR LEACHING TRIALS

Flat Braids	Width(in)	Braid Angle(θ°)	Packing(Plaits/in)
Sample #1	2.2	53	11
Sample #2	2.5	55	9
Sample #3	2.5	59	8
Tubular Braids			
Sample #1	1.2	48	13
Sample #2	1.5	58	18
Sample #3	1.1	42	16

As shown in Table 13, the packing of the braids was varied to enable a determination of the effects of the leaching process. It should be noted that the flat braids obtained in Table 13 were selected after numerous attempts to fabricate a high quality tape.

Refrasil - Trade Mark HITCO

Many problems were encountered during the preliminary fabrication of the flat braids which were related to non-uniformity of the braid angle. In many instances the braid angle varied from 30° at the edge of the tape to approximately 60° at the center. The problem was attributed to variation in yarn tension applied by the braid carrier. As a result, the tensioning springs and yarn guides were replaced on all seventy-seven (77) carriers.

The six (6) candidate braid designs were processed into silica at HITCO. The changes to the physical properties of the braids are listed in Table 14.

TABLE 14

Physical Properties of Tubular and Flat E-Glass Braids Before And After Leaching

Flat Braids	Width (inch)	Braid Angle (0°)	Packing (Plaits/in)
Sample #1 Glass	2.2	53	11
Silica	1.8	58	11
Sample #2 Glass	2.5	55	9
Silica	2.0	60	10
Sample #3 Glass	2.5	59	8
Silica	2.0	62	9
Tubular Braids			
Sample #1 Glass	1.2	48	13
Silica	1.0	56	15
Sample #2 Glass	1.5	58	8
Silica	1.0	68	8
Sample #3 Glass	1.1	42	16
Silica	1.0	49	18

Tubular braids Sample #2 and Sample #3 were unacceptable for subsequent tapewrapping or prepregging. Tubular braid Sample #3 contained maximum yarn packing which was increased by the leaching process. The resulting tape had negligable ability to stretch and conform to a wrap mandrel surface. Tubular braid Sample #2 contained minimal packing. During leaching the braid angle increased to an unacceptable level where it approached properties similar to a straight tape. It can be seen from reviewing Table 14 that flat braids were less

susceptable to braid angle and packing variations resulting from the leaching process. While a direct comparison or trend was not evident, there was evidence that flat braids were more adaptable to the leaching process, the major difference being the change in braid angle. It was hypothesized that the tubular braid was more restricted, thus limiting the ability of the tubular braid to change diameter during leaching. Therefore, as shrinkage occured during heat treatment, the braid angle increased significantly. The highest packed flat braid (i.e., flat braid Sample #1) exhibited the smallest changes in physical properties as a result of the leaching process. The braid angle increased during leaching to 58° from 53°; however, as determined in the baseline fabrication studies, braided tapes with angles less than 60° had conformability properties similar to bias-cut tapes. As a result of the braiding trials, two (2) designs were selected for prepregging evaluation. These were both Samples #1 of the tubular and flat braids.

Prepreg trials using the tubular braid indicated that it could not be used with the elastomeric modified phenolic resin. The rubber-modified-phenolic resin (RMP) had a very high viscosity and poor wetting characteristics. The RMP resin was supplied as a 15% solids solution by Fiberite, Inc. of Winona, Minnesota in a methyl ethyl ketone (MEK) solvent. The rapid volatization of the MEK, high viscosity nature of the resin and poor wetting characteristics prevented the RMP from penetrating the interior surface of the tubular braid. Process methods were attempted to penetrate the center of the braid. These consisted of pressure impregnation, resin soaking and repeat impregnations, but limited impregnation of the interior surfaces of the tubular braid occurred. A final approach consisted of first impregnating the braid in a tubular shape, followed by slitting, and then two (2) additional resin impregnations on the slit tubular braid. This approach was successful in that a 26% resin solids content was obtained; but the slitting of the tubular braid required an additional operation. The resin solids content achieved as a result of this approach is shown in Table 15.

TABLE 15

Resin Pick-Up of Tubular and Slit Tubular
Silica Braid Using RMP Resin as Impregnant

Tubular braid initial impregnation	-	8.36% resin solids
Slit tubular braid, second impregnation	-	18.37% resin solids
Slit tubular braid, third impregnation	-	25.60% resin solids

Similar results were obtained using the flat silica braids, however, the slitting operation was not required.

A secondary problem that was determined using the RMP resin was rapid volatilization of the MEK solvent. Plans called for the use of FMI's tapeline facility for the prepregging of the silica braid. However, the tapeline facility did not contain the necessary equipment to accommodate the large quantities of highly flammable solvent (i.e., MEK) which would be released when processing production quantities of braid. Thus, Fiberite was selected for prepregging the production quantity of material.

As a result of the braiding, leaching and prepregging trials, a flat E-glass braid was selected for demonstrating the manufacturing technology. The braid design established for the production quantity of braid is shown in Table 16.

TABLE 16

SELECTED E-GLASS BRAID DESIGN

Configuration	=	Flat
Yarn Ends	=	5 yarns ECG75 1/2 per carrier
Machine Carriers	=	77
Tape Width	=	2.2" to 2.4"
Packing	=	11-14 plaits/inch
Braid Angle	=	47° to 52°
Braid Angle Variations	=	35° to 57° maximum

4.2 Braided Tape Manufacturing Demonstration

Production quantities of flat braided tape were fabricated from E-glass. The flat braid design was selected because of the following; 1) A flat braid was required for use with the RMP resin because of its high viscosity and poor wetting characteristics; 2) The use of a flat braid eliminated the slitting operation required to successfully prepreg a tubular braid design; 3) The flat braids were more adaptable to the leaching process in that they were less restricted and there was less variation in the physical properties of the flat braids, 4) Flat braids demonstrated better control and reproducibility of physical properties because they had less tendancy to distort or stretch during leaching and prepregging.

A total of 1885 yards of flat braid was manufactured into seven (7) each spools. Each spool contained approximately 800 feet of continuous (i.e., splice less) braid. The flat braid was manufactureed in accordance to the braid design identified in Table 16. Each spool was subsequently inspected for design conformance by conducting physical measurements on the braid.

The quantity of braid fabricated was based on material allocations for demonstration and test hardware. It was determined that 100 feet of prepregged tape was required for fabrication of flat panels, 1500 feet for subscale cylinder 3300 feet for subscale frusta and 750 feet for supply to MICOM. The flat panels and cylinders were used for removal of test coupons and the subscale frusta were for demonstration hardware.

A test and evaluation plan was developed and submitted to MICOM. Testing consisted of mechanical, thermal, ablative and erosion evaluation. The mechanical tests consisted of axial tension and flexure at room temperature and 500°F. Thermal tests consisted of hoop expansion and thermal conductivity in the radial direction from room temperature to 500°F. Ablation testing

consisted of evaluating the material response to heat flux levels ranging between 420 Btu/Ft^2-sec to 880 Btu/Ft^2-sec at corresponding surface pressures of seven (7) to fifteen (15) atmospheres. Erosion testing consisted of determining material response to single particle impact using one (1) millimeter diameter glass beads launched at 8000 ft/sec.

Flat panels were needed for obtaining the erosion, ablation, and radial thermal conductivity specimens. The mechanical and hoop expansion test specimens were removed from tapewrapped cylinders. A detailed discussion of the material test and evaluation is presented in the subsequent section of this report.

The seven (7) spools of flat braided E-glass tape were forwarded to HITCO for leaching into silica. Problems arose at HITCO when attempting to process large quantities of flat braid in that residual acid was present on the tape during firing (i.e., heat treating). The residual acid caused severe local fiber damage where present. The incomplete acid removal was caused by the inability of the water rinsing process to penetrate the large spools. It was determined that maximum 50 foot lengths of glass braid could be successfully processed. Therefore, the remainder of the seven (7) each spools containing 800 feet each were sectioned into 50 foot spools and batch processed. A total of ninety-four (94) spools containing a minimum of fifty (50) continuous feet each were successfully leached. Table 17 lists the physical properties of the flat braided silica tapes after leaching.

It can be seen from Table 17 that changes to the flat braid as a result of the leaching process, were within the desired design parameters established. However, stretching of the braid did occur as indicated by the increase in braid angle and reduction in tape width. The silica tapes were very near to the upper limits in terms of braid angle and packing, but they still contained adequate stretch and conformability for tapewrapping.

TABLE 17

Physical Properties of Silica Tapes Manufactured By Acid Leaching of E-Glass

FMI Roll Ident.	50ft. Rolls Processed	Weight (lbs)	Length (yds)	Tape Width(in)	Packing Plaits/in)	Braid Angle (θ°)Min/Max
1	14	20.2	270	1.9	13.5	53/55
2	15	22.1	290	2.0	13.5	50/57
3	13	18.8	250	2.0	13.5	53/55
4	13	18.8	250	1.9	13.5	53/58
5	14	19.3	254	1.9	14.0	52/56
6	14	19.2	254	2.0	14.0	54/55
7	11	15.5	204	1.8	13.5	56/57

The ninety-four (94) spools of flat silica braid were prepregged at Fiberite, Inc. The rationale for selection of a vendor to perform this process has been discussed previously. Fiberite prepregged the silica tapes in accordance with the Material Specification for Impregnated Cloths and Tapes; MIS 22123. Fiberite uses a conveyer belt that carries the tape through the impregnation and staging ovens. In this manner, the tape is not pulled through, which could result in additional stretching of the tape.

A two (2) step procedure was used to prepreg the flat braided silica tape. The initial impregnation used a 15% resin solids solution followed by a 30% resin solids impregnation. Staging, which basically consisted of driving off the MEK solvent, was performed between impregnations. The two (2) step impregnation procedure was used because of the poor penetration properties of the RMP resin. The RMP resin has more of a tendancy to coat the fiber bundles rather than infiltrate them.

After prepregging, the edges of the braid were slit to the desired tape width. Three (3) different tape widths were required to fabricate test and

demonstration hardware. For fabricating tapewrapped cylinders, a 1.65" wide tape was required to obtain the desired wall thickness. Subscale frusta and flat laminates required a 1.4" wide tape and material supplied to MICOM was 0.75" wide.

After prepregging, the properties were measured. The resin solids content and volatiles content of selected spools of braid are listed in Table 18.

The average resin content of all the prepregged spools measured was 27.4% with an average volatile content of 6.7%. The resin content was within the desired property goals established early in the program (i.e., 30% ± 5%) as was volatiles content (i.e., 6% ± 3%). The prepreg process caused additional stretching of the tape and tensioning tests performed on the prepreg indicated only 10% elongation. These tests were performed by placing a one (1) pound weight at the end of the prepreg with the opposite end fixed. A heat gun was used on the gage section of the tape and percent elongation was determined.

The additional stretching of the tape was attributed to weight of the tape and resin mixture as it exited the resin bath just prior to the conveyor belt which carries it through the staging ovens. Also, the RMP resin shrinks considerably as the MEK solvent is driven off causing additional tape shrinkage (i.e., increase in braid angle).

There was concern of the tape's ability to conform during tapewrapping; however, as discussed in the following section the material was successfully wrapped.

4.3 Fabrication of Tapewrapped Cylinders and Frusta

Plans called for the fabrication of a flat laminate plus tapewrapped cylinders and frusta. A flat laminate was fabricated by hand lay-up techniques. A molding tool was fabricated to provide a finished 8"x12"x1/2" thick laminate.

TABLE 18

Prepreg Properties of RMP/Flat Silica Braided Tape

Roll No.	Resin Solids (%)	Volatiles (%)	Weight (lbs)
1.40" Wide tape (57 rolls)			
7	27.4	7.1	1.56
9	27.1	7.0	1.73
13	28.3	5.7	1.75
29	26.4	5.9	1.59
31	30.2	7.9	1.68
33	27.7	7.1	1.68
47	24.2	7.3	1.45
48	27.6	5.7	1.47
55	26.0	5.4	1.48
56	28.0	6.3	1.45
59	31.6	8.0	1.89
61	28.7	7.9	1.55
63	32.0	8.2	1.50
69	24.4	7.5	1.59
1.65" Wide Tape (26 rolls)			
5	27.2	7.1	1.79
6	28.1	7.0	1.77
14	28.8	6.1	1.68
51	26.4	4.5	1.73
52	28.3	4.6	1.74
79	25.7	7.6	1.70
81	25.0	7.7	1.76
82	25.4	6.8	1.75
0.75" Wide Tape (12 rolls)			
27	29.3	6.5	1.58
94	25.2	5.9	1.23

A sketch of the tool is shown in Figure 13. Strips of 1.65" wide prepreg were cut and stacked against the 20° starting ramp of the tool. This approach was used to simulate a tapewrapped material since the specimen geometries required for testing could not be machined from either a cylinder or frustum configuration. The entire assembly was then enclosed within a vacuum bag for autoclave curing. A minimum vacuum of 25" Hg was maintained on the vacuum bag and the laminate was cured under 500 psi pressure at 320°F for two (2) hours.

After molding, the plate was machined square and inspected. Test specimens as identified in Figure 14 were removed for test and evaluation. Each individual specimen was radiographed to insure that there were no delaminations or foreign inclusions. The resulting specimen data is listed in Table 19. The specimen data indicated that very uniform properties were obtained in that variation in specimen densities were minimal. However, it can be seen that the density level is low when compared to commercial RMSP.

Two (2) cylinders were fabricated using the 1.65" wide tape. A right-hand helix was used to wrap each cylinder. A steel wrap mandrel,(see Figure 15) was used which provided a nominal twenty (20) degree shingle angle and a laminate which was 7.8" inside diameter by 12" high with a 1/2" wall thickness. After wrapping each cylinder the assembly was removed from the wrap lathe and machined. The outside diameter surface was machined using single point tooling to provide a uniform surface for autoclave curing. After machining, a vacuum bag assembly was placed over the mandrel and sealed. The cylinders were cured at 500 psi and 320°F for two (2) hours while maintaining a minimum 25" Hg vacuum. The cylinders were then removed from the wrap mandrel and both interior and exterior surfaces were

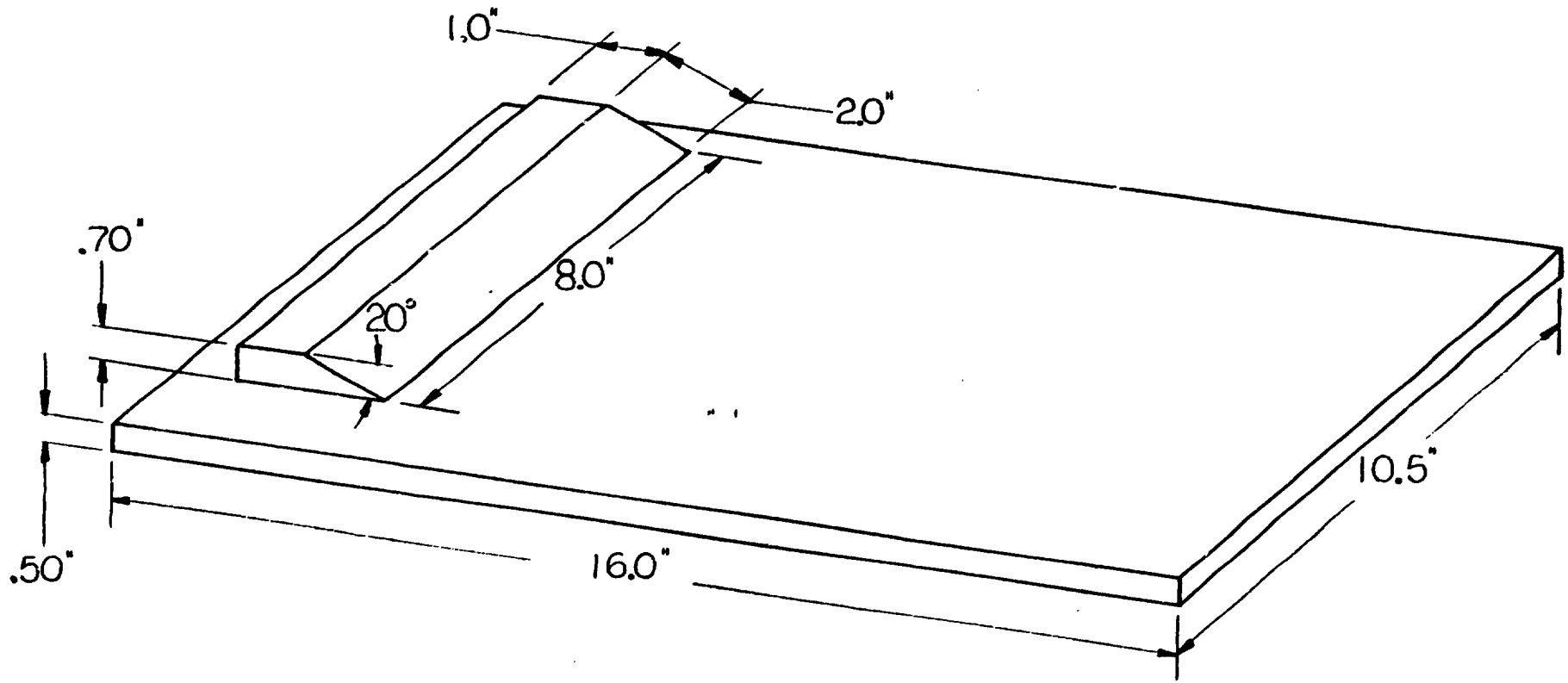

FIGURE 13. FLAT LAMINATE LAY-UP TOOL

Figure 14

CUTTING PLAN FOR MOLDED FLAT LAMINATE

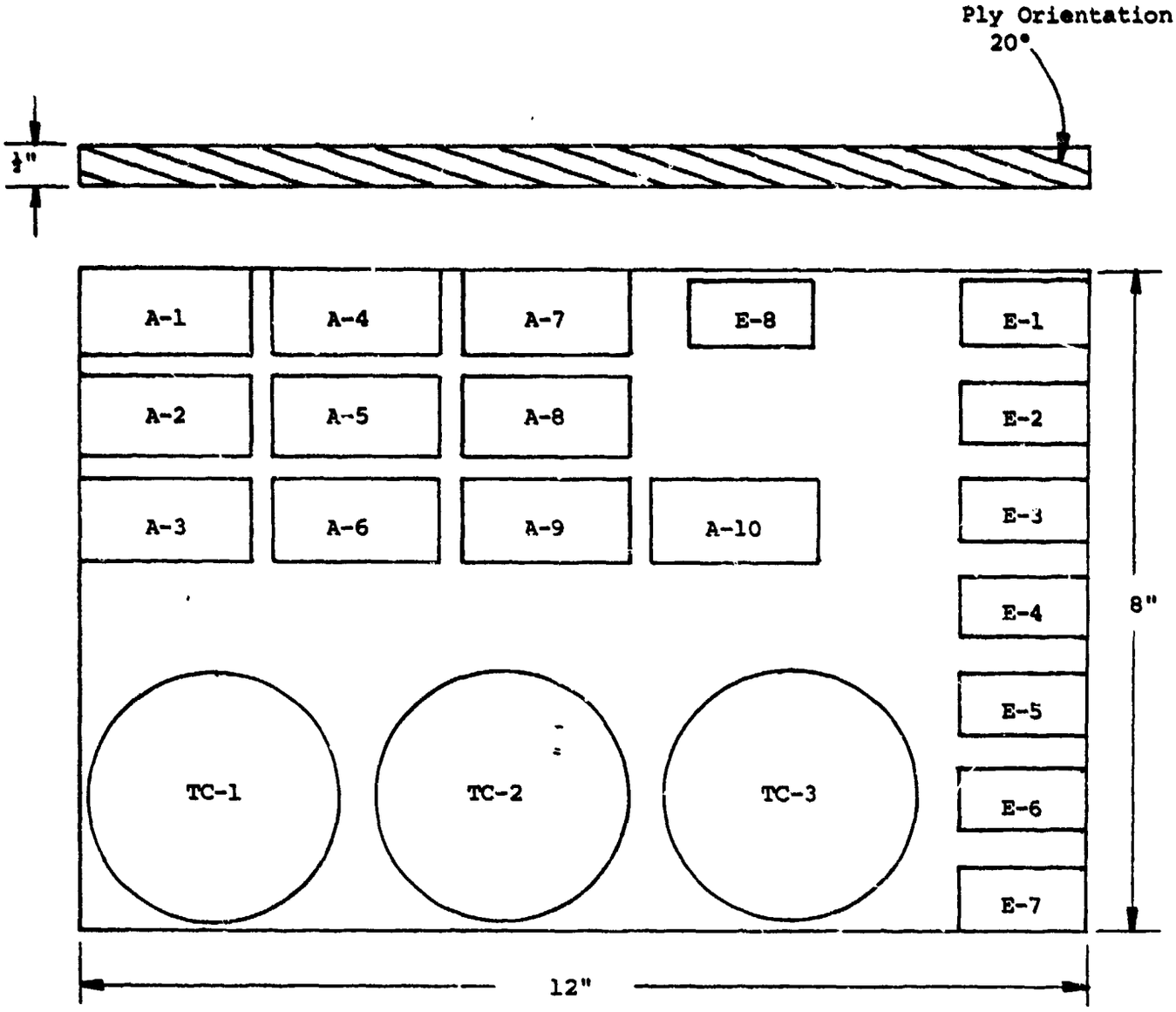

	No.	Lgth.	Width	Thick.
Tolerance	-	+ .010 - .000	+.005 -.000	+.005 -.000
Ablation	10	2.000"	1.000"	.500"
Erosion	8	1.500"	.750"	.500"
Thermal Cond.	3	3.000"D	-	.500"

A = Ablation Specimen

E = Erosion Specimen

TC = Radial Thermal Conductivity Specimen

TABLE 19

Flat Plate Specimen Data - 20° Lay-up Angle
Braided RMSP Tape

ID	Weight (gms)	Dimensions (inches)			Specific Gravity (g/cc)
TC-1	85.02	3006 dia x 0.503 thick			1.46
TC-2	85.26	"	"		1.46
TC-3	85.17	"	"		1.46
		Length	Width	Thickness	
E1	12.13	1.431	0.704	0.503	1.46
E2	12.13	1.433	0.704	0.503	1.46
E3	12.62	1.433	0.733	0.505	1.45
E4	12.21	1.436	0.703	0.504	1.46
E5	12.11	1.431	0.702	0.503	1.46
E6	12.11	1.431	0.702	0.503	1.46
E7	12.17	1.433	0.703	0.504	1.46
E8	12.60	1.506	0.698	0.502	1.45
A1	24.04	2.006	1.005	0.500	1.45
A2	24.14	2.006	1.004	0.502	1.45
A3	23.98	2.006	1.004	0.500	1.45
A4	24.20	2.006	1.004	0.502	1.46
A5	24.16	2.006	1.003	0.505	1.46
A6	24.13	2.006	1.004	0.502	1.45
A7	24.30	2.006	1.004	0.505	1.46
A8	24.11	2.006	1.005	0.502	1.45
A9	24.13	2.007	1.004	0.501	1.46
A10	24.10	2.006	1.005	0.503	1.45

Key

A = Ablation Specimen (wedge type)
E = Particle Impact Specimen
TC = Radial Thermal Conductivity Specimen

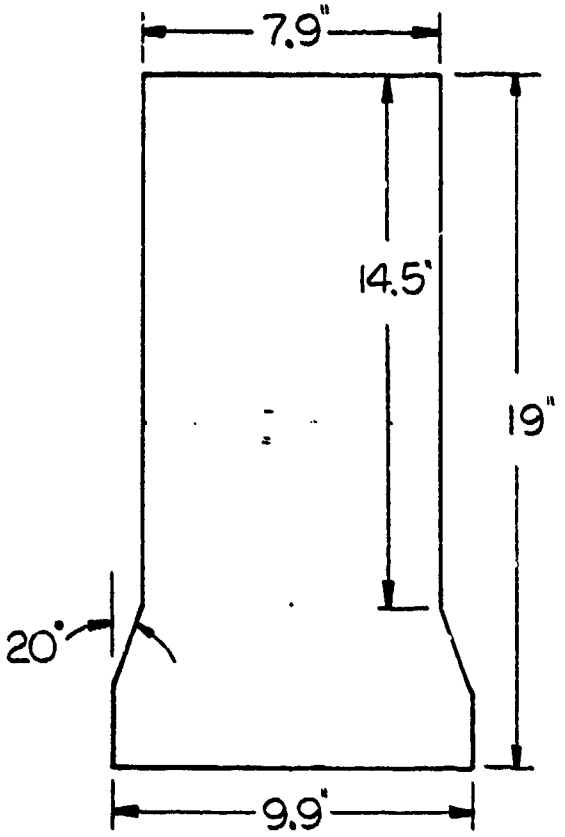

FIGURE 15. SCHAMETIC OF STEEL CYLINDER WRAPPING MANDREL

surface ground. Test specimens consisting of hoop thermal expansion, axial tension and axial flexure were machined from the cylinders. The specimens reomved from the tapewrapped cylinders are shown in Figure 16.

The subscale frusta for demonstration hardware were manufactured similar to the cylinders. The frustum configuration selected for demonstration was 18.7" major inside diameter, 15° half angle, 20" long with a wall thickness of 0.250". A wrap mandrel was designed and fabricated to provide a twenty (20) degree shingle angle and the part configuration identified. A sketch of the wrap mandrel is illustrated in Figure 17. A 1.4" wide braided RMSP tape was used to fabricate the frusta. Like the cylinders, a right-hand wrap helix was used. No problems were experienced wrapping the part even at the forward end where the wrap ratio increases. The frusta where cured at 500 psi and 320°F for two and one-half (2½) hours. After curing the frusta were machined to the desired wall thickness and forwarded to MICOM.

A tag ring was removed from the forward and aft end of the frustum to evaluate part uniformity and measure physical properties. The results of these tests are listed in Table 20.

TABLE 20

Tapewrapped RMSP Frustum - Tag Ring Properties

Test	FWD Ring	AFT Ring
Residual Volatiles (%)	1.90	1.80
	1.81	1.89
	1.87	1.82
	Avg. = 1.86	Avg. = 1.84
Resin Solids (wt %)	24.8	26.2
	24.9	25.9
	25.0	26.3
	Avg. = 24.9	Avg. 26.1
Specific (gravity (g/cc))	1.47	1.47
Apparent Density	1.57	1.54

*Note: Three specimens were removed at 120° segments on the tag rings.

FIGURE 16

TAPEWRAPPED CYLINDER CUTTING DIAGRAM

EXPANDED VIEW

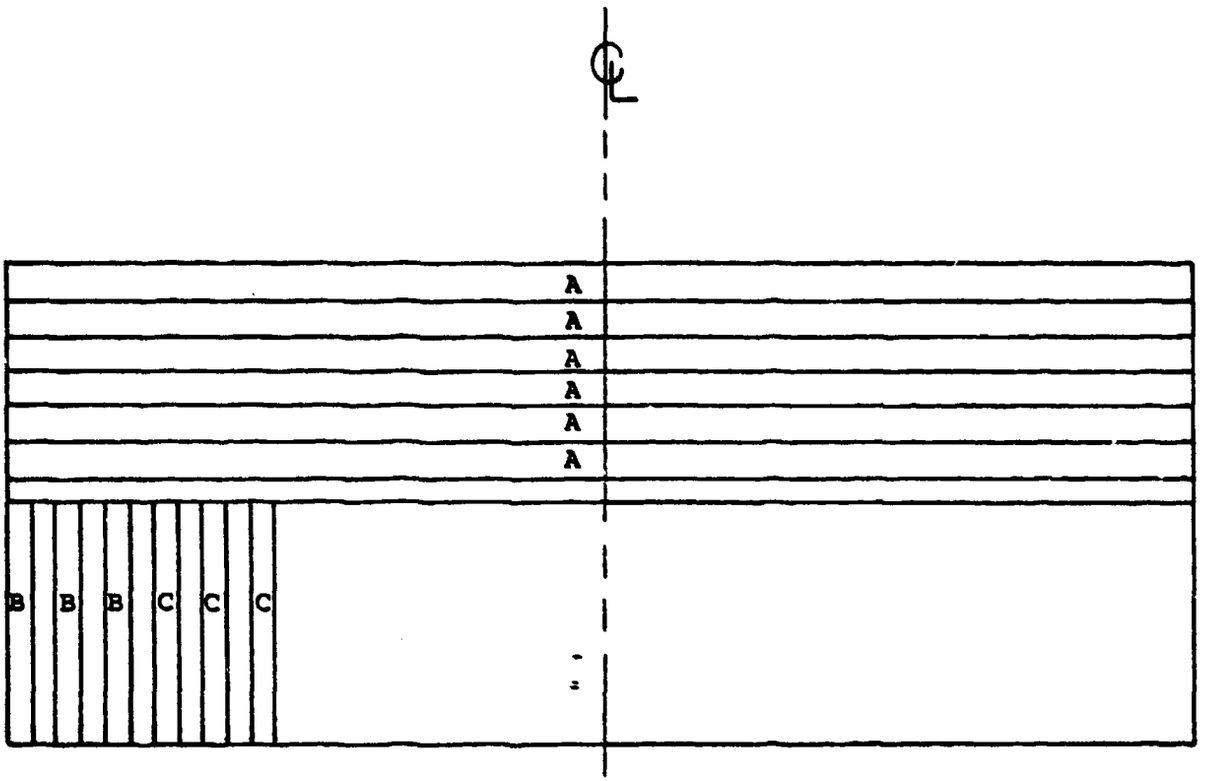

A = Hoop Thermal Expansion (8"ID x 1/2" Wall x 3/4" High)

B = Axial Tension (1/2" W x 3/8" Thick x 4" Long)

C = Flexure Strength (1/2" W x 3/8" Thick x 4" Long)

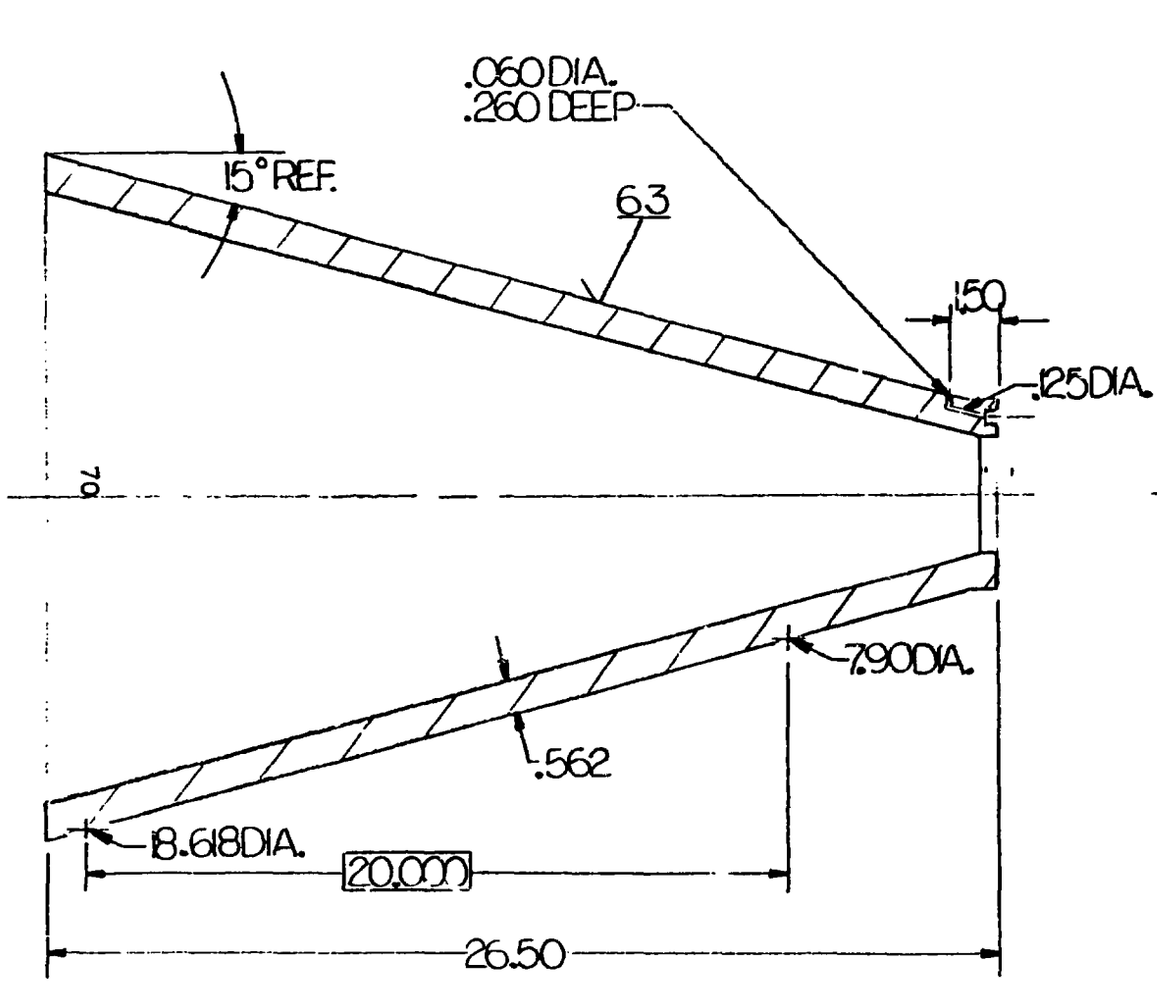

SECTION A-A

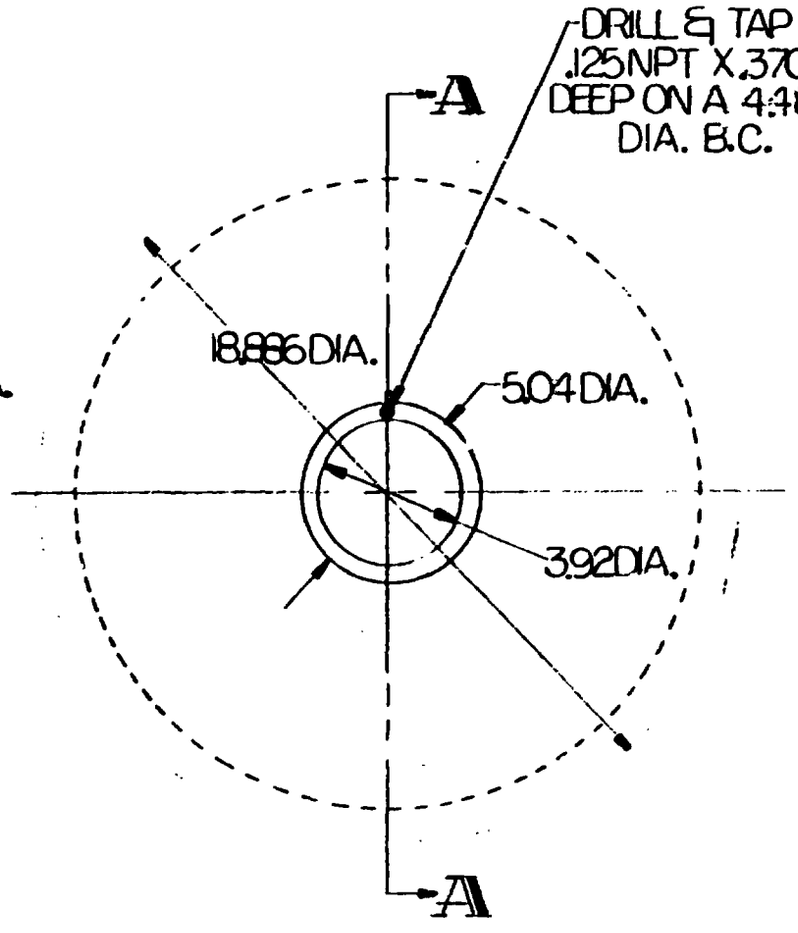

FIGURE 17. SUBSCALE FRUSTUM WRAP MANDREL

It can be seen that the physical properties were uniform; however, of concern was the difference between the specific gravity and apparent density. The difference between these values indicates that an open proosity of 4% to 6% was present. The porosity was attributed to the lower than desired resin content which is approximately 30% lower than commercially available RMSP tapes.

It should be noted that the wetting and infiltration of the tape by the RMP was poor. This was evident by the porosity values, density level, and mechanical strengths which are discussed in the subsequent report section. The braid that resulted from the leaching and prepregging processes was very highly packed, near the upper limits of the design goals. Resin penetration into the yarn bundles was not evident, therefore the resulting porosity of the tapewrapped cylinders and frusta and flat molded plates was high and the density was approximately 15% lower than desired.

An additional cylinder was tapewrapped using commercial bias-cut RMSP to determine whether the high porosity and low density properties could be attributed to fabrication procedures. The physical properties of this cylinder are summarized in Table 21 with a summary of the laminates fabricated with braided tape. It can be seen that the commercial RMSP contained had a higher density, which can be attributed to the higher resin content. Additional efforts would be required to increase the resin content of the braided silica material.

TABLE 21

SUMMARY OF TAPEWRAPPED MATERIALS PHYSICAL PROPERTIES

Part Identification	Raw Material		Prepreg Test Data		Cured Part Test Data		
	Reinforcement	Resin	Resin Solids	Vols	SP GR. (g/cc)	Resin Solids	Residual Vols
20° TW Cylinder	Braid	RMP	24.6%	3.4%	1.46	23.0%	3.0%
20° TW Cylinder	Braid	RMP	26.1%	4.5%	1.47	25.0%	3.9%
20° TW Cylinder	Bias Tape	RMP	29.1%	2.7%	1.62	29.5%	1.4%
20° Molded Panel	Braid	RMP	25%	2.3%	1.47	23.9%	3.4%
20° TW Frustum	Braid	RMP	22.6%	4.0%	--	--	--
20° TW Frustum	Braid	RMP	22.8%	3.1%	--	--	--

Note: The prepreg data listed was measured by FMI. The values obtained were lower than those presented in Table 18 which were determined by Fiberite.

5.0 MATERIAL CHARACTERIZATION

To afford the means to quantitatively assess the overall performance characteristics of the braided rubber modified phenolic material, a series of tests were conducted to ascertain the following properties:

- o Ablation
- o Erosion
- o Mechanical
- o Thermal

In performing these tests, the fundamental performance verification of material design and manufacturing technique was confirmed. Additionally, this information provided the opportunity to compare this material with the commercially available bias cut tape material at similar design loading requirements particular to the anticipated vehicle scenario.

The following sections describe the test techniques and procedures employed to conduct these tests. Specifically, the ablation, erosion, mechanical, and thermal testing are addressed in Sections 5.1, 5.2, 5.3, and 5.4 respectively.

5.1 Ablation Testing

Eight (8) ablation tests were conducted using the two dimensional (2D) wedge test configuration in the Avco Ten Megawatt Arc Facility. Two models each were tested at four different test environments. The tests provided the following comparative data for each of the test models:

a) Pre and post test mass and dimensional changes,

b) Surface brightness temperature and radiation response data,

c) Rear surface temperature response,

d) Motion picture histories of the ablating surfaces, and

e) Surface recession data.

The sections following detail this testing technique and report the results obtained.

5.1.1 Facility Description

Apparatus

Ablation testing was conducted at the Avco Ten Megawatt Arc (10MW) facility, Wilmington, Mass.

The 10 MW Arc Facility's basic components are shown in Figure 18. Its design incorporates a 4-inch diameter spherical plenum chamber into which four individual arc heads exhaust radially. The four arcs are mounted in a common plane, equally spaced at angles of 90 degrees around the periphery of the plenum chamber. The heated air mixes in the plenum chamber and exhausts through an exit nozzle in a direction perpendicular to the plane of the four radial plasma generators.

The power supply for the unit is a bank of 2080 heavy duty 12-volt lead-acid storage batteries. The arcs are initiated by means of fine steel wires. Air is injected tangentially into the arc chambers through sonic orifices and flows into the plenum chamber. When the power breaker is closed, steady state values of the current, voltage, and plenum pressure are achieved in less than 0.1 seconds. The 10 MW facility is described in detail in Reference 1.

Two-Dimensional Supersonic Wedge Test Configuration

A rectangular nozzle was used (Reference 2 and 3) to produce a uniform supersonic flow over a flat specimen. The high power capability of the 10 MW Arc, coupled with the destabilizing effects of a high level of free stream turbulence and the unfavorable pressure gradient by an oblique shock at the specimen leading edge, make possible the achievement of a turbulent boundary layer on a flat plate. A profile camera technique was adapted to the 2-D turbulent ablation test configuration in order to provide an accurate means

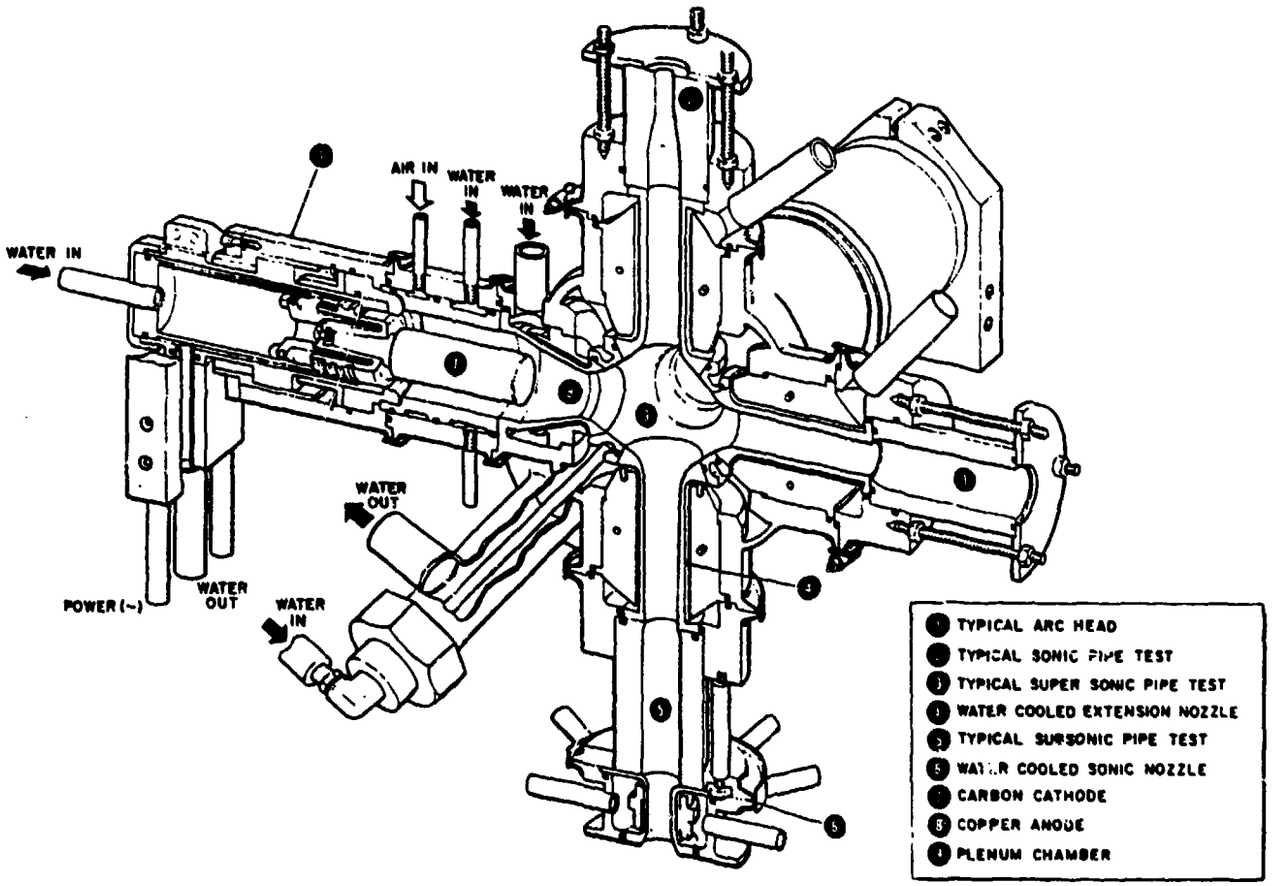

Figure 18

CUTAWAY VIEW OF 10MW ARC

SHOWING ARC PLENUM CHAMBER AND FOUR

ARC UNITS SET-UP FOR SONIC PIPE TESTS

of determining the steady-state recession rate as well as supersonic flow and ablating surface interaction.

The 2-D turbulent ablation testing configuration is described in Reference 4. The test configuration is shown schematically in Figure 19 with the standard specimen shape.

As shown in Figure 19, the test configuration consists of the specimen test surface placed flush with the lower edge of the nozzle and inclined at an angle of 15° to the flow. The inclination insures that, for reasonable test time, at least the downstream half of the specimen remains parallel to its original position and is subjected to a relatively constant environment (flow turned through a 15° compression angle) during the entire test. Under some conditions the shock thus produced may also aid in tripping the boundary layer.

Gas Enthalpy

The average gas enthalpy of the exhaust jet for both the model and calibration tests was determined from the sonic flow theory of Winovich (Reference 5). Measurements of gas enthalpy on the centerline of the exhaust jet with an enthalpy probe (Reference 6) have shown good agreement between the measured and calculated values. Figure 20 presents the fundamental curve of gas enthalpy versus a sonic throat mass flow rate parameter, derived by use of isentropic equilibrium flow relationships. The nozzles used during this test series were the Mach 2 and Mach 2.5 nozzles.

The gas mass flow rate is preset with adjustable sonic flow orifices located upstream of the arc firing chambers. This system provides a means of maintaining constant gas mass flow into the individual arcs. Adjustment of a precision type pressure regulator upstream of these orifices allows a total gas mass flow. A differential pressure transducer across the orifice

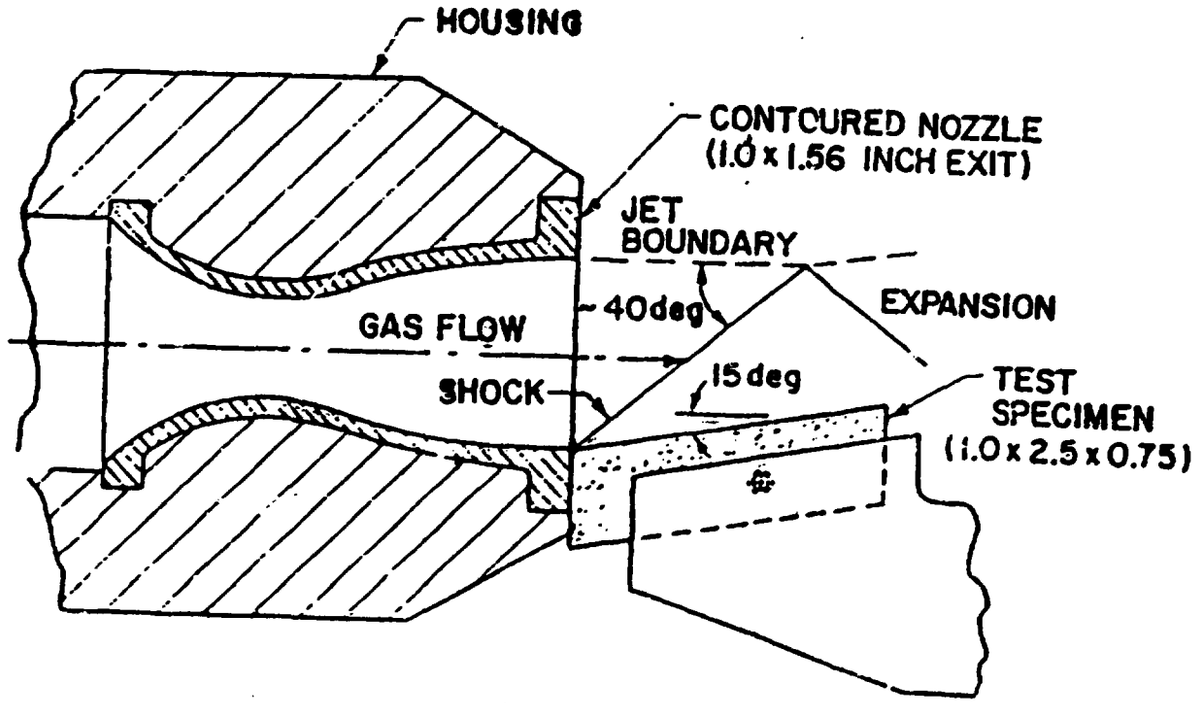

Figure 19
Specimen and Nozzle Configuration

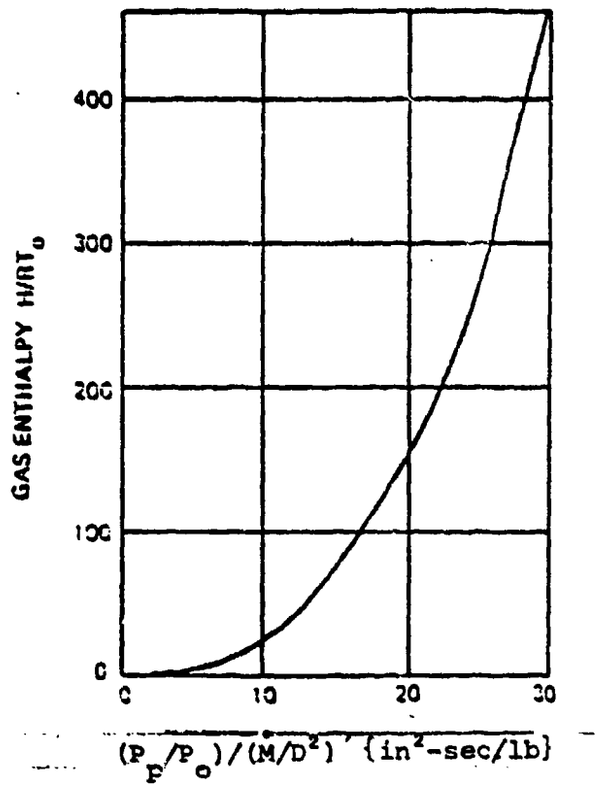

Figure 20

GAS ENTHALPY VS. SONIC THROAT
MASS FLOW RATE PARAMETERS

plate produces a signal on a continuous recording oscillograph. The arc plenum chamber pressure is measured by means of a standard pressure transducer which also produces a signal on a continuous recording oscillograph.

Heat Flux and Pressure

Heat flux and pressure calibration are accomplished through the use of a flat surface copper block, the same size and shape as the specimen, along the centerline of which are located three copper null-point transient calorimeters (Reference 7) and two pressure taps. The distances of the calorimeters and the pressure taps from the nozzle exit and their location relative to the sample position are shown in Figure 21. The calorimeter test consists of placing an uncooled solid copper model where the sample is normally located. The overall dimensions and shape of the copper model and ablative samples are normally identical. Briefly, the calorimeter consists of a small OFHC (oxygen free high conductivity) copper cylinder, into which a thermocouple is brazed in place. The thermocouple consists of 5-mil chromel and alumel wires contained in a 2-hole alumina rod, all placed in a stainless steel sheath. The thermocouple is brazed into the copper slug by means of 20 kv vacuum induction heater. The thermocouple is located at the so-called "null point," at which the temperature response matches the surface temperature of an uninstrumented copper cylinder. Once the surface-temperature history is determined for the one-dimensional heating of the copper slug, a digital computer program is employed to determine the heat flux as a function of time to the copper calorimeter (Reference 8).

The pressure measured at the upstream tap location (tap 1) is considered to be the static pressure behind the oblique shock. The Mach number behind the shock, M_2, is then found from the following equation:

$$M_2^2 = \frac{M_1^2 \left[(\gamma - 1)\, \xi + \gamma - 1 \right] \quad -2\,(\xi^2 - 1)}{(\gamma - 1)\, \xi + (\gamma - 1)\, \xi^2} \qquad (1)$$

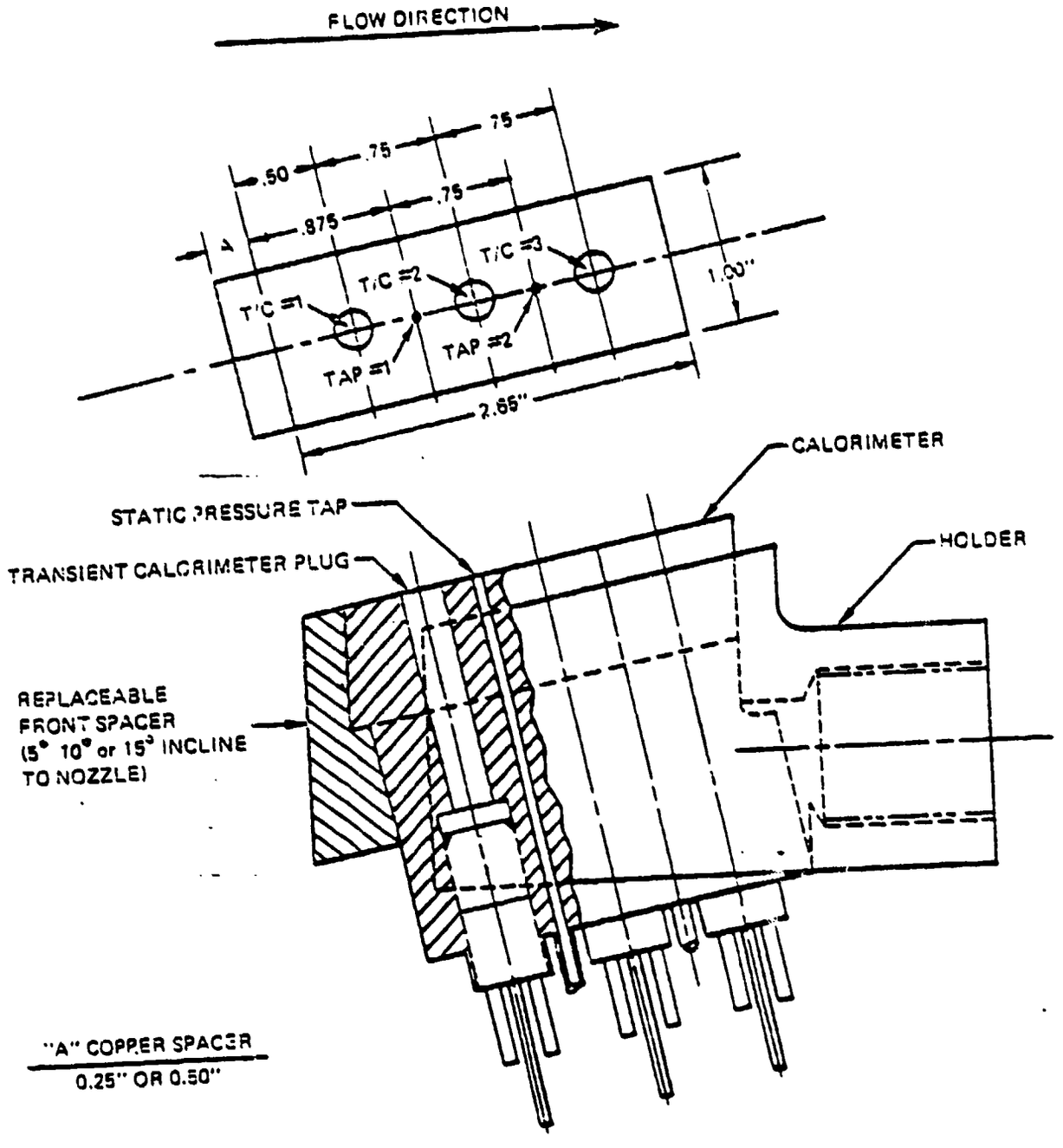

Figure 21 2D Wedge Heat Flux and Pressure Calorimeter

where M_1 is the nozzle design Mach No., ξ is the static pressure ratio across the shock, and γ is again taken as 1.2. Knowing the total enthalpy (H_s), the static pressure, and the Mach No., other properties of the flow behind the shock are found from the Mollier diagram for air with the use of an auxiliary scale solving the relation $U^2 = 2\Delta H$ as described in Reference 9 where U is the gas velocity and ΔH is the enthalpy change from static to stagnation conditions. Beginning just downstream of the first pressure tap location, streamlines begin to diverse (visible as erosion paths on certain types of specimens) due to the cross-flow pressure gradient. Therefore, the pressure measured at the second tap location is less than that at the first, although still greater than one atmosphere. If an isentropic expansion is considered to have taken place between taps 1 and 2, the Mollier diagram may be used to find the flow environment at the second tap location.

Shear Stress

In addition to the heat flux and other flow parameters which are recorded for a test, the shear stress is also calculated. The shear stress is assumed to be given by Reynolds' Analogy, that is:

$$\tau = \frac{q_{cw}\, U}{H_s} \qquad (2)$$

where

q_{cw} = cold wall heat flux

H_s = stagnation gas enthalpy

The methods used to determine the cold-wall heat flux and gas enthalpy were given previously. The gas velocity is determined by use of isentropic-flow and oblique-shock relationships, assuming a ratio of specific heats (γ) of 1.2, for the appropriate nozzle dimensions and specimen configuration.

5.1.2 Test Model Description

The nominal test model design for the reported test series is shown in Figure 22. One chromel alumel thermocouple was attached to the rear surface of each model as shown schematically in Figure 22. Pretest measurements on the "as received" models are recorded in Table 22. Each model's density was also calculated prior to machining and installation of the thermocouple. These data are presented in Table 22.

Pretest photographs (Figures 23 and 24) were taken of the eight instrumented prime test models showing the condition of the test surface. A typical view of the rear surface after thermocouple attachment is shown in Figure 25. An epoxy cement was used to assure the attachment of the thermocouple to the model. As shown in Table 22, each model was nominally 0.50 inch thick and had the same length and width. When the leading edge angle was machined on each model, the test surface length was decreased. The angle varied from 5 to 25 degrees, depending on the desired test environment.

5.1.3 Test Procedure and Results

Four steady-state test environments were employed. For each environment the model observations would be similar as discussed below. Prior to the model tests, a series of calibration tests were performed to confirm the four (4) test environments desired.

Calibration

As discussed in Section 5.1-1, the heat flux and pressure that a perspective test model would experience at the outset of the test is measured using a calorimeter having the same size and shape as the model (Figure 21). In order to obtain the desired enthalpy and heating rate, two different supersonic two-dimensional nozzles were used together with different model inclination

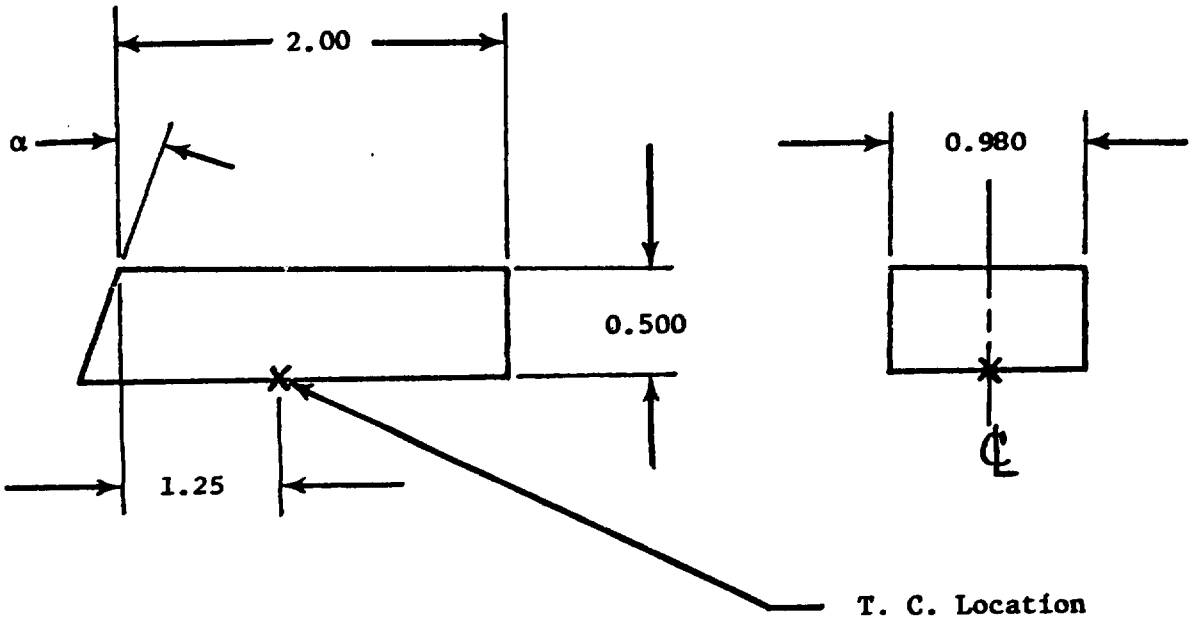

Figure 22

CHROMEL/ALUMEL NOMINAL 2D WEDGE
SAMPLE CONFIGURATION AND THERMOCOUPLE LOCATION

TABLE 22

PRETEST MODEL MEASUREMENTS OF BRAIDED RMSP

Model No.	Length Inches	Width Inches	Thickness Inches	Mass gms	Calculated Density gm/cm^3
A-1	2.007	1.004	0.500	24.19	1.47
A-2	2.007	1.004	0.502	24.28	1.47
A-3	2.007	1.004	0.501	24.15	1.46
A-4	2.007	1.004	0.502	24.33	1.47
A-5	2.007	1.003	0.505	24.30	1.46
A-6	2.007	1.004	0.500	24.29	1.47
A-7	2.007	1.004	0.504	24.41	1.47
A-8	2.007	1.005	0.501	24.25	1.46
A-9	2.008	1.004	0.501	24.25	1.47
A-10	2.007	1.004	0.503	24.24	1.46

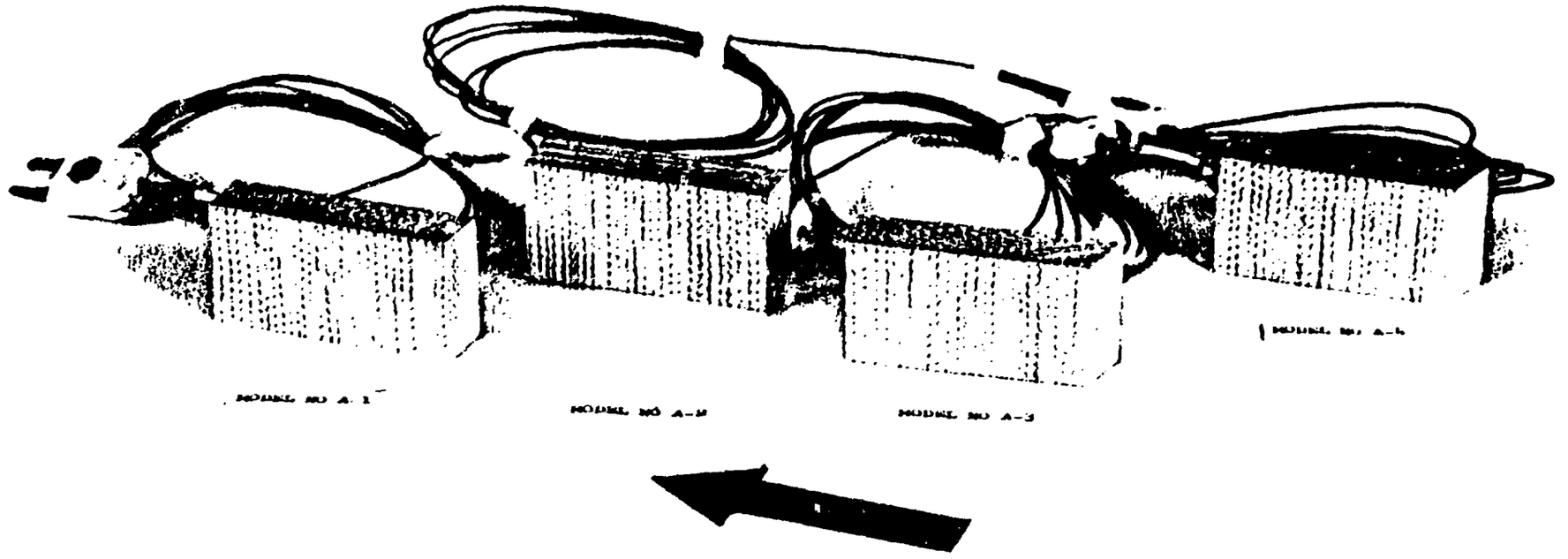

Figure 23 - Pretest Photograph of Test Specimens
A-1, A-2, A-3, and A-4

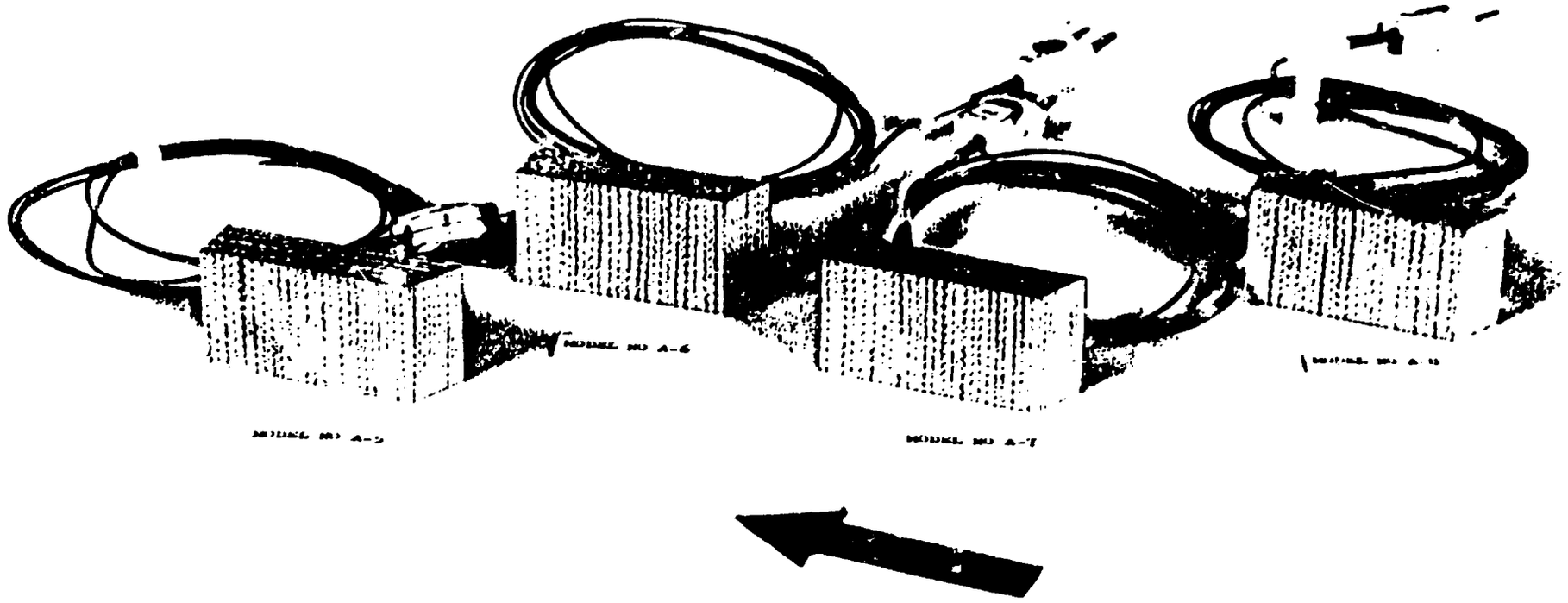

Figure 24 Pretest Photograph of Test Specimens A-5, A-6, A-7, and A-8

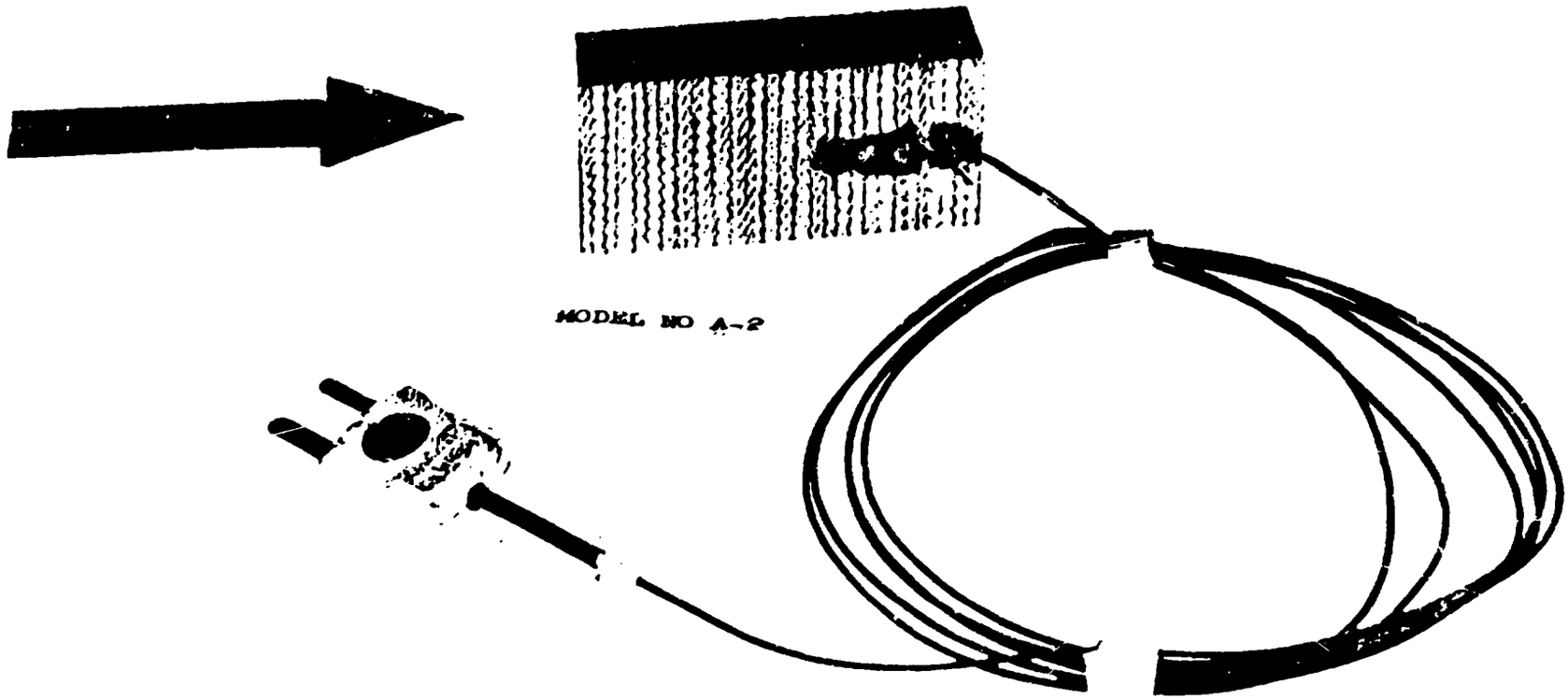

Figure 25 - Pretest Photograph of Rear Surface Showing Thermocouple Placement

angles. The arc parameters and test environments are given in Table 23 which presents the summary data for calibration and test specimen runs. For each of the four (4) test environments, the variation from run-to-run was very small. Figures 26 through 30 present the calibration heat flux and surface pressure distribution data for each of the four test environments. In all cases the surface pressure is slightly higher than one atmosphere decreasing slightly with axial position along the centerline of the model. The calorimeter heat flux values so determined are assumed to correlate using the approximate turbulent heating relationship:

$$\dot{q}_{cw} \approx (\dot{m}^{0.8} H_s) \qquad (3)$$

where

$\dot{q}_{cw}$ = cold wall heat flux

$\dot{m}$ = total air mass flow rate in arc

H_s = stagnation gas enthalpy

This relationship was used to determine the cold wall heat flux for each specimen test. For each test environment, the model location and inclination angle was the same as that for the calorimeter.

During the test series, starting with AVCO, Run 12503, an arc-operating problem occurred which may have influenced the material ablation. To circumvent the problem, the arc-operating condition for this test point was slightly altered, namely, decreasing the air mass flow which lowered the heat flux slightly. Calibration data for both points are presented, as are the ablation

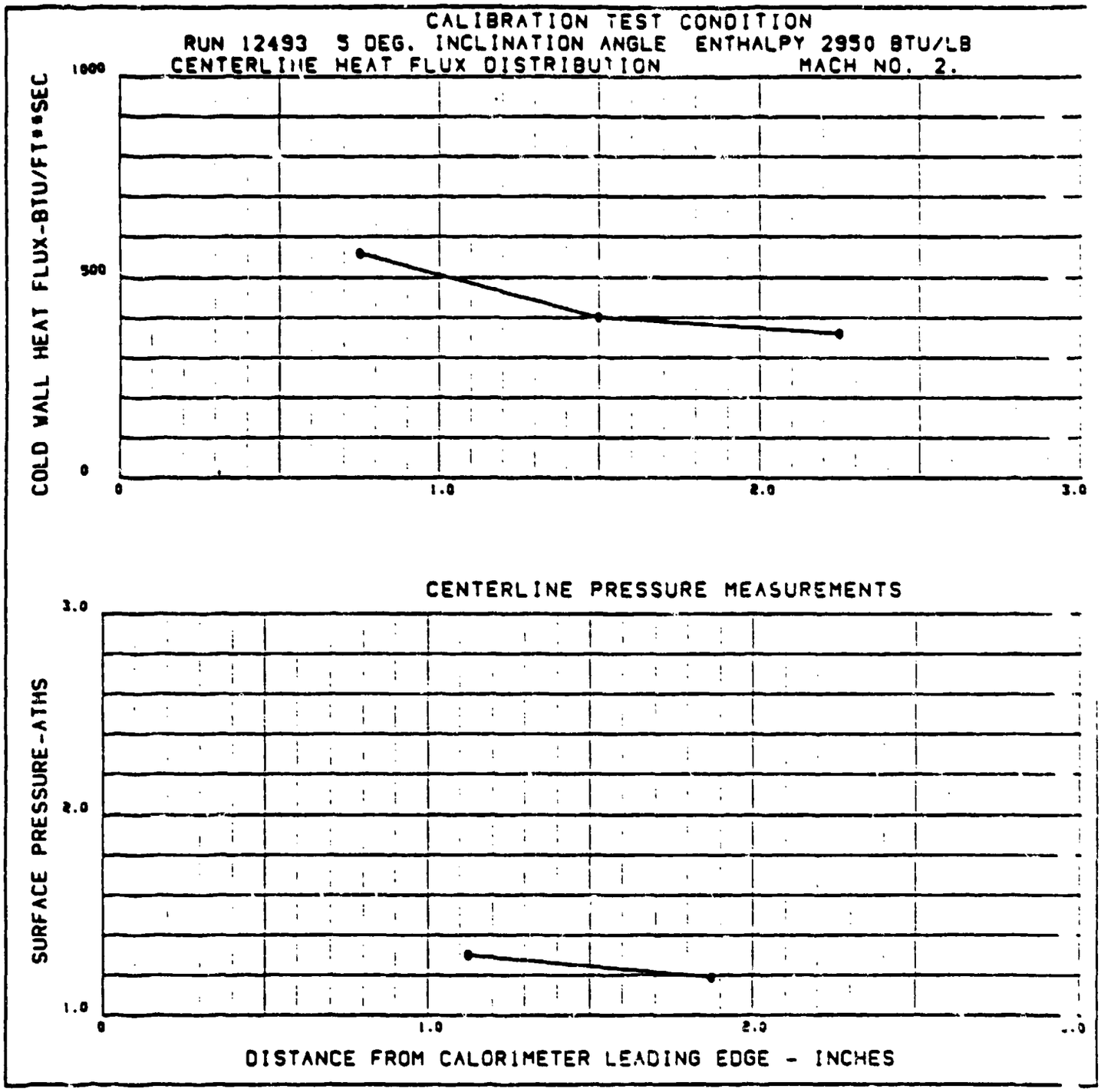

Figure 26 - Calibration Test Results, Run No. 12,493

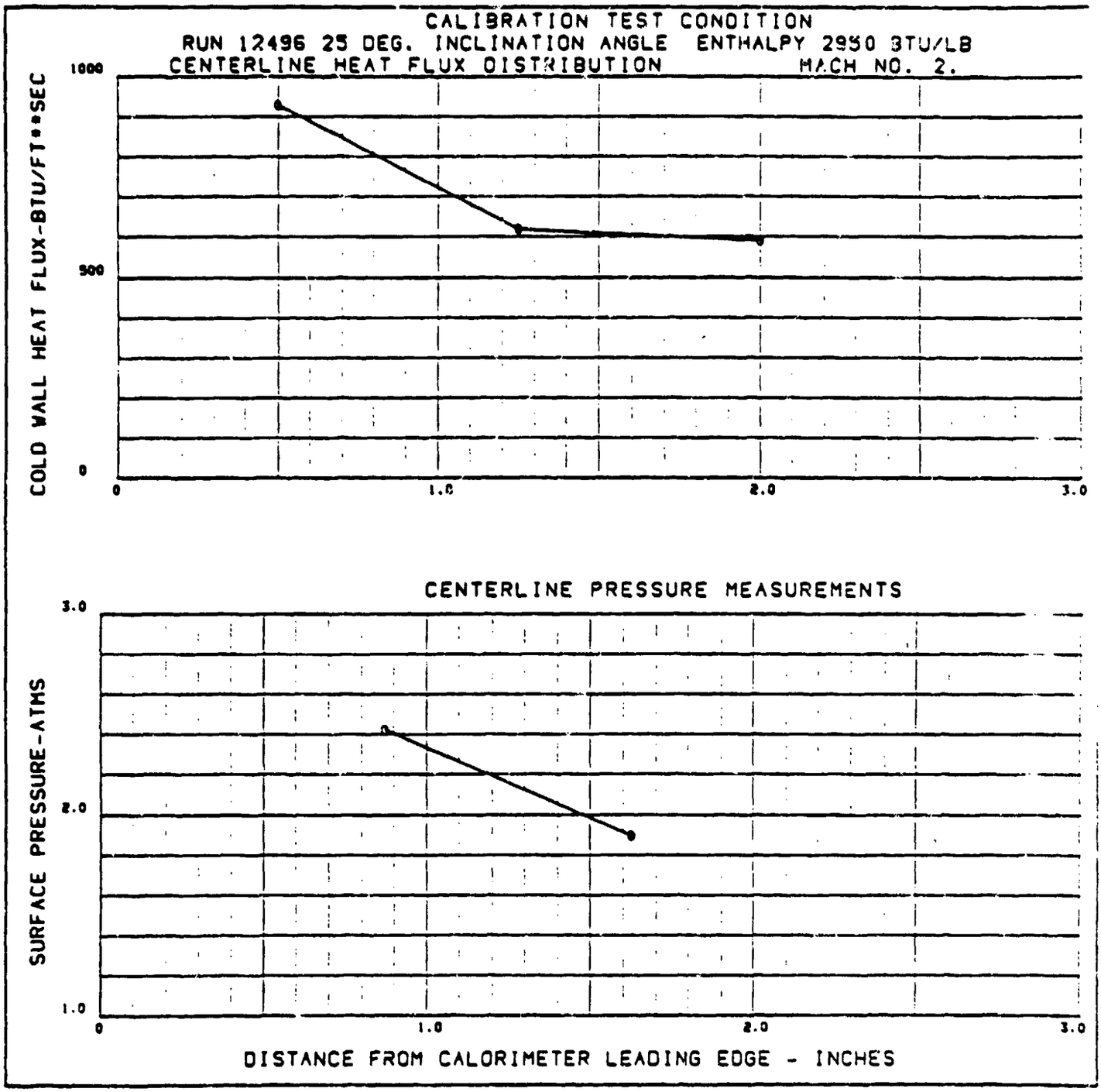

Figure 27 - Calibration Test Results, Run No. 12,496

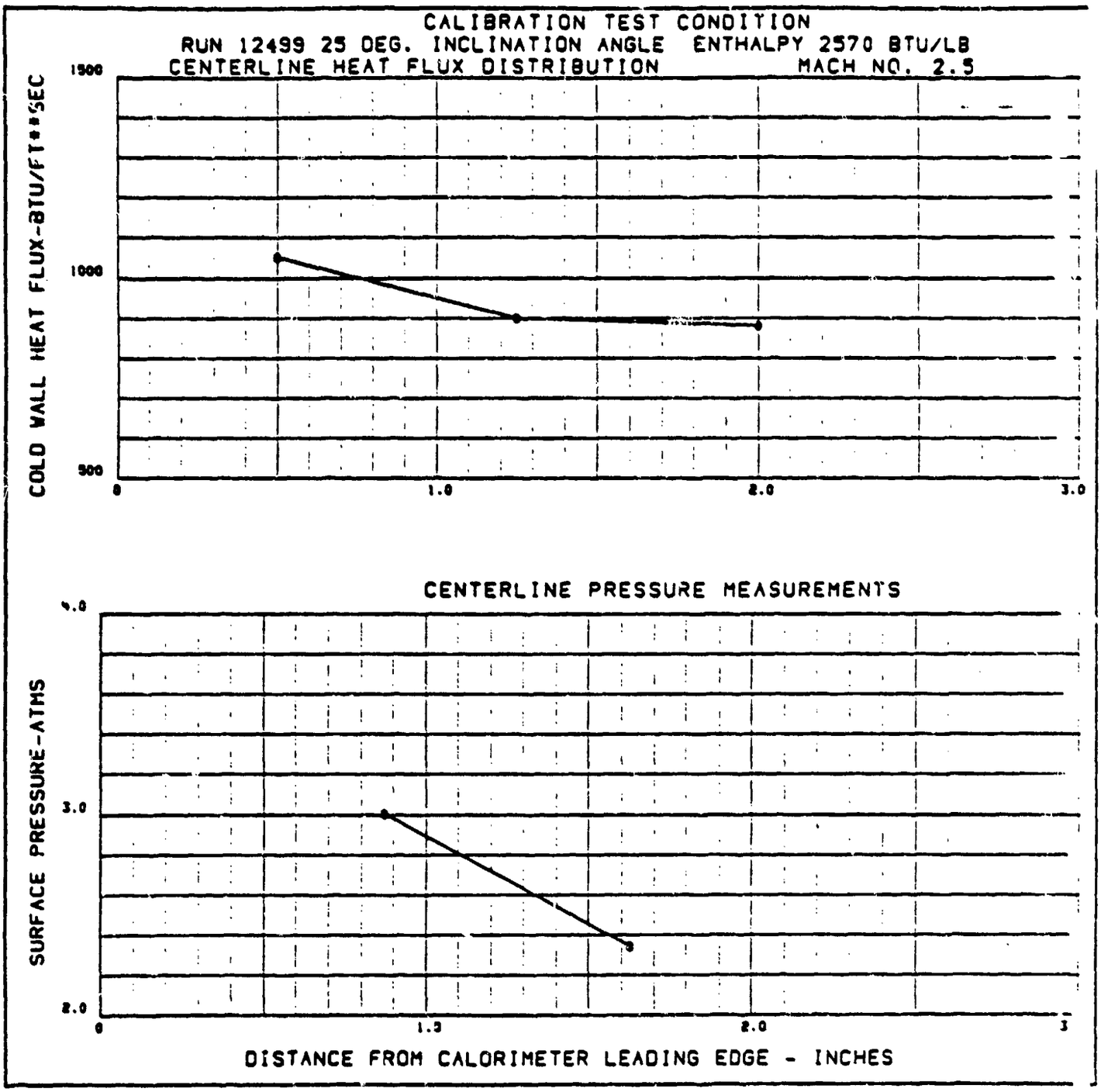

Figure 28 - Calibration Test Results, Run No. 12,499

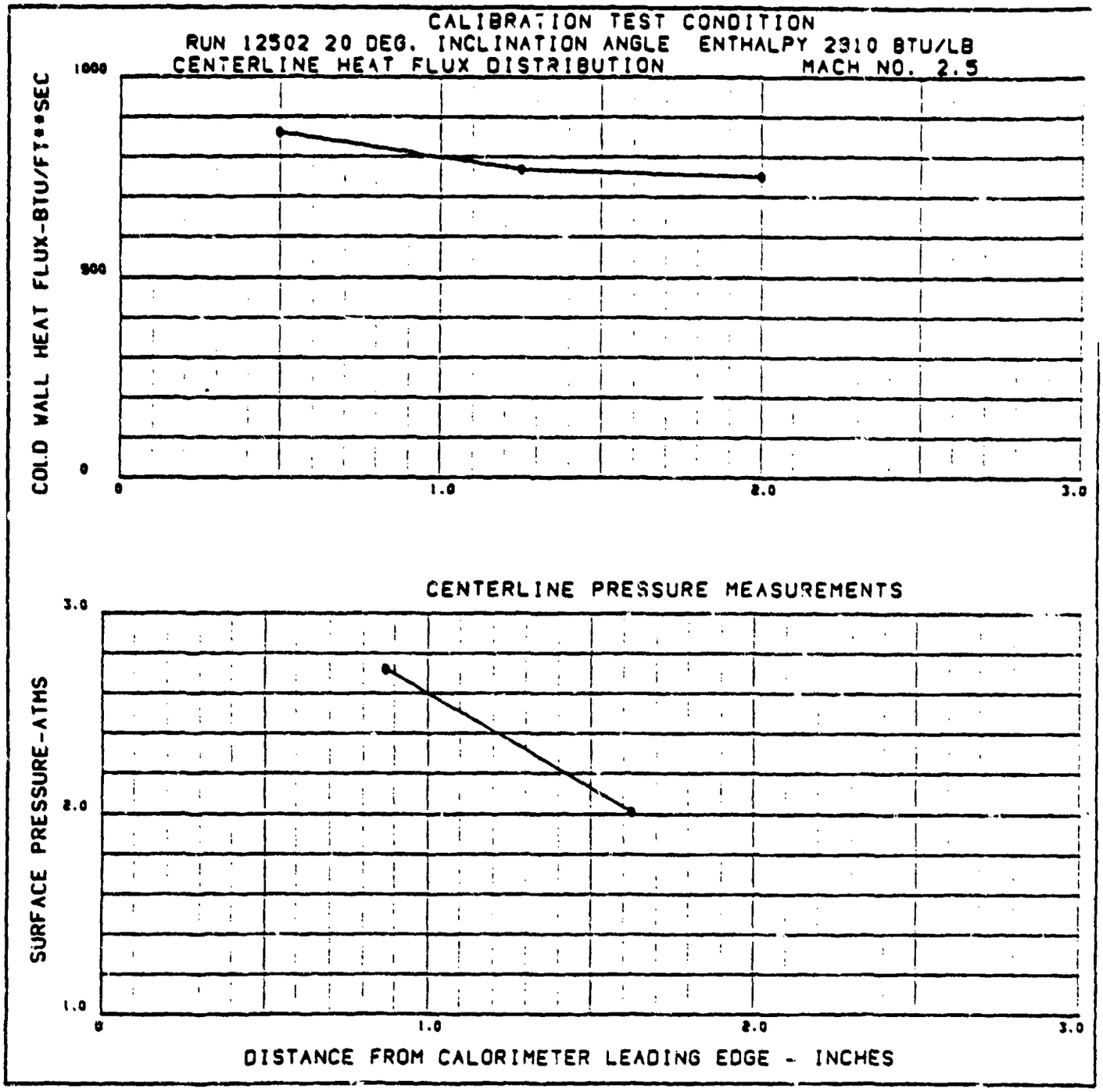

Figure 29 - Calibration Test Results, Run No. 12,502

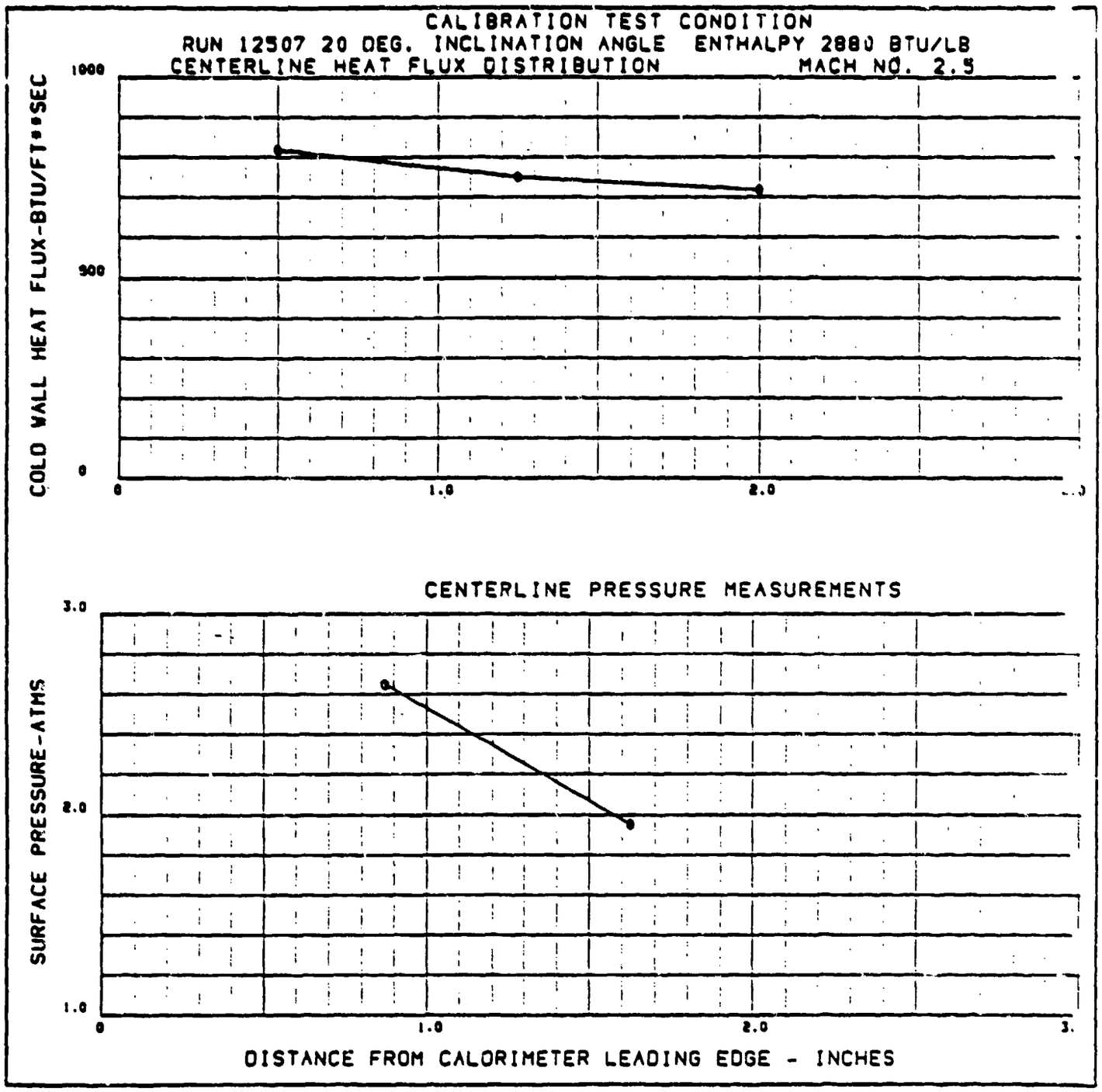

Figure 30 - Calibration Test Results, Run No. 12,507

results for the test models.

5.1.3.1 Test Setup and Environment

The ablation test setup is schematically shown in Figure 31. The high speed cameras, recording optical pyrometer, high resolution camera polavision and recession profile camera are shown in their respective positions. Each of the cameras was individually controlled such that all the cameras were operating at least one second before the arc was initiated. The output of the optical pyrometer was continually recorded once the test was underway. All emf signal outputs, such as those from the thermocouple hot junction or the recording pyrometer, were recorded on magnetic tape at a centralized data acquisition system. Electronic data processing equipment was used to recover and process the data. A two-way intercommunication capability allowed coordination of efforts between the test and signal recording site. Individual arc currents and voltages also were recorded continuously on the facility CEC oscillograph. The total test time is determined from timing lines on the oscillograph. The start of the test is taken when the recorded pressure and current traces respond (approximately 0.01 second). The end of the test is taken when the arc current is terminated.

Recession Rate Determination

The Nikon 35mm variable frame rate camera was used to obtain films (about two (2) per second) of the specimen surface. Through the use of a split filter technique, it was possible to obtain a clear image of both the heated specimen surface and the cooled specimen holder (which had a fixed position reference marker (scale) attached). The recession data are obtained using a Telecomputing Corporation film reader. Readings so obtained are entered into a program to obtain a least mean squares fit recession rate and a plot for each test. In addition to the recession data, the Nikon films also show the shock patterns

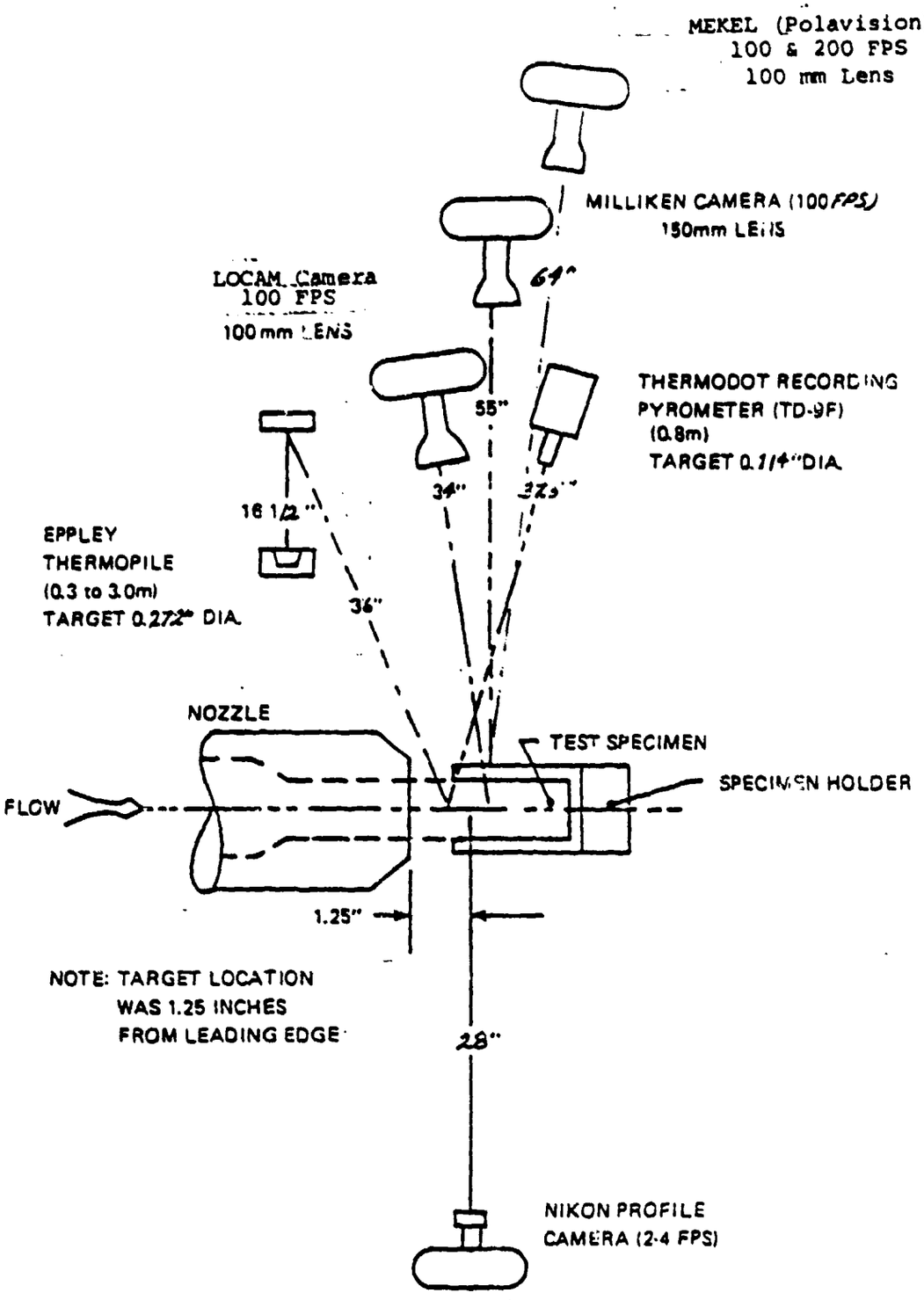

Figure 31 - Schematic of Facility Instrumentation Layout

on the heated surface due to the reaction of the supersonic air flow with any significant surface roughness or distrubance that may exist as a result of nonuniform surface ablation. All surface recession data were obtained for the specimen station at 1.250 inches from the leading edge.

Surface Brightness Temperature and Surface Radiation

Surface brightness temperature was measured and recorded continually during each test by a high resolution Thermodot (Infrared Industries Model TD-9F) recording optical pyrometer. This instrument is sensitive to radiation at a 0.80 ± 0.015 micron wavelength. The optical head was focused 1.250 inches from the specimen's test surface leading edge, along the centerline, covering a circular viewing area of 0.114 inch diameter. Coupled with this measurement was the total radiation measurement taken at the same station using an Eppley thermopile sensitive to radiation in the range from 0.3 to 3.0μm and covering a spot of 0.272 inches diameter. The total emittance of the surface material can be calculated by dividing the total radiation, as measured by the Eppley thermopile, by the black-body radiation corresponding to the true surface temperature.

High Speed Motion Picture Coverage

Two (2) 16mm high speed cameras were used to record model ablation-phenomena. These were a Milliken (D.B. Milliken Co., Model DBM55) and a LOCAM (Redlake, Photo Instrument, Model 51) high speed motion picture cameras using color motion picture film. Both cameras were operated at framing rates of 100 frames per second. The framing rate was recorded on the film using a high frequency pulse generator operating at 1000 cycles per second. Each camera had a slightly different viewing angle of the test surface and used a different viewing lens.

In addition to the above described cameras, a polavision camera was used for instant review of the surface ablation phenomena. This camera uses 8mm color motion picture film which is developed within 2 minutes after a test is concluded and is projected on a special viewer.

Internal Temperature Measurements

As described in Section 5.1.2, instrumented models were tested. These models were each instrumented with one backface thermocouple as shown in Figure 22.

Thermocouple signals were recorded on magnetic tape and processed by computer. An ice bath, in the test cell, served as the reference junction for the thermocouple circuit.

5.1.3.2 Test Data Presentation

General Discussion of Test Results

Although an arc malfunction occurred in one model test, the tests in general were performed without any other model or other arc malfunctions. Tables 23 and 24 present a summary of the arc test parameters and ablative performance of the test models respectively. Table 25 present a summary of the post test and motion picture observations.

In general, all of the test models developed a flowing viscous liquid layer on the heated surface. Although the motion picture coverage did not show any significant surface spallation to have occurred during the tests, the post test appearance (Figures 32 through 36 of some of the models showed significant loss of char material (all occuring at the higher shear level test environments). It has been concluded that this char layer loss occured after the test was ended. This may have been due to sublayer pressure forces which literally blew away a weak char layer after the pressure forces on the surface

TABLE 23

ARC PARAMETERS AND TEST ENVIRONMENT

Sample Code	Enthalpy Btu/lb	Test Time (Sec.)	Cold Wall[a] Heat Flux $\dot{q}_{cw}$, (Btu/ft^2-sec)	Plenum Pressure (Atm.)	Nozzle Throat Size (Inch)	Flow Mach No.	Model Inclination Angle, (Degrees)
Calib.	2950	1.16	450	6.92	1.0 x 0.8	2.0	5°
A-1	2950	10.00	450	6.92	1.0 x 0.8	2.0	5°
A-2	2950	9.95	450	6.92	1.0 x 0.8	2.0	5°
Calib.	2950	1.25	620	7.96	1.0 x 0.8	2.0	25°
A-3	2950	9.98	620	7.96	1.0 x 0.8	2.0	25°
A-4	2950	4.98	620	7.93	1.0 x 0.8	2.0	25°
Calib.	2570	1.24	900	15.63	1.0 x 0.464	2.5	25°
A-5	2570	4.98	900	15.68	1.0 x 0.464	2.5	25°
A-6	2570	9.96	900	15.68	1.0 x 0.464	2.5	25°
Calib.	2910	1.18	770	15.88	1.0 x 0.464	2.5	20°
A-7	2880	10.00	760	15.33	1.0 x 0.464	2.5	20°
Calib.	2880	1.18	750	15.58	1.0 x 0.464	2.5	20°
A-9	2910	5.00	760	15.53	1.0 x 0.464	2.5	20°
A-10	2910	9.98	760	15.53	1.0 x 0.464	2.5	20°

a) INTERPOLATED AT 1.25 INCH CENTERLINE STATION

TABLE 24

ABLATIVE PERFORMANCE OF BRAIDER RMSR HEATSHIELD MATERIAL

Sample Description	Weight			Thickness[a]			Peak Surface Brightness Temperature (°R)	Recession Rate s,
	Pre	Post	Loss	Pre	Post	(Gain) Loss		
A-1	31.0	29.9	1.1	0.499	0.506	(0.007)	3960	b
A-2	31.1	30.1	1.0	0.502	0.511	(0.009)	3850	b
A-3	30.1	26.5	3.6	0.499	0.417	0.082	4340	0.01074
A-4	30.0	28.2	1.8	0.501	0.477	0.024	4210	0.00674
A-5	29.9	27.3	2.6	0.504	0.460	0.044	4380	0.00967
A-6	29.9	25.1[c]	4.8[c]	0.500	0.368[c]	0.132[c]	4360	0.00927
A-7	28.3	24.2[c]	4.1[c]	0.504	0.364[c]	0.140[c]	4310	0.00503
A-9	29.6	28.0	1.6	0.500	0.457	0.043	4270	0.00393
A-10	30.5	26.0[c]	4.5[c]	0.502	0.362[c]	0.140[c]	4280	0.00491

a) Centerline location 1.25 inches from test surface leading edge.

b) Surface expanded.

c) Surface spalled.

TABLE 25

POST TEST MODEL AND MOTION PICTURE OBSERVATIONS

Run No.	Sample No.	Post Test Model Surface Observations	Motion Picture Observations
12,494	A-1	Uniform light gray, glassy surface layer covering all of the heated surface. Ablation was uniform both laterally and axially. Downstream portion of model showed silica flow pattern.	Upon arc initiation the model surface temperature increased. Liquid (silica) flow became evident after 2.3 seconds and covered the surface with a relatively slow moving viscous rivulet-like flow. Some minor interlaminar surface eruptions were evident. Liquidus material flowed off the sides of the model with some of the liquid material freezing to the sides of the model.
12,495	A-2	Similar in appearance to Model A-1.	Similar to Run 12,494. Flow became evident after 2.5 seconds.
12,497	A-3	Glassy, grayish surface layer slightly rougher to the touch than models A-1 and A-2. Surface recession was uniform laterally and from the 0.5 inch station to the trailing edge.	The model's surface brightness increased quickly and uniformly after arc ignition; silica flow was evident after 0.5 sec. The liquidus surface flow was moving very rapidly but uniformly and flowed off the model's side and downstream edge. Some very minor random surface interlaminar spall areas were evident throughout the test.
12,498	A-4	Similar to model A-3 except that dark lateral striations were evident. Surface recession was smaller than for sample A-3.	Similar to Run 12,497 except surface flow became evident after 0.6 sec.

TABLE 25 (Cont.)

POST TEST MODEL AND MOTION PICTURE OBSERVATIONS (Cont'd)

Run No.	Sample No.	Post Test Model Surface Observations	Motion Picture Observations
12,500	A-5	Thin glass-like surface layer with dark black zones evident on left side of model's heated surface. Dark lateral surface striations also evident. Surface recession was uniform laterally and from the 0.5 inch station to the trailing edge.	Upon arc ignition the sample surface increased very rapidly in temperature and developed a freely flowing liquidus layer after 0.35 seconds. Also throughout the test very small surface spall "spots" developed but soon disappeared but then developed at another surface location. No large spall zones developed however. The liquidus layer flowed off the sides of the model.
12,501	A-6	Similar to Run 12,500 except for a large continuous dark zone extending from the 3/4 inch station to the trailing edge. Surface recession was relatively uniform laterally and from the 0.5 inch station to the trailing edge.	Similar to Run 12,500. Liquid surface flow developed after about 0.37 seconds.
12,503	A-7	Nonuniform surface showing a large zone of exposed virgin material. This zone extended from the 5/8 inch model station to the trailing edge. Surface appears to have eroded badly with the weak char partially removed.	Upon arc ignition the model surface began to heat up uniformly. However, at about 0.35 seconds a burst of particles (lasted 0.01 seconds) issued from the arc nozzle and impacted the model which produced some spall zones on the surface. Following this a liquid layer developed (0.57 sec.) and essentially covered the zones which then continued to ablate in a normal manner. Some local, very small spall zones developed throughout the test. Because of the flow anomalie this test was repeated (Run 12,504).

TABLE 25 (Cont.)

POST TEST MODEL AND MOTION PICTURE OBSERVATIONS (Cont'd)

Run No.	Sample No.	Post Test Model Surface Observations	Motion Picture Observations
12,504	A-8	Very rough, eroded surface having numerous spall-like zones. Much of the silica layer removed. Some ply delamination is evident.	Upon arc ignition the sample surface temperature increased and liquid layer flow became evident after 0.5 seconds. A uniform but freely flowing liquid layer was in evidence when a large mass from the arc (broken graphite electrode material) hit the model and caused a large section of char layer at the trailing edge to be dislodged. This occurred at about 2.3 seconds. This damaged zone appeared to be healed (covered by liquid flow) and the surface again appeared to flow and ablate normally. However, at 9.8 seconds a large spall (mid-section of model) occurred (no debris from the arc was in evidence). The test was concluded at 10 seconds and showed a model with a severally damaged surface. Once again, the test was repeated (Run 12,506).
12,505	A-9	Rough surface having a silica-like deposit over the surface. Indication of surface spallation (dark spots) randomly distributed over the surface.	Upon arc ignition the model's surface temperature increased and a liquid layer developed after 0.6 seconds. The liquid layer flow was very rapid, continuous, and uniform throughout the test. No flow anomalies were evident. Some local, but small surface spall zones developed but "healed" over due to the liquid flow.
12,506	A-10	Similar to Run 12,503 having a large zone of virgin material where apparently the char layer was pulled away during the test.	Similar to Run 12,505. The liquid layer flow became evident after 0.6 seconds. No evidence could be seen on the film of any char removal. Char removal occurred after the test was concluded.

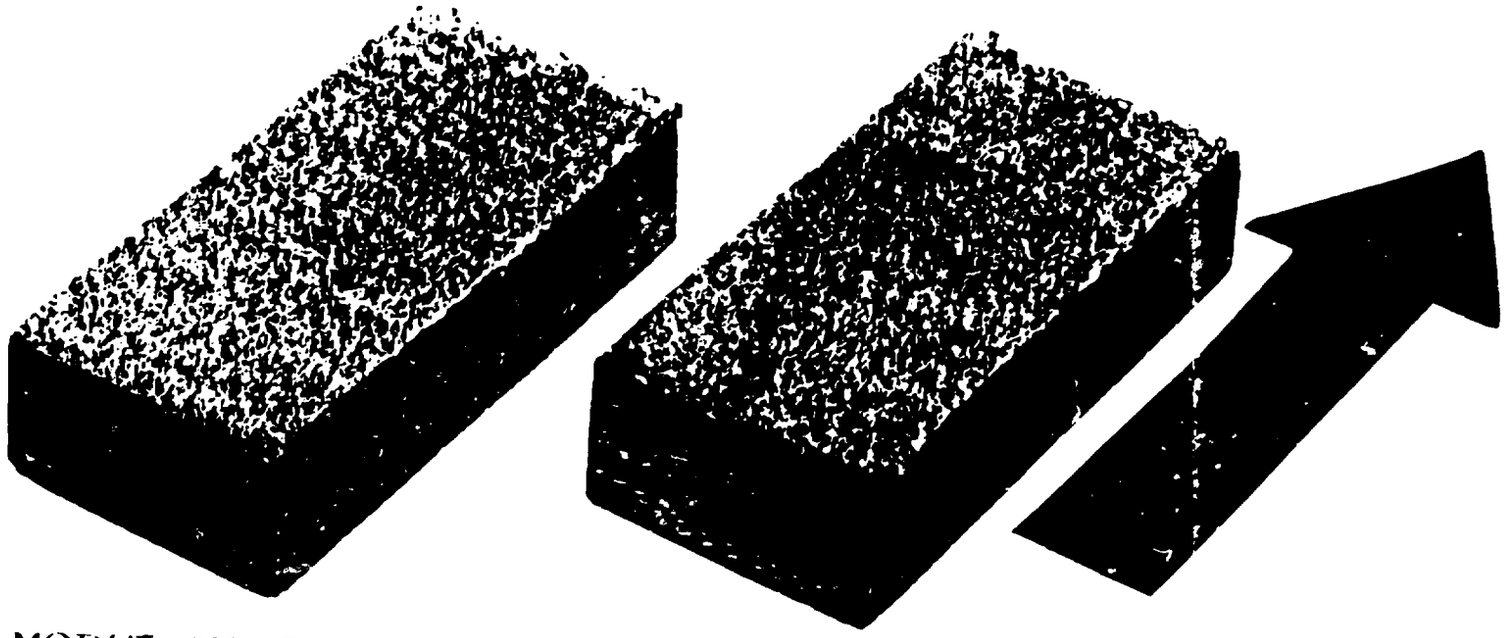

Figure 32 -- Post Test Photograph of Models A 1 and A 2

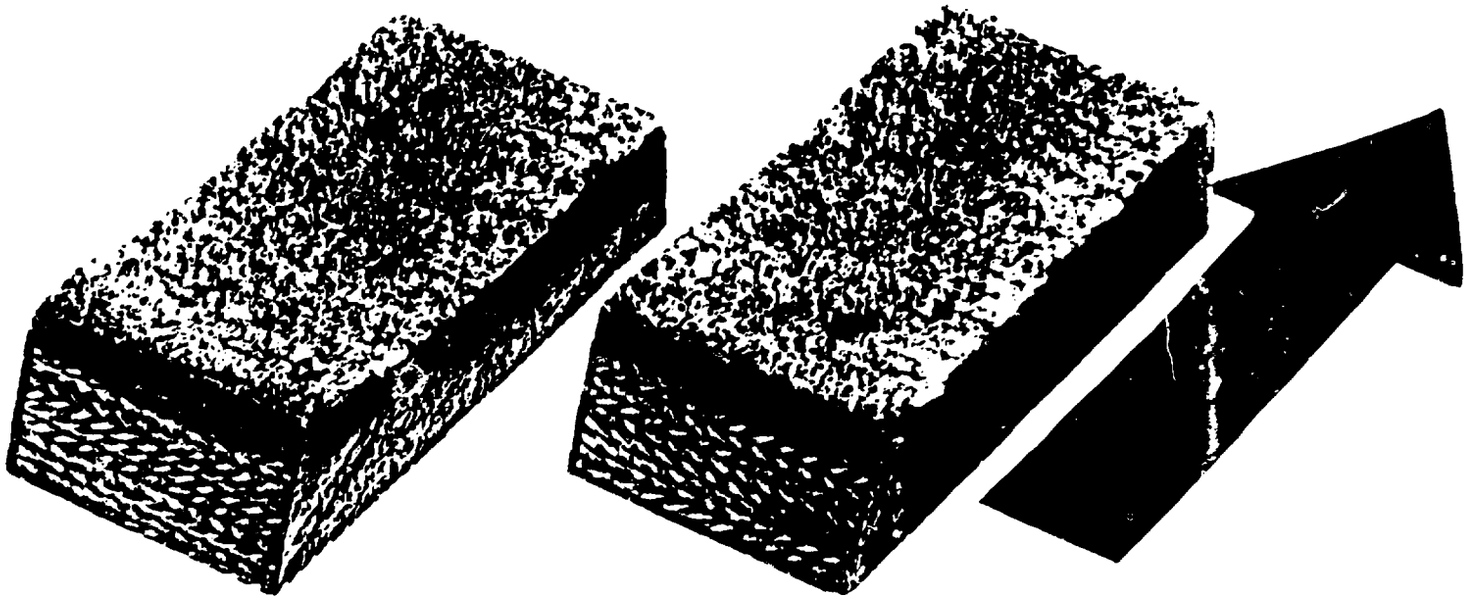

Figure 33 - Post Test Photograph of Models A-3 and A-4

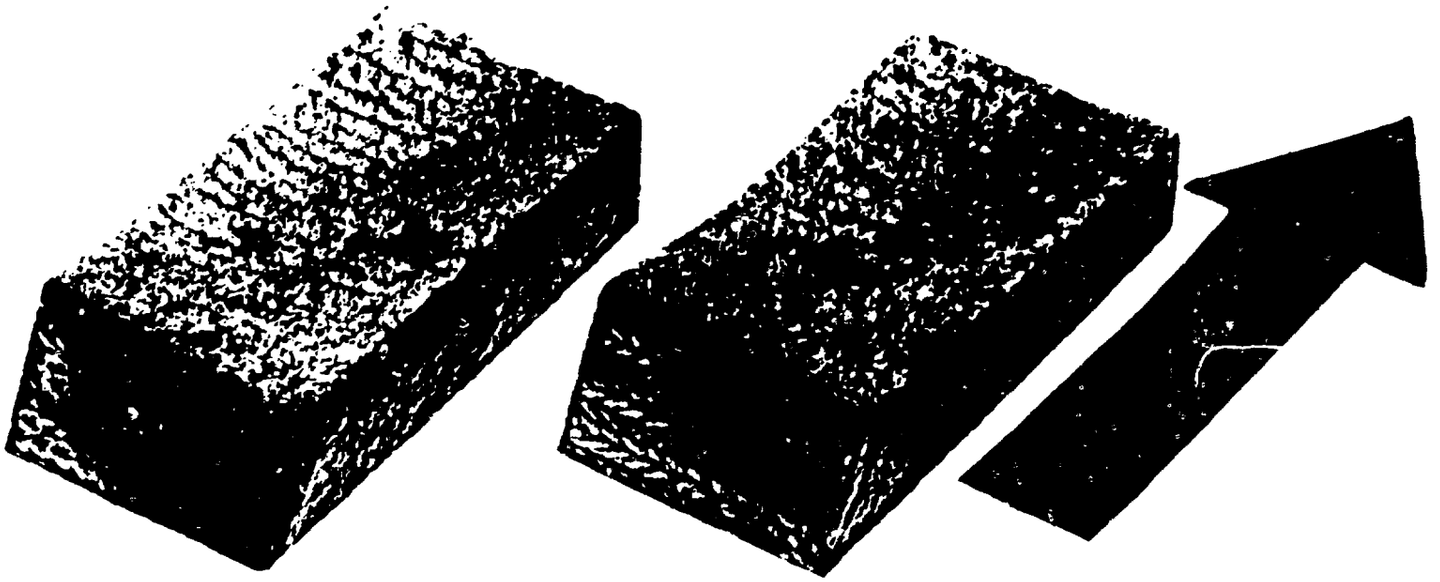

Figure 34 - Post Test Photograph of Models A 5 and A 6

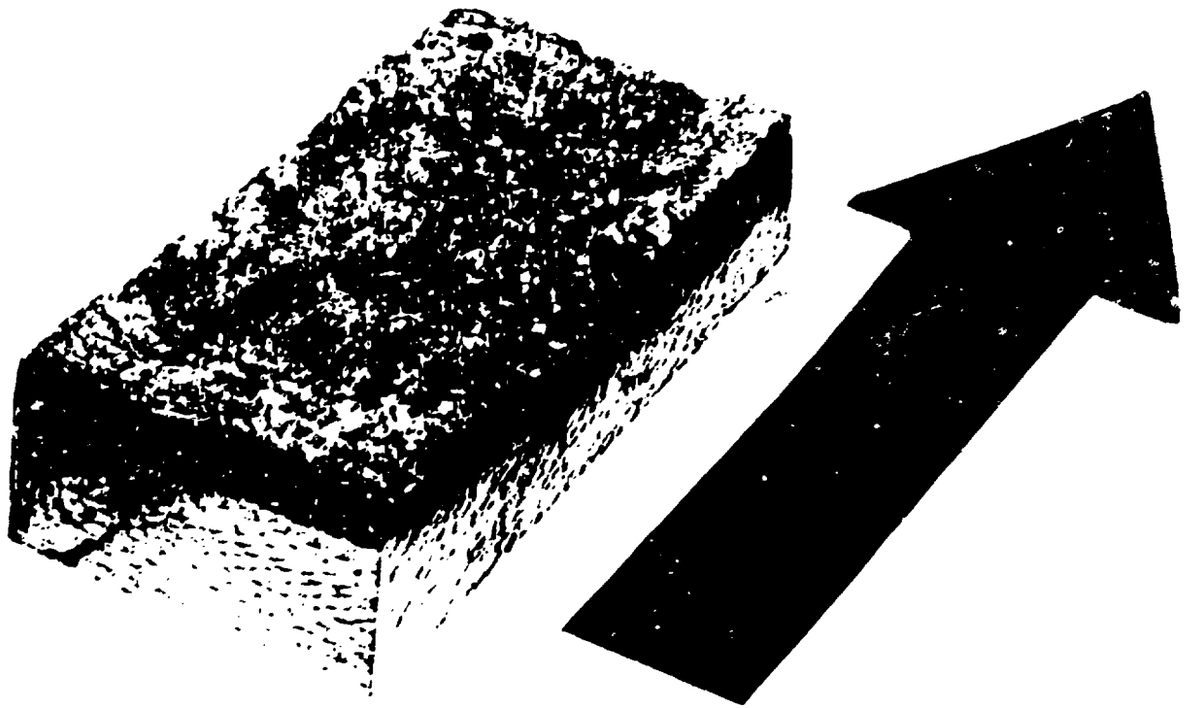

Figure 35 Post Test Photograph of Model A 8

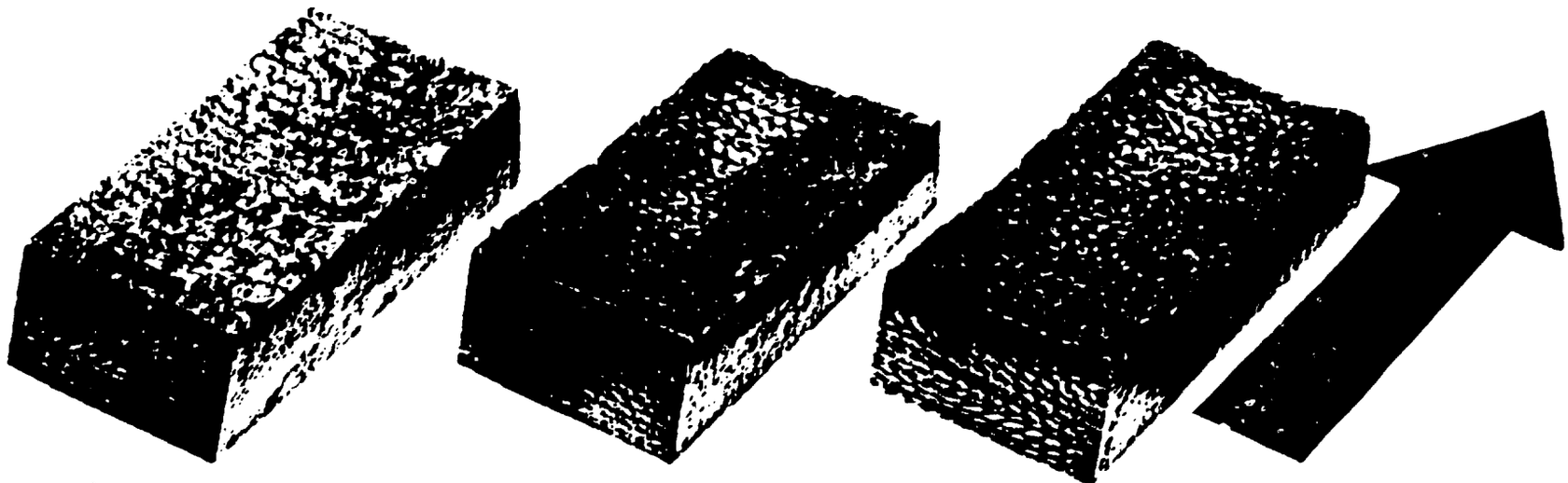

Figure 36 - Post Test Photograph of Models A 9, A 7 and A 10

of the model were reduced following the conclusion of the test. Presented below are the results of the test measurements and post test observations.

Post Test Sample Profile Measurements

Following the tests, each sample was weighed and measured. These data are presented in Table 24. Data for Sample A-8 have been omitted because of an arc malfunction which resulted in abnormal material loss of the model. As noted in Table 24, the models tested at the low heating environments expanded. All other test models showed a loss in physical dimension. The surface profile measurements of all models are presented in Figures 37 to 40. These profiles were generated by mechanical measurement using a dial indicator micrometer equipped with a 0.032 inch diameter tapered tip. Readings were taken starting from the test surface leading edge at 0.125 inch increments along the specimen centerline. Model profiles were similar for those models tested at the same environment for the same test time (Figure 40, Samples A-7 and A-10).

Post Test Model and Motion Picture Observations

Figures 32 to 36 present the post test photographs of the test models. Table 25 presents the post test observations for each of the models as well as the observations taken from the motion picture films. In general, it appears that under certain flow environments the material being characterized was susceptible to surface shear forces and in some cases had developed a weak char which following the test was partially removed. This latter phenomena occurred only at the shear levels of 60 and 74 psf (Figures 34 and 36). In all cases, there was a time period (induction time) before steady-state ablation occurred. These times are noted in Table 25 under the motion picture observation column. Under the lowest heating environment the induction time of

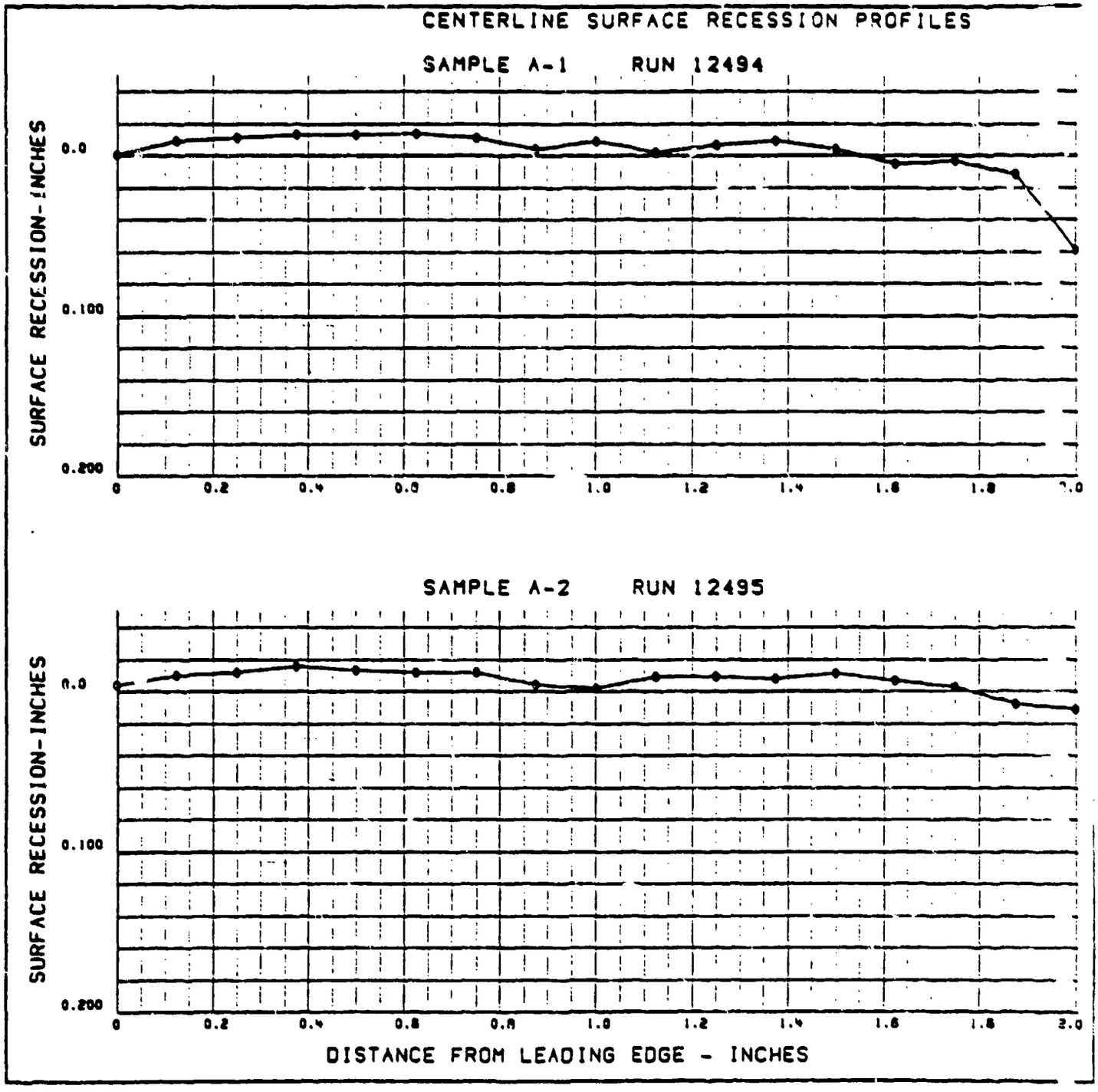

Figure 37 - Centerline Surface Recession Profiles of Models A-1 and A-2

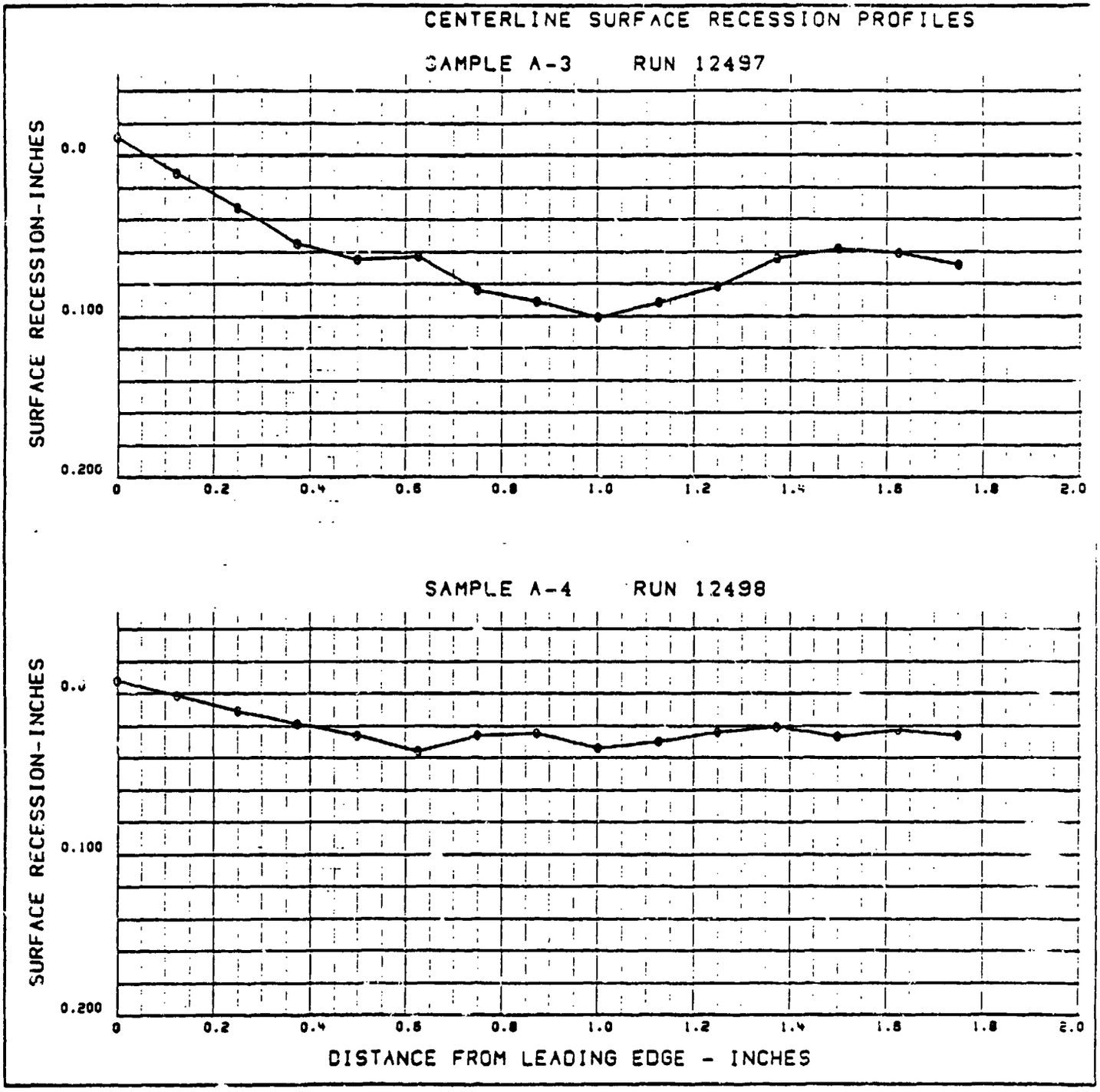

Figure 38 - Centerline Surface Recession Profiles of Models A-3 and A-4

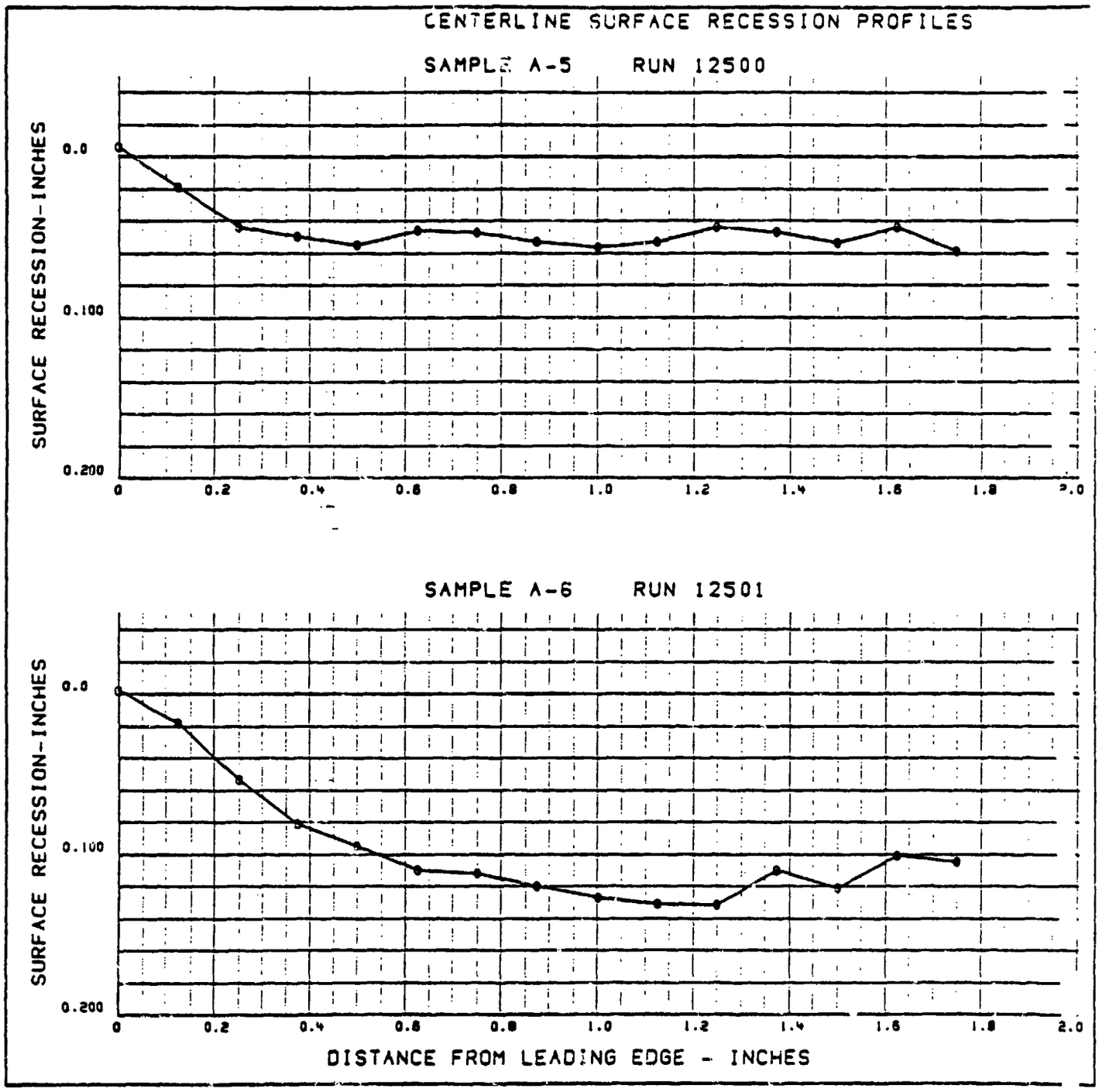

Figure 39 - Centerline Surface Recession Profiles of Models A-5 and A-6

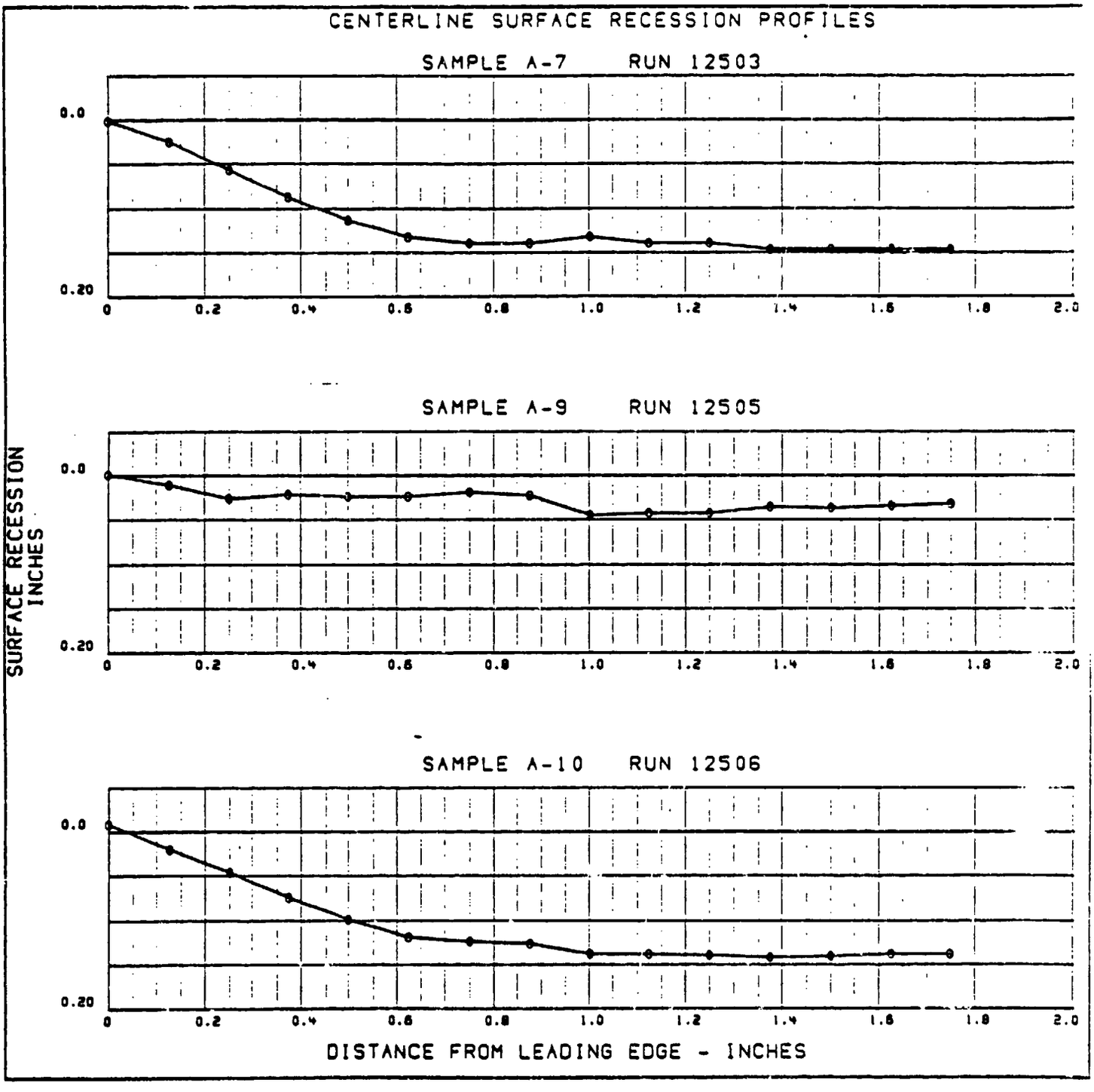

Figure 40 - Centerline Surface Recession Profiles of Models A-7, A-9 and A-10

2.3 seconds was evident while an induction time of 0.35 seconds occurred at the highest heating level.

Recession Rate Measurement Results

Data obtained from the NIKON 35mm camera enabled surface recession measurements to be obtained at the 1.25 inch model station. These film data were reduced using the Telecomputing Corporation film reader and measuring the distance from a reference plane to the test surface at the selected station. Readings so obtained are entered into a special program to obtain at least mean squares fit recession rate. Figures 41 through 49 present the results of the measurements and recession rate values. The induction time (time required to achieve steady state ablation) in all cases was significantly larger than the time required for flow to stabilize before steady-state ablation was established. Also length of test time is important in establishing a creditable recession rate as is evident in data from Run 12497 (10 sec) and Run 12498 (5 sec), Figures 43 and 44 respectively. Obviously, the greater the number of data points the more likely a more accurate measure of recession rate will result.

Surface Brightness Temperature and Surface Radiation Measurement Results

The time histories of recorded surface brightness temperature and surface radiation (1.25 inch model station) are presented in Figures 50 through 67, respectively. In general, the higher heat flux produced higher values of surface brightness temperature and surface radiation. Near steady state values of brightness temperature and surface radiation were achieved for all test environments except for the lowest test conditions. The relative smoothness of the traces also indicates no spallation or other adverse surface ablation during the test period.

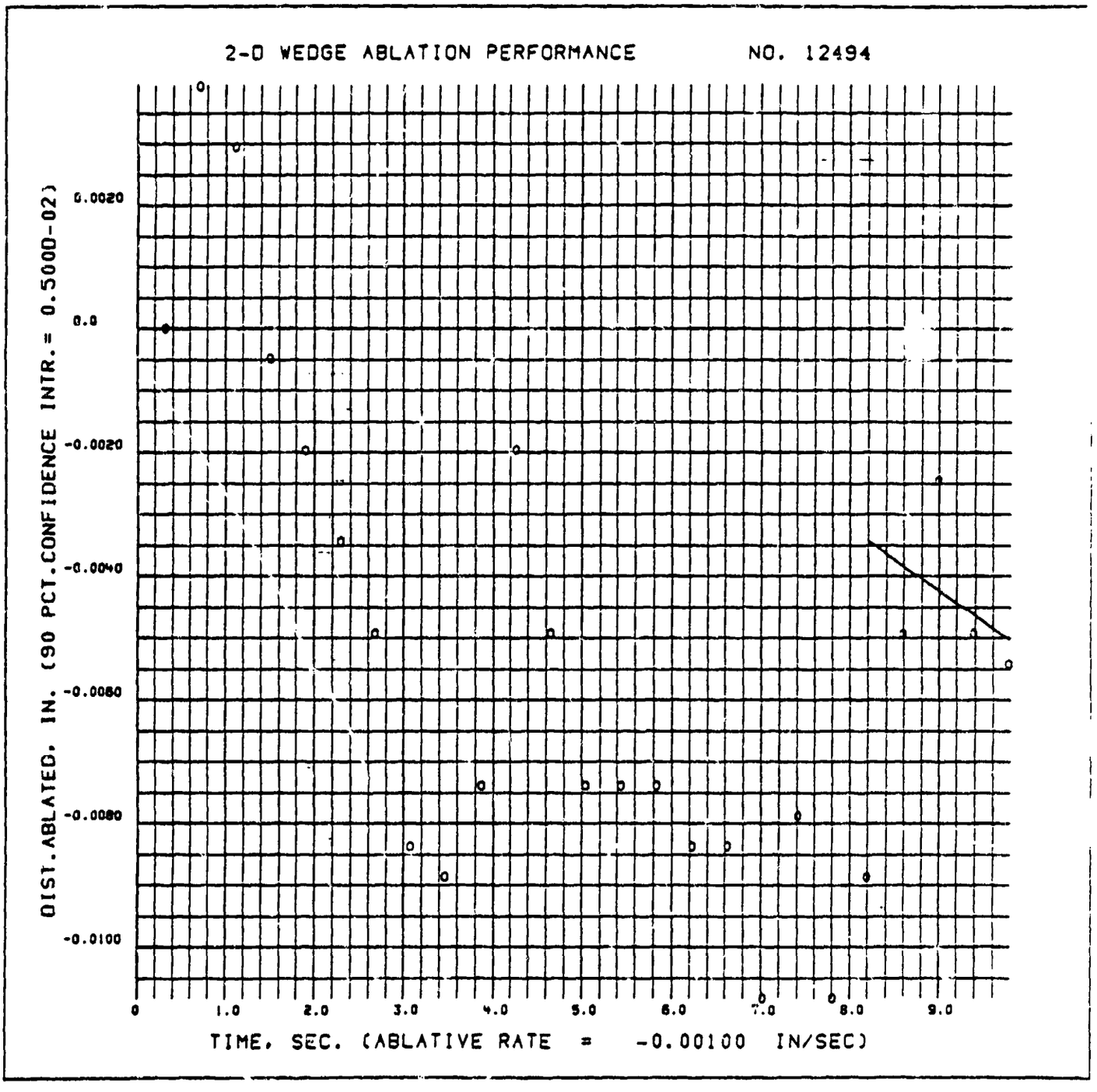

Figure 41 - Surface Recession Versus Time-Station
1.25 Inches - Model A-1

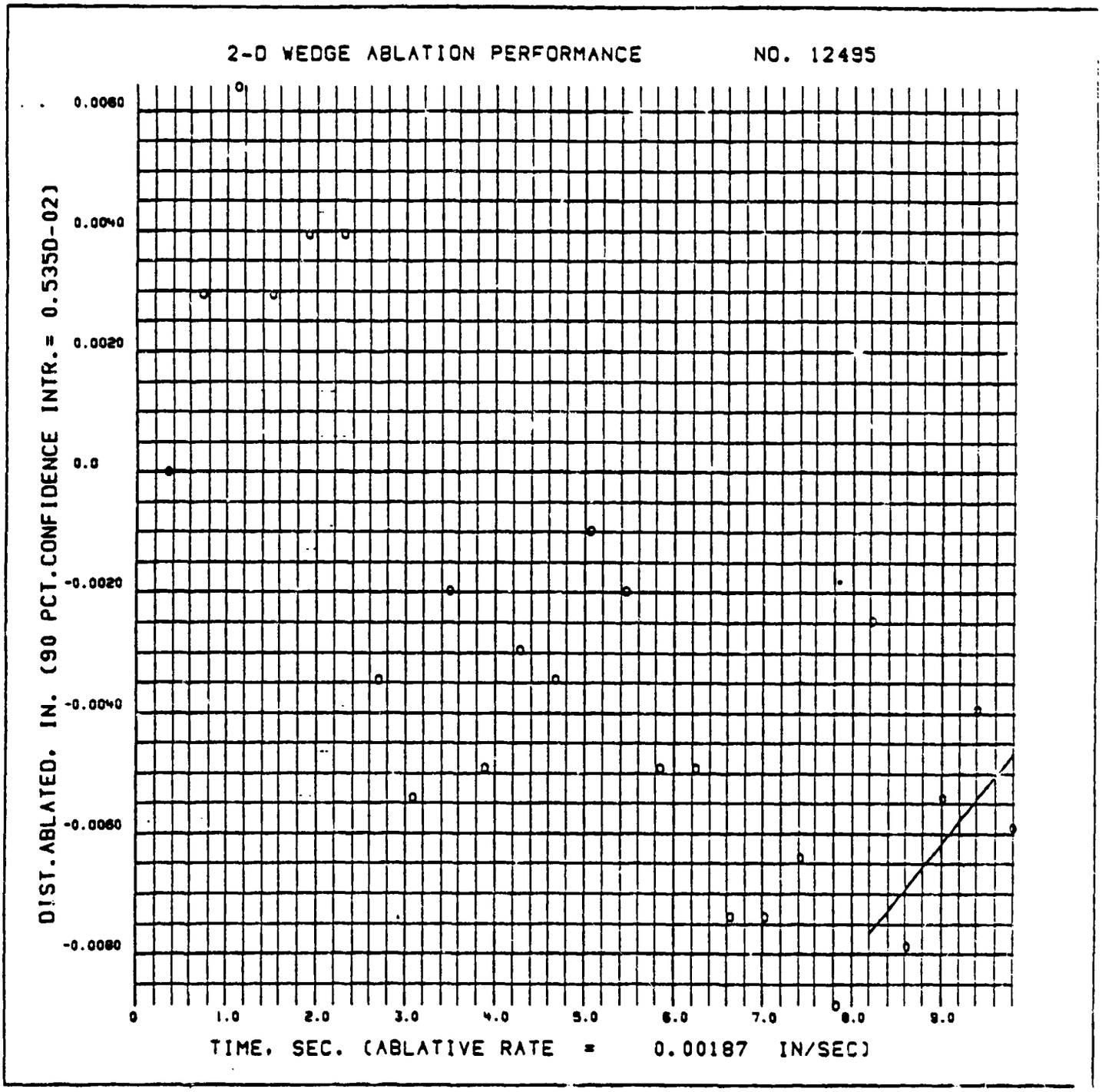

Figure 42 - Surface Recession Versus Time-Station
1.25 Inches - Model A-2

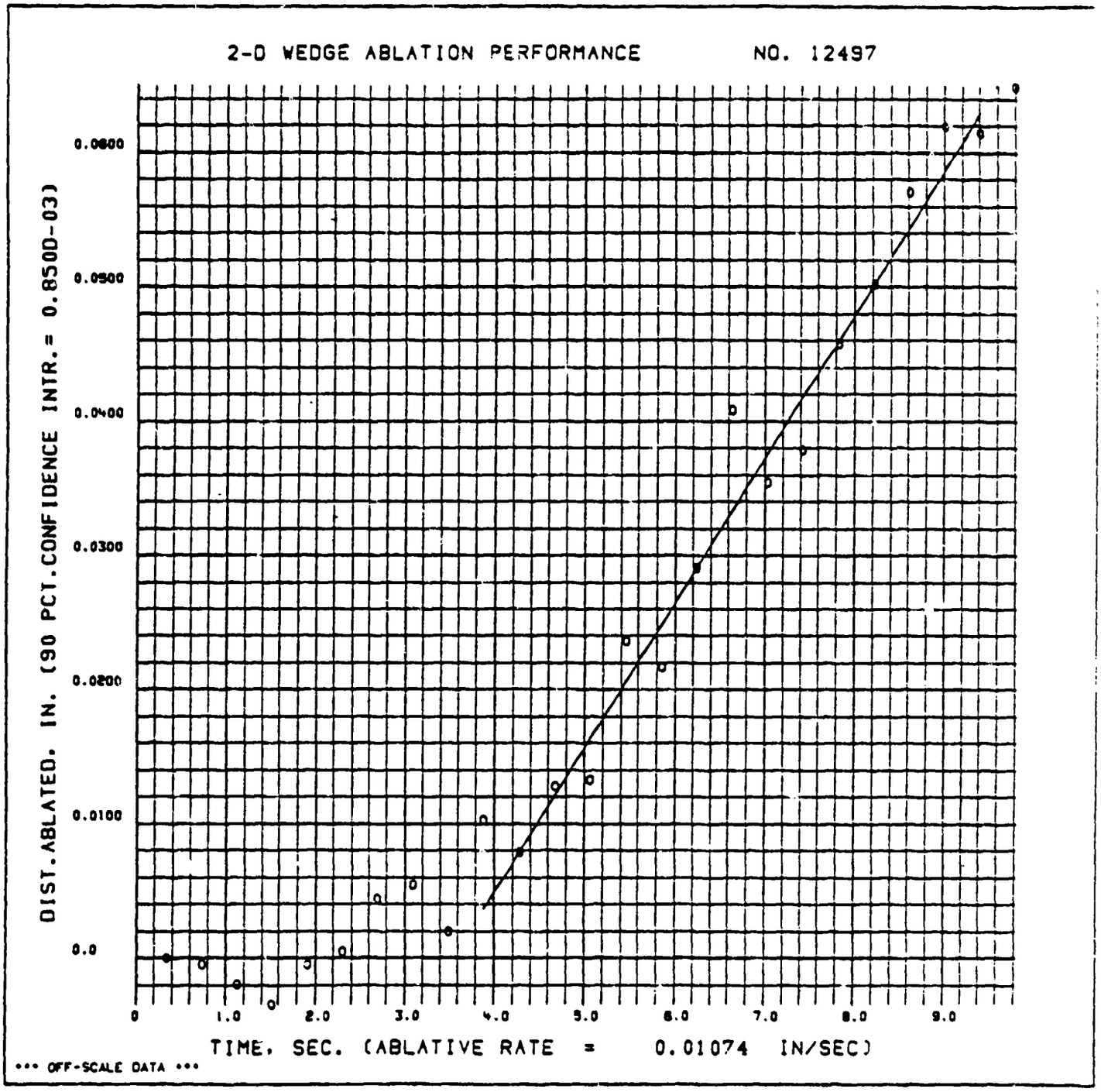

Figure 43 - Surface Recession Versus Time-Station
1.25 Inches - Model A-3

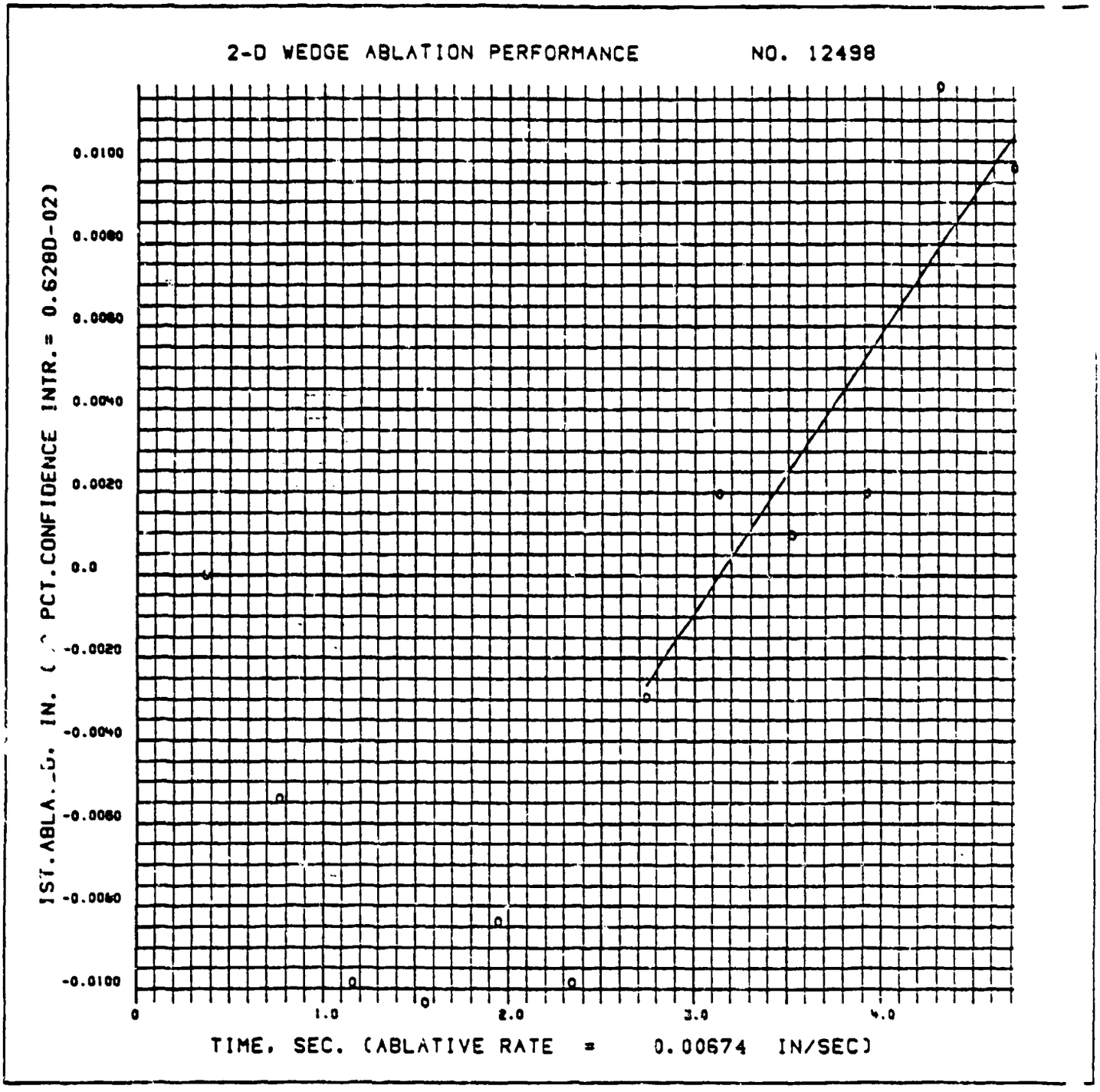

Figure 44 - Surface Recession Versus Time-Station
1.25 Inches - Model A-4

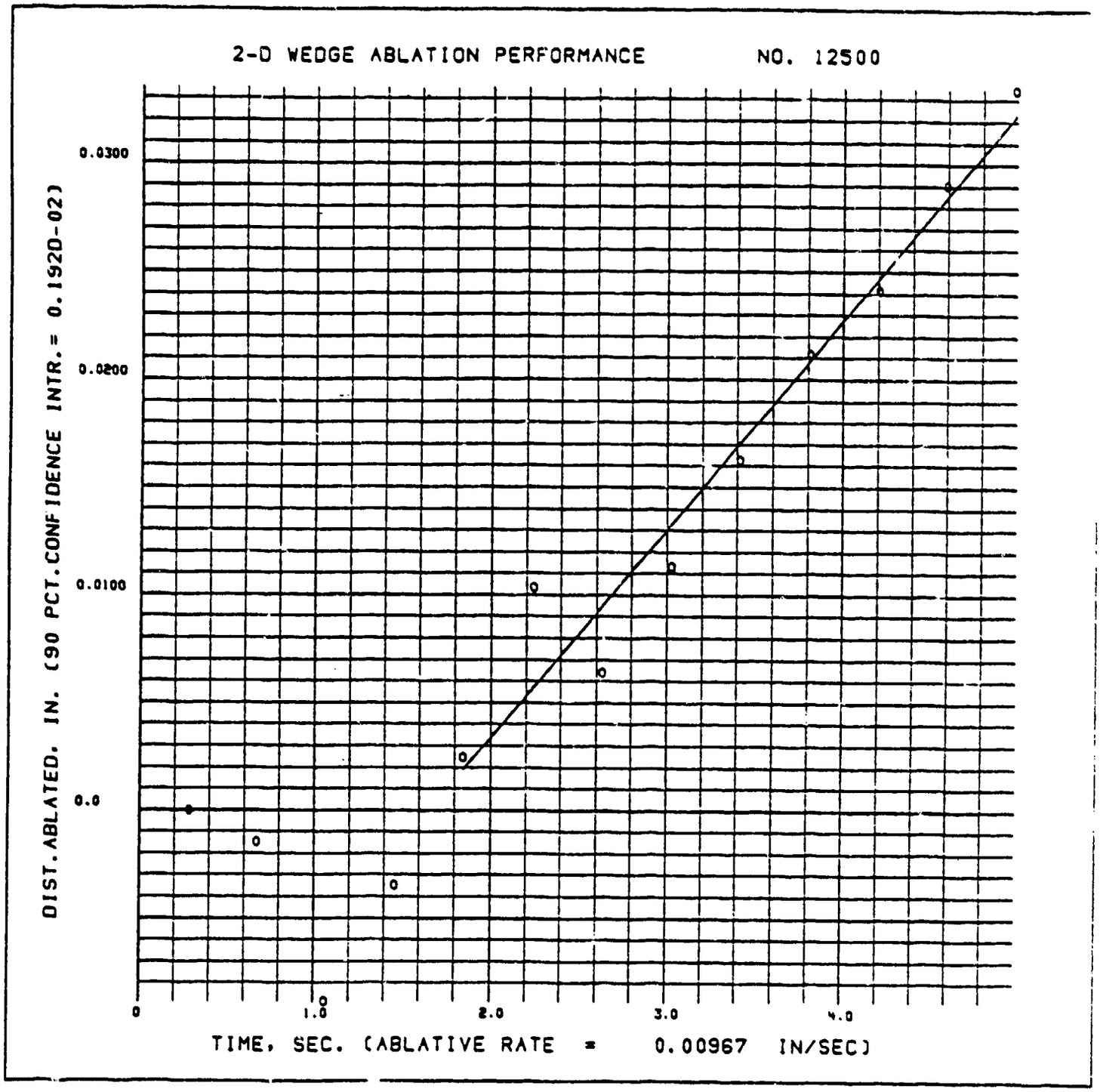

Figure 45 - Surface Recession Versus Time-Station
1.25 Inches - Model A-5

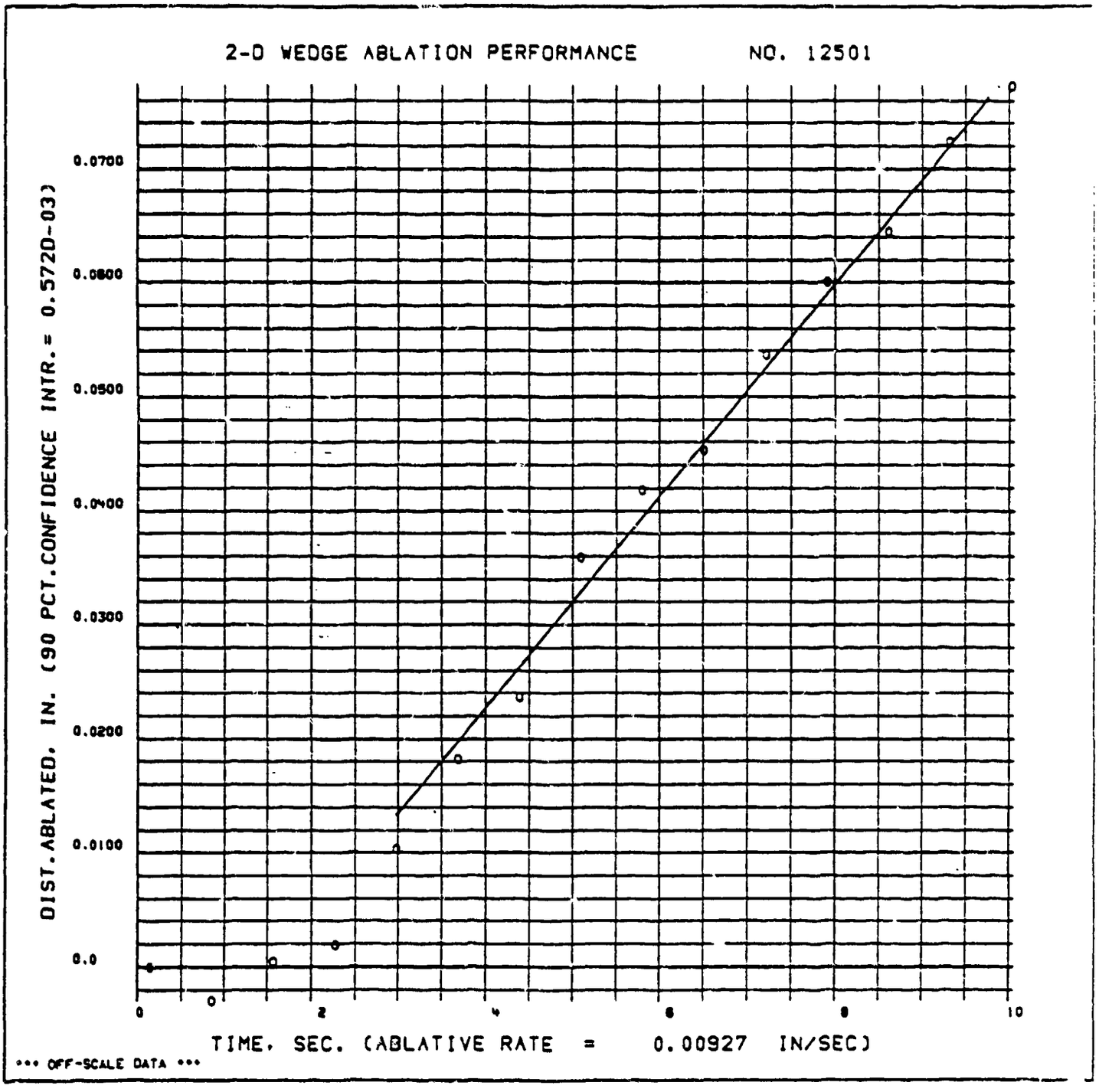

Figure 46 - Surface Recession Versus Time-Station
1.25 Inches - Model A-6

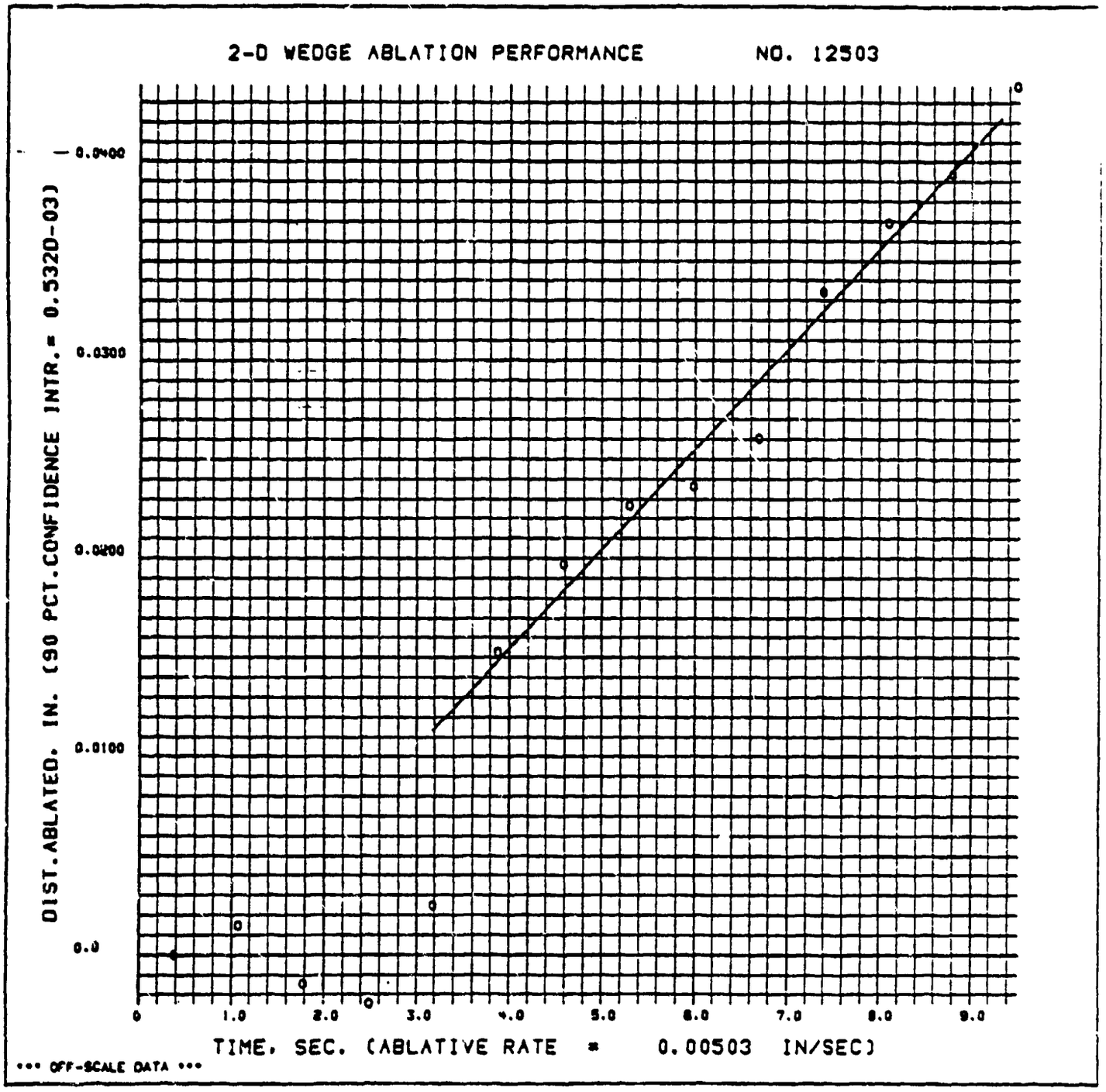

Figure 47 - Surface Recession Versus Time-Station
1.25 Inches - Model A-7

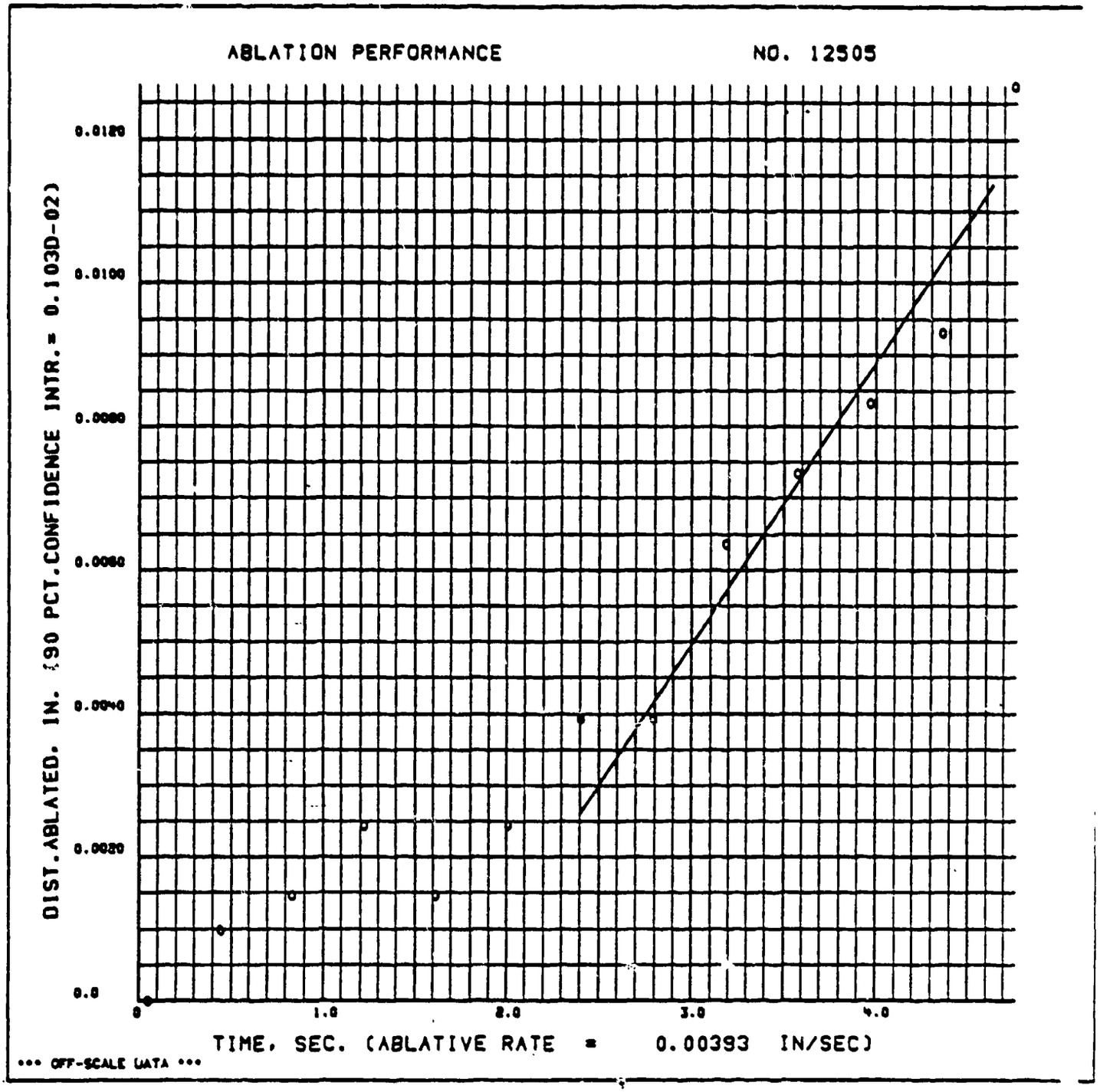

Figure 48 - Surface Recession Versus Time-Station
1.25 Inches - Model A-9

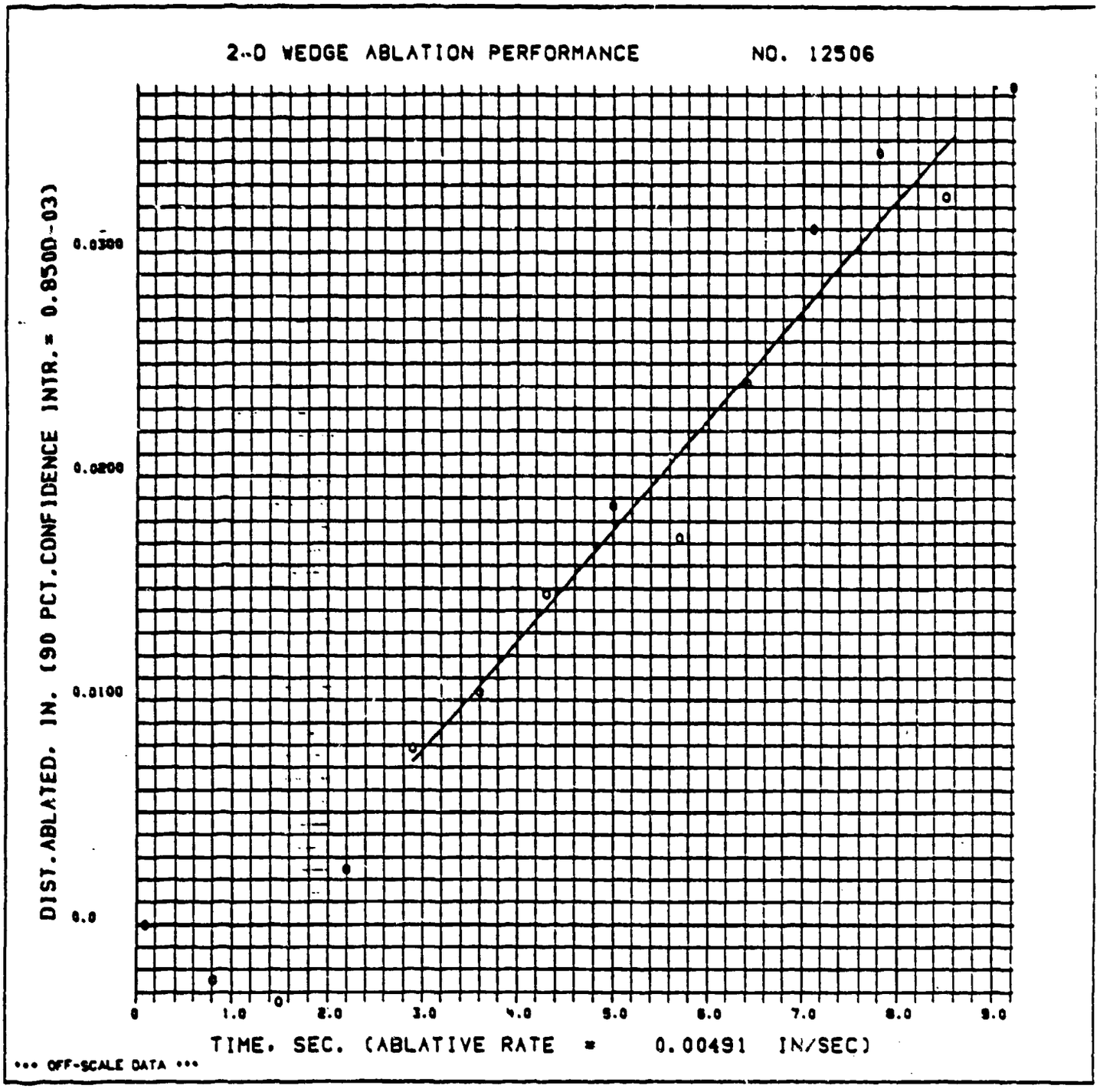

Figure 49 - Surface Recession Versus Time-Station
1.25 Inches - Model A-10

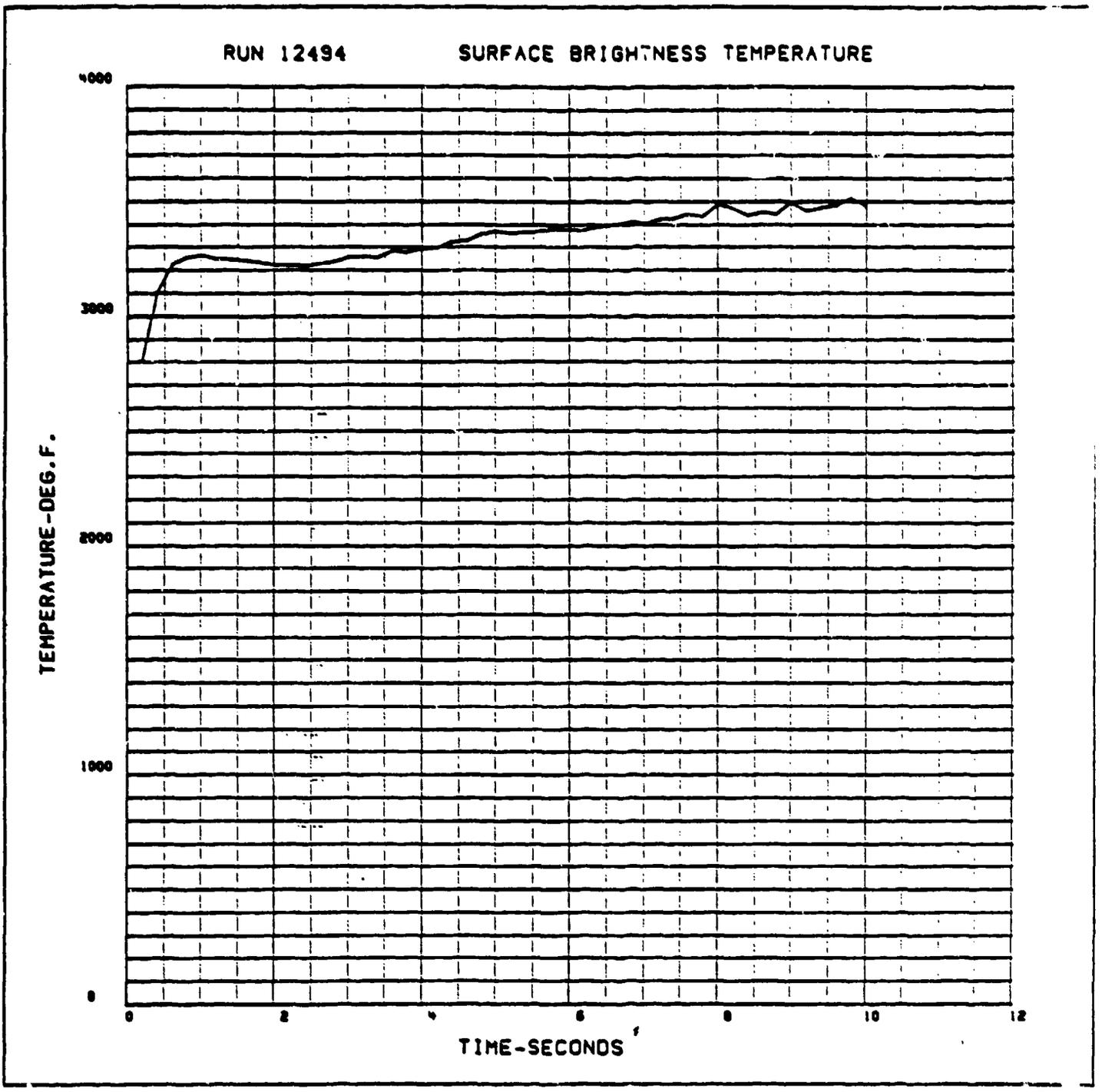

Figure 50 - Surface Brightness Temperature Versus Time
Model A-1

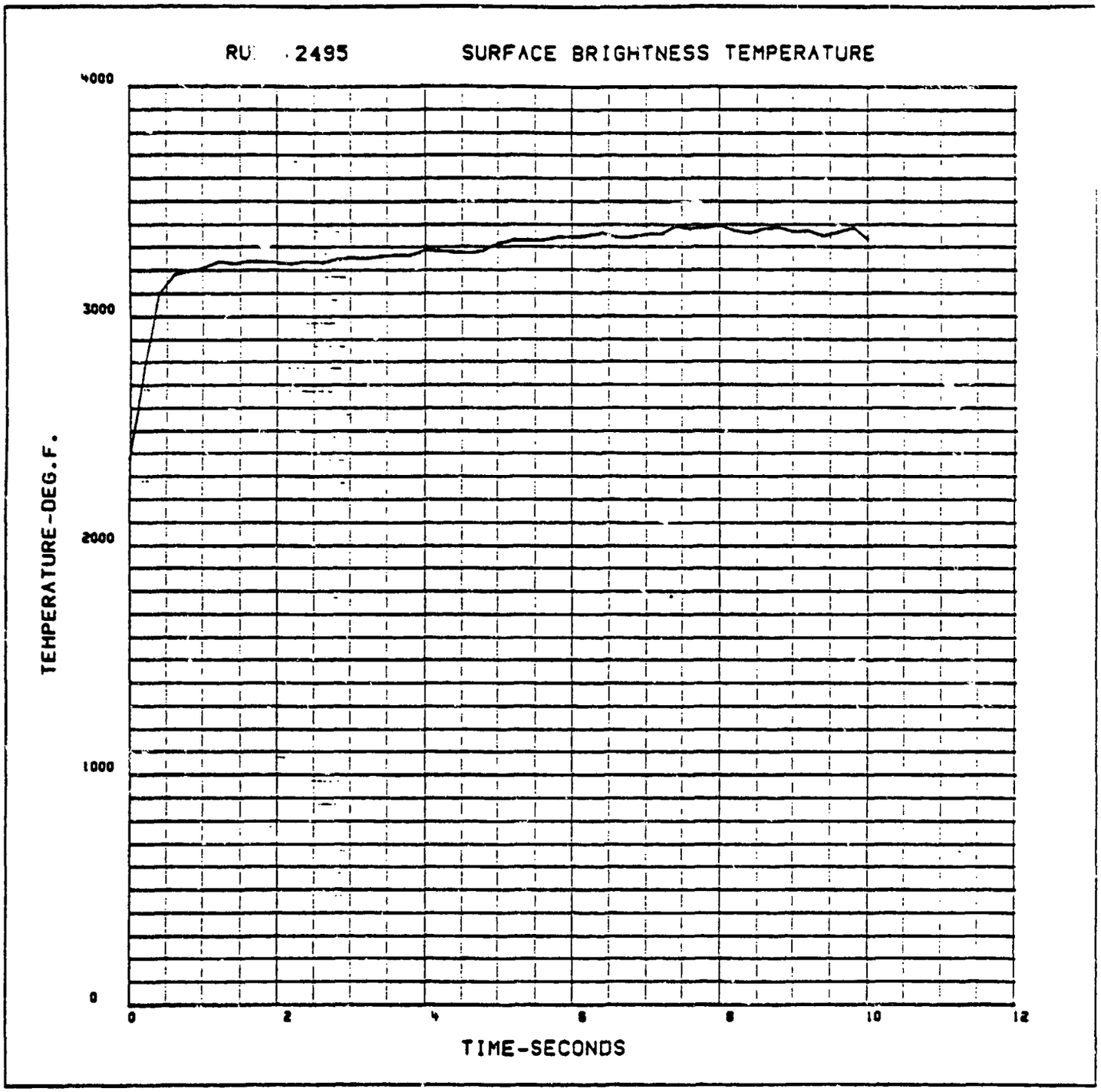

Figure 51 - Surface Brightness Temperature Versus Time
Model A-2

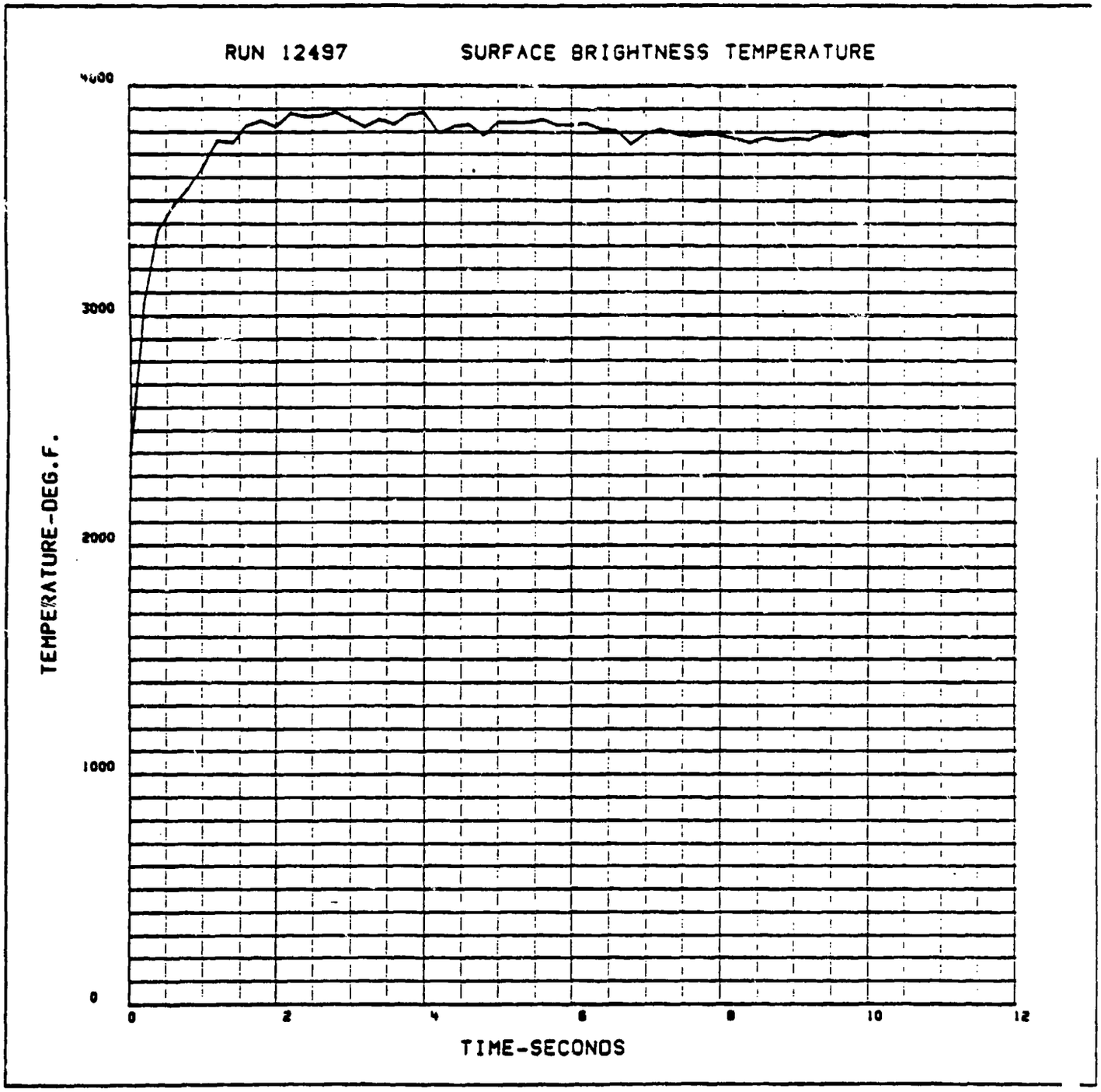

Figure 52 - Surface Brightness Temperature Versus Time
Model A-3

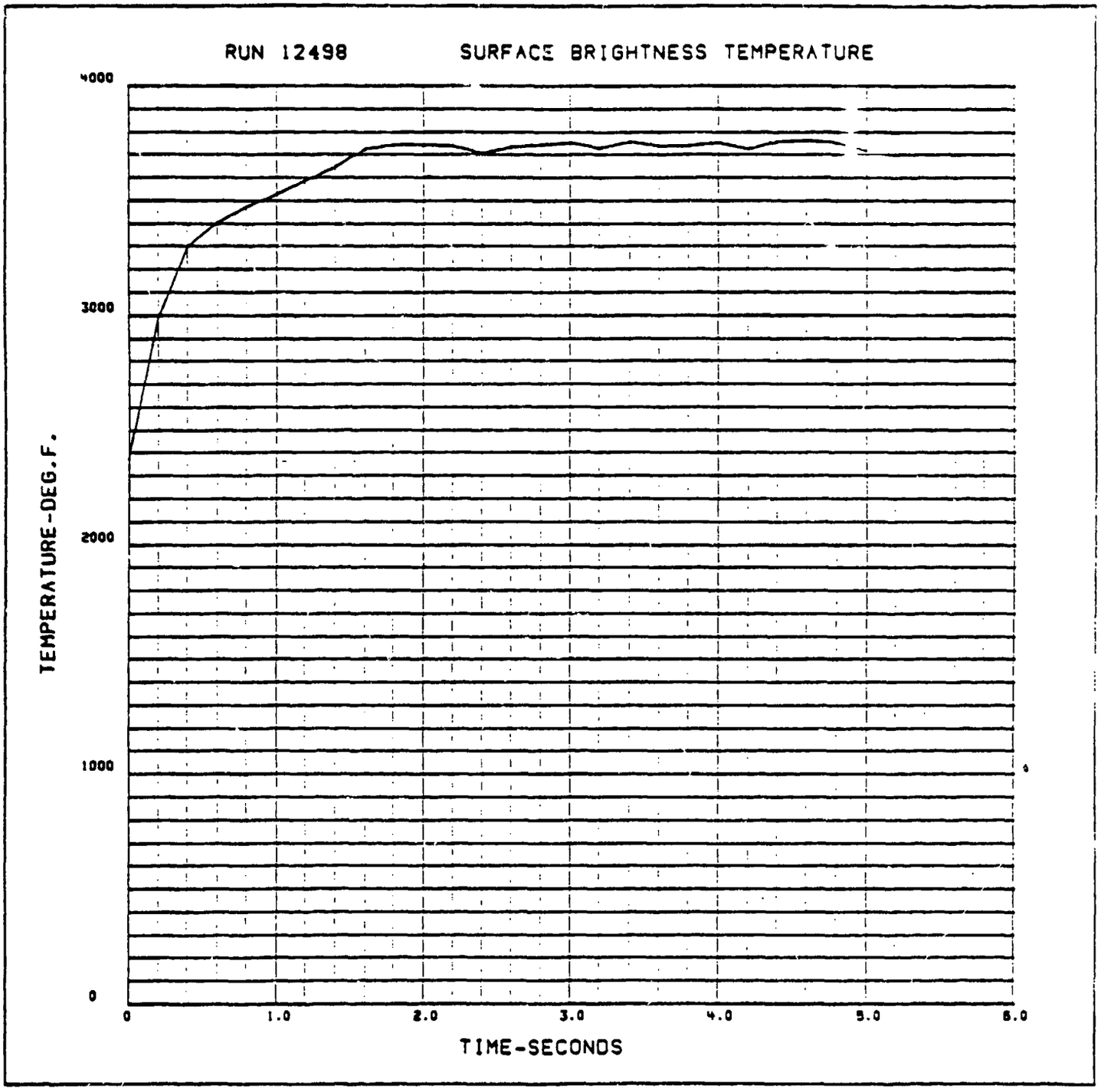

Figure 53 - Surface Brightness Temperature Versus Time
Model A-4

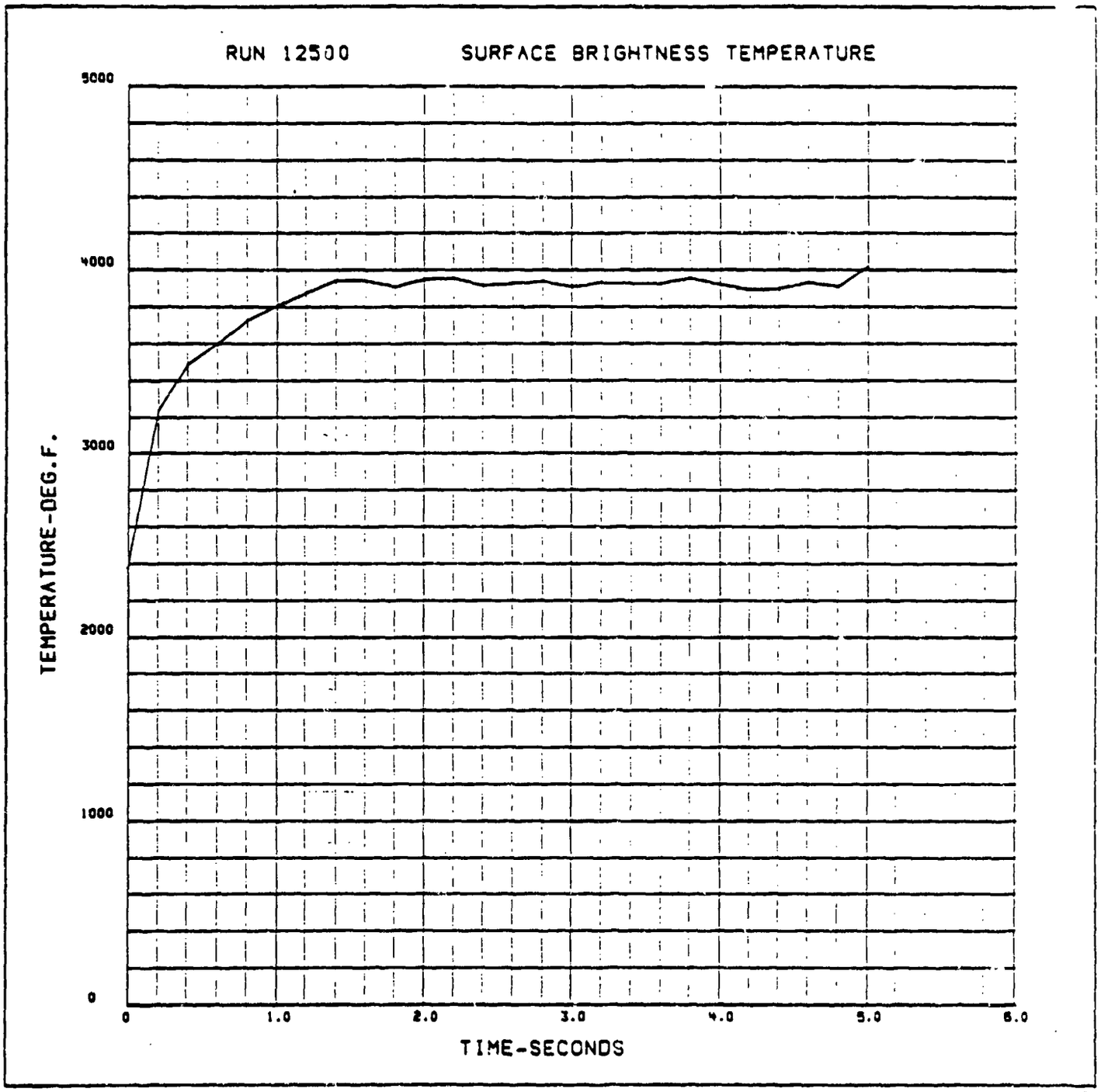

Figure 54 - Surface Brightness Temperature Versus Time
Model A-5

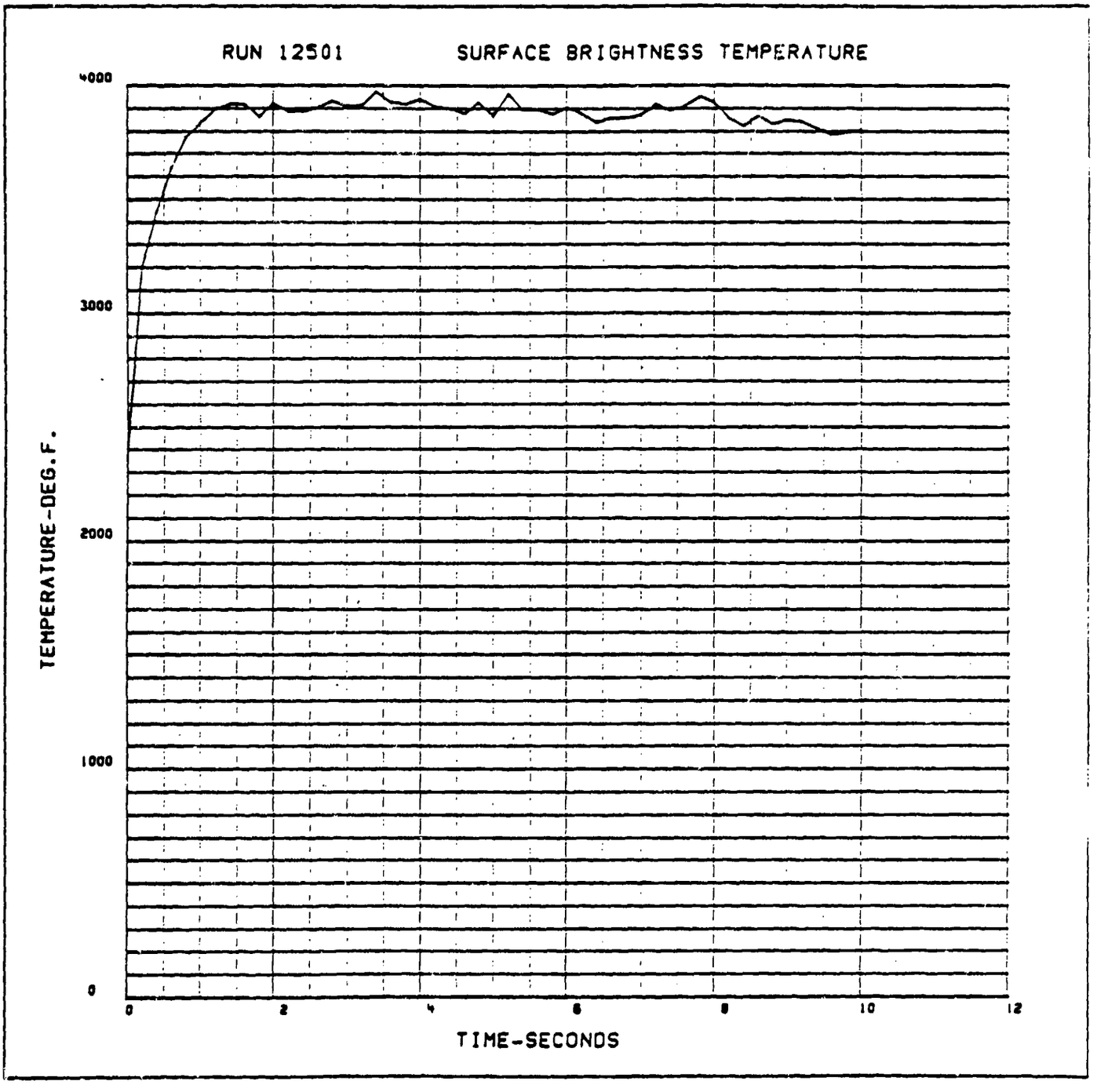

Figure 55 - Surface Brightness Temperature Versus Time
Model A-6

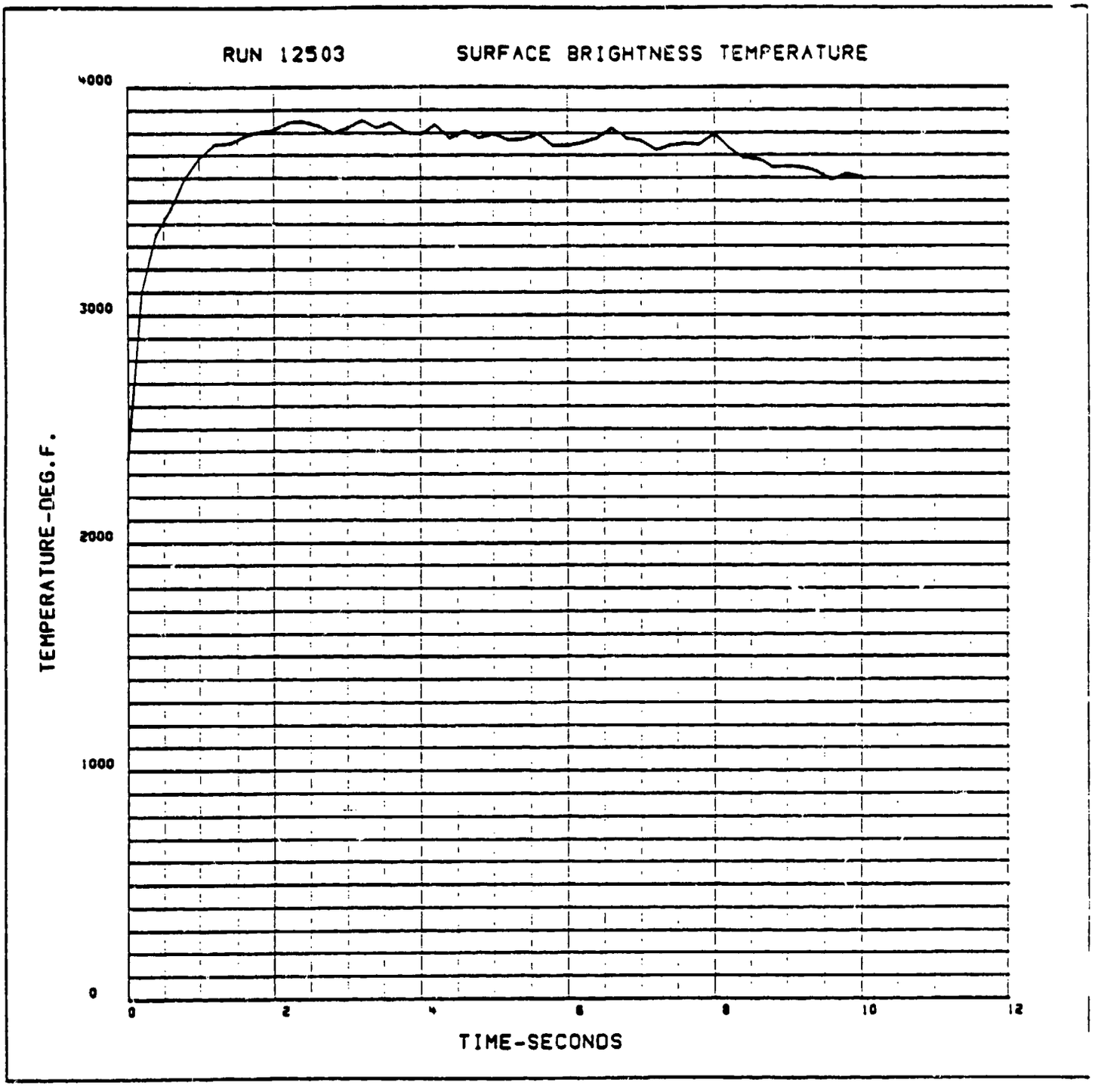

Figure 56 - Surface Brightness Temperature Versus Time
Model A-7

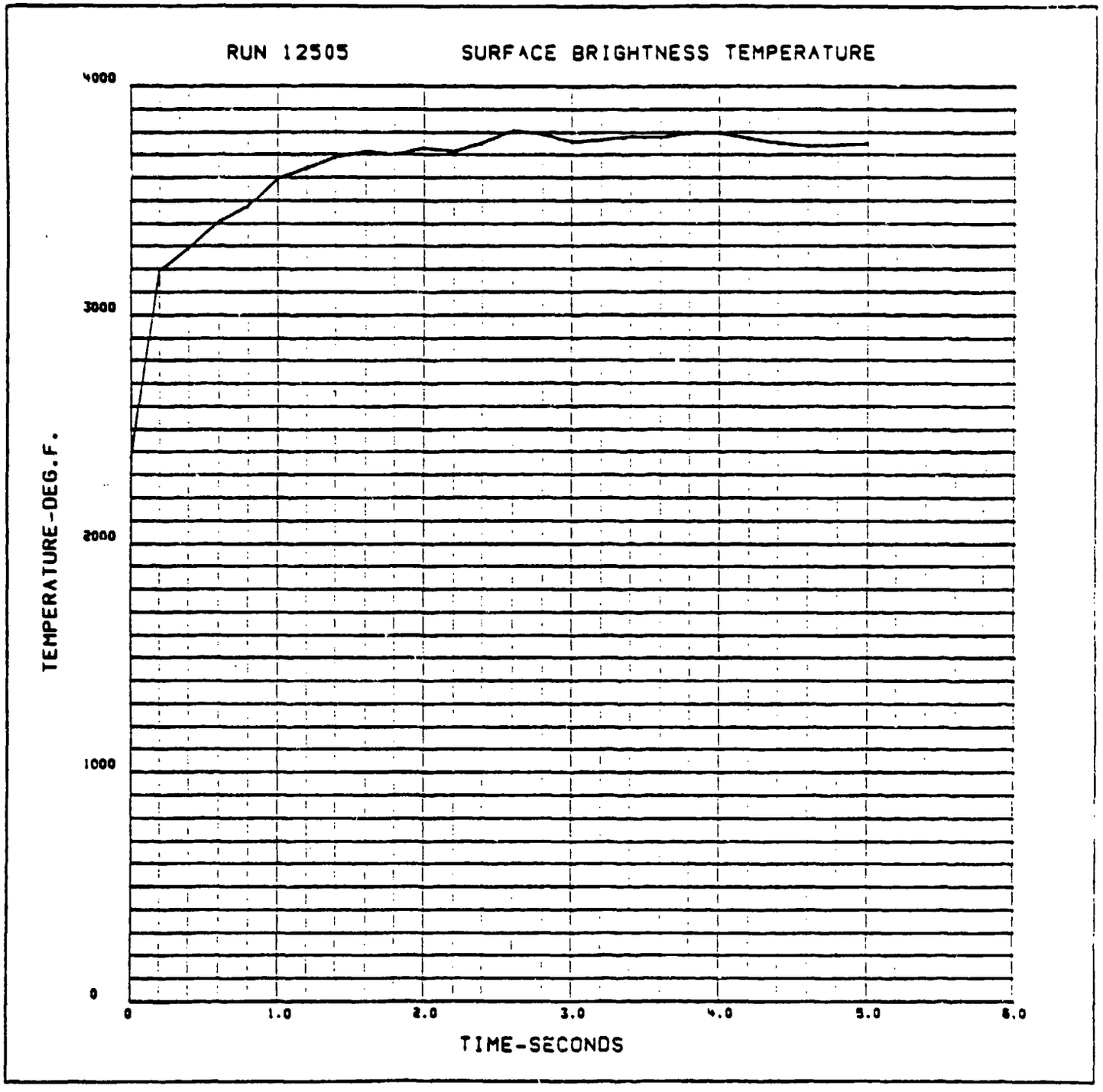

Figure 57 - Surface Brightness Temperature Versus Time
Model A-9

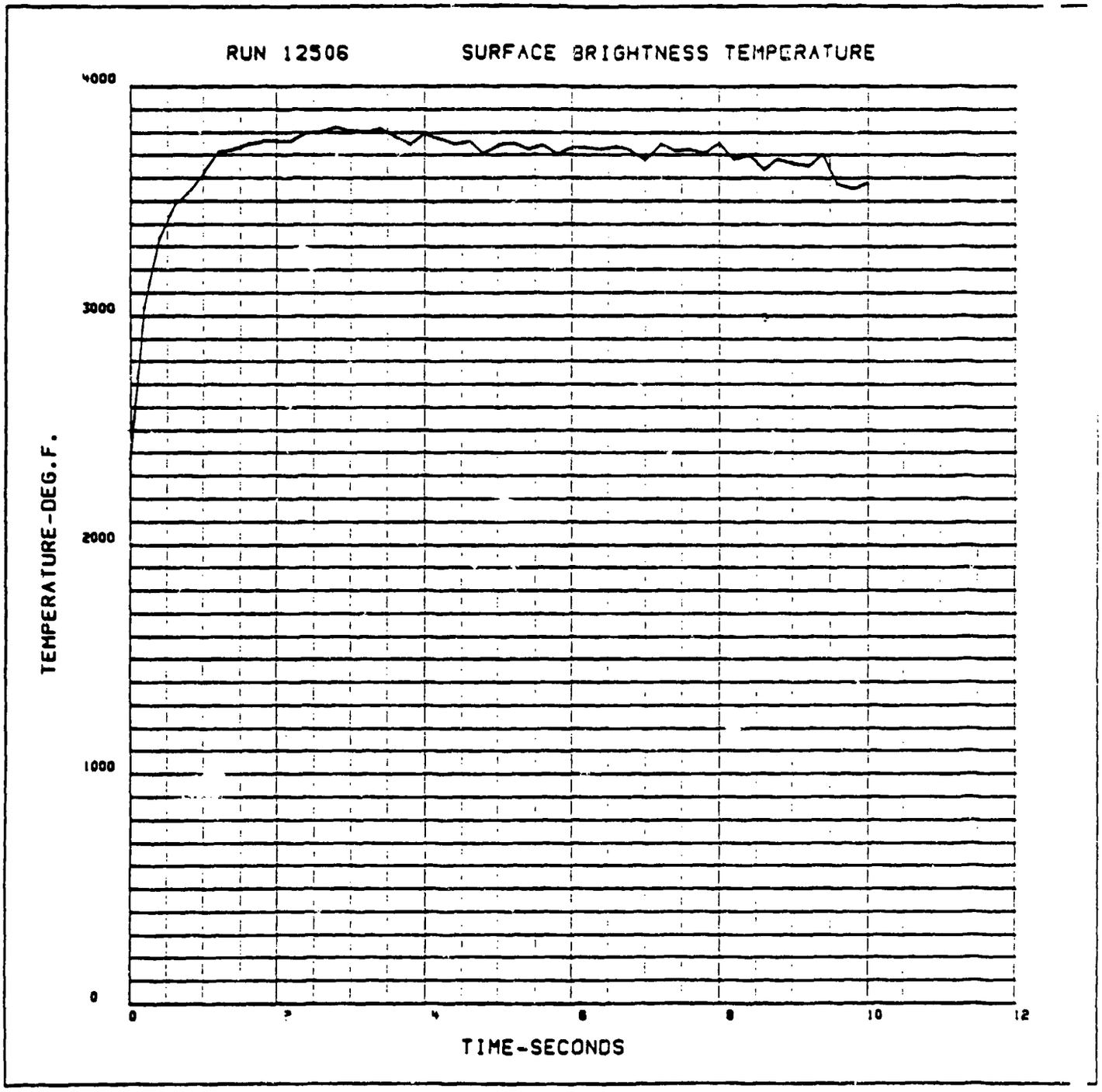

Figure 5(- Surface Brightness Temperature Versus Time
Model A-10

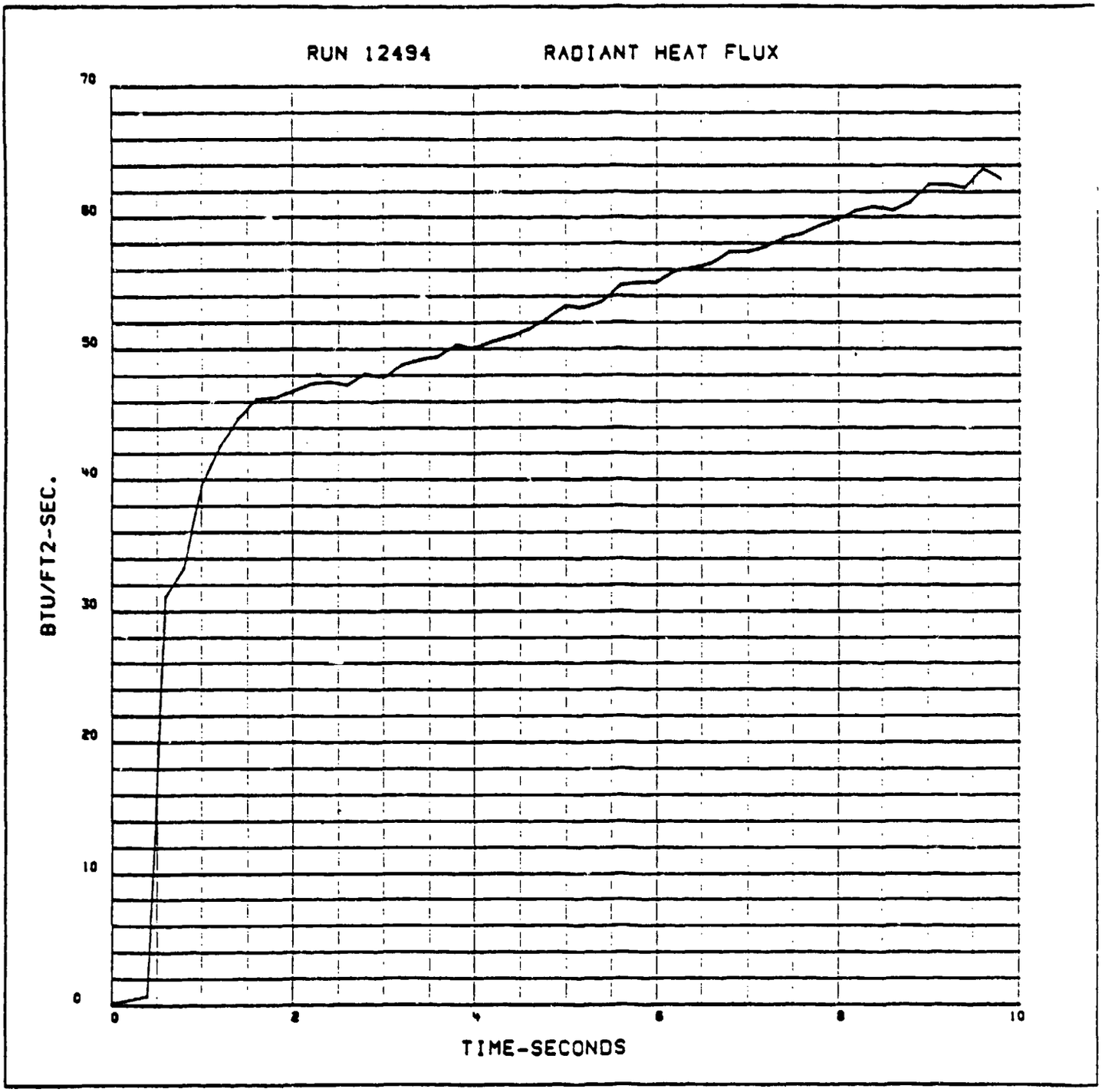

Figure 59 - Surface Radiation Versus Time
Model A-1

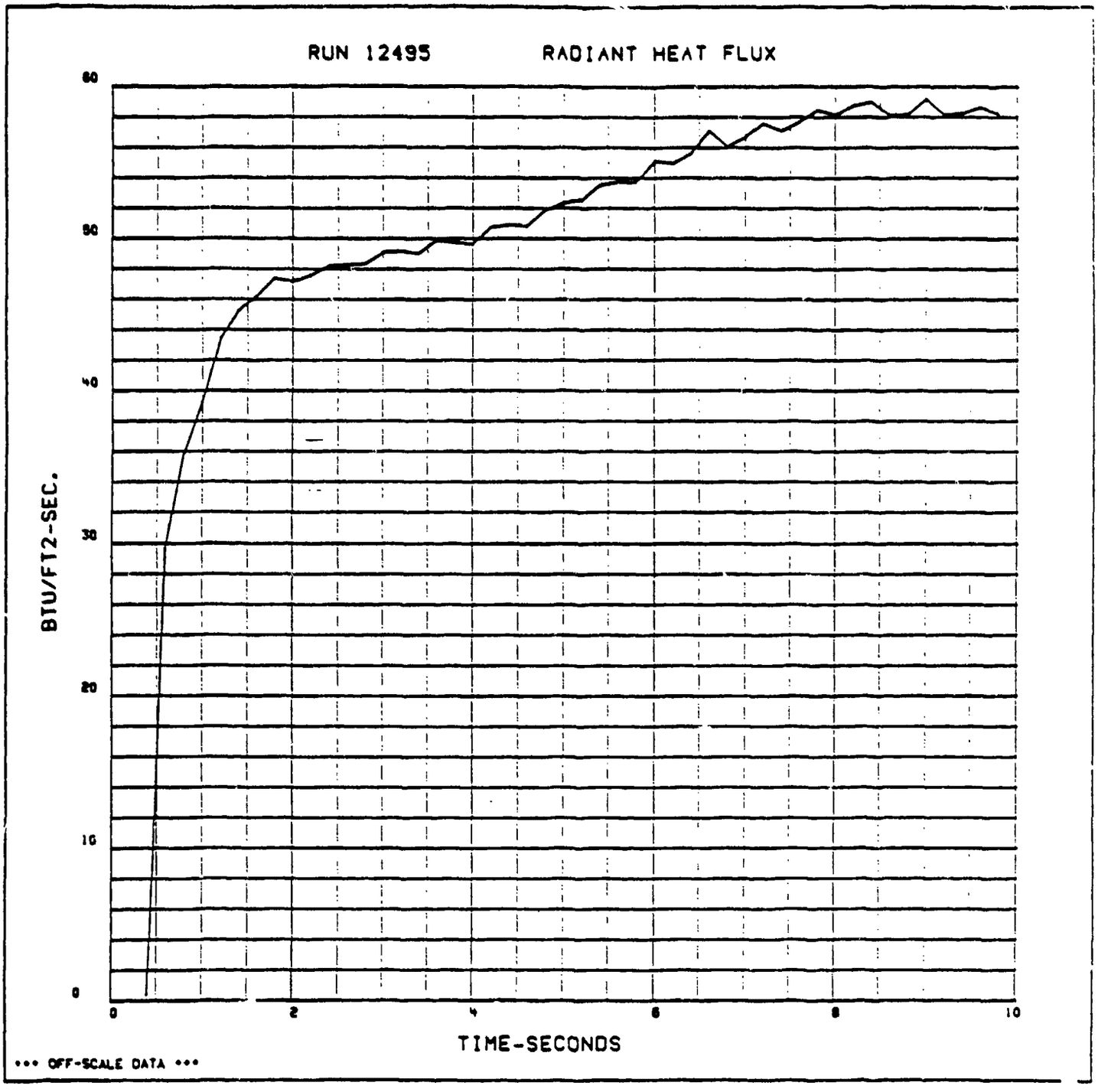

Figure 60 - Surface Radiation Versus Time
Model A-2

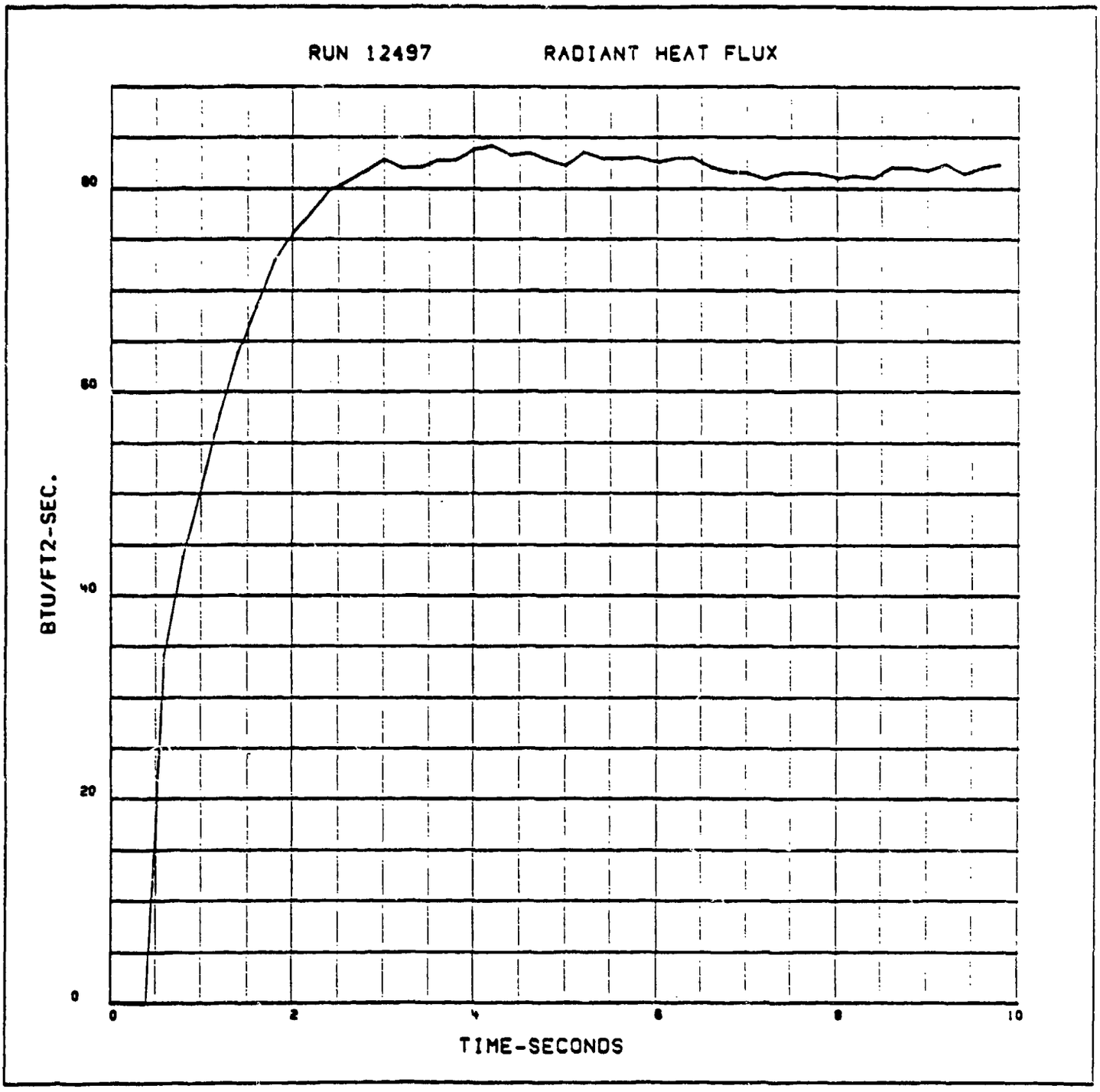

Figure 61-Surface Radiation Versus Time - Model A-3

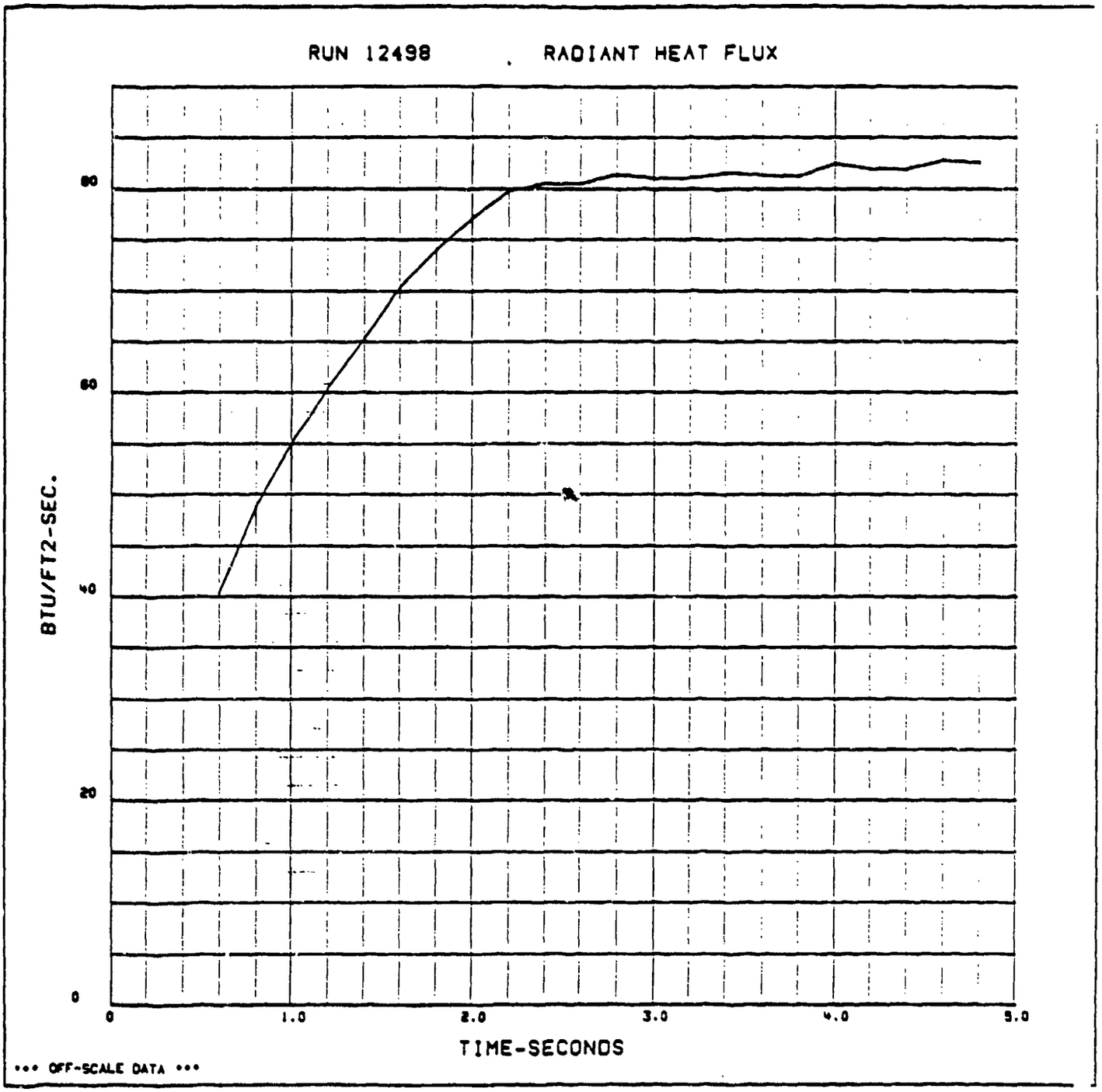

Figure 62 - Surface Radiation Versus Time - Model A-4

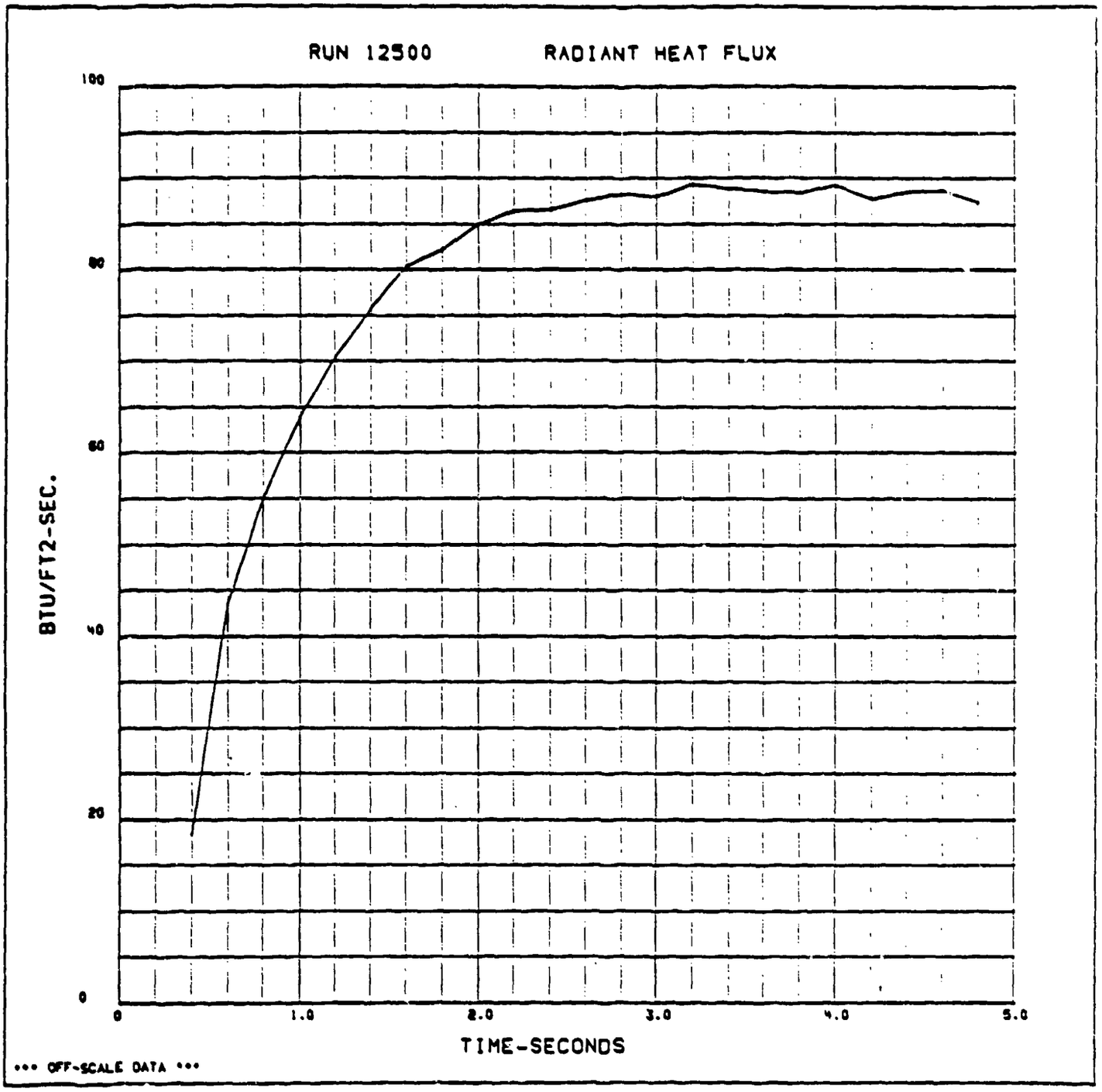

Figure 63 - Surface Radiation Versus Time - Model A-5

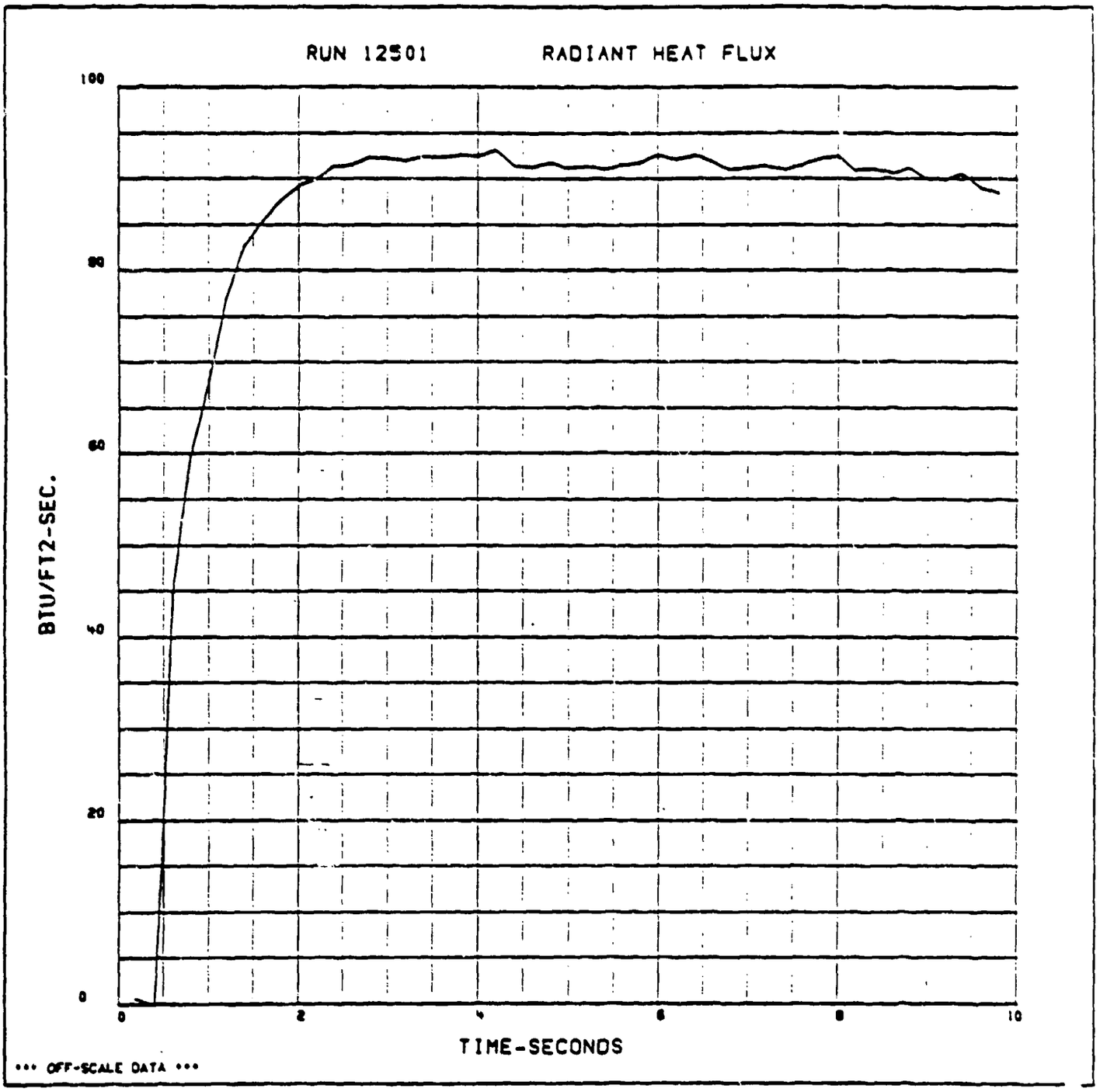

Figure 64 - Surface Radiation Versus Time - Model A-6

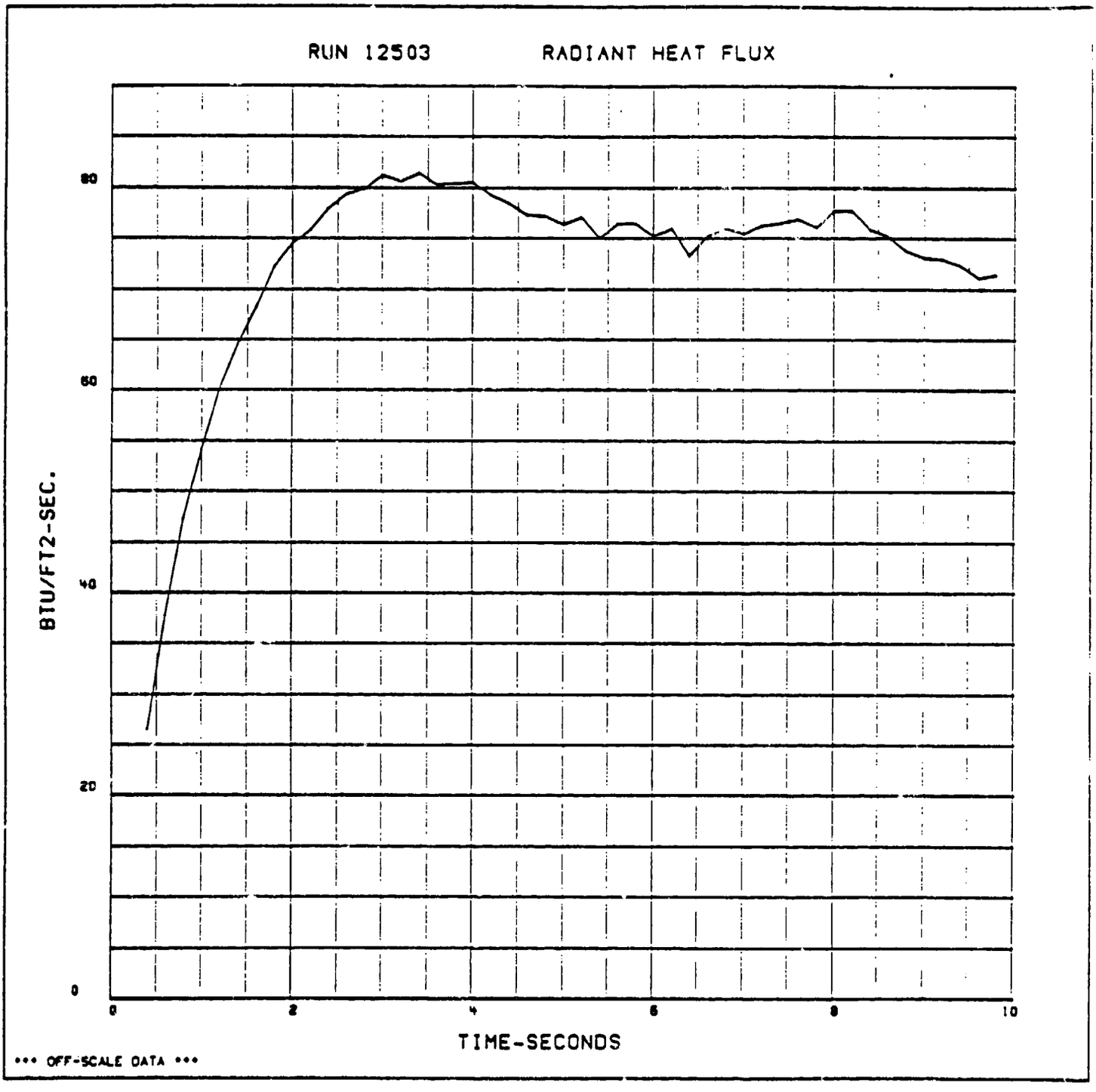

Figure 65 - Surface Radiation Versus Time - Model A-7

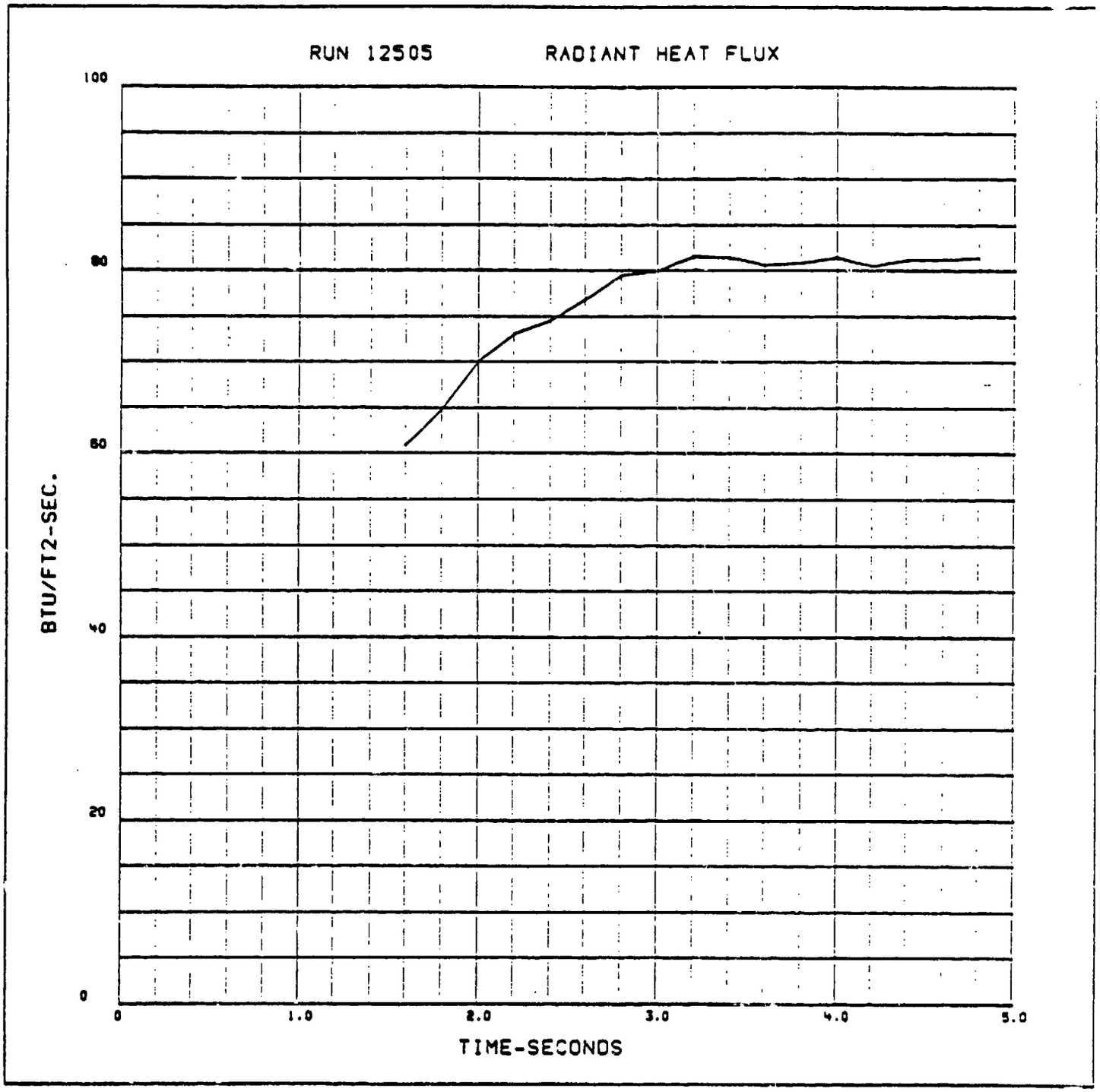

Figure 66- Surface Radiation Versus Time - Model A-9

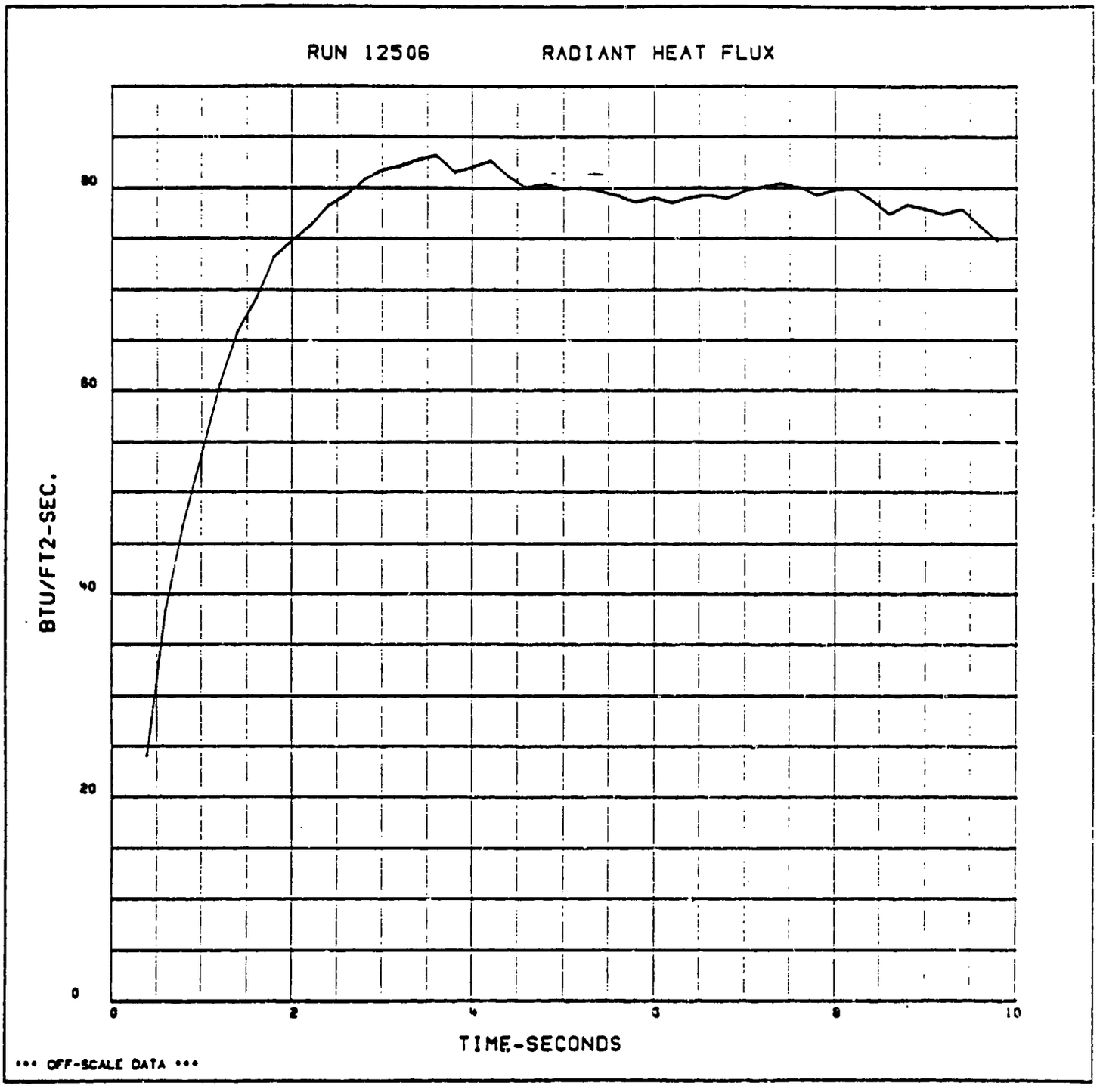

Figure 67 - Surface Radiation Versus Time - Model A-10

Rear Surface Temperature Measurement Results

As shown in Figure 22, each model was instrumented with a chromel-alumel thermocouple located on the back side of the model at the 1.25 inch model station. Although temperature data were obtained in all test runs, it was apparent from some traces that hot gas had contacted the back side material and produced a small (20°F) temperature response during the heating portion of the test. As a consequence, some of the recorded data are in error and are not reproduced. Those data which are considered reliable are shown in Figures 68 to 72. In general, the back side temperature response was negligible during the heating cycle. The only temperature response occurred well into the cool down or soak cycle. The material is essentially an insulator having a low thermal diffusivity. It might be noted that the gas leakage that occurred developed at the trailing edge of the model where a gap existed in the holder because the model length was shorter than normal. The gap was filled with a silica phenolic material (butted against the model's trailing edge) which apparently permitted a small quantity of hot gas to infiltrate to the base of the model and produce a small temperature increase on the rear surface on some of the models.

5.2 Erosion Testing

Six (6) single particle impact tests were conducted: Two (2) in the virgin and four (4) in the charred material state. Two impact angles were employed (10 and 20 degrees) using a glass particle fired at nominally 8 kft/sec. The test series provided the following comparative data:

- o Pre and post test mass
- o Post test photographs

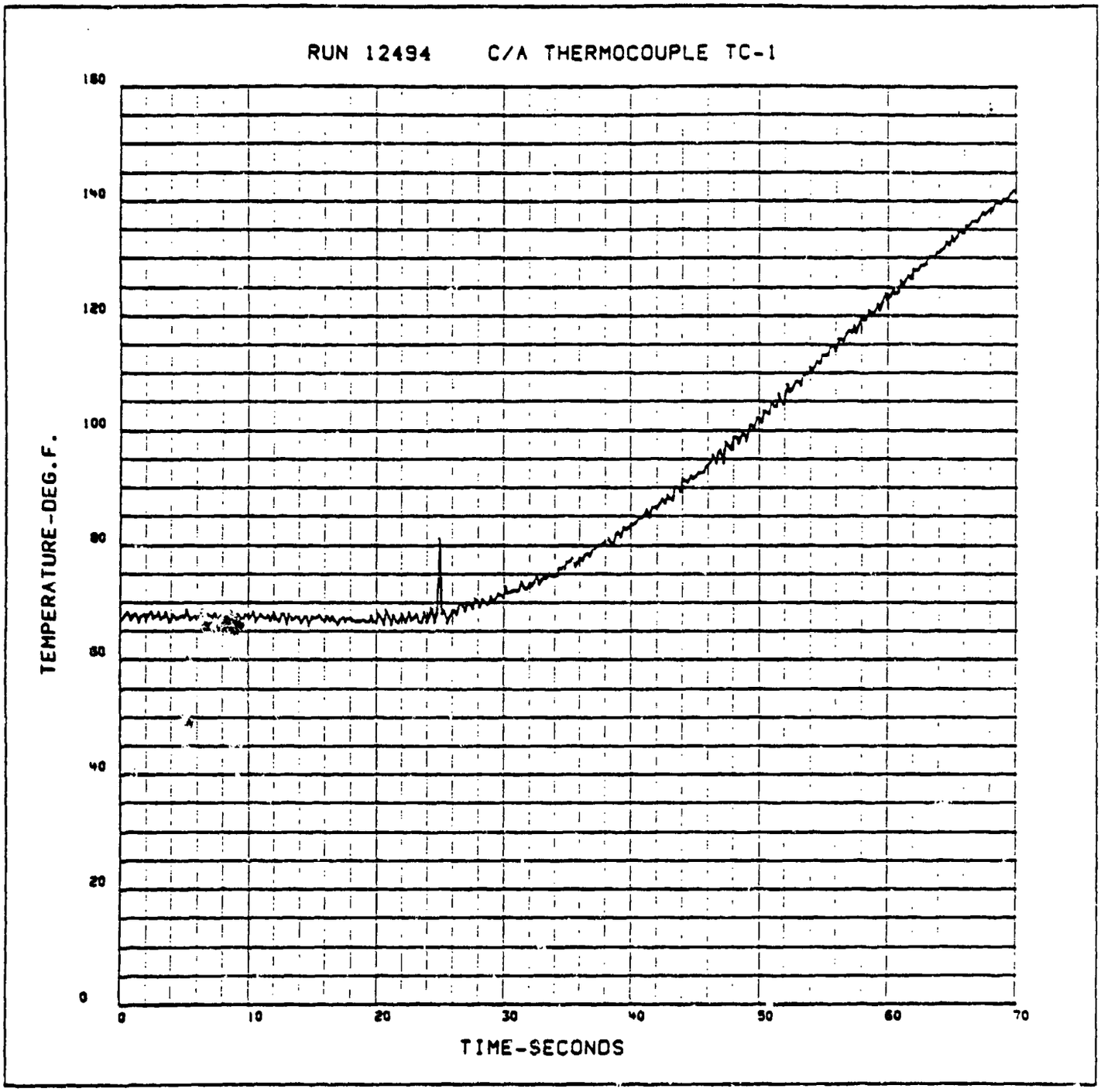

Figure 68 - Rear Surface Temperature Versus Time - Model A-1

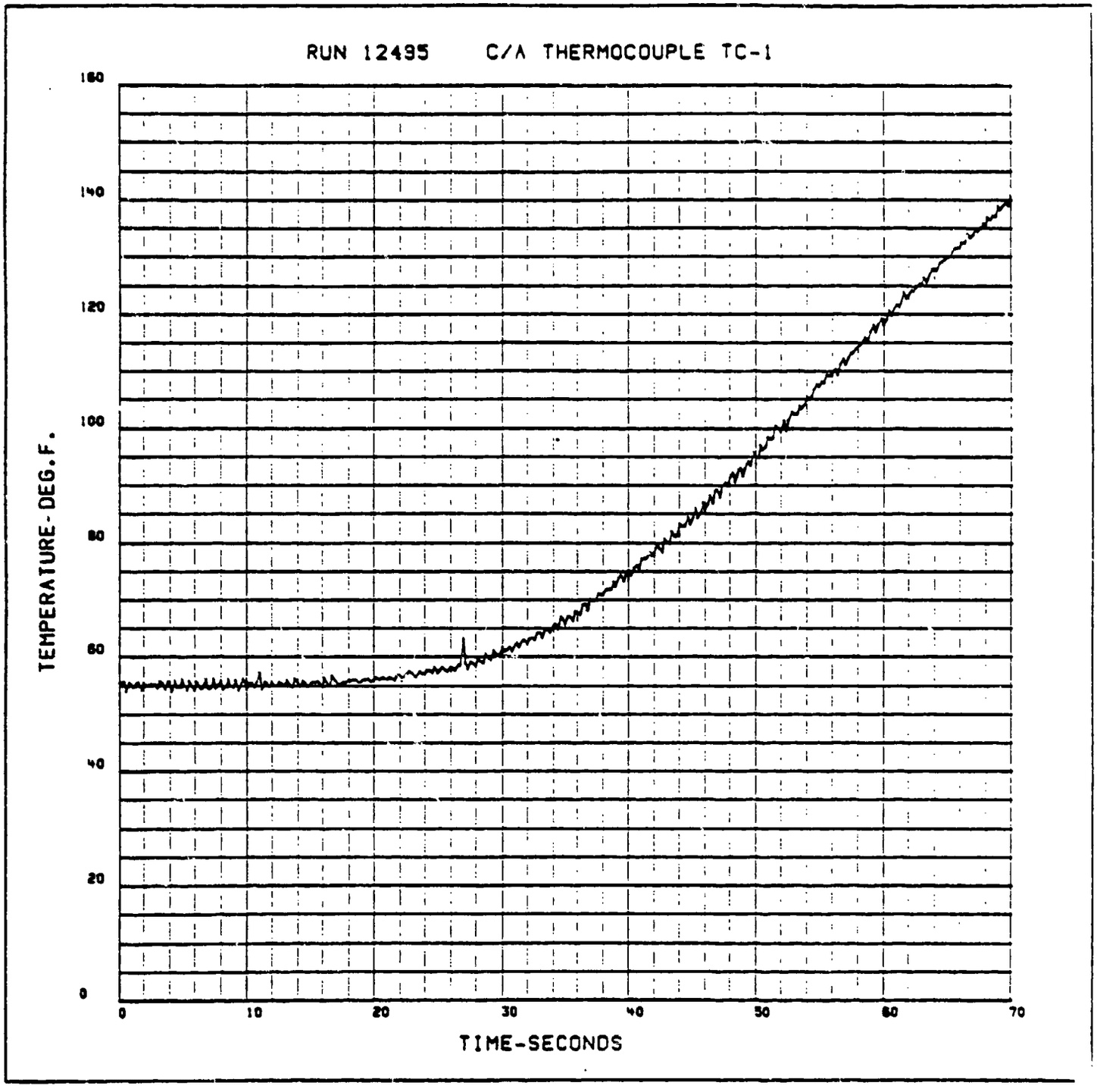

Figure 69 - Rear Surface Temperature Versus Time - Model A-2

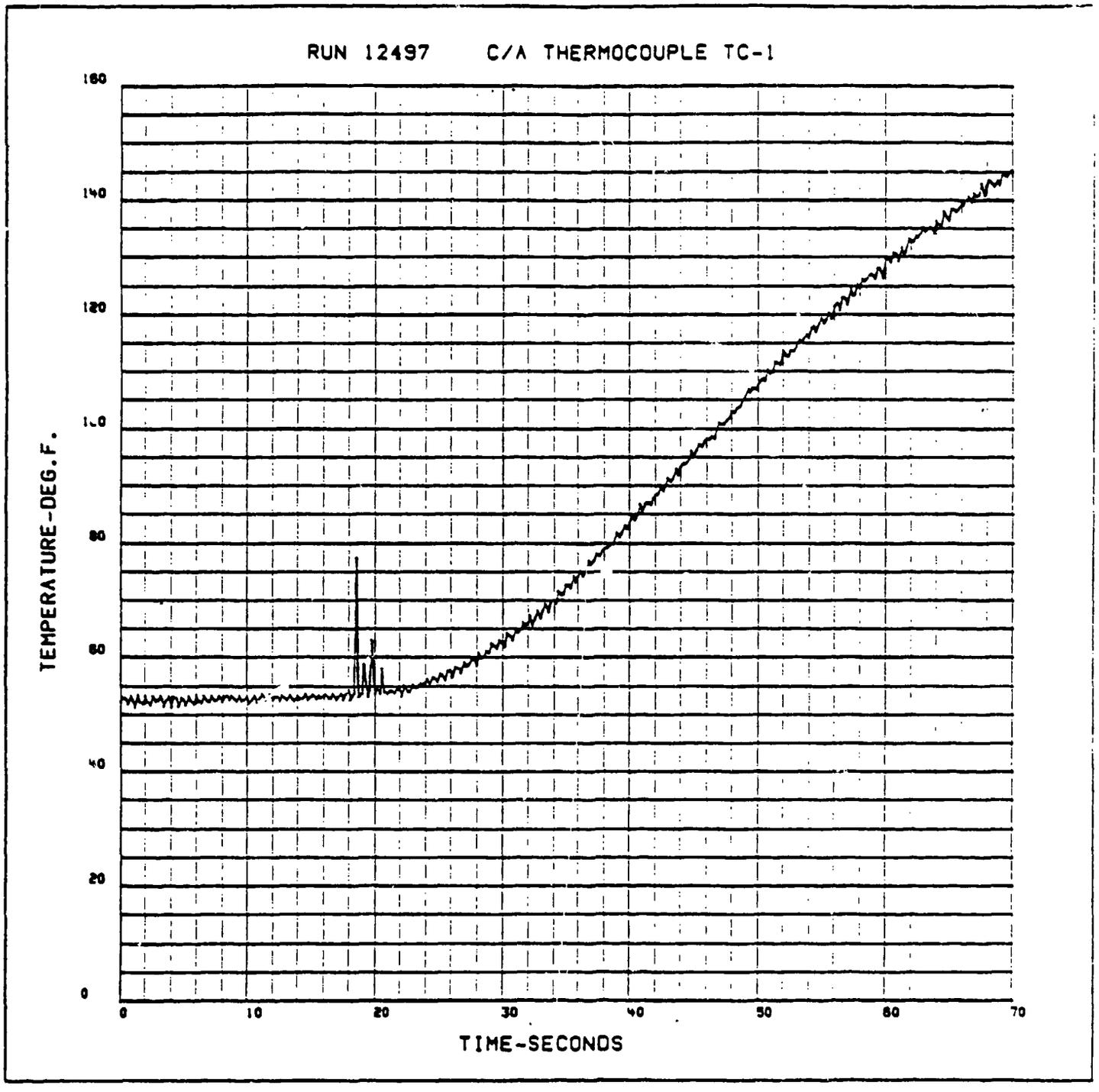

Figure 70 - Rear Surface Temperature Versus Time - Model A-3

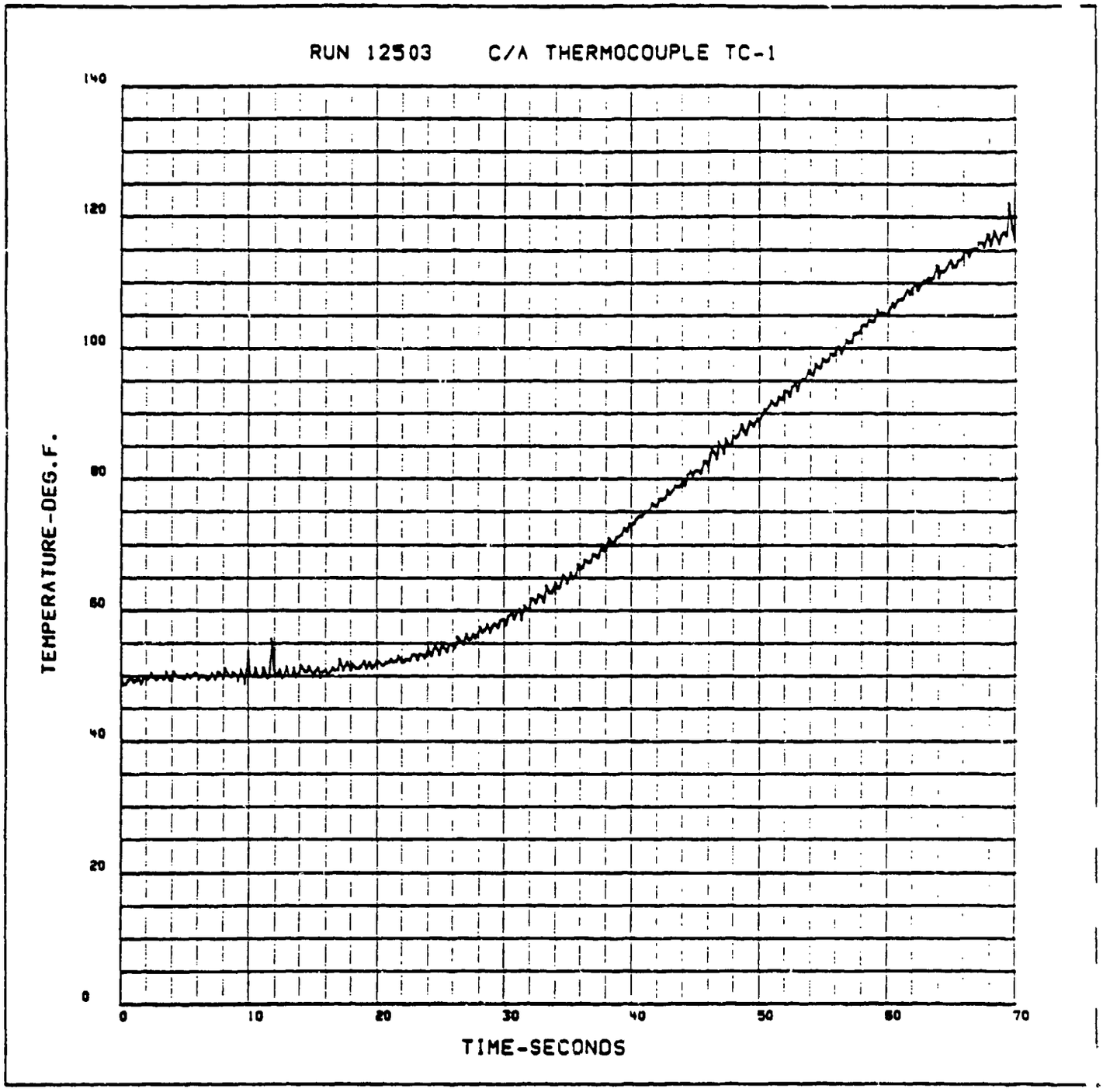

Figure 71 - Rear Surface Temperature Versus Time - Model A-7

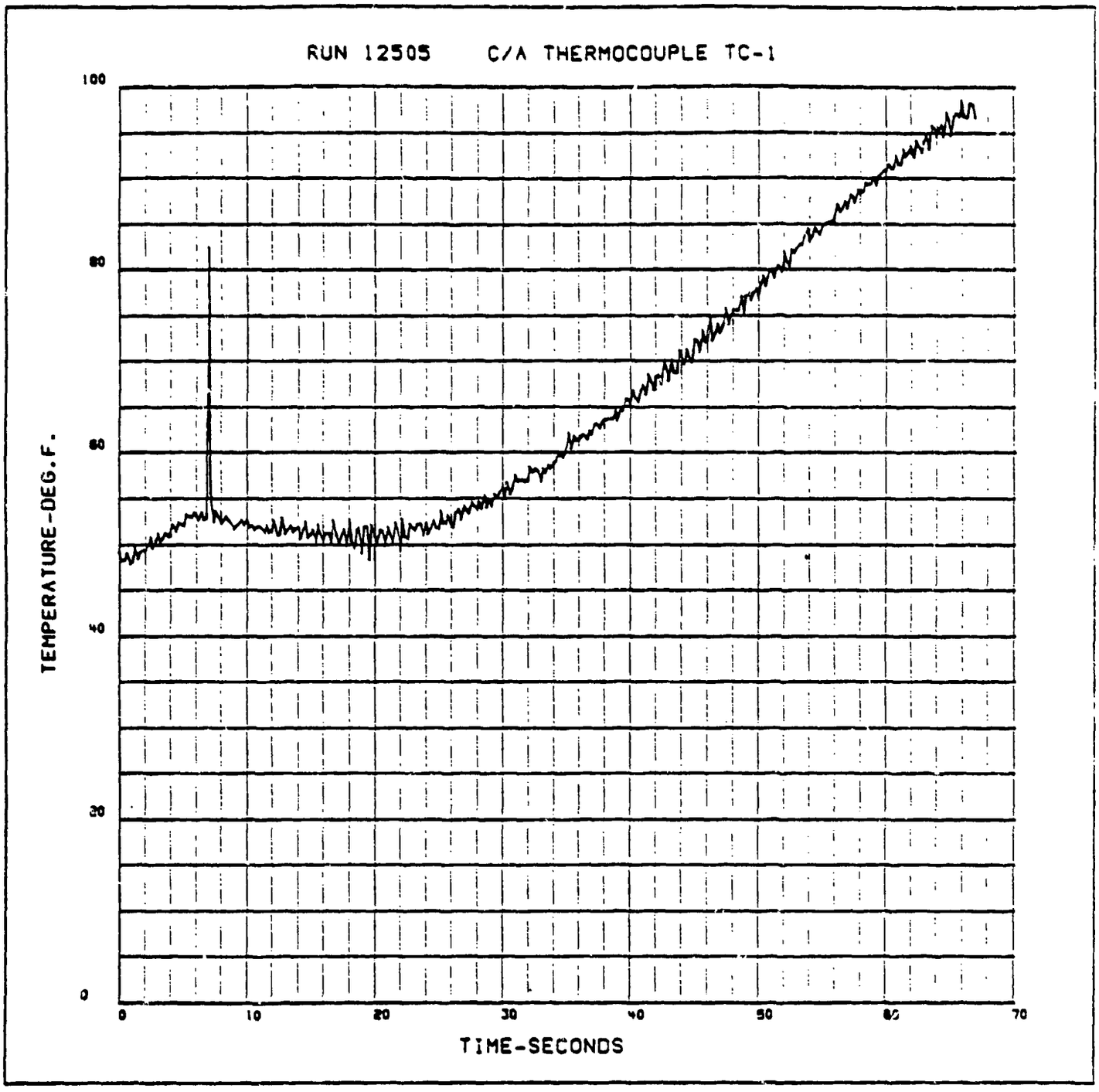

Figure 72 - Rear Surface Temperature Versus Time - Model A-9

- o Crater volume
- o Gravimetric and volumetric mass loss ratios

The particle testing was performed at Effects Technology, Inc. in Santa Barbara, California. A description of the test technique is given in the following subsections.

5.2.1 Facility Description

The method of launching small particles is based upon established exploding foil technology. This technology has been used for many years as a means of accelerating thin plastic plates to high velocities. Exploding wire particle impact testing draws heavily on the extensive calibration data available from exploding foil plate impact testing.

Energy Storage System

The circuit diagram of the ETI particle impact test system is shown in Figure 73. The capacitor bank consists of four 14 μf, 20 KV capacitors which can be connected in parallel to provide 3, 6, 9, or 12 K Joules in a rapid, high current discharge.

When the exploding element is connected into the circuit and the capacitor bank is charged to the desired voltage, a solenoid is activated which disconnects the bank from the power supply. The fire button is then depressed, sending a low voltage pulse to the primary of the trigger transformer. The output of the transformer is a short duration, 80 KV pulse which is applied to a pair of electrodes located within the spark gap. This high voltage pulse causes ionization of the air between the spark gap electrodes, thereby initiating the discharge of the capacitor causing the wire to explode. A current viewing resistor is used to monitor the bank current during each test.

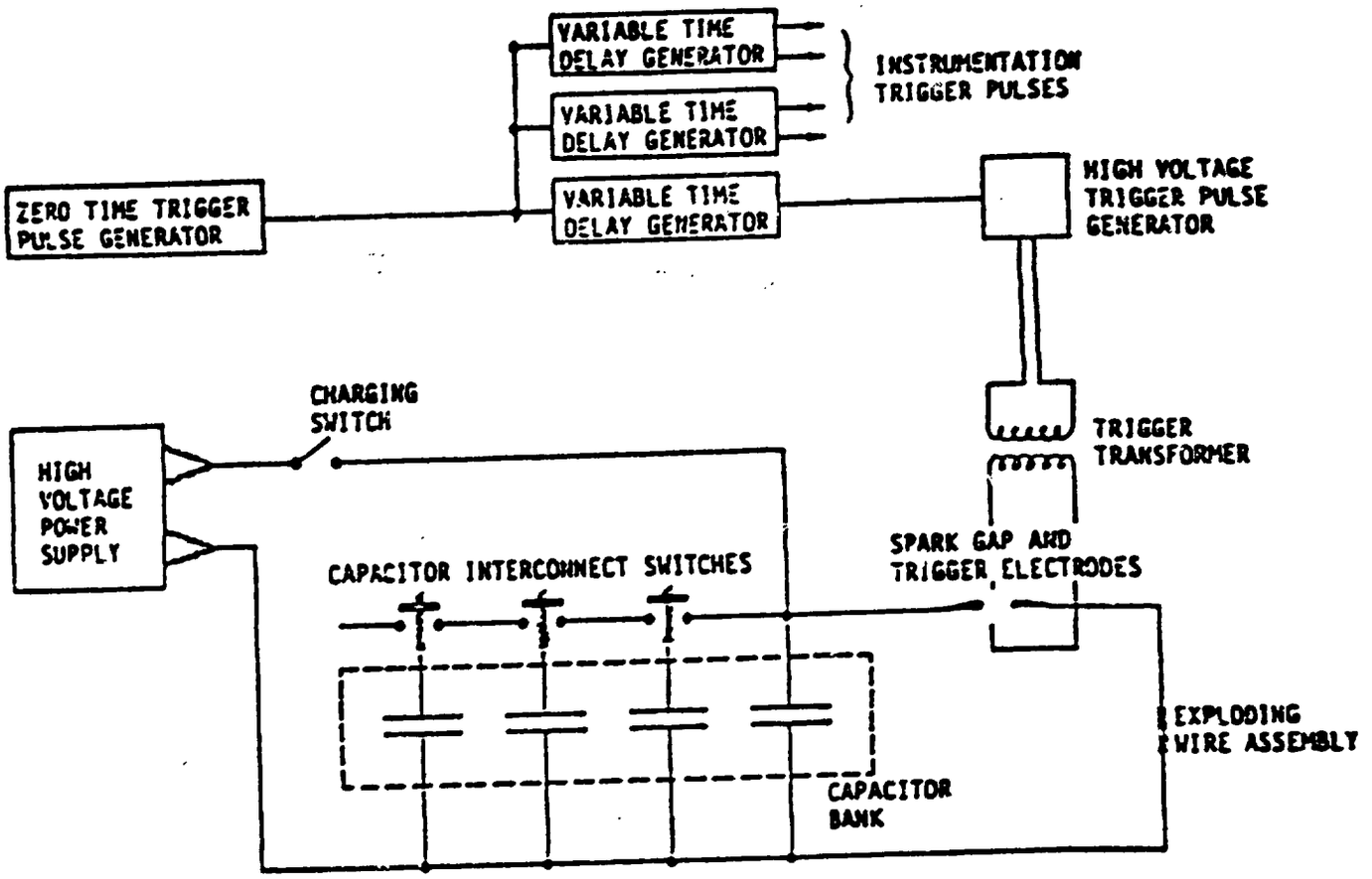

Figure 73

CIRCUIT DIAGRAM OF EXPLODING WIRE SYSTEM

Particle Launch Assembly

The primary assembly type used for particle impact testing is illustrated in Figure 74. In this approach, the driving force is provided by an electrically exploded wire. Initially, the wire is confined in an insulator block. The insulator block sizes vary as a function of exploding wire length. Typical block dimensions are 7.3 cm x 7.3 cm x 2.5 cm for 0.025 cm to 0.10 cm diameter wires. The barrel is aligned with, and centered on the wire. The particle is placed in contact with the wire prior to the test. Expansion of the exploded wire vapor is limited primarily to the path through the barrel, so that the particle is accelerated to a high velocity. The maximum launch velocities obtainable for a single particle depends primarily on the particle material and size. Typically, spherical 1.0 mm glass, 1.0 mm nylon, 0.4 mm aluminum oxide, and 1.00 mm tungsten carbide particles have been successfully launched to velocities of 6,000m/sec, 3,600m/sec, 4,600m/sec, and 2,700m/sec, respectively.

Aiming

For tests requiring extreme accuracy in the prediction of impact location, a laser alignment system is used. With this system, a laser beam passing through the barrel projects a spot onto the surface of the test specimen.. The specimen is then fixed in position for firing. Using this technique, the impact location can be predicted to an accuracy of 0.5 mm for a 1.0 mm diameter particle.

Shallow Angle Impact for Cold Specimens

For shallow angle impact tests, a special specimen holder has been designed. In this design, illustrated in Figure 75, the angle of incidence is fixed by the preset angle of the holding bracket. In general, specimens involving shallow impact angles are required to be lengthened in the direction

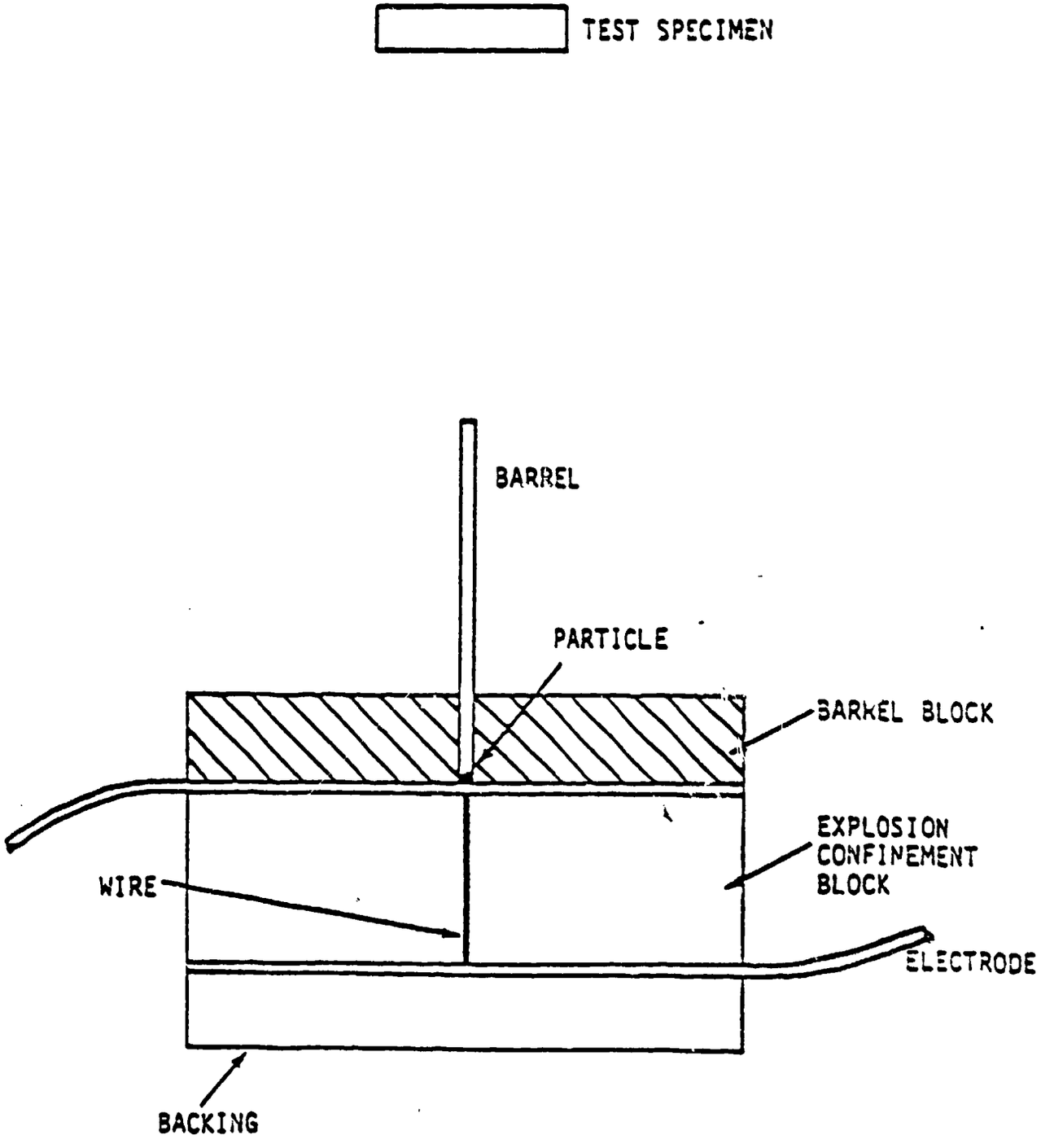

Figure 74

EXPLODING WIRE PARTICLE LAUNCHING ASSEMBLY

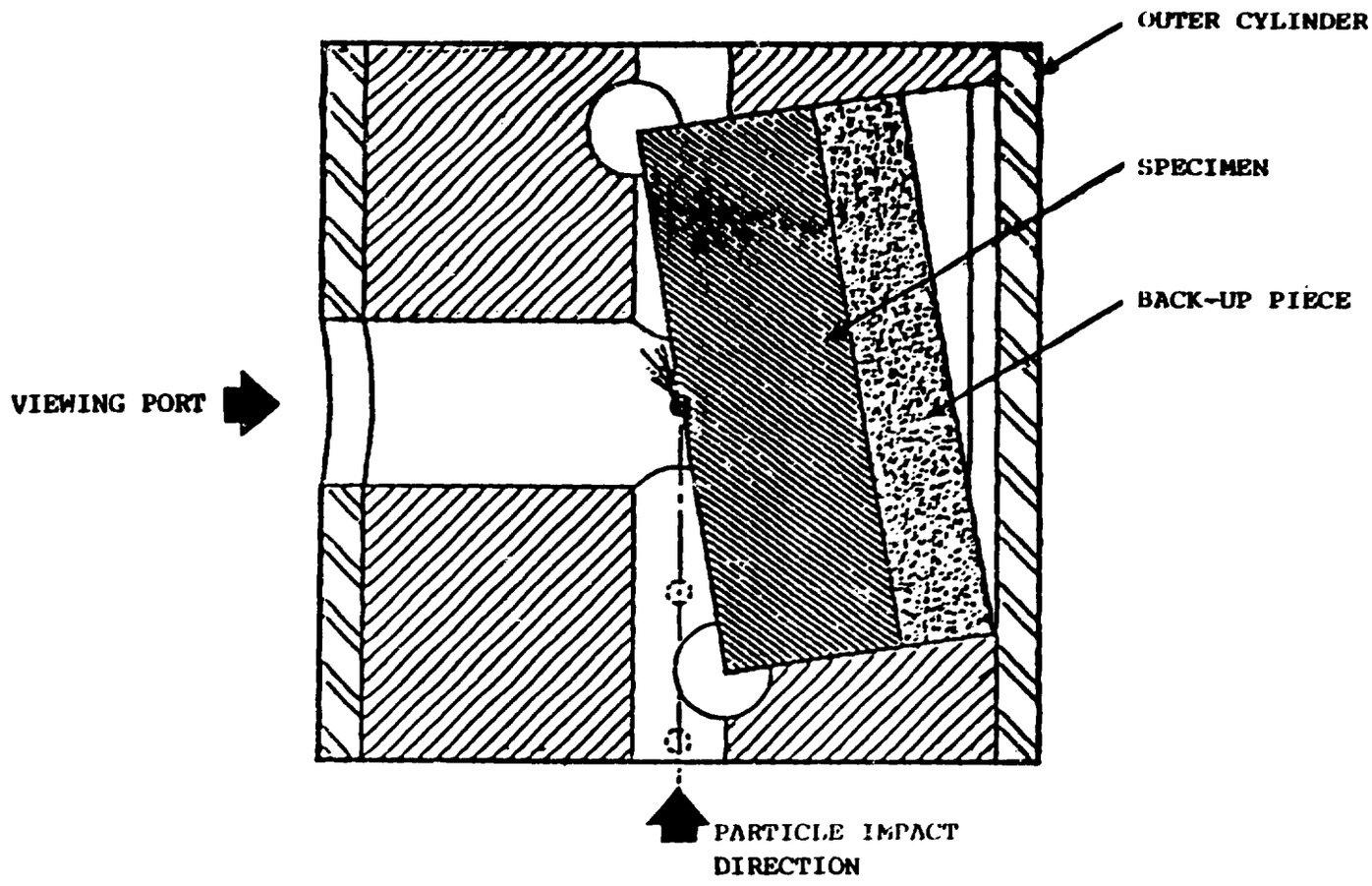

Figure 75 SPECIMEN HOLDER CONFIGURATION FOR IMPACTS NOT NORMAL TO SPECIMEN SURFACE

of tilt. This requirement arises because the aiming error, defined in terms of the projected distance perpendicular to the particle trajectory, is constant so that miss distances are amplified in the direction of tilt. Also, in some cases, the craters elongate in the direction of tilt. However, even for shallow angle impacts at a high velocity, the specimens can be relatively small because of the aiming accuracy attainable by the approach described here.

Thermal Gradient System

In general, all materials of a hypervelocity vehicle that are exposed to the external world and susceptible to erosion are potentially subject to high thermal flux and correspondingly high surface temperatures, i.e., temperatures close to melting or sublimation. In addition, a steep thermal gradient is present in which the material temperature decreases with increasing distance from the surface. Two fixtures have been developed at ETI for laboratory testing under thermal gradient conditions; one for testing in a controlled atmosphere. Each of these thermal gradient fixtures consists of a graphite susceptor placed within the RF load coil, which upon RF inductive heating, acts as a graybody radiator to a nearby specimen. Figure 76 is a schematic view of the graphite susceptor mounted in the induction load coil. Radiating surfaces up to 5.08 cm diameter can be constructed with spatial variation in temperature being 56°K (100°F) at most. A protective sleeve of boron nitride or alumina ceramic is usually placed between the coil and the graphite heater in order to minimize the occurence of coil damage caused by the hot particulates emitted by the graphite.

Figure 77 depicts the geometry of a specific thermal gradient apparatus as used in conjunction with a particle launcher (backface surface temperature is monitored). The actual firing position of the particle launcher can be

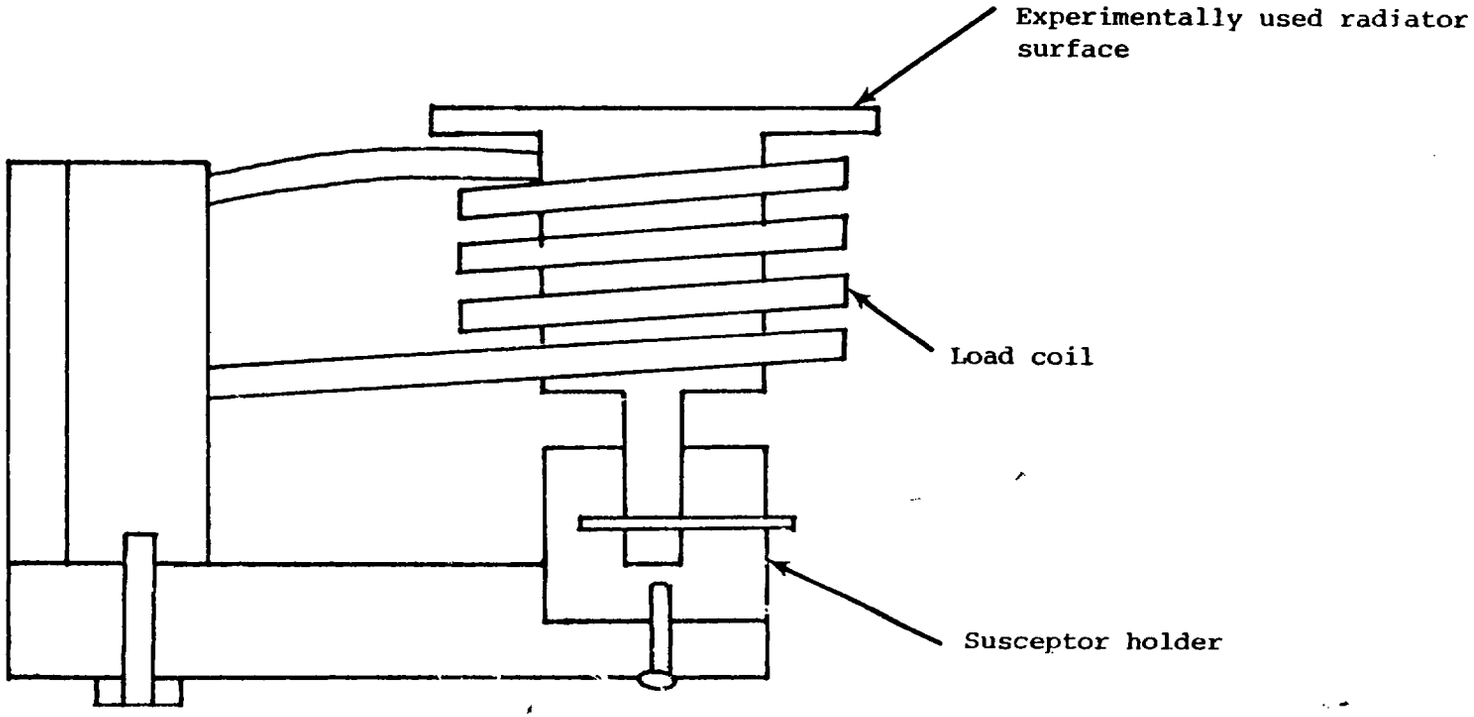

Figure 76

SCHEMATIC VIEW OF THE THERMAL FLUX RADIATOR MOUNTED IN INDUCTION LOAD COIL

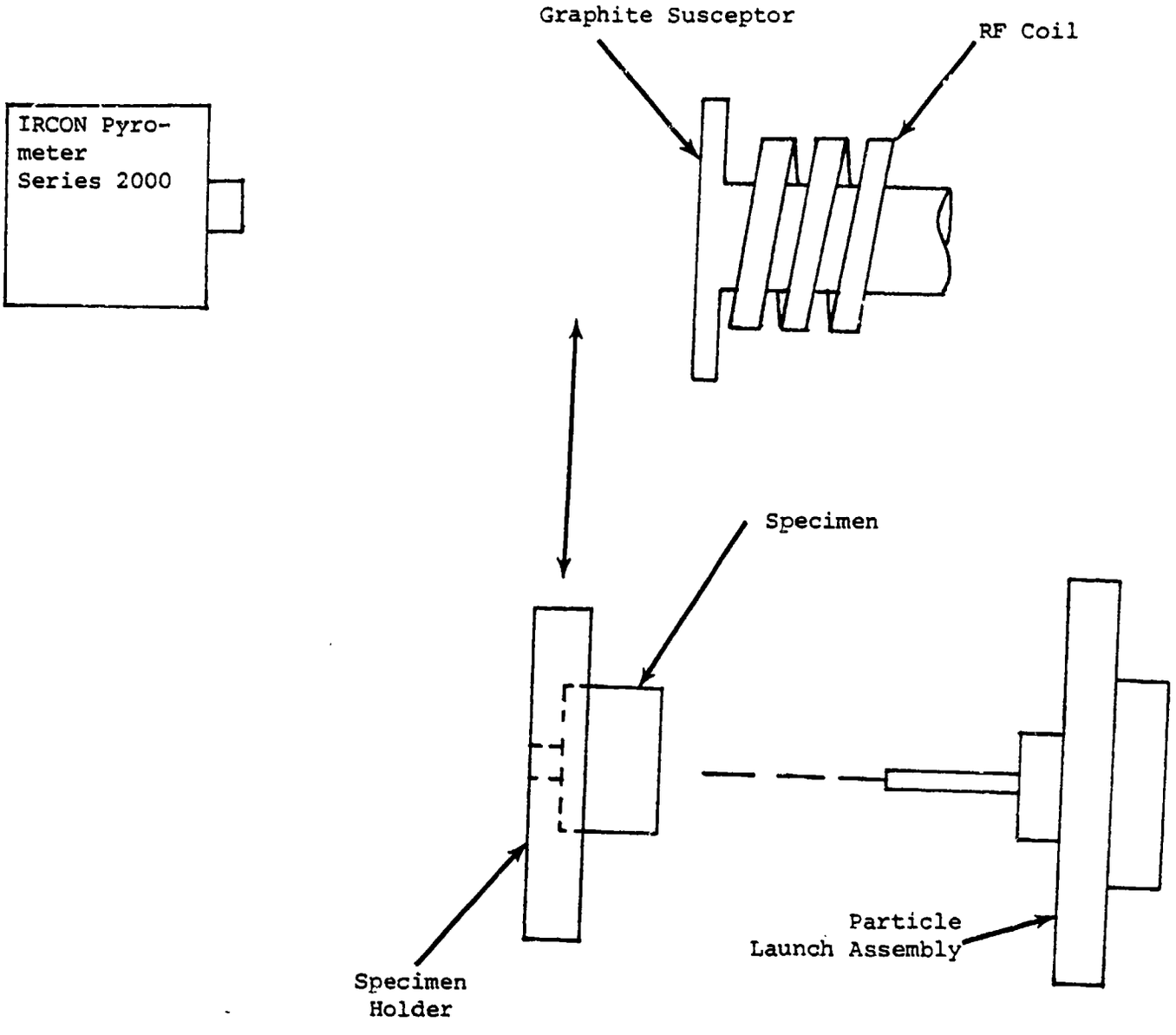

Figure 77

MAIN GEOMETRY FOR THE THERMAL GRADIENT/
PARTICLE LAUNCHER APPARATUS

oriented such that the particle will impact at the desired angle with respect to the specimen's surface. A mechanical coupling between the specimen holder and an electromagnetic solenoid allows the specimen to be moved from its neutral or particle impact position to the heating position and back.

In order to provide the desired test parameters (radiator temperature, heating pulse time, and particle impact velocity), a precise sequence of events is necessary. First the radiator is brought to the calibrated temperature and stabilized. The solenoid is then pulsed so as to position the specimen in front of the thermal radiator. The solenoid is activated with a preset pulse duration so as to provide the desired time of specimen heating. The specimen then drops into the firing position and the reverse motion activates a microswitch which provides the launch system trigger pulse. This trigger pulse immediately discharges the capacitor bank through the wire in the shot assembly and launches the particle. The trigger pulse also activates the high speed framing camera in order to obtain in-flight photographs of the particle prior to impact. The sequence of events is the same for the multiple particle thermal gradient tests. Each of the test fixtures can expose a specimen to a predetermined thermal flux for pulse durations on the order of 20 msec to minutes. However, for heating times less than 0.8 seconds, the heat pulse reduces to a sawtooth form.

The horizontal motion of the linear solenoid is converted to vertical motion of the specimen by a mechanical linkage yielding a 5:1 amplification between the solenoid movement and the specimen holder motion (see Figure 78). The movement of the initially cool specimen from its neutral position to the heating position or from the heating position to the neutral position takes about 0.1 second. The associated rise and fall times of the heat pulse may or may not be significant, depending on the selected heating time. The

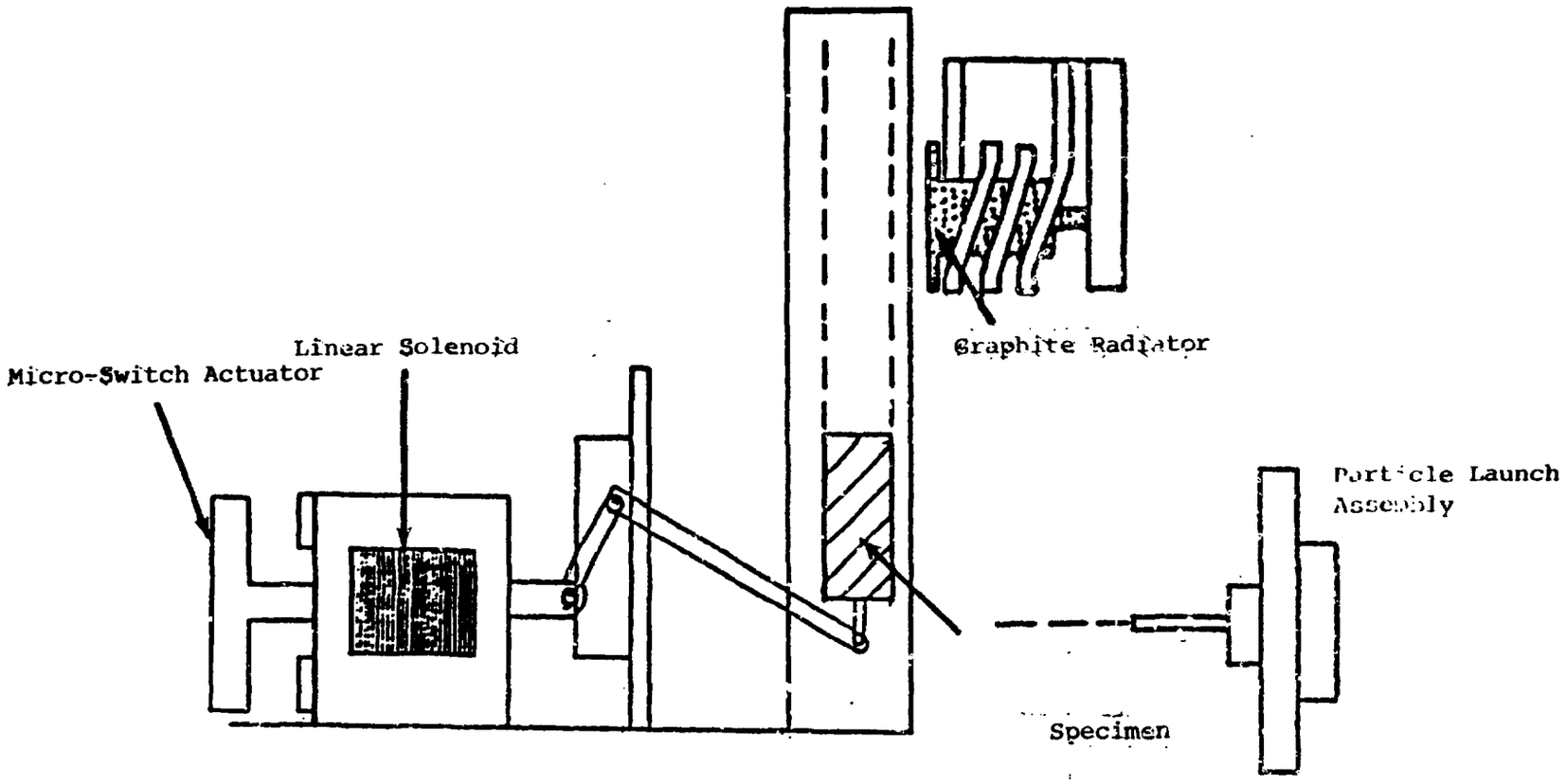

Figure 78

LINEAR SOLENOID THERMAL RADIATOR TEST FIX[illegible] AND EXPLO[illegible]NG WIRE LAUNCHER IN LAUNCH POSITION

relatively fast entry and exit of the specimen to the heating position yield a reasonably square heating pulse for pulse lengths greater than 0.5 second. For a temperature of 2255°K (3600°F), established at the specimen's surface at the end of the heating pulse, it is estimated that there will be a 22°K (40°F) reduction in temperature by the time the specimen drops to the firing position. A position monitoring signal is available for recording the total time that the specimen is in the heating position.

Note that the specimen does not have to be electrically conductive in order to be heated by the thermal gradient test system. A graphite susceptor is heated instead which in turn radiatively heats the specimen. Even materials such as fused quartz, which is 70% spectrally transparent below 3 μm, have been heated in such a fixture to a surface temperature of 1922°K (3000°F).

An important use for the thermal gradient test system is the exposing of heatshield specimens to thermal fluxes. Unlike the nosetip materials, typical heatshield materials pyrolyze at temperatures lower than sublimation temperature of carbon. Attempts to rapidly induce high uniform temperatures within conductive heatshield materials lead to material explosions. Using slow heating rates, or by means of the thermal gradient system, heatshield specimens may be taken to high temperatures without catastrophic failure. Portions of a heatshield that have been pyrolyzed completely leave just the graphite structure known as char with a density about 20% less than the density of unpyrolyzed virgin heatshield material. The difference in material strengths between virgin and char material is significant, resulting in different erosion responses for the virgin and charred materials. Figure 79 represents a typical density profile in a heatshield material exposed to a heater at 2477°K for 10 seconds. Note that even though the heater was turned off so that there was no net heat flux entering the heatshield at times later than 10 seconds

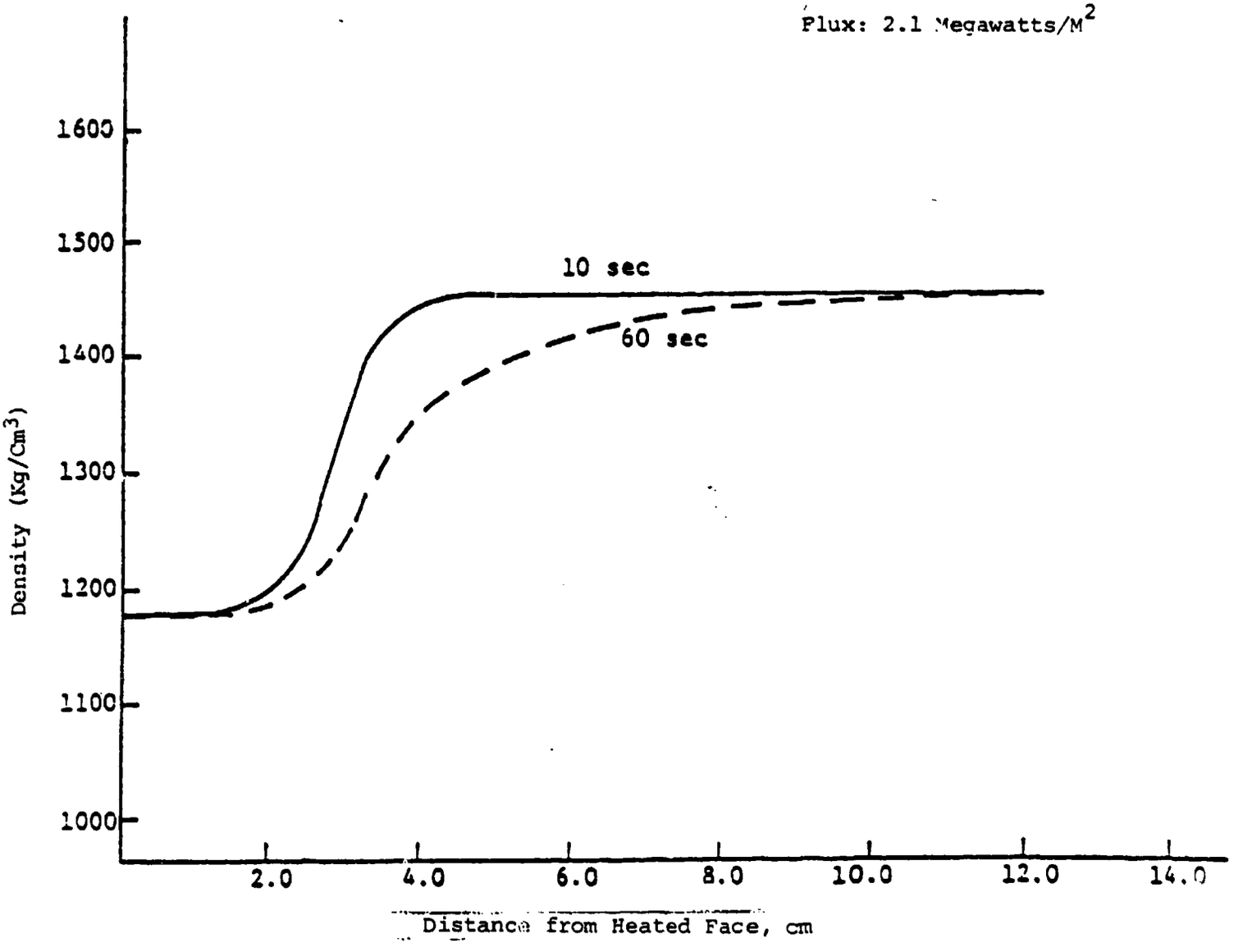

Figure 79

DENSITY PROFILES FOR TYPICAL HEATSHIELD MATERIALS
(Heated for 10 sec)

pyrolysis is still present deep within the material up to a minute later. A heater surface temperature of 2477°K (4000°F) corresponds to a heat flux rate per unit area of 2 Megawatts/m^2 (180 Btu/Ft^2-sec).

The open air linear solenoid thermal gradient test system is used routinely in thermal experiments with heatshield materials. The closed environment thermal gradient test system can be used for higher heat flux experiments for these materials. It is also known that the charring process in heatshields is dependent on the surrounding ambient gaseous environment and again the closed environment thermal gradient system lends itself in experimentally determining the atmospheric effects on char and its erosion response. A summary of the ETI thermal radiator specimen position or capabilities is presented in Table 26 below.

Table 26. THERMAL RADIATOR SPECIMEN POSITIONOR CAPABILITIES

Specimen Dimensions	Max. 5.08 cm square x 1.91 cm thick
Specimen Type	Conductor or Non-conductor
Radiator Temperature	1255°K-3866°K (1800°F-6500°F) Variable
Pulse Length	20 msec $\leq \tau^*$
Angle of Incident	$6^\circ \leq \theta \leq 90^\circ$
Environment	Up to 3310°K (5500°F) in air, complete temperature range in nitrogen
Specimen Instrumentation	Imbedded thermocouples
Impacting particle	Size 0.3 mm-1.0 mm diameter velocity 0.31-5.5 km/sec (1-18 kfps)

*The maximum pulse duration is limited by the environmental chamber's ability to withstand extended periods of operation which depends primarily on the peak operating temperature and radiator size.. However, normal operating periods are limited to 1-2 minutes.

5.2.2 Diagnostics

Diagnostic systems which are used in the ETI particle impact test facility include active systems for dynamic measurements performed during the test (e.g., particle velocity, impact time, particle integrity) and passive systems for determining test parameters and results (e.g., particle mass, particle diameter, mass loss, crater dimensions) as listed in Table 27 below.

Table 27 DIAGNOSTIC CAPABILITIES

Measured Quantity	Method	Accuracy
Particle Diameter	Microscope	± 2%
Particle Mass	Microbalance	± 1μg
Mass Loss	Microbalance	± 5%
Impact Velocity	Framing Camera	± 5%
Impact Simultaneity*	Framing Camera	± 10%
Impact Location (Aim)	Laser Alignment	0.500 mm

*Simultaneity of impact for two particles launched on a single test.

High Speed Photography

Measurements of projectile velocity are typically performed on each test using a high speed framing camera. The high speed camera which is used for these measurements is a TRW Model 1D Image Converter with a 3-frame head. The camera is capable of recording at framing rates of 10^7 per second. An example of a 3-frame photographic series of a particle in flight recorded by the camera is presented in Figure 80. The timing sequence for control of the shuttering time, the firing time of the capacitor bank, and the high intensity light source are provided by a variable time delay generator.

TRW Model 1D Image Converter Camera

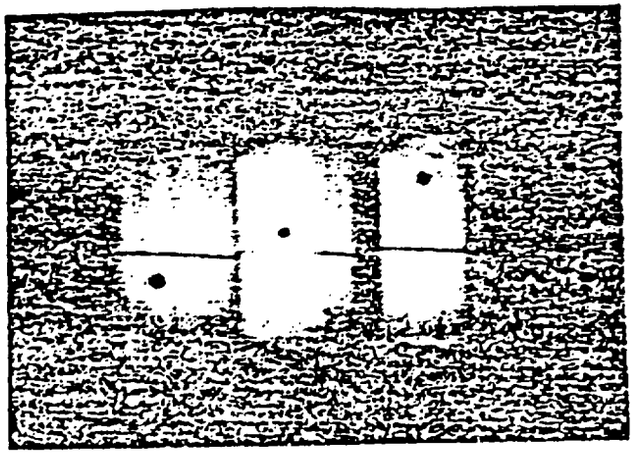

0.75 μsec. Between Frames--1mm, GRID

Figure 80

TYPICAL HIGH SPEED PHOTOGRAPH
IC DATA FOR PARTICLE IMPACT TESTING
FROM A HIGH SPEED CAMERA

In addition, an important advantage of high speed photography in particle impact testing is direct visualization of the condition of the particle in flight. Although the particle remains intact in a high percentage of the tests, breakup will occur in some cases and it is important to be able to clearly distinguish between the two conditions.

Pre-Test and Post-Test Measurements

Passive diagnostics which are used on erosion tests include size and mass measurements on both particle and specimen. The particles are examined and measured with the microscope, and weighed on a micro-balance prior to insertion in the erosion test assembly. Specimens are examined microscopically and weighed before and after testing to determine extent of damage and mass loss. Sectioning, polishing, and photomicrographic equipment is also used to permit internal examination of the crater region of the specimen. Mass loss due to particle impact is determined by both direct measurement and mercury displacement techniques. Also, sections of test specimens for microradiography can be taken to study sub-surface damage.

As an aid to the erosion modeling development, additional information is obtained from the post-test specimen in terms of crater profiles. From such crater profiles, particular aspects of the crater geometrics can be determined. Figures 81 and 82 are examples of crater profile data.

Temperature Measurements

For all heating experiments, temperatures are monitored with one or two ICRON Series 2000 automatic optical pyrometers available at ETI. Temperatures are indicated visually on a meter. The stated accuracy of the meters is 0.3% of full scale. The spectral response of the sensing unit of the optical pyrometer is within the 0.7 - 0.97 μm band. The sensing unit responds to the

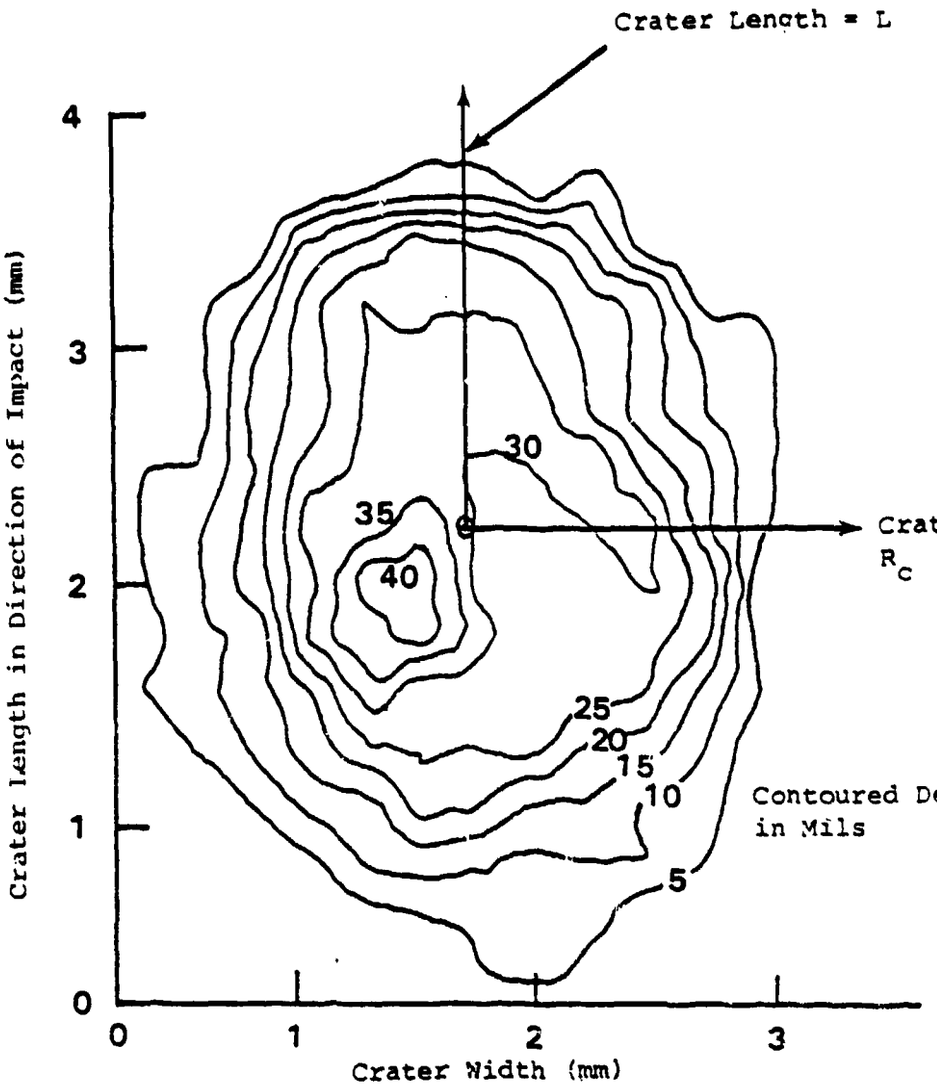

D(Y,X)

X-AXIS, 0 DEGREES

X	1	2	3	4	5	6	7	8	9	10	11
Y											
1	0	0	0	2	0	0	7	0	0	0	0
2	0	0	2	21	20	23	7	6	0	0	0
3	0	1	1	22	30	31	37	20	0	3	0
4	0	0	34	36	45	44	46	35	36	13	0
5	0	11	39	44	35	70	59	40	24	10	6
6	0	13	40	48	75	74	64	48	45	18	0
7	0	20	39	49	59	70	62	40	41	16	0
8	0	13	35	39	40	62	44	35	40	15	5
9	0	1	32	32	44	42	47	25	38	14	0
10	0	0	0	19	26	25	19	27	5	3	0
11	0	0	0	6	10	11	13	11	0	0	0
12	0	0	0	0	0	0	9	0	0	0	0
13	0	0	0	0	0	0	7	0	0	0	0
14	0	0	0	0	0	0	5	0	0	0	0

An Array of Crater Depth Points (mils)
For a 0.5 mm Grid.

Figure 81
EXAMPLE OF CRATER CONTOUR PROFILE FOR LOW ANGLE (14°) IMPACT ON GRAPHITE

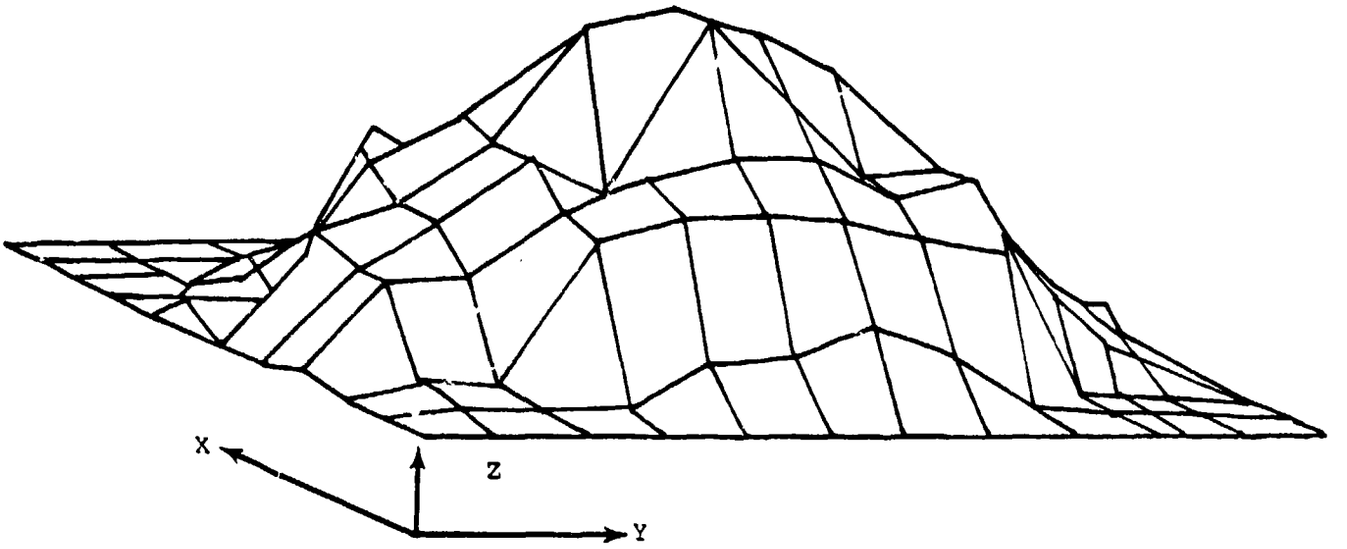

Example of Optical Crater Profile Measurement Three-Dimensional Projection Plot

Figure 82

CRATER PROFILE EXAMPLES

radiative power falling onto a detector. The radiative power within the total blackbody spectrum is proportional to the fourth power of the absolute temperature according to Stefan's law. The IRCON pyrometer's narrow spectral response makes it more sensitive to the temperature of the object's surface being monitored than is indicated by Stefan's law. Mathematically stated, the radiative power that falls within the spectral band of the sensing detector is given by:

$$\underline{P}_D = K \int_{0.7\mu}^{0.97\mu} \varepsilon_\lambda \, \lambda^{-5} \, (\exp(ch/k\lambda T) - 1)^{-1} \, d\lambda$$

The spectral band is narrow; therefore, the integral in the above Equation can be approximated by:

$$\underline{P}_D = k\lambda^{-5} \, \varepsilon_\lambda \, ((\exp(c_2/\lambda T) - 1)^{-1} \, \Delta\lambda$$

where: ε_λ = emissivity

λ = average wavelength in the spectral band = 0.834 μ

c = speed of light

h = Planck's constant

k = Boltzmann's constant

T = absolute surface body temperature

K = proportionality constant

P_D = spectrally responsive power on the detector

c_2 = constant = $ch/k = 1.4388 \times 10^4 \mu^{\circ}K$

$\Delta\lambda$ = 0.97μm - 0.7μm = 0.27μm

It can be shown that the fractional change in spectrally responsive power on the detector, P_D in terms of a fractional change in temperature, T, is given by:

$$\frac{\Delta P_D}{P_D} = \left\{ \frac{c_2/\lambda T}{1-\exp(-c_2/\lambda T)} \right\} \frac{\Delta T}{T}$$

5.2.3 Erosion Test Results

A hypervelocity particle impact on a material leaves the material with a discernible crater. This crater represents the region of mass ejected due to the particle impact. Hence, test results that characterize the erosion response of the material consist of various spatial dimensions and quantity of mass removed. Specifically, the erosion response is expressed in terms of either gravimetric or volumetric mass loss or crater volume. The following two subsections contain descriptions of these two methods of expressions.

Volumetric Mass Loss or Volume Loss

A particular crater is measured volumetrically by filling the crater volume with mercury (Hg). A special assembly is available that allows the liquid mercury to be forcibly injected into the crater void such that the large surface tension of mercury is overcome and hence, small crevices within the crater that represent portions of the crater volume are filled with mercury. The mercury volume represents the crater volume. The mercury volume is obtained by measuring the mass of mercury on a microbalance and dividing this mass by the density of mercury (13.54 gm/cm^3). The mass loss represented by the crater volume is calculated by multiplying crater volume by the density of the material before ejection. Note that the density of material must be known. This may be difficult in the case of a charring heatshield having a

"thin" char layer and hence, a density gradient. Volume losses rather than mass losses represent primary measurement quanitities.

Gravimetric Mass Loss and Volume Loss

Gravimetric measurements entail mass measurements of an impact specimen before and after a particle impact. The difference in measured masses, in many cases, corresponds to the mass loss due to an impact. Of course, in the case where the specimen is subjected to mass loss mechanisms other than those due to the impact, one obtains the combined mass loss. This is the case in the charring erosion tests. The mass loss represents the combination of the particle impact, pyrolysis, and possibly ablation. In the case where the mass loss is due solely to the particle impact, the gravimetric method is useful. In the situation where crater volumes are small, the gravimetric method is more accurate than the volumetric method. Extremely small craters are difficult to completely fill with mercury because of the combination of the high surface tension of mercury and the comparatively high ratio of "brushlike filaments" protruding at the crater surface to crater volume for small craters.

The crater volume is inferred from gravimetric data (if the density of the expected material is known) by dividing the measured mass loss by the assumed density.

Mass Loss and Volume Loss Ratios

The primary quantities measured either volumetrically or gravimetrically (mass or volume loss) are additionally buffered to yield experimental quantities that are meaningful for data interpretations. Two quantities of interest are mass loss and volume loss ratios. The definitions for these quantities are:

$$G = \text{mass loss ratio} = \frac{\text{Mass of crater material}}{\text{Mass of impact particle}}$$

If the density of the material and particle are ρ_t and ρ_p, respectively, V_c the crater volume, and D_p the particle diameter, then the volume loss ratio is given by:

$$\nu = \text{Volume loss ratio} = \frac{\text{Crater Volume Loss}}{\text{Impacting Particle Volume}}$$

$$= V_c / \left(\frac{\pi}{6} D_p^3 \right)$$

Note that $G = \rho_t \nu / \rho_p$

Reporting Format

The tables contained within are usually partitioned into the following columns.

- Test No./Specimen Number - The test number is assigned by Effects Technology, Inc. to the specific impact test. The specimen number is assigned to the specimens.

- Specimen Density - If uncharred, the density is inferred by measuring the width, length, height, and mass of the specimen. Some error results because the specimens are portions of a curved frustum and not rectangular blocks. If charred, then the specimen density reported represents the assumed density of char and not of the whole specimen. Note that this is reported even in the case of a thin char layer test and henceforth, not a valid representative density. The crater volume measured volumetrically is of more and valid importance in this case. The density is usually reported in terms of grams per cubic centimeter.

- Nominal Particle Diameter - The nominal diameter of the impacting particle. The particles are very close to being spherical. If this assumption is used, a more accurate estimate of the particle diameter is made by referring to the particle mass column and dividing this mass and quanitity by the particle

density to obtain the particle volume and then calculate the diameter. For glass and nylon, the respective densities are 2.54 and 1.14 grams per cubic centimeter. The diameters are reported in units of millimeters. Particle type is usually indicated in this column. If no special note is found, the particle is glass; if nylon, it is so designated.

- Particle Impact Velocity - The impact speed inferred from the in-flight framing camera pictures. Reported in units of kilofeet per second and kilometers per second in parentheses.

- Specimen Test Temperatures - This column has some designation that characterizes the specimen thermal state - the following expressions are used:

- o 70 - Room temperature specimen usually uncharred (degrees Fahrenheit)
- o (X) seconds @ 4000°F - The specimen impact surface is exposed to a graphite heater (RF inductively heated) whose surface temperature is measured by an optical pyrometer to be 4000°F (at an emissivity setting equal to 1.0). The heater is stabilized at a fixed temperature before the specimen is exposed to the heater for (X) seconds and removed from the source of heat and impacted within 0.1 seconds.
- o Cold Char - A specimen preconditioned. The specimen is exposed to a graphite heater for 30 seconds at 4000°F and allowed to cool down to room temperature.

- Impact Angle - The angle of the incoming particle with respect to the surface. A normal impact is 90°, a particle moving parallel to the surface impacts at an angle of 0 degrees. Units are degrees.

- Particle Mass - The measured mass of the impacting particle. Units are milligrams.

- Gravimetric Mass Loss - The difference in mass measured of the impact specimen before and after the impact event. Units are in milligrams. For the charring erosion tests, the mass loss represents both impact and pyrolysis mass loss; hence, not useful for extracting erosion data. However, this data is useful when compared to charring predictions and to note consistency amongst all charring tests of the same thermal state.

- Gravimetric Mass Loss Ratio - The ratio of the gravimetric mass loss to the impacting particle mass.

- Volumetric Volume Loss - The mercury displaced volume of the impact crater of the post-test impact specimen. Units are in cubic millimeters.

- Volumetric Volume Loss Ratio - The ratio of the volumetric volume loss to the impacting particle volume.

- Calculated Gravimetric Volume Loss - The gravimetrically measured mass loss divided by the assumed target density. Units are in cubic millimeters.

- Calculated Gravimetric Volume Loss Ratio - The ratio of the calculated gravimetric volume loss to particle mass divided by particle density.

- Profiled Crater Volume - The crater volume calculated by the crater profile technique. Units are in cubic millimeters.

5.2.3.1 Erosion Data

Tabular summaries of the erosion data are found in Table 28. This table summarizes the erosive properties obtained on virgin and charred braided rubber modified silica phenolic.

Although a volumetric mass loss was measured for Test E4361, a gravimetric mass loss measurement was not obtained due to an apperaturing problem that allowed some hot aluminum plasma to deposit on the specimen.

Photomicrographs of the resulting damage (crater) for each of the tests are presented in Figures 83 through 89.

TABLE 28

SINGLE PARTICLE IMPACT TEST RESULTS

Test No./ Specimen Number	Specimen Density (gm/cm^3)	Nominal Particle Diameter (mm)	Specimen Test Temp. (^oF)	Impact Angle (^oC)	Gravimetric		Volumetric		
					Mass Loss	Mass Loss Ratio G_G	Mass Loss	Mass Loss Ratio G_V	Crater Volume
E4361	1.345	1.0	70	10	--	--	1.02	0.71	0.77
E4362	1.397	1.0	70	10	1.166	0.84	1.38	0.99	0.99
E4363	1.481	1.0	70	10	1.373	0.99	1.69	1.22	1.14
E4364	CHAR	1.0	30 sec @ 4000	10	1040	747	--	--	9.1
E4365	CHAR	1.0	30 sec @ 4000	10	996	714	--	--	13.5
E4366	CHAR	1.0	30 sec @ 4000	10	1043	740	--	--	25.5
E4367	CHAR	1.0	30 sec @ 4000	10	1078	786	--	--	27.9

*Calibrated velocity - not measured due to high speed camera misfire
- this test re-done as Test E4363.

Damaged Material
(Post-test Photo)

Mag = 2.9x

Impact Direction ——→

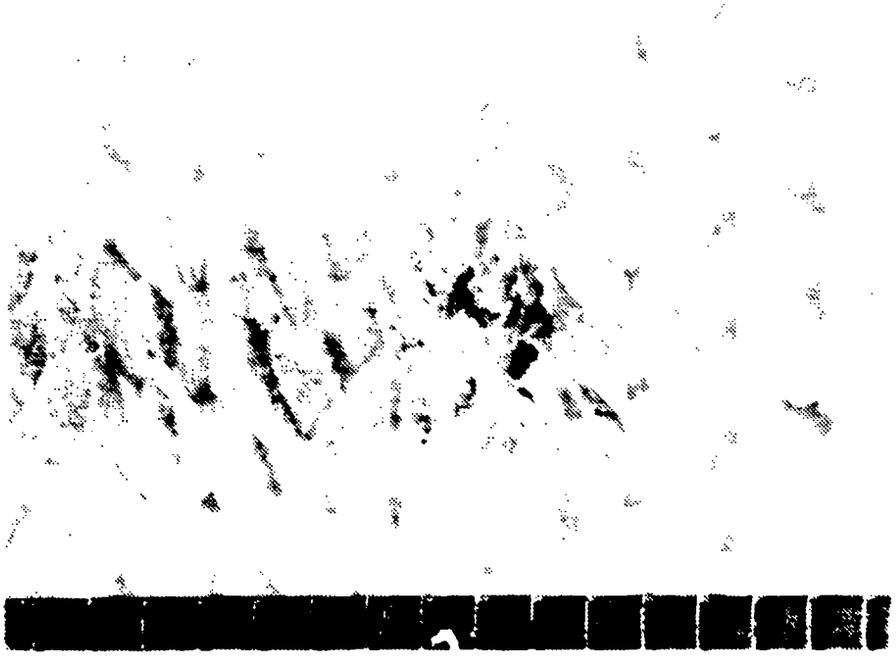

Damaged Material
(Post-test Photo)

Mag = 7.5x

Figure 83 Photomicrographs of damage resulting from a 1 mm glass sphere (10°) impact at 8 kft/sec and 70 $^{\circ}$F.

Test No. E4362

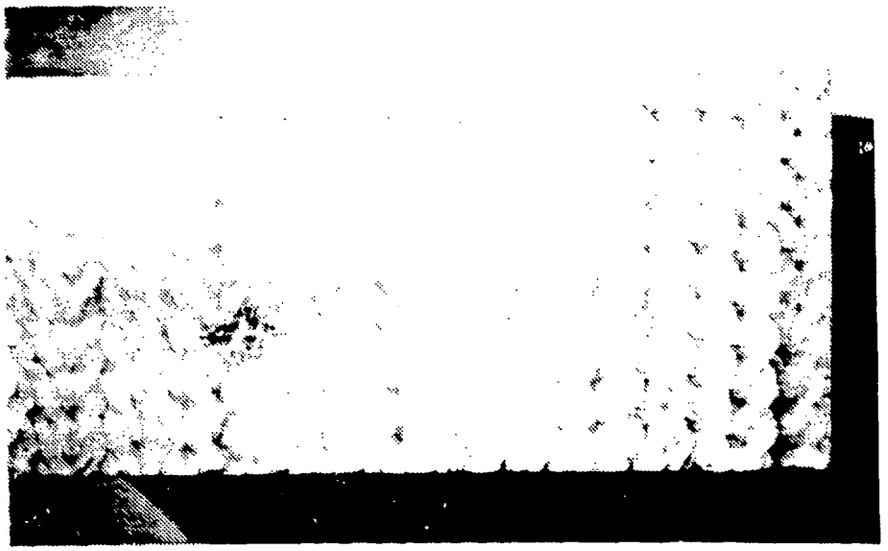

Virgin Material
(Pre-test Photo)

Mag. = 2.8x

Impact Direction ⟶

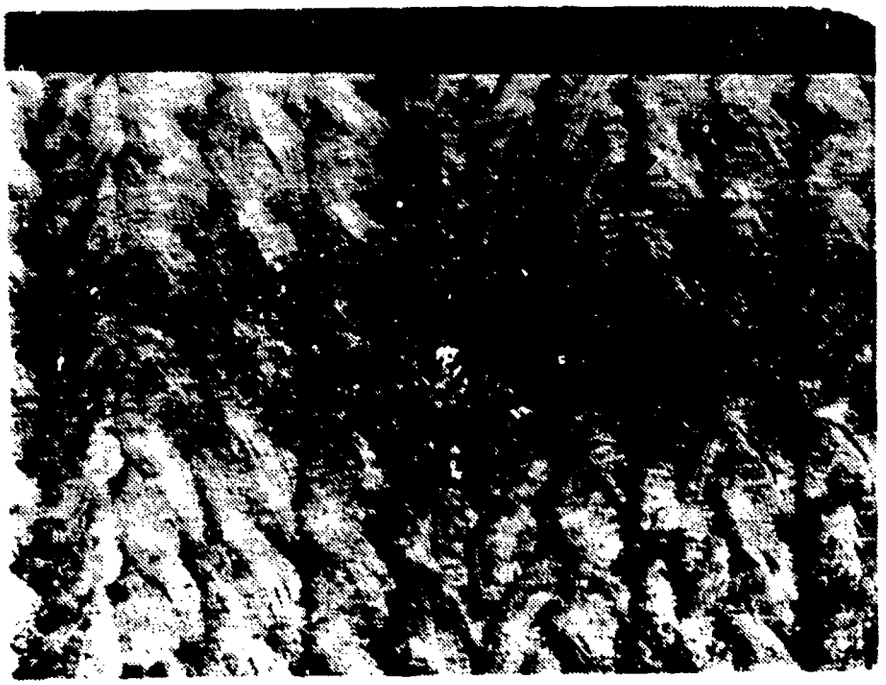

Damaged Materia
(Post-test Phot

Mag. = 7.5x

Figure 84 Photomicrographs of damage resulting from a 1 mm glass sphere (10°) impact at 8 kft/sec on material radiatively charred for 30 sec at 4000 $^{\circ}$F.

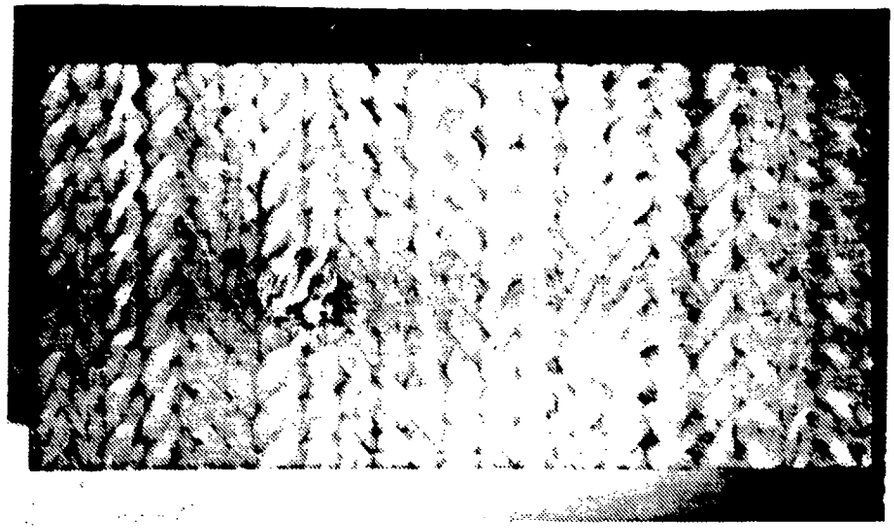

Virgin Material
(Pre-test Photo)

Mag. = 2.8x

Impact Direction ⟶

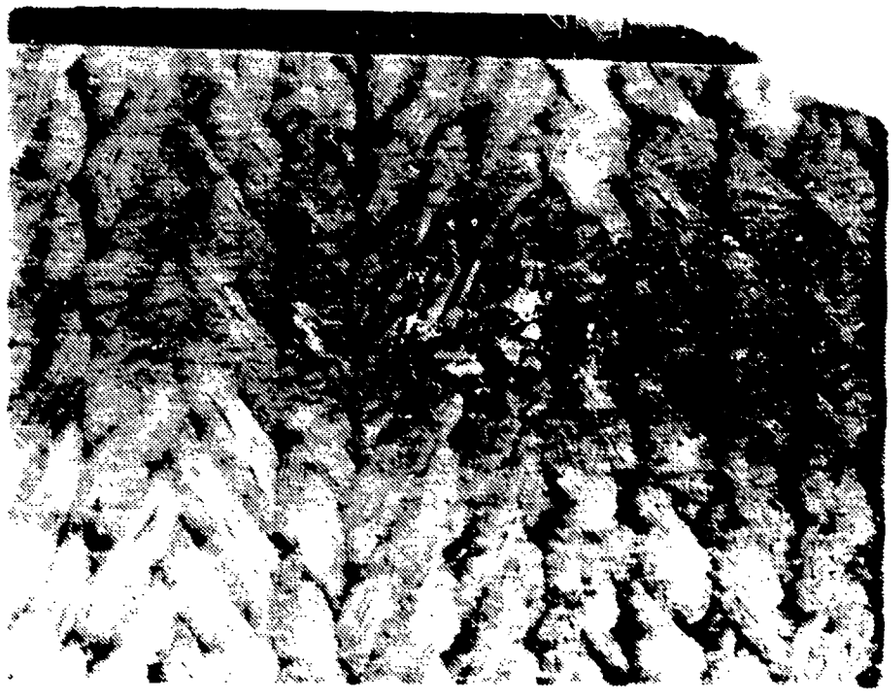

Damaged Material
(Post-test Photo)

Mag. = 7.5

Figure 85 Photomicrographs of damage resulting from a 1 mm glass sphere (10^{o}) impact at 8 kft/sec and 70 ^{o}F.

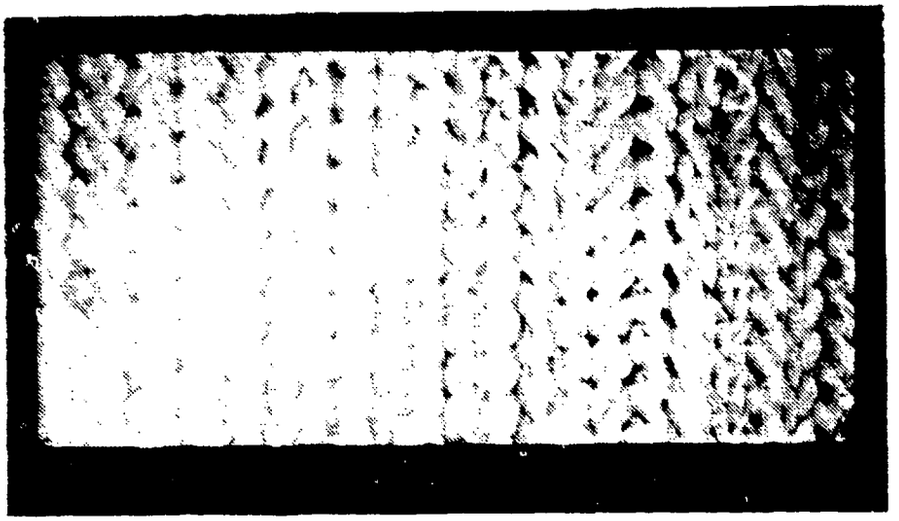

Virgin Material
(Pre-test Photo)

Mag. = 3.0x

Impact Direction ⟶

Damaged Material
(Post-test Photo)

Mag. = 2.75x

Figure 86 Photomicrographs of damage resulting from a 1 mm glass sphere (10°) impact at 8 kft/sec and 70 °F.

Test No. E4365

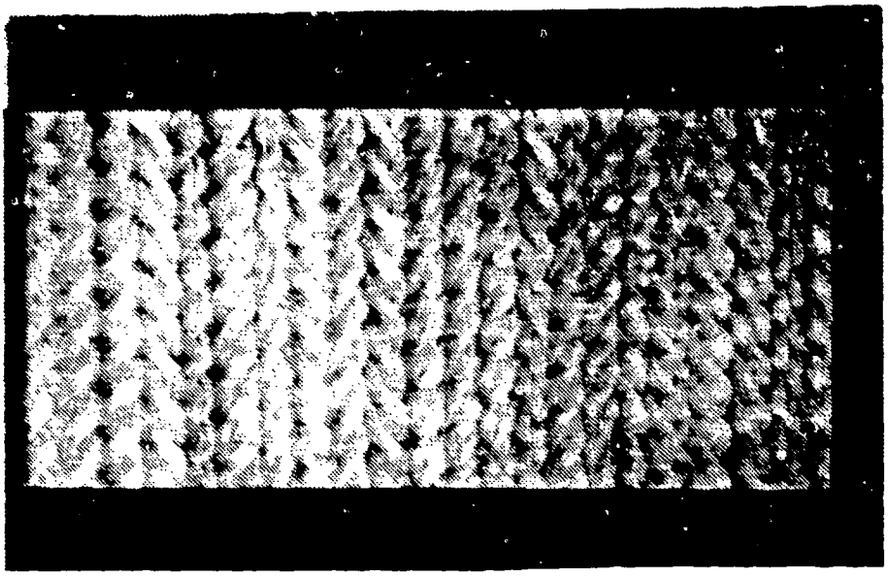

Virgin Material
(Pre-test Photo)

Mag. = 3.0x

Impact Direction ⟶

Damaged Material
(Post-test Photo)

Mag. = 2.7x

Figure 87 Photomicrographs of damage resulting from a 1 mm glass sphere (10°) impact at 8 kft/sec on material radiatively charred for 30 sec at 4000 $^{\circ}$F.

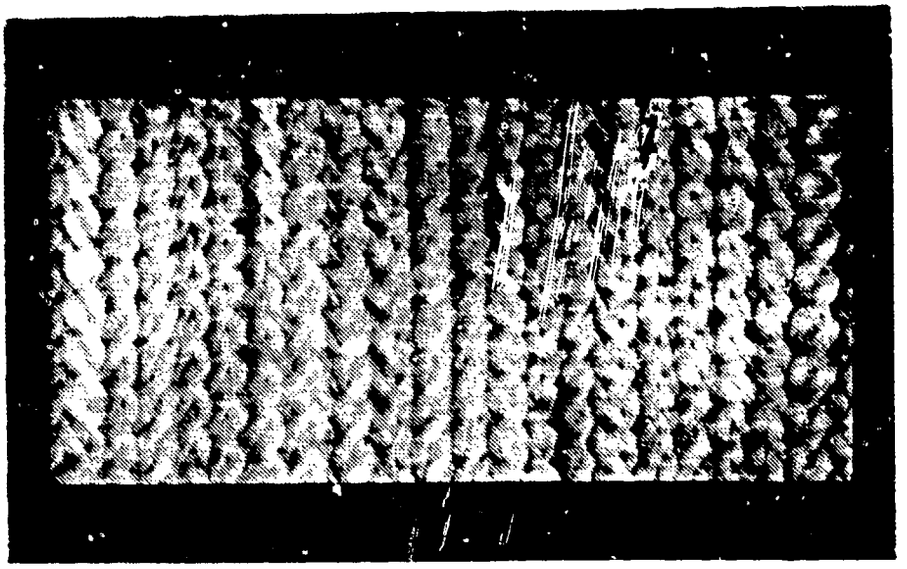

Virgin Material
(Pre-test Photo)

Mag. = 3.0x

Impact Direction ⟶

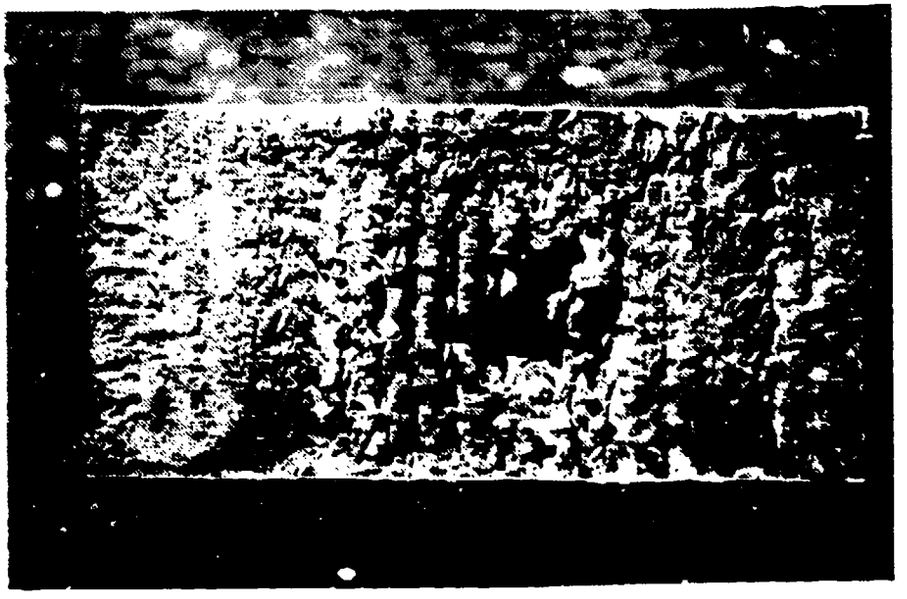

Damaged Material
(Post-test Photo)

Mag. = 2.7x

Figure 88 Photomicrographs of damage resulting from a 1 mm glass sphere (20°) impact at 8 kft/sec on material radiatively charred for 30 sec at 4000 °F.

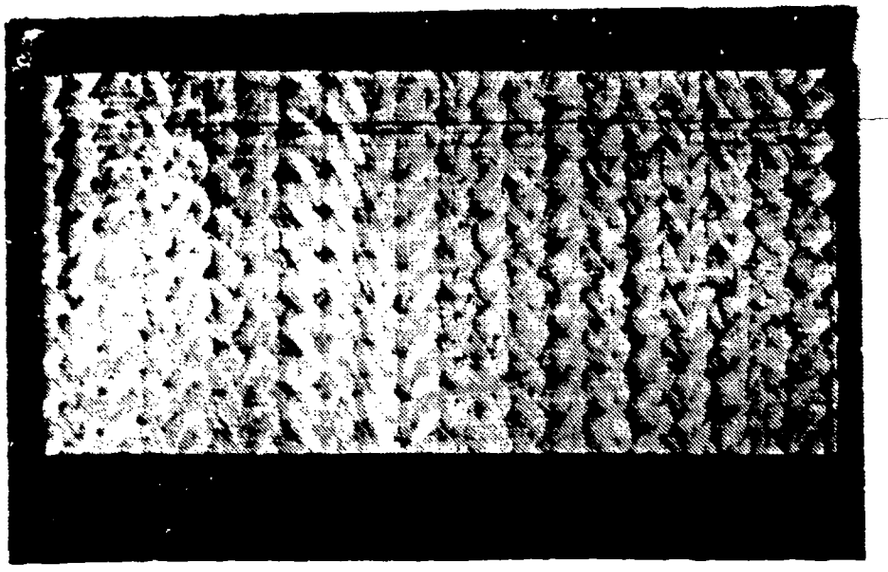

Virgin Material
(Pre-test Photo)

Mag. = 3.0x

Impact Direction ⟶

Damaged Material
(Post-test Photo)

Mag. = 2.9x

Figure 89 Photomicrographs of damage resulting from a 1 mm glass sphere (20°) impact at 8 kft/sec on material radiatively charred for 30 sec at 4000 °F.

5.3 Mechanical Properties

Two testing procedures were employed to obtain axial mechanical properties representative of the braided RMSP material. These were:

- o Axial Tensile
- o Axial Flexure

The following sections describe the test procedures and results particular to each.

5.3.1 Axial Tensile Properties

Classical tensile properties can be termed as the tensile stress, the tensile strain, and the tensile elastic modulus. The material being tested is subjected to a uniaxial tensile load distributed uniformly over the cross-sectional area of the test section. This is written as:

$$\sigma = \frac{f}{a} \qquad (1)$$

Where

σ = tensile stress in the axial direction

f = force acting on specimen

a = initial cross sectional area of specimen

The tensile strain is defined as the axail deformation of a material with respect to an original length when the material is subjected to a uniaxial tensile load distributed uniformly over the cross-sectional area of the test section. This is written as:

$$\varepsilon = \frac{\Delta \ell}{\ell_o} \qquad (2)$$

Where

ε = tensile strain in the axial direction

$\Delta \ell$ = linear gage length deformation in the axial dimension

ℓ_o = original gage length axial dimension

The tensile elastic modulus is defined as the ratio of the tensile stress to tensile strain below the proportional limit when the material is subjected to an uniaxial tensile load distributed uniformly over the cross-sectional area of the test section. This is written as:

$$E = \frac{\sigma}{\varepsilon} \qquad (3)$$

The test apparatus used employs a stock Instron with a strain gage network load cell. Strain is measured by bonding strain gages to the gage length of the specimen and recording strain during the test using the Instron strain gage amplifier. Figure 90 is a schematic of the test system.

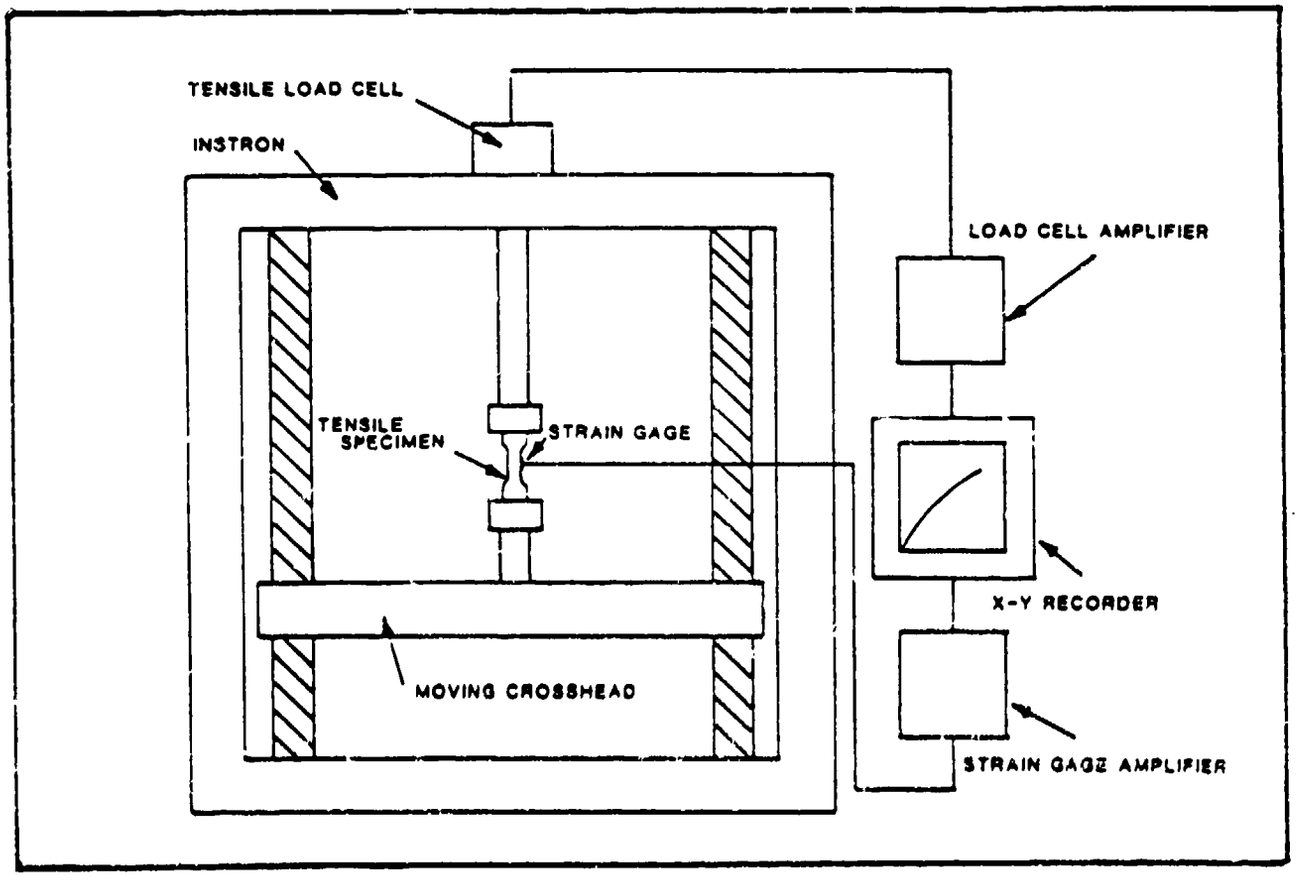

Figure 90
TENSILE TEST APPARATUS

5.3.1.1 Data Reduction & Results

The data is reduced to three parameters:

1) Tensile stress at failure

2) Tensile strain at failure

3) Tensile modulus

Tensile stress at failure is calculated from Equation (1) where the force acting on the specimen is the load read from the x-y recording at failure.

The tensile strain at failure is calculated from Equation (2) where $\Delta\ell$ is the linear gage length deformation in the axial dimension at failure.

The tensile elastic modulus is measured by taking a tangent to the initial straight line portion of the force/strain x-y recording. The modulus is calculated from:

$$E = \left(\frac{df}{d\varepsilon}\right)\frac{1}{a} \qquad (4)$$

Where

$\frac{df}{d\varepsilon}$ = tangent of force/strain initial curve

a = initial specimen cross-sectional area

The percent coefficient of variance is typically calculated for a set of data to indicate the statistical uniformity of the information. This is calculated as:

$$CV = \frac{s_x 100}{\bar{x}} \qquad (5)$$

Where

$$s_x = \frac{\Sigma_i (x_i - \bar{x})^2}{n-1} \qquad (5)$$

x = value of data point

Table 29 summarises the axial tensile properties obtained for the braided rubber modified silica phenolic material tested at room temperature and 500°F.

5.3.2 Axial Flexural Properties

Three Point Flexure Properties - An Instron model 1114 screw-driver mechanical test machine, used in conjunction with a three point beam deflection fixture, was employed to determine shear strength. A schematic representative of this flexure fixture is illustrated in Figure 91. The load delivered by the fixture is monitored by a strain gage network load cell. The load cell output is then amplified and recorded versus beam center deflection. Deflection was obtained by recording of dial gage movement or LDVT signal output.

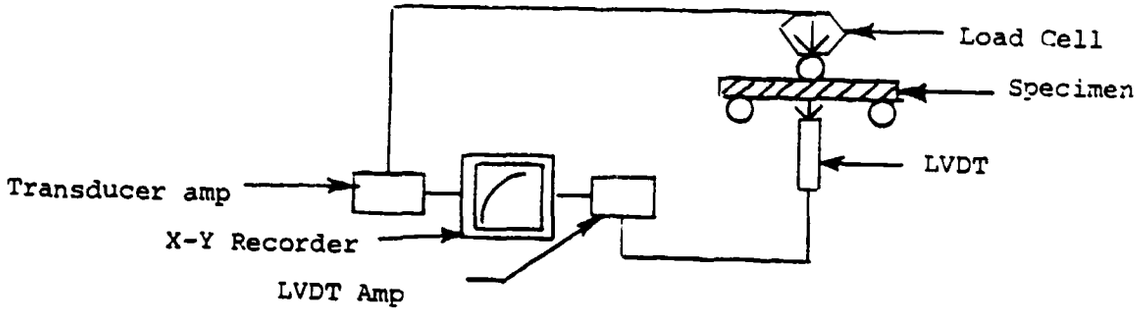

Figure 91
FLEXURE APPARATUS

Ultimate flexural strength is calculated by the following equation:

$$\sigma = \frac{MC}{I}$$

Where

σ = ultimate flexure strength (psi)

M = maximum applied bending moment ($M=\frac{PL}{4}$) (in.-lbs.)

C = maximum height of material from neutral axis (in.)

TABLE 29

BRAIDED RUBBER MODIFIED SILICA PHENOLIC
AXIAL TENSILE PROPERTIES

Test Temp.	Property	Units	Value
75°F	Modulus	10^6 psi	0.6
	Ultimate Strength	10^3 psi	1.8*
	Strain	%	0.6
500°F	Modulus	10^6 psi	0.2
	Ultimate Strength	10^3 psi	0.9*
	Strain	%	0.7

* Failures Intra Laminar

Table 30 summarizes the axial flexural properties obtained for the braided rubber modified silica phenolic material tested at room temperature and 500°F.

5.4 Thermal Properties

Two testing procedures were employed to obtain thermal properties representative of the braided RMSP materials. These include:

- o Hoop Thermal Expansion
- o Thermal Conductivity

The section following describe the test procedures and results particular to each.

5.4.1 Hoop Thermal Expansion

Diametral Thermal Expansion Property - Circumferential thermal expansion is defined as the change in circumference per unit initial circumference, when a cylindrical object is heated over a specified temperature range. Because some materials are anisotropic, it is necessary to measure the circumferential thermal expansion of cylindrical parts sampled as hoops. In order to measure this property, three parameters must be examined: the initial circumference, the change in circumference, and the temperature of the material during that change. This technique measures the change in diameter of the hoop in order to calculate the change in circumference.

The diameter of the hoop is measured to the nearest .001 inch using calipers traceable to NBS, and periodically calibrated by FMI Q.C. The change in diameter is detected by an LVDT (at three to six locations), which can detect a change in diameter of less than 4×10^{-5} inch. The temperature of the hoop is measured using a thermocouple or an Ircon infrared radiometer.

TABLE 30

BRAIDED RUBBER MODIFIED SILICA PHENOLIC
AXIAL FLEXURAL PROPERTIES

Test Temp.	Property	Units	Value
75°F	Ultimate Strength	10^3 psi	3.7
500°F	Ultimate Strength	10^3 psi	1.1

The material's characteristic is simulated using the following equation:

$$\alpha = \frac{\Delta D}{D \Delta T}$$

Where

α = diametral thermal expansion coefficient $(\frac{in.}{in. \ ^{o}F})$

ΔD = change in diameter (in.)

D = diameter (in.)

ΔT = change in temperature

The scope of this task included the diameter thermal expansion of three hoop specimens in the range of RT-250C (482 F).

Thermal expansion was measured by a recording quartz dilatometer. The technique is illustrated in Figure 92. The specimen was run in air. The heating time for each run was approximately two hours.

Table 31 lists room temperature dimensions of the thermal expansion hoop specimens, before and after the tests. As indicated, one hoop specimen each of three heights was investigated: 1/2 inch, 3/4 inch, and 1 inch. The table also shows percent changes in the dimensions, resulting from the heating cycle to slightly over 250°C for these tests.

Figure 93 is a composite of the thermal expansion curves for the three hoops, identified by hoop length. In all cases, expansion is evident up to at least 150°C, above which contraction accompanies apparent transformations in the materials.

5.4.2 Thermal Conductivity

Thermal conductivity was measured by a steady-state, comparative technique, using Pyroceram 9606 as the heat-flow meter (see Figure 94). The runs were made under static air.

TABLE 31

DIMENSIONS OF THERMAL EXPANSION
HOOP SPECIMENS

Dimension	Ring Identification 1/2" LE-1495	3/4" LE-1498	1" LE-1499
OD, in:			
Before	8.808	8.810	8.814
After	8.804	8.808	8.808
Change, %	-0.045	-0.023	-0.068
ID, in:			
Before	7.801	7.779	7.791
After	7.803	7.798	7.802
Change, %	+0.026	+0.244	+0.141
Length, in:			
Before	0.505	0.7533	1.0028
After	0.499	0.7505	1.0005
Change, %	-1.188	-0.372	-0.229
Weight, g:			
Before	158.6	238.8	316.3
After	151.4	226.8	303.1
Change, %	-4.54	-5.03	-4.17

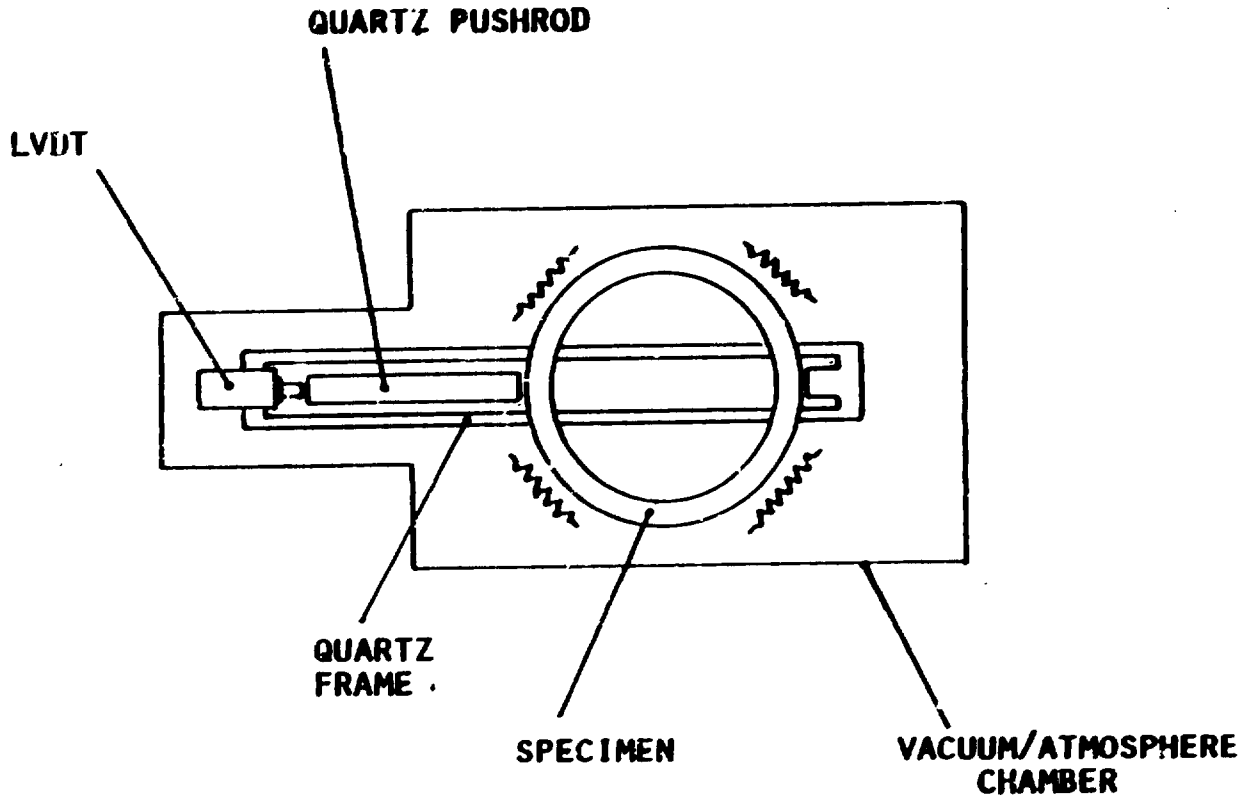

Figure 92

SCHEMATIC HCOP DILATOMER

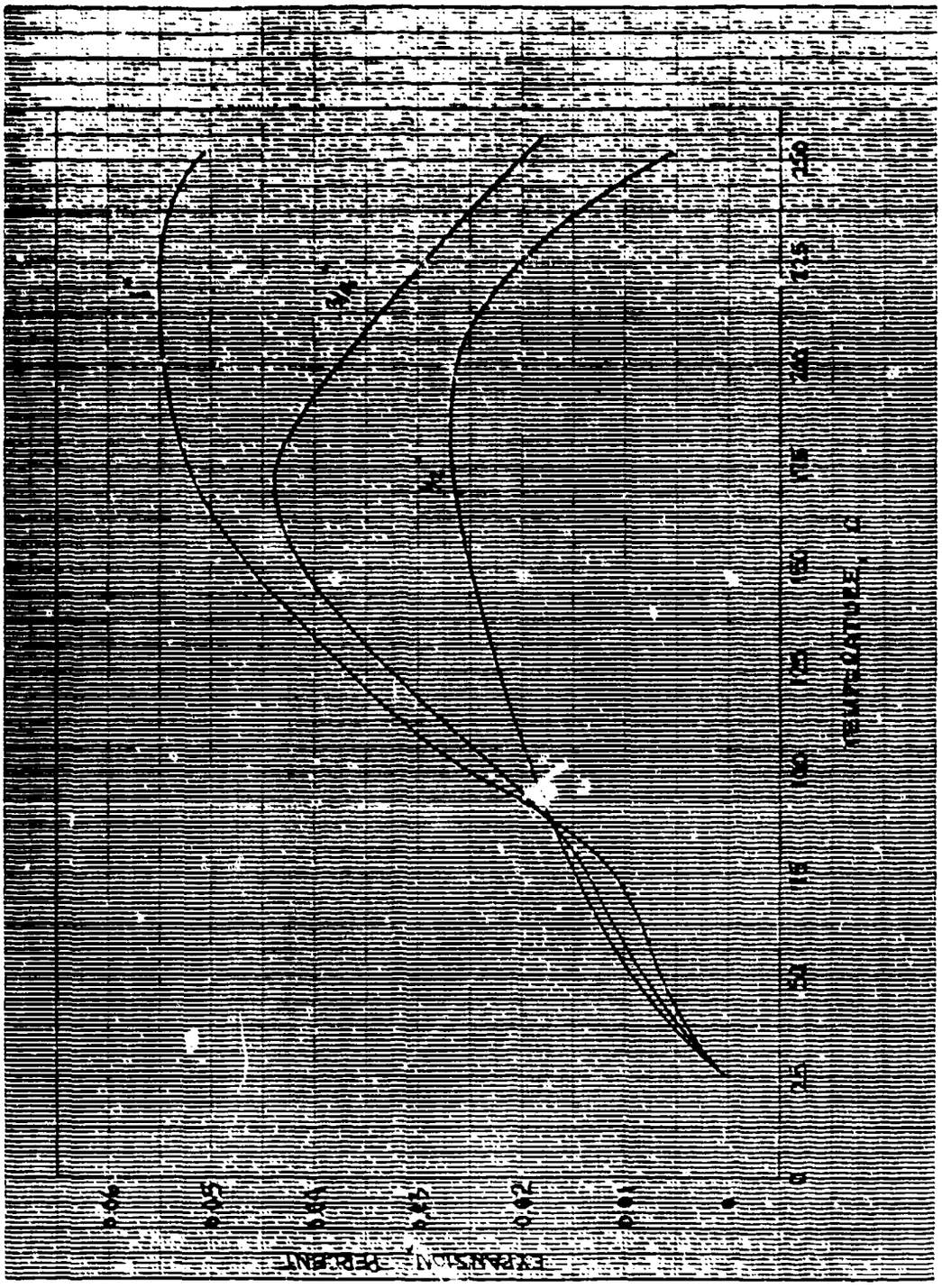

Figure 93

DIAMETRICAL THERMAL EXPANSION OF BRAIDED RMSP

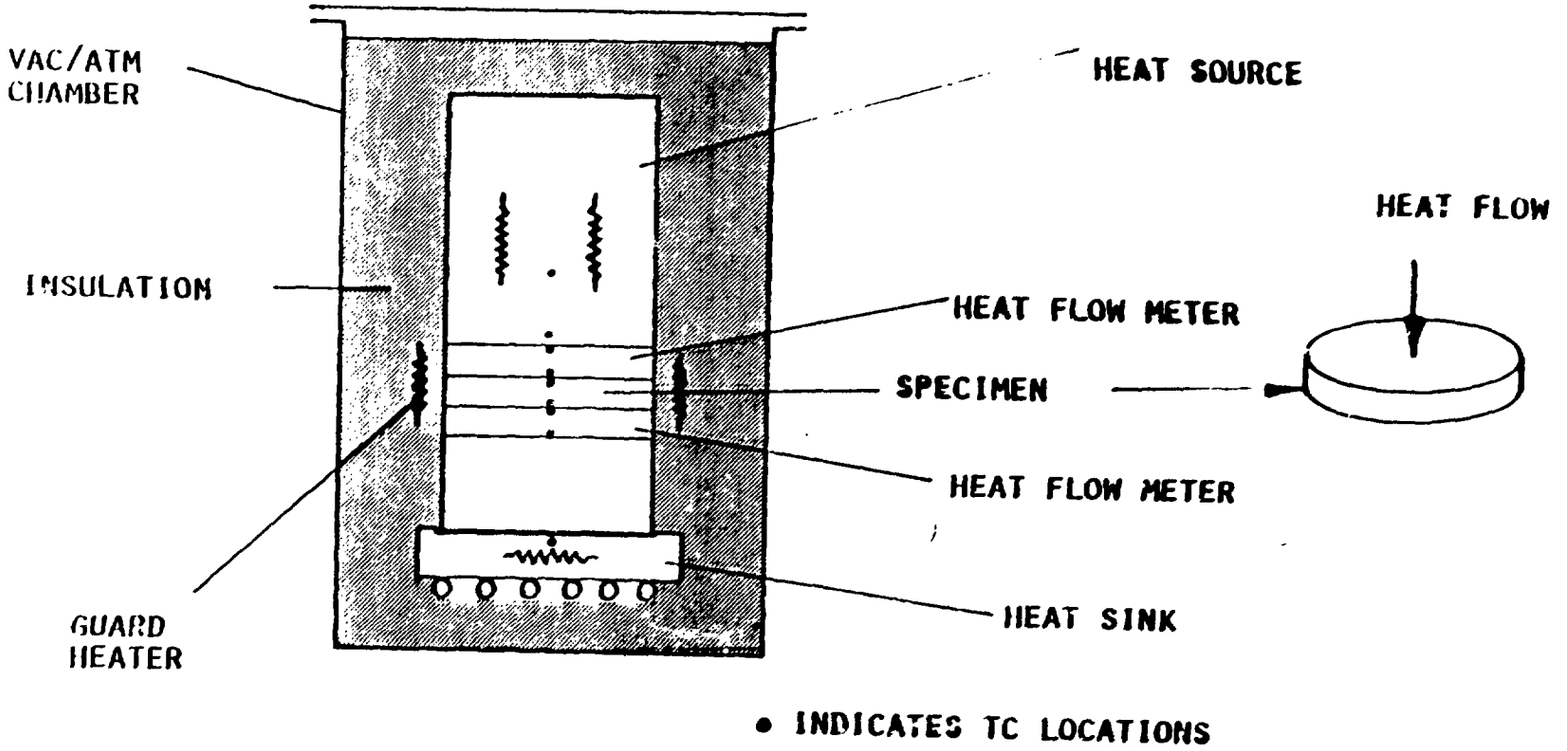

Figure 94

SCHEMATIC; STEADY-STATE COMPARATIVE CONDUCTIVITY

In this test, a resistance heater introduces a heat flow through the specimen and then to a heat flow detection meter. This meter is constructed with integral guard cylinders to inhibit non-axial (with respect to the specimen) heat flow. It is assumed that the central section of the apparatus collects all the heat which passes through a similar section of the specimen. Adjacent to the meter, a liquid gas cooled heat sink is located.

Under steady-state conditions, the conductivity of the specimen is determined by the following expression:

$$\lambda = q\Delta X/A\Delta T$$

Where

λ = thermal conductivity

q = heat flow rate

A = specimen cross-sectional area

ΔX = axial distance between temperature measuring points

ΔT = temperature difference along ΔX

The value of λ is the average thermal conductivity which corresponds to the average of the two temperatures along ΔX. The value of q is determined by the heat flow meter using a form of the preceeding equation.

Tables 32, 33, and 34 present results of the thermal conductivity measurements on two specimens of the silica phenolic. Tables 32 and 33 present primary data on two disk specimens, nominally three inches in diameter, by one-half inch thick. Table 34 lists additional values measured on the second specimen, to explore the range above 250°C (482°F). In all cases, the values are listed in the order measured; each measurement involved a heat soak of about two hours at the indicated temperature. The Table 34 data illustrate attempts to identify permanent changes in transport

TABLE 32

THERMAL CONDUCTIVITY OF BRAIDED RMSP

SPECIMEN 1

Temperature, C	Conductivity, $Wm^{-1}C^{-1}$
75	0.338
140	0.360
210	0.356
74	0.345
174	0.358
268	0.381
103	0.336

TABLE 33

THERMAL CONDUCTIVITY OF BRAIDED RMSP

SPECIMEN 2

Temperature, C	Conductivity, $Wm^{-1}C^{-1}$
76	0.327
125	0.339
193	0.357
232	0.365
267	0.375
171	0.354
76	0.321

TABLE 34

THERMAL CONDUCTIVITY OF BRAIDED RMSP

SPECIMEN 2, EXTENDED TEMPERATURE RANGE

Temperature, C	Conductivity, $Wm^{-1}C^{-1}$
67	0.330
78	0.348
138	0.353
190	0.381
194	0.380
228	0.388
230	0.348
111	0.349
237	0.390
66	0.332
231	0.389
65	0.350
230	0.383
266	0.371
330	0.383
395	0.361
199	0.329
511	0.373
588	0.450
696	0.418
280	0.337
612	0.303
734	0.523
735	0.557
322	0.391

characteristics, through repeat measurements at low temperature following measurements in the range above 250°C. Although data were recorded as high as 735°C (1355°F), no clear trend relating conductivity to heat-treatment could be defined. Figure 95 summarizes the data presented in Tables 32, 33, and 34.

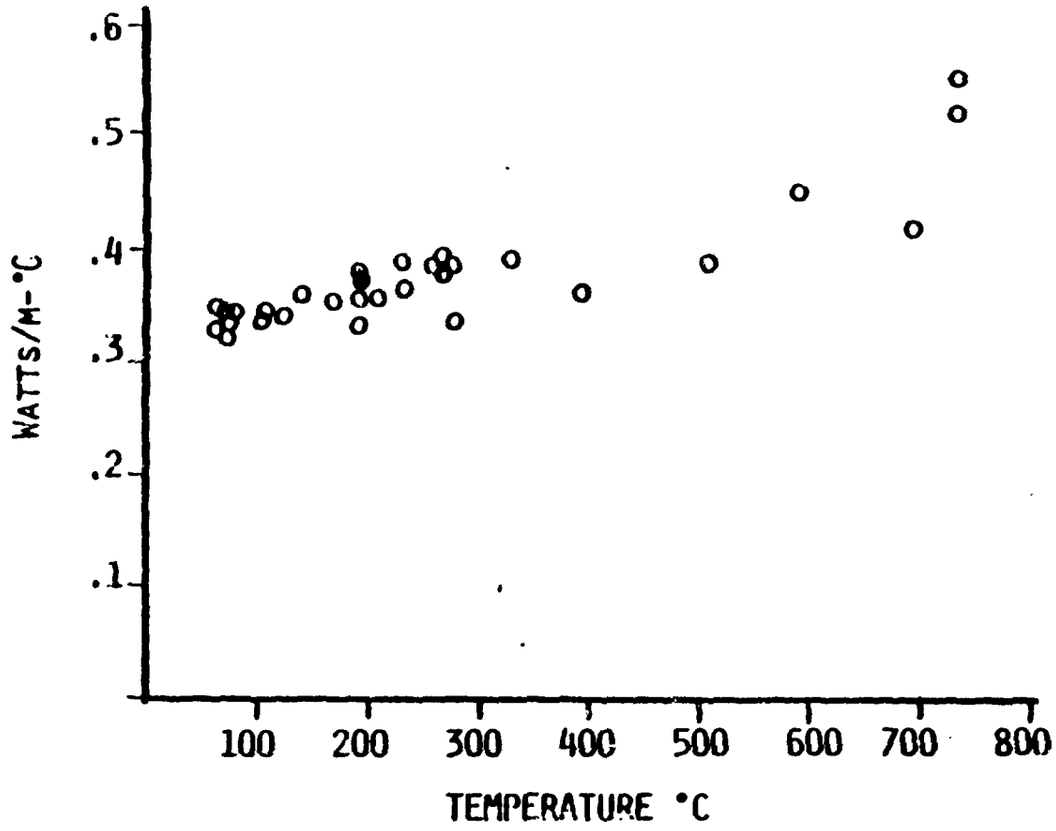

Figure 95

THERMAL CONDUCTIVITY OF BRAIDED
RUBBER MODIFIED SILICA PHENOLIC MATERIAL

6.0 CONCLUSIONS AND RECOMMENDATIONS

This program has resulted in the successful fabrication of ablative heatshield materials using braided silica and glass tapes. Both cylinders and frusta shapes were manufactured using rubber-modified-silica-phenolic tapes (RMSP) obtained by braiding E-glass yarn into a flat braid design, and subsequently leaching the glass into silica using an acid digestion and heat treating process. Tubular glass braids (i.e., glass phenolic) were also successfully manufactured and used for tapewrapping both cylinders and sub-scale frusta.

Test and evaluation of materials fabricated with braided prepreg have shown that similar or improved properties were obtained with the exception of mechanical characteristics.

Ablation test conditions were selected on the basis of anticipated flight environment and test conditions in which RMSP materials fabricated from conventional bias-cut tapes had been previously preformed. Figure 96 illustrates a comparison of recession rate for conventional bias RMSP versus braided RMSP where test conditions were the same. It can be seen that the ablation response of the material constructions are very similar.

Erosion testing indicated that the volumetric mass loss of braided RMSP was similar to other elastomeric modified phenolic reinforced heatshield materials. A bar chart of normalized volumetric loss ratios is presented in Figure 97. The performance of rubber modified materials is relatively poor as compared to other ablative heatshields, but the response of the braided construction was similar to other elastomeric resin reinforced materials.

A comparison of hoop thermal expansion characteristics between bias RMSP versus braided RMSP is shown in Figure 98. These tests were conducted on identical specimen sizes to eliminate differences due to circumferential yarn length effects.

FIGURE 96
RECESSION RATE VS. COLD WALL HEAT FLUX
BRAIDED AND BIAS RMSP

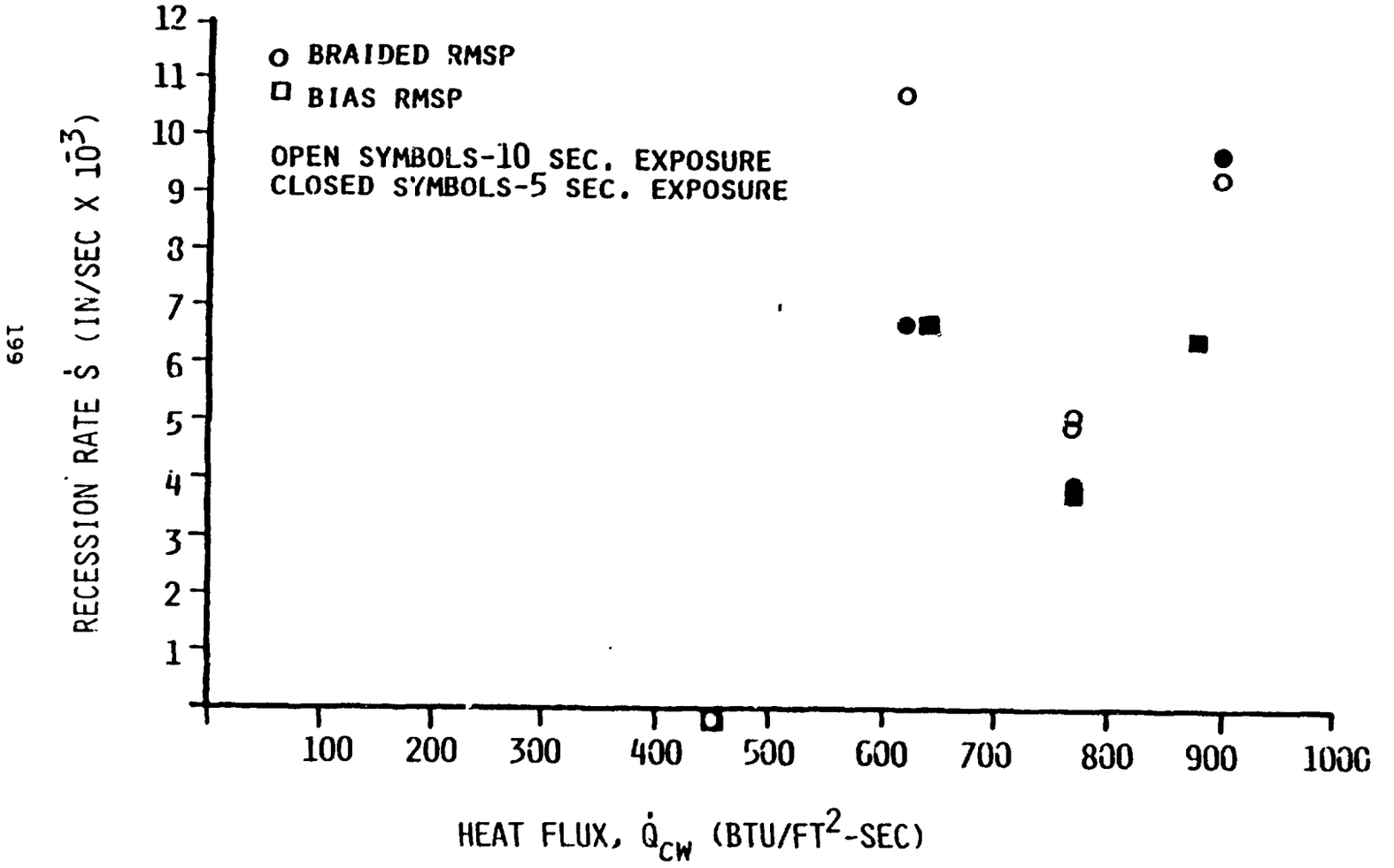

FIGURE 97
RELATIVE COMPARISON OF EROSION RESPONSE
BRAID VS. VARIOUS 45° BIAS TAPE
HOT CHAR

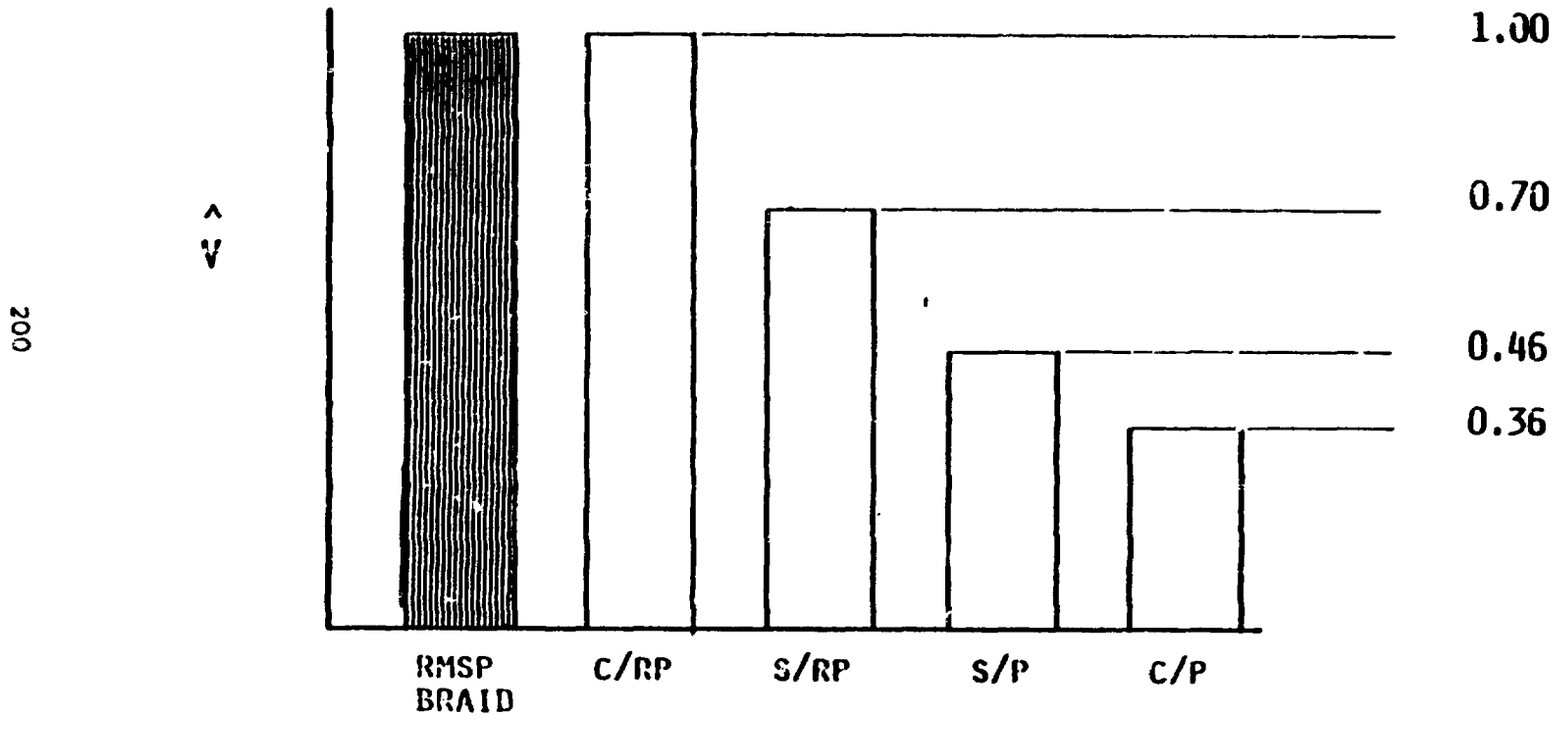

FIGURE 98
HOOP THERMAL EXPANSION
BRAIDED AND 45° BIAS TAPE

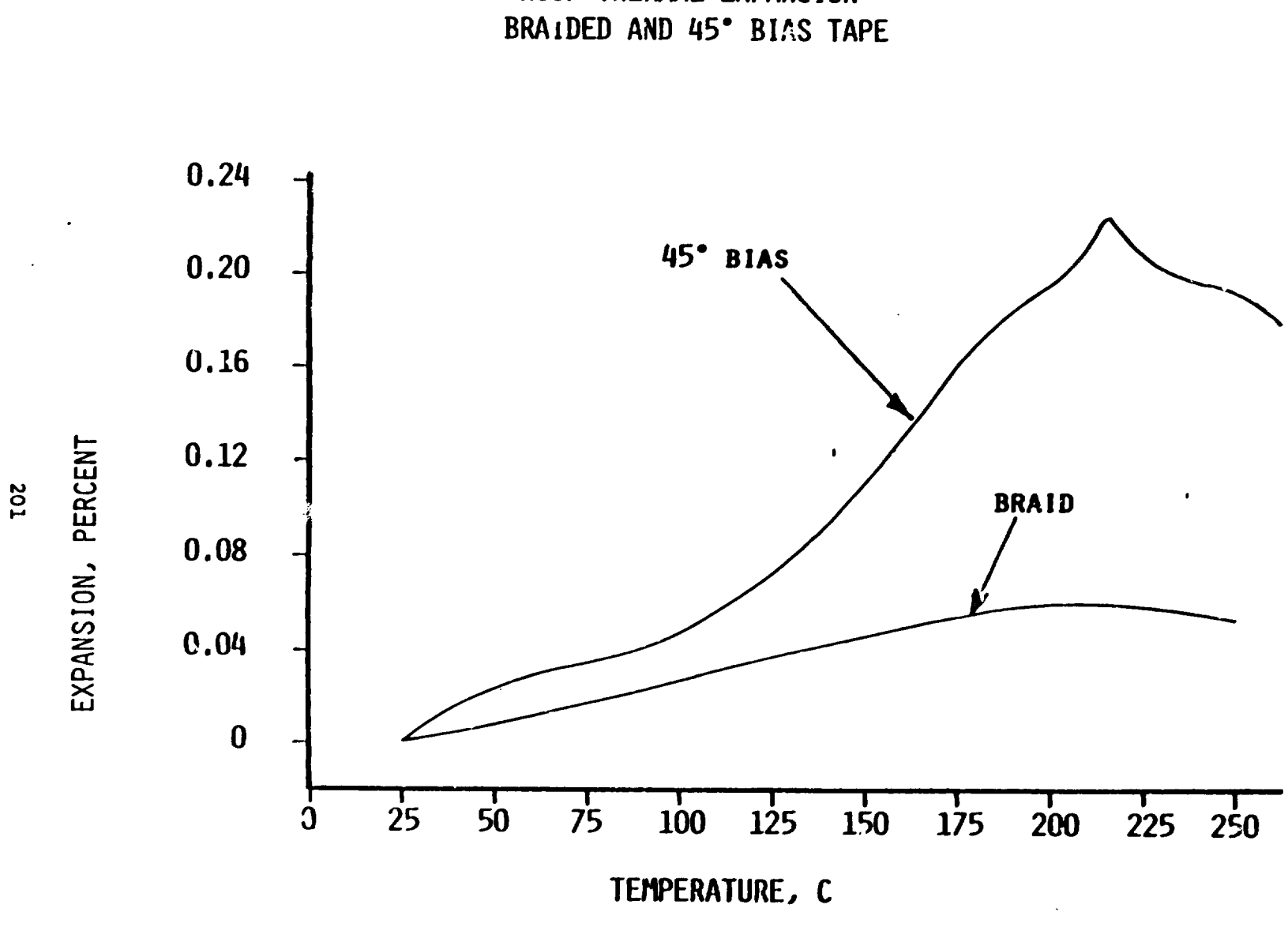

It can be seen that the braided material had a significantly lower percent expansion. However, it is felt that this difference resulted from the low resin content and high fiber volume of the braided material.

The low resin content in the braided RMSP, specifically the lack of resin penetration into the fiber bundles, was responsible for the poor mechanical properties exhibited by the braided RMSP. Table 35 lists a comparison of mechanical properties between the braided and bias RMSP materials.

TABLE 35

Axial Tensile and Flexure Properties of Braided and Bias RMSP

Temperature (°F)	Property	Units	Braid	45° Bias
Axial Flexure Properties				
75°F	Strength	10^3 psi	3.7	12.7
500°F	Strength	10^3 psi	1.1	1.2
Acial Tensile Properties				
75°F	Modulus	10^6 psi	0.6	1.1
75°F	Strength	10^3 psi	1.8	5.4
75°F	Strain	%	0.6	1.1

Examination of specimen failure indicated that 45° bias tape materials failed interlaminar (i.e., between the plies of tape) while the braided materials failed intralaminar (i.e., failure was in the tape) due to the lack of resin present in the yarn bundles.

Additional efforts are required to further develop the manufacturing technology for fabricating heatshield materials using braided tapes. Two issues remain unresolved. First, the resin content of the fabricated laminates must be increased and the potential yarn damage must be further investigated in the

braided tape. These issues are interrelated in that low resin content was the result of very high yarn packing in the braid. The high yarn packing resulted from the leaching process required to convert the glass to silica where significant shrinkage occurred. The braid design selected for demonstration was based on three trial samples. To further develop the technology for braided materials, optimization of the initial braid design and characterization of the leaching process effects are required.

The technology developed on the program is not limited to just silica or glass reinforced materials. Any material which can be handled on standard commercial braiding equipment can be braided.

Cost savings may be realized from the application of braiding. Assessment of manufacturing costs indicates that a 5% to 20% savings can be achieved. These savings are the result of eliminating the fabric slitting and stitching operations required for bias materials. Additional cost savings can be realized from reduced scrap. Braided material can be fabricated to very narrow tape widths thus eliminating excess material which must be machinced from the final heatshield product.

Further work is required to establish the technology for braided heatshield materials. The efforts conducted in this program have demonstrated that braiding can provide cost benefits plus the ability to manufacture continuous tapes with a balanced construction. The foundation for braiding manufacturing technology has been established in this program. The results substatiate further technology development.

REFERENCES

1) "AVCO Hyperthermal Simulation Capabilities," AVCO Systems Division Report No. AVSD-0006-70-CA, 15 January 1970.

2) Puckett, A. E., "Supersonic Nozzle Design," Journal of Applied Mechanics, December, 1946.

3) Foelsch, K., "The Analytical Design of an Axially Symmetric Novel Nozzle for a Parallel and Uniform Jet," J. Aero. Sci. 16, 161-166 and 188 (March 1949).

4) Comfort, E. H., "Ablation Measurements in Turbulent Flow," AIAA Paper No. 70-226, AIAA Eighth Aerospace Sciences Meeting, New York, January 1970.

5) Winovich, W., "On the Equilibrium Sonic-Flow Method for Evaluating Electric-Arc Air Heater Performance," NASA TND-2132, March 1964.

6) Cilmi, P., "Enthalpy Probe Measurements in the 10 Megawatt Arc Facility," Memorandum R720-67-103, AVCO Space Systems Division, Wilmington, Massachusetts, 23 August 1967.

7) O'Connor, T. J. and J. V. Morgida, "Null Point Transient Calorimeters, Theoretical Concepts and REsults," ISA Preprint No. 16, 5-2-66, October 1966.

8) Beck, J. V. and H. Wolfe, "Digital Program to Calculate Surface Heat Fluxes from Internal Temperatures in Heat Conducting Bodies," AVCO/RAD-TR-62-27, August, 1962.

9) Vincenti, W. G. and C. H. Krugar, Jr., Introduction to Physical Gas Dynamics, John Wiley and Sons, New York, 1965, p. 185.

10) "ABM Aeromechanical and Materials Design Volume II," Martin Marietta Corporation, Orlando, Florida, Report #OR 12,029, August 1972.

11) Katsikas, C. J., et al, "Ablation Handbook Entry Materials Data and Design," AVCO Corp. Technical Report AFML-TR-66-262. September 1966.

12) Schutzler, J. C., et al, "Thermal Protection Materials for Advanced Terminal Defense Interceptors," Prototype Development Associates, Inc. TR-1046-94-22, March 1977.

13) Martin, John J., "Atmospheric Reentry," Prentice-Hall, Inc., Englewood Cliffs, N.J., 1966.